Spectral classification & physical parameters of the IPHAS CBe stars in the BCD system.

by

Leonardos Gkouvelis

Doctorat en Física

Supervised by Prof. Juan Fabregat

in the

Departament d Astronomia i Astrofisica

Universitat de València

May 29, 2017

Declaration

Juan Fabregat Llueca, Catedratico de Astronomía y Astrofísica de la Universidad de Valencia

Certifica:

Que la presente memoria, titulada *Spectral classification & physical parameters of the IPHAS CBe stars in the BCD system*, ha sido realizada en el Departamento de Astronomía y Astrofísica de la Universidad de Valencia por Leonardos Gkouvelis bajo su direccion, y constituye su Tesis Doctoral para optar al grado de Doctor en Ciencias Fisicas.

Valencia, 25 de mayo de 2017

Juan Fabregat

Abstract

The INT Photometric $H\alpha$ Survey (IPHAS) has detected tens of thousands of emission line objects in the Northern Galactic Plane. Spectroscopic follow-up has shown that the vast majority of them are Classical Be (CBe) stars, rapidly rotating main sequence B type stars which develop an outflowing circumstellar disk by mechanisms not yet completely understood. In this work we present a study of the full catalogue of the CBe stars discovered by IPHAS. We have analyzed 805 low resolution spectra of 732 IPHAS CBe stars. With a semi-automatic procedure, which we evaluate at the first part of this work, we obtained the relevant physical parameters, including the effective temperature, surface gravity, absolute magnitude and distance, based on the techniques of the Barbier-Chalonge-Divan (BCD) spectrophotometric system.

Also, we plot an HR diagram from which we extracted masses and ages. From the data in the catalogue we have determined for the sample a mean rotational velocity of 82% of the critical velocity, without any trend of variation with the spectral type. The data also confirm that the circumstellar discs rotate following a Keplerian velocity law. We found the ages of the stars evenly distributed between the ZAMS and the TAMS, and hence our results do not support claims of an evolutionary nature of the Be phenomenon.

The distribution of the stars does not present an apparent clustering in or around the Perseus or the Outer Arm regions. Instead, they appear scattered along the two arms and the space in between, with some stars spreaded along larger distances, beyond the expected location of the Outer Arm. The density of the stars beyond the Perseus Arm displays a similar exponential decline at all longitudes

along the Northern Galactic Plane. No evidence of an outer Arm beyond the Perseus Arm is present in our data.

Leo Gkouvelis May 29, 2017

Declaration of Authorship

I, Gkouvelis Leonardos, declare that this thesis titled, ' Spectral classification & physical parameters of the IPHAS CBe stars in the BCD system.' and the work presented in it are my own. I confirm that:

- This work was done wholly or mainly while in candidature for a research degree at this University.
- Where any part of this thesis has previously been submitted for a degree or any other qualification at this University or any other institution, this has been clearly stated.
- Where I have consulted the published work of others, this is always clearly attributed.
- Where I have quoted from the work of others, the source is always given. With the exception of such quotations, this thesis is entirely my own work.
- I have acknowledged all main sources of help.
- Where the thesis is based on work done by myself jointly with others, I have made clear exactly what was done by others and what I have contributed myself.

Signed:

Date:

"Aunque la halles pobre, Itaca no te ha engañado. Así, sabio como te has vuelto, con tanta experiencia, entenderás ya qué significan las Itacas."

C.P. Cavafis

"If you find Ithaca wanting, it's not that she's deceived you. That you have gained so much wisdom and experience will have told you everything of what such Ithacas mean."

C.P. Cavafy

'Κι ἂν πτωχικὴ τὴν βρῇς, ἡ Ἰθάκη δὲν σὲ γέλασε. Ἔτσι σοφὸς ποὺ ἔγινες, μὲ τόση πείρα, ἤδη θὰ τὸ κατάλαβες ἡ Ἰθάκες τί σημαίνουν.'

Κωνσταντῖνος Καβάφης

Abstract

Departament d Astronomia i Astrofisica

Universitat de València

Doctor of Philosophy

by Leonardos Gkouvelis

Doctorat en Física

Supervised by Prof. Juan Fabregat

Resumen

Capítulo 1. Introducción.

Las estrellas Be clásicas (CBe) son estrellas tipo B de la secuencia principal que tienen en sus espectros líneas de emisión, o las han tenido alguna vez en el pasado. También presentan un exceso de emisión en el continuo, en los rangos ultravioleta, óptico e infrarrojo. La emisión tanto en las líneas como en el continuo se origina por el procesado de la radiación ultravioleta de la estrella central en una envoltura de materia circunestelar con geometría de disco. Todavía no se dispone de una explicación completa de los procesos de eyección de materia que dan lugar a la formación del disco, aunque se acepta de forma casi unánime que la velocidad de rotación rápida, la presencia de pulsaciones no radiales y la posible existencia de campos magnéticos están en el origen de dichos procesos.

Las estrellas CBe, y en especial las de tipos más tempranos, son objetos de vida corta, que no han dispuesto de tiempo para alejarse significativamente de sus lugares de nacimiento. Es poco probable que todavía estén inmersas en las nebulosas en las que se formaron, debido a que son objetos relativamente evolucionados. Son además estrellas intrínsecamente brillantes, con lo que pueden ser detectadas a lo largo de todo el plano galáctico, al menos en regiones sin excesiva extinción interestelar. Por lo tanto pueden considerarse como trazadores para el estudio de la estructura espiral de la Galaxia.

El INT Photometric Hα Survey (IPHAS) es un cartografiado fotométrico del Plano Galáctico norte que ha detectado decenas de miles de objetos con la línea de Hα en emisión. La fotometría de IPHAS se obtiene a partir de imágenes en los filtros r' e i' del sistema de Sloan, y un filtro de banda estrecha centrado en la línea de Hα. Una primera lista de objetos mostrando la línea de Hα en emisión fue presentada por Witham et al. (2008). Varios miles de objetos detectados con líneas de emisión han sido también observados espectroscópicamente. Este seguimiento espectroscópico ha confirmado que la mayoría de ellos son estrellas Be clásicas (CBe).

El objetivo principal del cartografiado IPHAS es la detección de objetos con líneas de emisión en el plano galáctico norte. Algunos de estos objetos corresponden a

fases muy rápidas de la evolución de las estrellas masivas, tanto aisladas como en sistemas binarios, y por tanto se conocen muy pocos ejemplares en la Galaxia. La detección de un número significativo de ellos permitirá aumentar hasta en un orden de magnitud las muestras conocidas en la actualidad, lo que a su vez permitirá estudiar fases de la evolución estelar que todavía no son bien conocidas.

El sistema espectrofotométrico BCD se empezó a desarrollar en los años 40 por Barbier y Chalonge, y ha continuado desarrollándose durante los años 70 mediante los trabajos de Chalonge y Divan. El sistema está basado en la medida de parámetros observables en la región espectral de la discontinuidad de Balmer, entre los 3500 y los 4600 Å. Los parámetros básicos son: D, profundidad de la discontinuidad de Balmer, que es un indicador de la temperatura efectiva; λ_1, el punto medio de la discontinuidad de Balmer en el rango espectral; Φ_b, el gradiente del flujo en la zona del continuo de Paschen; y Φ_{uv}, el gradiente del flujo de la zona del continuo de Balmer.

Los parámetros D y λ_1 son independientes de la extinción interestelar, y permiten la determinación de la temperatura efectiva y la gravedad superficial a partir de las calibraciones correspondientes. El tercer parámetro Φ_b, que mide la pendiente del continuo de Paschen, es una función de la temperatura efectiva y de la extinción interestelar, y puede usarse para la determinación de esta última.

La discontinuidad de Balmer es una característica espectral fácilmente visible en estrellas de los tipos O hasta F tardíos. Una descripción moderna del sistema BCD con una presentación de sus ventajas con respecto a otros sistemas espectroscopios ha sido presentada por Zorec at al. (2009).

Sin embargo, los procedimientos estándar para la determinación de la profundidad de la discontinuidad de Balmer no son aplicables, en general, a las estrellas CBe. Debido a la menor presión en la envoltura circunestelar, éstas presentan una segunda discontinuidad en la region ultravioleta, que puede estar en emisión o en absorción. Por esta razón no es posible utilizar el método clásico BCD para analizar las estrellas Be. Sí resulta posible, sin embargo, utilizar un gradiente diferente a Φ_{uv} para medir la profundidad de la discontinuidad fotosférica original.

Las ventajas del sistema BCD en comparación con otros sistemas de clasificación son que puede aplicarse a espectros de baja resolución y ofrece muchas facilidades a la hora de implementarse en procesos automatizados. El sistema BCD dispone de varias calibraciones para la determinación de los parámetros astrofísicos a partir las cantidades observables descritos.

El objetivo de este trabajo es el análisis de los espectros de seguimiento de IPHAS para la elaboración de un catálogo de estrellas Be clásicas, a partir del cual obtener los parámetros físicos de cada estrella, estudiar su estado evolutivo, su velocidad de rotación y la estructura de velocidades en el disco. Además, y aprovechando el area cubierta por IPHAS, se ha determinado la distancia a las estrellas mediante la técnica de la paralaje espectroscópica, con el objeto de explorar la posibilidad de uso de las estrellas CBe de IPHAS como trazadores de la estructura galáctica, y en particular de la estructura espiral.

El trabajo está dividido en dos partes. En la primera describimos los métodos que hemos desarrollado para la determinación de los parámetros físicos de las estrellas a partir de los espectros de baja resolución. En la segunda presentamos el catálogo completo de las estrellas CBe de IPHAS con sus parámetros físicos, y hacemos un análisis estadístico de sus propiedades. Por último exponemos las conclusiones de este trabajo y posibles planteamientos para el futuro.

Capitulo 2. Análisis.

IPHAS empezó a observar en 2005, y las observaciones se prolongaron hasta 2015. Durante este periodo se han descubierto decenas de miles de objetos con la línea Hα en emisión, más del 70% de los cuales son estrellas Be. Para complementar los datos de fotometría se ha realizado seguimientos espectroscopicos, de los cuales el más extenso se ha realizado en el Fred Lawrence Whipple Observatory (FLWO) en Estados Unidos, con el espectrógrafo FAST, durante un periodo de 7 años, desde 2005 hasta 2012, obteniendo 2624 espectros en todo el plano galáctico norte. La gran mayoría de ellos pertenecen a estrellas CBe, y el objetivo de este trabajo es analizar esos datos.

Los espectros de FAST son de baja resolución, y constituyen una gran cantidad de datos, por lo que resulta difícil analizarlos uno a uno mediante métodos estándar.

Por esta razón hemos desarrollado un método semiautomático para poder realizar el análisis en un tiempo razonable. Nuestro método de análisis esta basado en el sistema espectrofotométrico de Barbier, Chalonge y Divan (BCD), descrito anteriormente.

La magnitudes absolutas en la banda V de Johnson (M_V) se obtienen directamente de los parámetros D y λ_1 por medio de la calibración de Zorec y Briot (1991). Posteriormente se transforman en magnitudes absolutas en la banda r de IPHAS usando los colores intrínsecos ($V - R_C$) para estrellas B de la secuencia principal, y suponiendo que las magnitudes R_C y r de IPHAS en el sistema de Vega son idénticas dentro de los errores de nuestro procedimiento.

Las distancias se obtienen por medio de la técnica de la paralaje espectroscopia, comparando la magnitud absoluta M_r con las magnitudes r aparentes publicadas en el segundo catálogo fotométrico de IPHAS (Barentsen et al. 2014), corregidas de absorción interestelar y de extinción circunestelar añadida por al emisión en el continuo del disco. Para corregir de la emisión circunestelar seguimos el método descrito por Raddi et al. (2013), basado en la correlación existente entre la anchura equivalente de la línea Hα y el exceso en el continuo.

Para la determinación de los parámetros físicos fundamentales mediante las técnicas del sistema BCD descritas es necesario que los espectros tengan al menos una calibración en flujo relativa los suficientemente precisa. Dado que los espectros originales no disponían de esta calibración, se ha procedido a realizarla noche por noche utilizando estándares de calibración del archivo del FLWO/FAST, de forma que cada espectro ha sido calibrado en flujo utilizando estándares observadas durante la misma noche. Posteriormente se ha comprobado la precisión de la calibración, comparando espectros de los mismos objetos obtenidos en noches diferentes. El error medio de la calibración en flujo se ha estimado en el 5% en la región de los 4000 Å, y en el 15% en 3600 Å. Esto se traduce en errores en los parámetros D y λ_1 comparables con los rangos que subtienden estos parámetros a lo largo de un subtipo espectral y una clase de luminosidad respectivamente.

Por otra parte, para poder utilizar las calibraciones del sistema BCD tenemos que transformar los espectros a una resolución espectral aproximadamente de 8 Å, que

es la resolución con la que dichas calibraciones fueron desarrolladas. Aunque el parámetro D es independiente de la resolución, la posición media de la discontinuidad de Balmer, y por tanto el parámetro λ_1, sí que varía con la resolución espectral. Como la determinación de las magnitudes astrofísicas fundamentales depende de los parámetros medibles del sistema BCD, para medir éstos últimos necesitamos reducir la resolución de nuestros espectros a la resolución original del sistema. Esto lo hacemos convolucionando los espectros con un filtro gaussiano de la anchura adecuada.

Una vez calibrados los espectros en longitud de onda y transformados a la resolución adecuada, el siguiente proceso ha sido medir los parámetros del sistema BCD, y a partir de dichos parámetros determinar las magnitudes físicas de los objetos observados. El parámetro D se calcula midiendo la diferencia entre el continuo de Paschen y la línea que une los fondos de las líneas de Balmer de orden alto, ambos extrapolados a una longitud de onda de 3700 Å. Para determinar la posición media de la discontinuidad de Balmer se calcula un ajuste del continuo espectral, y a continuación se calcula su intersección con el valor medio de las líneas que trazan el continuo de Paschen y los fondos de las líneas de Balmer. El parámetro Φ_b se calcula como el gradiente del continuo espectral entre 4000 y 4600 Å.

Para calcular estos parámetros para todas las estrellas de la muestra se ha desarrollado un proceso semiautomático, que solo requiere intervención humana para evaluar diagramas generados en algunos pasos intermedios relevantes en el tratamiento de cada espectro. La entrada del programa la constituyen los espectros calibrados en flujo y longitud de onda, junto con la anchura del filtro gaussiano requerido para convolucionar los espectros y transformarlos a la resolución requerida por las calibraciones del sistema BCD. El flujo es normalizado en 4600 Å, y a continuación se obtiene una medida preliminar de la profundidad de la discontinuidad de Balmer, que se denomina D_1. A partir de D_1 se deriva un valor aproximado de la temperatura efectiva, y se divide el espectro por el de una curva de cuerpo negro a esa temperatura. De esta forma el continuo de Paschen se aproxima a una línea recta, y se puede extrapolar de forma precisa. La determinación final de

D como un cociente de flujos en 3700 Åcancela la contribución de la función de cuerpo negro.

Para calcular la posición de la discontinuidad de Balmer, se calcula en primer lugar la línea paralela al continuo de Paschen extrapolado, a una distancia de $D/2$. El continuo espectral se caracteriza como un ajuste parabólico al pseudo-continuo entre los 3700 y 3850 Å. La intersección entre ambas líneas determina el valor del parámetro λ_1. Para cada espectro el programa traza una serie de diagramas que pueden ser inspeccionados para controlar el proceso.

Como resultado final, el sistema determina también el tipo espectral y la clase de luminosidad, la temperatura efectiva, la magnitud absoluta y la extinción interestelar, usando las calibraciones del sistema BCD.

A partir de la magnitud absoluta en la banda r' y la extinción interestelar, y de las magnitudes aparentes en r' obtenidas del segundo catálogo fotométrico de IPHAS, se ha determinado las distancias a los objetos mediante la técnica de la paralaje espectroscopia. En esta determinación se ha tenido en cuenta la contribución de la emisión en el continuo de la envoltura circunestelar a la magnitud aparente. Esta contribución se ha determinado a partir de su relación con la anchura equivalente de la línea Hα, que también se ha medido para todos los objetos observados.

Para validar nuestro método y los resultados obtenidos hemos analizado una parte de los espectros, con el objeto de compararlos con datos de las mismas estrellas que aparecen en la literatura, obtenidos por otros autores con métodos diferentes. En primer lugar hemos analizado estrellas CBe que han sido observadas con el Isaac Newton Telescope (INT) y Nordic Optical Telescope (NOT) en la isla de La Palma. Raddi et al. (2013) determinaron sus tipos espectrales y exceso de color mediante el ajuste de sus distribuciones de energía espectral a modelos de atmósfera apropiados, en la parte azul del espectro, entre los 3800 y 5000 Å. Para la comparación hemos utilizado los espectros de 35 estrellas en común entre la muestra de Raddi et al. y la nuestra. Para 29 de ellos el tipo espectral coincide con un margen de uno o dos subtipos. También hemos comparado los excesos de color, obteniendo una diferencia media en el $E(B-V)$ de 0.04±0.15 magnitudes, lo que representa un acuerdo satisfactorio.

Por otra parte, también hemos analizado quince estrellas en común con Mongió et al (2013), donde se presenta fotometría $uvby\beta$ de una muestra de estrellas en el plano galáctico norte. Para esos objetos, a partir de la fotometría hemos determinado la extinción interestelar, el tipo espectral y la magnitud absoluta usando las calibraciones del sistema de Strömgren-Crawford. Hemos seguido los procedimientos descritos por Fabregat y Torrejón (1998) para aplicar dichas calibraciones a las estrellas CBe, para las cuales la emisión circunestelar en los continuos de Balmer y Paschen y en la línea Hβ tienen importantes efectos en los índices fotométricos.

Las diferencias obtenidas entre los dos análisis en la determinación del tipo espectral son menores de un subtipo. En la determinación de la extinción interestelar el acuerdo entre los dos procedimientos muy bueno, con una diferencia media en el $E(B-V)$ de 0.00$\pm$0.10 magnitudes. Cabe destacar que tanto en las calibraciones del sistema $uvby\beta$ como del BCD los colores intrínsecos se determinan a partir de la profundidad de la discontinuidad de Balmer, que se mide mediante el índice c_1 en el sistema $uvby\beta$, y el parámetro D en el BCD, lo cual justifica el muy buen acuerdo obtenido.

Capítulo 3. Análisis global de los espectros de FAST.

En este capítulo presentamos un análisis detallado de la muestra completa de 2627 espectros de baja resolución obtenidos con el espectrógrafo FAST. A partir de estos datos abordamos varios problemas fundamentales relativos a las estrellas CBe como clase, y en particular sus velocidades de rotación, estado evolutivo y distribución de velocidades en el disco circunestelar. También usamos nuestra muestra para contribuir al estudio de la estructura espiral de la galaxia en el hemisferio norte, usando nuestros objetos como trazadores después de determinar su distancia mediante la técnica de la paralaje espectroscopia.

En primer lugar, mediante inspección visual se ha encontrado 1120 espectros de 1026 estrellas con características espectrales correspondientes a estrellas de los tipos O y B con líneas de emisión. De entre ellos hemos seleccionado los espectros con el continuo bien definido y una relación señal/ruido superior a 30 en la región de la discontinuidad de Balmer. Esto ha dado lugar a una muestra final de 823 espectros de 732 estrellas CBe, para las cuales hemos obtenido sus

parámetros físicos fundamentales mediante las técnicas y calibraciones del sistema BCD. Dichos parámetros incluyen la temperatura efectiva, clasificación espectral, magnitud absoluta, extinción interestelar, magnitud bolométrica y distancia, esta última obtenida mediante la técnica de la paralaje espectroscópica.

Presentamos un catálogo final con datos para 732 estrellas Be, de las cuales 649 son nuevas detecciones sin publicar en anteriores trabajos. Presentamos además un catálogo adicional con estrellas cuyas características espectrales permiten clasificarlas como estrellas CBe, pero que la calidad de los espectros no es suficiente para la determinación de los parámetros físicos. En total, presentamos una muestra de 1089 estrellas CBe débiles, detectadas a partir de la fotometría de IPHAS y confirmadas con espectros de seguimiento. Nuestro catálogo aumenta el número de estrellas Be clásicas conocidas en un 40%.

Se ha determinado la anchura equivalente y otros parámetros de línea Hα, para todas las estrellas de la muestra. Los valores mayores de la anchura equivalente obtenidos son -92, -66 y -62 Å. Para el resto de las estrellas la anchura equivalente es inferior en módulo a -60 Å. A continuación hemos comparado las determinaciones espectroscópicas de la anchura equivalente con las obtenidas a partir de la fotometría mediante interpolación de los colores de IPHAS en las curvas de HαEW constante presentadas por Drew et al. (2005). Existe una buena correlación entre ambas determinaciones, aunque los valores derivados de la fotometría son sistemáticamente más altos, con una diferencia media de 2.6 Å.

Los espectros de veinte estrellas, que representan un 2.7% de la muestra, presentan la línea de Hα en absorción; sus colores fotométricos, sin embargo, las sitúan en la región ocupada por las estrellas con líneas de emisión en los diagramas color-color de IPHAS. Por el contrario, seis estrellas que aparecen en la región del diagrama fotométrico correspondiente a las estrellas con líneas de absorción, muestran la línea de Hα en emisión en sus espectros. Estas diferencias las interpretamos como debidas a transiciones de fase entre emisión y absorción o viceversa, originadas por la bien conocida variabilidad del fenómeno Be, a lo largo del tiempo transcurrido entre la obtención de los datos fotométricos y los espectroscópicos. El hecho de que más estrellas cambien de emisión a absorción que al contrario es un

efecto de selección de la muestra. La mayor parte de las estrellas seleccionadas para seguimiento espectroscopio lo fueron porque sus colores fotométricos eran característicos de estrellas con líneas de emisión.

A partir de la temperatura efectiva y la luminosidad de cada estrella hemos situado nuestra muestra en un diagrama HR, a partir del cual hemos estimado la masa y la edad de cada estrella interpolando en los caminos evolutivos de Ekstrom et al. (2012). Con esos parámetros hemos realizado diagramas para estudiar el estado evolutivo de las estrellas Be.

La cuestión del estado evolutivo de las estrellas CBe es todavía sujeto de debate. Fabregat y Torrejón (2000) propusieron que el fenómeno Be es un efecto evolutivo que tiene lugar en la segunda parte de la vida de una estrella de tipo B en la secuencia principal. Zorec et al. (2005) encontraron un resultado similar para estrellas CBe de tipo tardío, pero propusieron que las de tipo temprano se dan principalmente en la primera mitad. Sin embargo, Martayan et al. (2007) encontraron un porcentaje significativo de estrellas CBe en la ZAMS, lo que implicaría que el fenómeno Be es una característica innata de algunas estrellas B, y no adquirida en el curso de la evolución. Muchos otros autores se han ocupado de este problema en la bibliografía reciente, alcanzando conclusiones en general contradictorias. Nuestros resultados muestran que el conjunto de estrellas CBe estudiado se distribuye uniformemente a lo largo de toda la secuencia principal del diagrama HR, entre el ZAMS y el TAMS, y por tanto no confirman las propuestas que presentan el fenómeno Be como un proceso evolutivo.

En la actualidad es un hecho bien establecido que las estrellas CBe son una clase de retadores rápidos, con velocidades de rotación distribuidas entre el 75% y el 100% de la velocidad de ruptura, definida esta como la velocidad a la cual la materia que constituye la estrella escaparía por el ecuador debido a la fuerza centrífuga. Para obtener la velocidad media de rotación de nuestra muestra, a partir de los perfiles de las líneas de HeI hemos obtenido la velocidad de rotación proyectada $v \sin i$, obteniendo un valor medio del 65%. Corrigiendo del efecto de proyección obtenemos que la velocidad media de nuestra muestra es del 82% de la velocidad de ruptura, en buen acuerdo con trabajos anteriores. Hemos podido comprobar

también que la velocidad de rotación con respecto a la velocidad de ruptura es independiente del subtipo espectral.

Para las estrellas que presentan una estructura de doble pico en la línea de emisión de Hα hemos calculado la separación entre los picos, y a partir de ella la distribución de velocidades de la materia en el disco circunestelar. Nuestros resultados confirman un régimen de rotación kepleriano, como se ha encontrado en trabajos anteriores.

En cuanto a la distribución espacial, nuestra muestra presenta una distribución irregular en función de la longitud galáctica, con una alta densidad en la región comprendida entre los 110 y 140 grados, y areas muy poco pobladas alrededor de los 40 y 80 grados. Esta distribución está relacionada con la variación de la extinción interestelar a lo largo del plano galáctico, de forma que las regiones con menor densidad de estrellas se corresponden con las direcciones en las que la extinción es mayor. Cabe destacar la aparente falta de estrellas en la dirección del anticentro galáctico, a latitudes positivas, en una región de muy baja extinción. Este hecho puede deberse a la curvatura o alabeo del disco galáctico en la dirección del anticentro.

A partir de la determinación de distancias no hemos encontrado ningún agrupamiento de nuestros objetos en las regiones ocupadas por los brazos espirales predichas por los modelos actuales de estructura de la Galaxia. Nuestros objetos se distribuyen de forma exponencial, hasta distancias del orden de los 12 Kpc. Solo 8 estrellas se encuentran en distancias mayores de 15 Kpc., más allá de los límites de la Galaxia predichos por los modelos actuales. Planeamos obtener en el futuro datos de mayor calidad de esas estrellas, con el objeto de comprobar las distancias y estudiar los límites espaciales del disco galáctico.

Capitulo 4. Conclusiones.

En este trabajo hemos elaborado un catálogo de parámetros físicos fundamentales para una muestra de de 732 estrellas Be clásicas, detectadas fotométricamente por el cartografiado del plano galáctico IPHAS. Analizando la espectroscopía de seguimiento hemos determinado tipos espectrales y clases de luminosidad, temperaturas efectivas, velocidades de rotación proyectadas, extinción interestelar y

magnitudes absolutas. La combinación de los datos espectroscopios y la fotometría de IPHAS nos ha permitido determinar la emisión circunestelar del continuo, la distancia, mediante la técnica de la paralaje espectroscopia, la magnitud bolométrica y la luminosidad. Finalmente, hemos obtenido la masa de las estrellas y su edad mediante interpolación en los caminos evolutivos de Ekström et al. (2012).

Este catálogo constituye la mayor muestra de datos homogéneos para estrellas CBe compilada hasta la fecha, y representa un aumento significativo sobre el número de unas dos mil estrellas CBe conocidas hasta la fecha en la Galaxia y las Nubes de Magallanes.

Hemos utilizado los datos del catálogo para investigar cuestiones básicas relativas a la física de las estrellas CBe como clase. Hemos determinado una velocidad media de rotación del 82% de la velocidad crítica de ruptura, en buen acuerdo con otros trabajos recientes. Hemos demostrado también que no hay dependencia entre la velocidad de rotación y el tipo espectral. Nuestros datos confirman además que la distribución de velocidades en el disco sigue una ley kepleriana.

También hemos analizado la distribución de edades de la muestra. Hemos encontrado estrellas CBe de todas las edades distribuidas uniformemente entre el ZAMS y el TAMS, y unas pocas ligeramente más evolucionadas. Nuestros resultados no confirman resultados previos que proponen una interpretación evolutiva del fenómeno Be.

Finalmente hemos estudiado la distribución de las posiciones de las estrellas en el plano galáctico. Dicha distribución no presenta agrupamiento en torno a los brazos espirales que definen la estructura de la Galaxia. Por el contrario, las estrellas aparecen distribuidas en el espacio entre ellos, con algunas situadas a grandes distancias, más allá de la posición esperada del brazo de Cisne o exterior.

Acknowledgements

First of all, I would like to thank my supervisor, Juan, for trusting me and being patient since the beggining of this project, which was based mainly on his ideas and guidance. Secondly, I would like to thank Dr. Pablo Reig for trusting me and proposed me for this project. And also for various moments of scientific collaboration. A big thanks to Prof. Juan Zorec for always being there for us with his support in the BCD system and providing us the right solution at the right time.

I thank all the IPHAS collaboration, but mostly Janet and Roberto for their support all those years.

Also, Paul Groot for giving me the opportunity to make observations for the UVEX survey in INT telescope at La Palma.

Vicent Martinez for supporting economically with his project the period I didn't have a scholarship.

Alberto, Amelia, Fermando, Lluis, Lorena, Rebeca, Xusa, Sofia, Vicent P. for making me feel like home in the Observatory.

My family for making easier the difficult periods. Laura and her family for being patient the last year and making this possible. My friends Tilemachos, Georgios A., George Stamokostas, Giannis Gennarakis, Giannis Malamos and so many others for their support and scientific chats we had all those years.

The Observatory of Valencia, the university of Valencia and the "Negrito" bar.

Contents

List of Figures

List of Tables

Abbreviations

BD	**B**almer **D**iscuntinuity
BCD	**B**arbier **C**halonge **D**ivan
CBe	**C**lassical **B**e
CCD	**C**harge - **C**oupled **D**evice
EW	**E**quivalent **W**idth
FLWO	**F**red **L**aurence **W**hipple **O**bservatory
INT	**I**saac **N**ewton **T**elescope
IRAF	**I**mage **R**eduction (and) **A**nalysis **F**acility
IPHAS	**I**NT **PH**otometric **H**α **S**urvey
IPHAS DR2	**IPHAS Data R**elease **2**
ISM	**I**nter**S**tellar **M**edium
NOT	**N**ordic **O**ptical **T**elescope
SAO	**S**mithsonian **A**strophysical **O**bservatory
WFC	**W**ide **F**ield **C**amera
ZAMS	**Z**ero **A**ge **M**ain **S**equence

Physical Constants

astronomical unit	au, A	=	149597870700 m
parsec ($1au/1arcsec$)	pc	=	3.0×10^{16} m
light year	ly	=	$0.30...pc$
Speed of Light	c	=	2.9×10^{8} $\mathrm{ms}^{-\mathrm{S}}$
Solar mass	$M_\odot$	=	$1,9 \times 10^{30}$ kg
Solar bolometric luminosity	$L_{\odot,bol}$	=	3.8×10^{33} erg/s
Solar bolometric magnitude	$M_{\odot,bol}$	=	$+4.72mag$
Solar absolute magnitudes	$M_{\odot,B}, M_{\odot,V}$	=	$+5.48mag, +4.83mag$
Solar equatorial radius	$R_\odot$	=	6.9551×10^{8} m
Standard gravitational acceleration	g_N	=	9.80665 $ms^{-2} \approx \pi^2$
Solar circular velocity v_0	v_0/R_0	=	30.2 ± 0.2 $kms^{-1}kpc^{-1}$
Solar distance from Galactic center	R_0	=	8.35 kpc
Solar apparent B magnitude	$m_{B,\odot}$	=	-26.08mag
Solar apparent V magnitude	$m_{V,\odot}$	=	-26.73mag
Solar effective temperature	$T_{\odot,eff}$	=	$5780K$
ABsolute monochromatic magnitude	AB	=	$-2.5log_{10}f_\nu + 8.90$ (for f_ν in $Wm^{-2}Hz^{-1}$)
Galactic diameter	G_D	=	31–55 kpc
Galactic stellar population	N_{star}	=	$2.5 \times 10^{11} \pm 1.5 \times 10^{11}$
Oldest known star		=	≥ 13.7 Gyr
Wien's law constant	I_pT	=	$2.8 \times 10^{7} \mathring{A}K$

To science . . .

Chapter 1

Introduction

Classical Be (CBe) stars are main sequence O, B and early A-type stars whose spectra show -or have shown- Balmer and other lines in emission. They are characterised by excess continuum emission in the ultraviolet, optical and infrared spectral ranges. Both the line and continuum emission arise from recombination processes in a hot, dense circumstellar decretion disk. The formation of these disks is not yet completely understood, although fast rotation, nonradial pulsations and magnetic fields are believed to be at their origin. A recent review of the nature of CBe stars and their main characteristics is presented by Rivinius et al. (2013).

It has been proposed that the Be-phenomenon is an evolutionary effect which appears during the second half of a B star main sequence lifetime (Fabregat & Torrejón, 2000). Zorec et al. (2005) found a similar result for late-type CBe stars, but propose that early-type CBe stars appear mainly in the first half of the main sequence. However, Martayan et al. (2007) found a significant number of CBe stars at the ZAMS, rotating faster than young B stars in general. This would imply that the CBe nature is innate, and not an acquired characteristic of a fraction of B stars. In the recent literature many other authors have addressed these issues with different, often contradictory, conclusions.

Be stars are $\approx 20\%$ of the total population of B-type stars (Zorec & Briot, 1997). The total known population of Be stars are about 2000, Galactic and in the Magellanic clouds (Neiner et al., 2011). In this work we raise this number by almost 40%, presenting not only the identification of 732 Galactic CBe stars, but a complete catalogue with their stellar parameters and statistics from their properties.

CBe stars, mainly those of the earlier types, are short lived objects which in general have had relatively little time to move far away from their birthplaces. Being main sequence or slightly evolved stars, they are unlikely to be embedded in their

parental clouds. In addition, they are intrinsically bright, with absolute magnitudes ranging from ~ 0 to ~ -4, enabling their detection across the whole Galactic Plane, at least in regions not affected by heavy interstellar absorption. As such, they are tracers relevant to the investigation of the spiral structure of the Galaxy. The INT Photometric Hα Survey of the Northern Galactic Plane (IPHAS, Drew et al. 2005; Barentsen et al. 2014) is a 1800 deg^2 imaging survey covering the entire northern Milky Way at $\mid b \mid < 5^o$ in the r, i and Hα filters, using the Wide Field Camera (WFC) on the 2.5-metre Isaac Newton Telescope (INT) in La Palma. A first list of objects displaying Hα emission was presented by Witham et al. (2008). Most of them, at $r < 17mag.$, have been followed up spectroscopically from 2005 to 2012, leading to a database of low resolution spectra of 2627 objects. Preliminary analysis reveals that about 70% of this sample are CBe stars.

The general aim of this work is to obtain the fundamental physical parameters of the newly uncovered population of IPHAS CBe stars, which significantly increases the number of these objects known in the Galaxy. In addition, we aim to use this sample to contribute to the investigation of the spiral structure of the Galaxy in the Northern Hemisphere, using them as tracers and the standard techniques of spectroscopic parallax to measure their distances. These sources will likely obtain accurate trigonometric parallaxes from Gaia in the near future. Therefore, their proper characterisation would also aid their future exploitation for more detailed studies of Galactic structure with Gaia data.

To deal with such a large set of spectra we have developed a semi-automatic procedure to obtain the relevant physical parameters of the CBe stars, including the spectral type and luminosity class, effective temperature, interstellar extinction and absolute magnitude. We have used for this purpose the techniques and calibrations of the BCD (Barbier-Chalonge-Divan) spectrophotometric system (Barbier & Chalonge 1941; Chalonge & Divan 1952).

The Spectral types vary in all sub-types of B and the majority of luminosity classes are found as V-IV and the distances from $\sim 1.4 - 12$ Kpc, with some exeptions.

1.1 INT Photometric Hα Survey

The Hα spectral line (6562.8 Å) comes from the transision of the electron, at the hydrogen atom, of the excited state $n = 3$ to $n = 2$. It is the first of the Balmer line series, in which, if they are in emission, all the transisions end to the $n = 2$ atomic energy state. The energy to ionize a hydrogen atom is at the same order

of magnitude as it does to excite the atom's electron to the n = 3 energy state. In fact, it is very rare for an electron to be excited to this energy state without being removed from the atom. Once an atom is ionized, the nucleus and removed electron can recombine to form a new atom with the electron typically in a higher energy state. This electron will then cascade back to the ground state, a process which produces Hα emission and other Balmer lines about half of the time. Thus, observing Hα emission in a region indicates that hydrogen is being ionized there. Major astronomical objects that can have the Hα emission line at their spectrum are: compact planetary and symbiotic nebulae; rapidly evolving post-AGB stars, Be stars of all types (including young Herbig stars, and B[e] supergiants), lower mass young stellar objects and dMe stars, a range of interacting binary stars (symbiotics, 'supersoft' compact binaries, WD/NS/BH accreting binaries generally), H-rich white dwarfs, large numbers of near-main-sequence A stars and M giants. At this work we are working exclusively with Be stars.

In the begining of the IPHAS survey, the existing catalogues of emission-line objects were not bigger than few hundred sources. The recent years technological advance, i.e. large area CCD-mosaic detectors, allowed to produce large surveys and at the same time the quality of the data has totally changed the statistics of stellar evolutionary study. The Isaac Newton Telescope Photometric Hα Survey (IPHAS) (www.ipha.org), of the Northern Galactic plane, is a programme that began taking data with the INT Wide Field Camera (WFC) in August of 2003 (more inforamtion about the INT/WFC can be found at the webpage:http://www.ing.iac.es/astronomy/instruments/wfc/) . IPHAS has surveyed the entire northern Galactic in the latitude range $-5^o < b < +5^o$: a sky area of 1800 deg^2. which targets to discover emission-line objects. Actually, since the begginng of IPHAS till now the population of known emission line objects grew, due to the survey, by more than an order of magnitude.
The INT Wide Field Camera (WFC) offers a pixel scale of 0.33 arcsec, allowing on-sky structures above 1 arcsec in size to be resolved. The magnitude range for point sources is $13 \leq r', i'$,H$\alpha \leq 21$.

The Sloan filters have been preferred over Harris alternatives because of their squarer transmision profiles. The Sloan r' filter is the most blue sensitive of the three (central wavelength 6240 Å), with the Hα filter positioned towards the red end of its bandpass (central wavelength 6568 Å). With an FWHM transmission of 95Å, the Hα filter is more than broad enough to capture all likely Doppler shifts due to Galactic motions of up to a few hundred kms^{-1} or $\sim$ 10 Å due to the

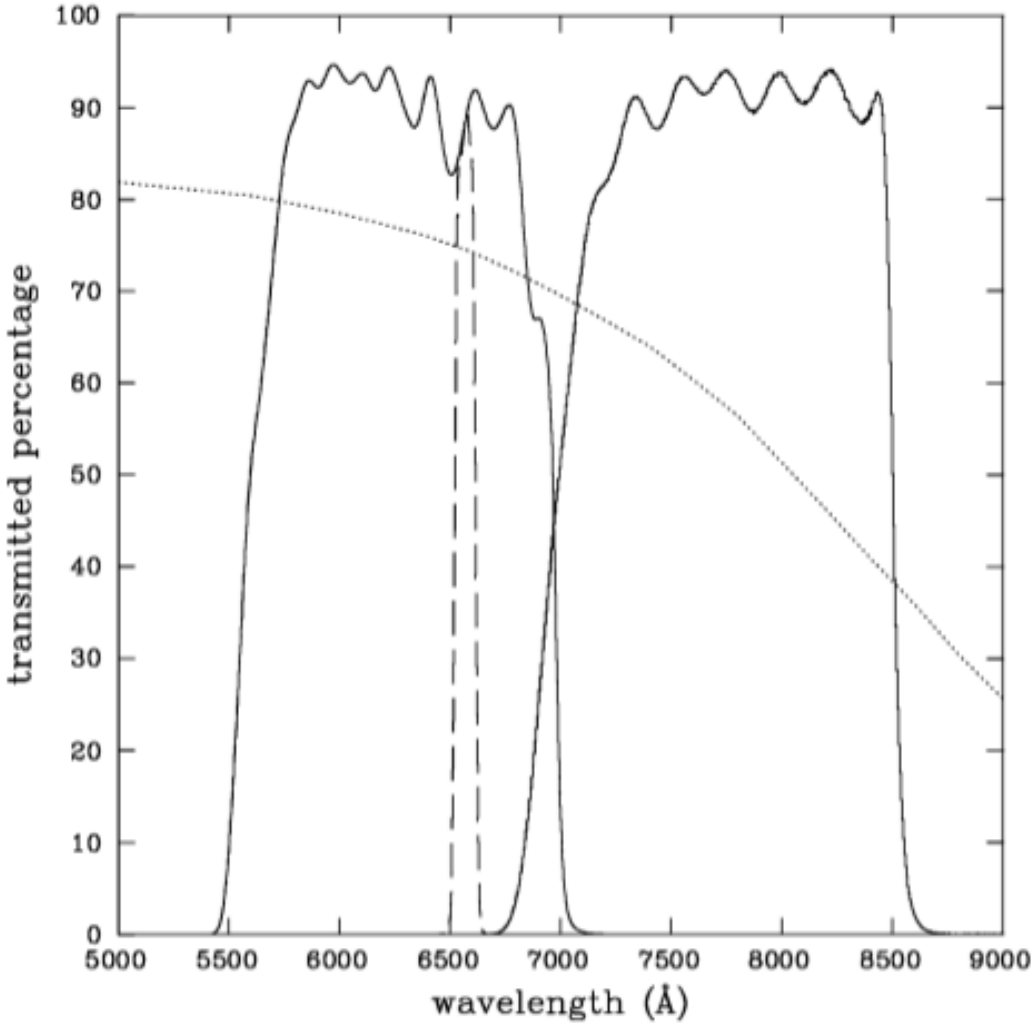

FIGURE 1.1: The transmission profiles of the Hα, Sloan r' and i' filters used in all IPHAS observations. The r' and i' filter profiles are plotted as solid lines, whilst the Hα profile is shown dashed. The dotted line is the mean WFC CCD response at the cooled working temperature. (figure from Drew et al. (2005).)

converging beam of the INT/WFC. The central wavelength of the Sloan i' filter is 7743 Å. The survey has two broad-band filters in order to give a continuum-dominated colour with which the (r'-Hα) excess measurement can be compared. It has been shown in the past (Robertson & Jordan, 1989) that this is importand for distinguishing between a genuine Hα emission excess and a molecular band dominated late-type stellar spectrum: in such cases, large (r' - Hα) 'colour' will correlate with relatively extreme ($r' - i'$). More information of the strategy can be found on the description of the IPHAS survey (Drew et al., 2005) in Section 3. The exposure times in the three filters were set at 120 s (Hα), 30 s (r') and 10 s (i').

1.1.1 Spectroscopic follow-up

IPHAS has had several spectroscopic follow-up runs since its first campaing. Besides the large follow ups, the collaboration runned smaller spectroscopic observations for first exploration of the bright sources. The survey chiefly targets emission line point sources, but is also sensitive to (resolved) emission from low-surface-brightness planetary nebulae (PNe). These can be detected out to large galactocentric radii, their radial velocities can constrain mass models for our Galaxy, while nebular line analysis will reveal the abundance distribution and ISM enrichment. Another key issue is the evolution of massive stars. Our observational knowledge of the post-main sequence evolution of massive stars such as luminous blue variables (LBVs), extreme B[e] objects and hyper-giants is based on a rather sparse collection of such objects. The IPHAS survey can pick up such objects anywhere in the Galaxy even through high extinction since their absolute magnitudes range from -6 to -10. The large sample of early-type emission line objects coming out of the follow-up was expected to allow us to map out the Galactic structure, in particular beyond the solar circle. Similarly, the survey detect many Wolf-Rayet stars, for which no systematic Northern Hemisphere survey has been performed for decades.

The high luminosity and low surface gravities in (post)-AGB stars consistently lead to the production of photospheric Hα emission. With IPHAS, we were able to get good samples of both dusty and dust-free stars and thus their overall core mass distribution. In addition to these objects representing post-MS evolution, Hα emission also picks up the chromospherically active MS stars as well as young pre-MS objects.

Many of the currently known accreting binaries have been discovered through their optical variability (outbursts) or via their X-ray emission. Large differences between the observed populations of CVs, X-ray binaries and symbiotics compared to the predictions of binary population synthesis models strongly suggest that severe observational selection effects are at play, and the majority of these populations still lie undetected. Hα emission is a key common characteristic of practically all interacting binaries. IPHAS will permit quantitative tests of our binary evolution models and a better (and complementary) understanding of the existing variability/X-ray selection effects. Key populations include the large number of expected short period CVs Witham et al. (2006), high-mass accretion rate white dwarf binaries as potential Type Ia progenitors and neutron star/black hole binaries.

Although focusing on emission line objects, the survey also has uncovered populations of non-emitting systems that are nonetheless very interesting. Examples include the search for extremely late-type stars, instrinsically red objects and single white dwarfs and related systems.
With the imaging part of the survey finished, as well as an efficient reduction pipeline that is delivering source catalogs with magnitudes, a spectroscopic follow-up strategy formed the next crucial stage of the project. IPHAS large collaboration has access to a wide range of facilities. Thus, the aim was to use a multi-telescope and multi-instrument approach to share the resources and optimise the scientific return for the international team and the community (time has been awarded on several facilities).
Fiber-feb multi-object spectrographs such as HectoSpec were essential for a thorough follow- up strategy. However, having objects with a bright and clear Hα emission line, we do definitely wanted spectroscopic identifications for them since they cover a large area on the sky. To obtain these identifications it was most efficient to use long-slit spectrographs on small to medium sized telescopes, such as the 1.5m+FAST on the Fred Lawrence Whipple Observatory (FLWO). The Fred Lawrence Whipple Observatory is an astronomical observatory owned and operated by the Smithsonian Astrophysical Observatory (SAO) and is their largest field installation outside of their main site in Cambridge, Massachusetts. It is located near Amado, Arizona on the slopes of Mount Hopkins, USA.

The IPHAS colaboration requested to use the 1.5m+FAST combination to obtain spectroscopic identification of Hα emission line sources with $r' < 16$. The request was low-resolution spectroscopy to be used for classification. The 1.5m+FAST was an ideal combination for this sample, due to its flexible nature. Since these observations are not time or weather critical they are ideal 'filler' observations and had been done at all times posible. This program was started in 2005 A, when the first batch of targets was observed. The data are of excellent quality and revealed a large number of emission line stars including a few binaries. Bright early-type emission line objects make up the largest fraction of this sample. Since these closely track star formation, they can be used to study Galactic structure all the way along the plane since they are intrinsically bright and high quality spectroscopic follow-up is straightforward. The selections efficiency was very high with over 90% of selected targets being true emission line objects.
The 300 grating was a standard set-up to cover the wavelength region 3500- 7500 Å. Based on the observations the set-up was obtaining a S/N=25 on a r'=16 mag

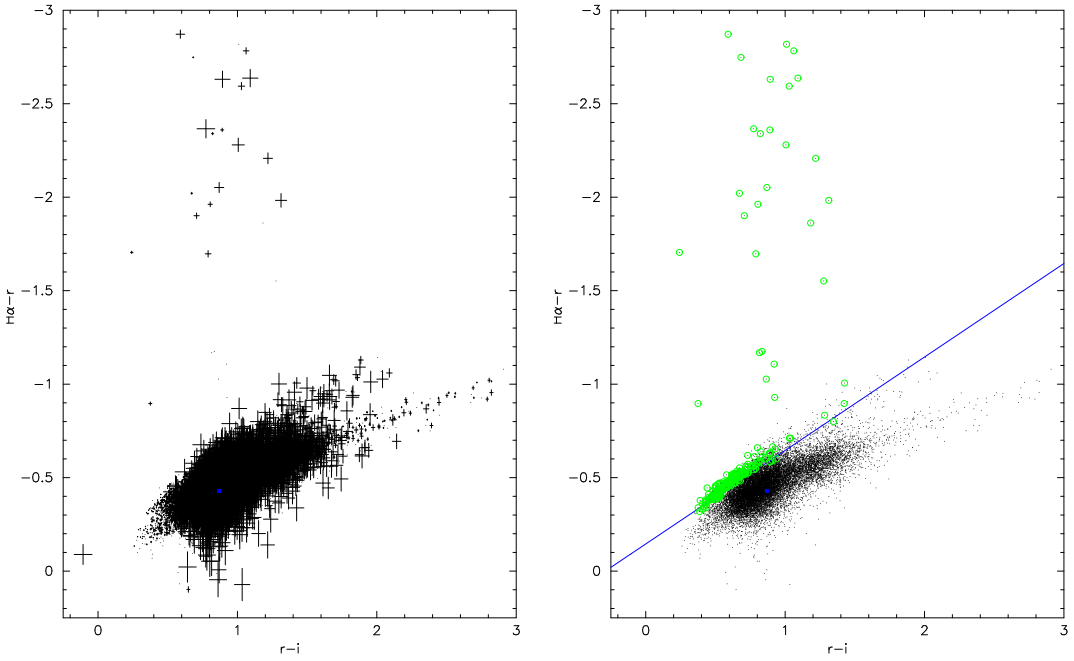

FIGURE 1.2: a) Typical $r - i$ versus Hα $- r$ color-color plot derived from one INT WFC field including error-bars (44,347 sources). b) Example of a color-color selection criterion (line). Objects lying significantly away from the main-sequence distribution are marked by circles if their color and photometric accuracy satisfy a sigma-clipping requirement. This project targets the very small fraction of targets that are bright and have strong strong Hα excess.

star in 10 minutes exposures. Including 5 minutes overhead per object for telescope pointing, CCD read-out etc. FAST's optics are primarily reflective, are adequately sized to prevent vignetting, and use high-performance coatings. The high measured system peak efficiency of 26% (fraction of light incident on the primary detected at the CCD) demonstrates that the throughput of reflective optics can be quite competitive with that of refractive optics. FAST's structure is constructed from graphite-epoxy composite panels, which have an excellent stiffness-to-weight ratio and low thermal expansion, resulting in low flexure and excellent focus stability.

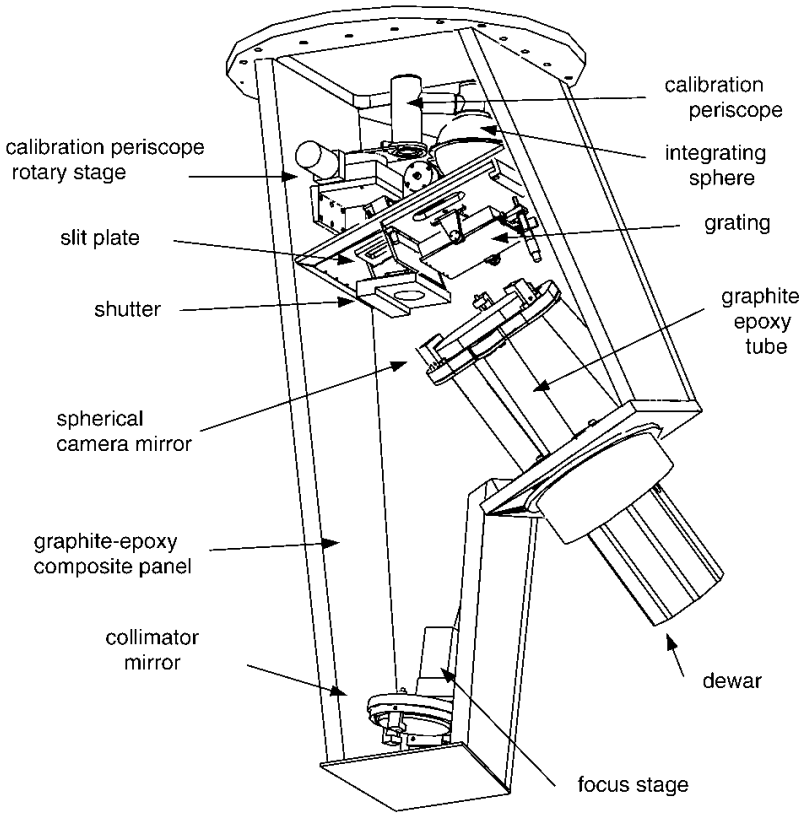

FIGURE 1.3: FAST spectrograph with its access hatch removed. The calibration periscope is shown in the calibration position where it conducts light from the integrating sphere to the focal plane. The Schmidt corrector plate is hidden behind the spherical camera mirror. The fold mirror (also hidden) is mounted on the flat plate that supports the dewar. (Fabricant et al., 1998).

1.2 Classical Be stars

1.2.1 The Classical Be stars

Classical Be (CBe) stars are O-B and early A-type stars which have Balmer Hydrogen and other lines in emission, or they had in the past. B refers to the spectral type and letter "e" (emission) that has emission lines. Most of the times we observe also spectral emission lines of other neutral or ionized atoms, in the spectum of the source, but usualy weaker. Other typical observational characteristics are that they show linear polarization in the optical spectrum and emission in the infrared, that is stronger than in other B-type stars. We also know that B-type stars may evolve to Be stars (meaning that, at some moment of their life may show emission lines). The majority of the Be star population is in the main sequence. The first observed Be star is Gamma Cassiopeia, which was observed by Angelo Secchi in 1866, and was also the first star which has been observed with emission lines.

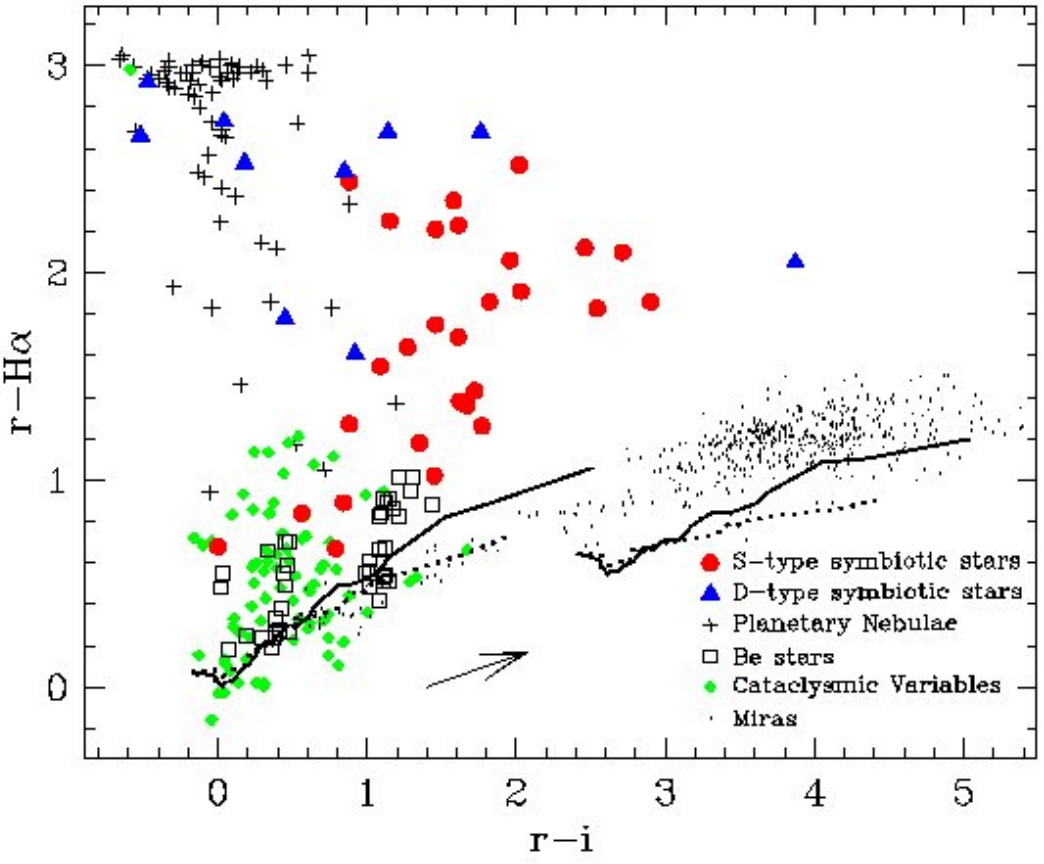

FIGURE 1.4: This figure is a schematic representation of the (r-Hα, $r-i$) colour-colour plane that IPHAS data define. The points plotted are the IPHAS colours of already-known objects falling into the object classes specified in the key. The main stellar locus, occupied by the great majority of normal stars, is located in between the synthetic tracks drawn in black, corresponding to unreddened (left) and reddened ($E(B-V)$ = 4, right) main sequences. The dotted tracks crossing this area are the unreddened and $E(B-V)$=4 giant-star sequences. The figure is from (Corradi et al., 2008). A discussion of the properties of the colour-colour plane, IPHAS survey methodology and sample data, was presented in (Drew et al., 2005).

However, at the time, they couldn't understand what the spectral lines mean. At the begining of the 20th century with the revolution of quantum mechanics, it became clear the nature of the spectral lines. However, it was not before the 50's that the understanding of the Be emission lines rise from a circumstellar disk envelope. All the observational evidence and theoritical knowledge can be explained if we consider the star with a circumstellar disk made by gas in its equatorial plane. The disk is made by matter ejected from the star. High-resolution data, found the disk to be Keplerian Meilland et al. (2012). The polarization and the infrared flux comes from the scattering of the radiation of the star in the matter of the disk, and the emission lines comes from absorption of ultraviolet radiation on the matter of the disk, which is re-emitted. We know in general that Be stars are fast rotators (Confirmed as well from interferometric observations), some of

them reach the speeds of almost 100% of the speed needed for a star to fall apart. However, The rotational velocity itself can not form the disk alone. We need also an additional mechanism of ejecting matter from the star, i.e. a strong magnetic field or non-radial star pulsations.
Gravity darkening, affects the determination of the rotational velocity $vsini$, because the most rapidly rotating part of the star is becoming inconspicuous. Recent interferometric results corroborate this effect, (van Belle, 2012) notes that \actual oblateness values are always well in excess of the simple predictions from $vsini$\. This has effectively reopened the discussion of how close Be stars rotate to the critical limit, and given rise to codes explicitly taking it into account, like FASTROT by Frémat et al. (2005), or CHARRON by Domiciano de Souza et al. (2012).

In the literature we can find the observational techniques tha specifies the observational parameters we have about these objects. Stee et al. (2005) reviewed the methods and techniques of interferometric observations of hot star disks with application to Be and B[e] stars. In the optical region, Tycner et al. (2005) and Tycner et al. (2006) carried out narrow-band Hα interferometry using the Navy Prototype Optical Interferometer (NPOI) and found the intensity distribution in the envelopes for gamma Cas and phi Per, and a relationship between Hα emission and linear size of emission-line forming region for eta Tau and beta CMi. They attributed this relationship to the large optical thickness of Hα radiation. Grundstrom & Gies (2006) calculated numerical model of disks for the Ha emission line, and found that the Hα disk radii as theoretically predicted are consistent with Hα interferometric observations. In the infrared spectral regions, varius types of long baseline interferometers and interferometric array systems were used. Gies & Bagnuolo (2007) in K band and Kervella & Domiciano de Souza (2006) carried out interferometric observations of the Be stars Alpha Arae in the N band at VLT, and derived the upper limits of the envelope size to be approximately 4 mas, corresponding to 14 stellar radius. The formation and dissipation of the envelopes of Be stars are considered by Meilland et al. (2006) and Rivinius (2005). Meilland et al. suggested two scenarios: one is the successive outbursts of central stars to form disks and rings, and the other is the slowly decreasing mass loss until the disks vanish. Rivinius considered the lifecycles of classical Be stars, similar to the successive outburst scenario of Meilland. If not replenished by subsequent outbursts, the ring will finally dissipate and Be stars will become B star.
Neiner & Hubert (2005) reviewed the indirect and direct methods of magnetic fields detection based on oblique rotator models. Rotational modulation of spectral lines and X-ray fluxes provide a promising method. Smith & Balona (2006)

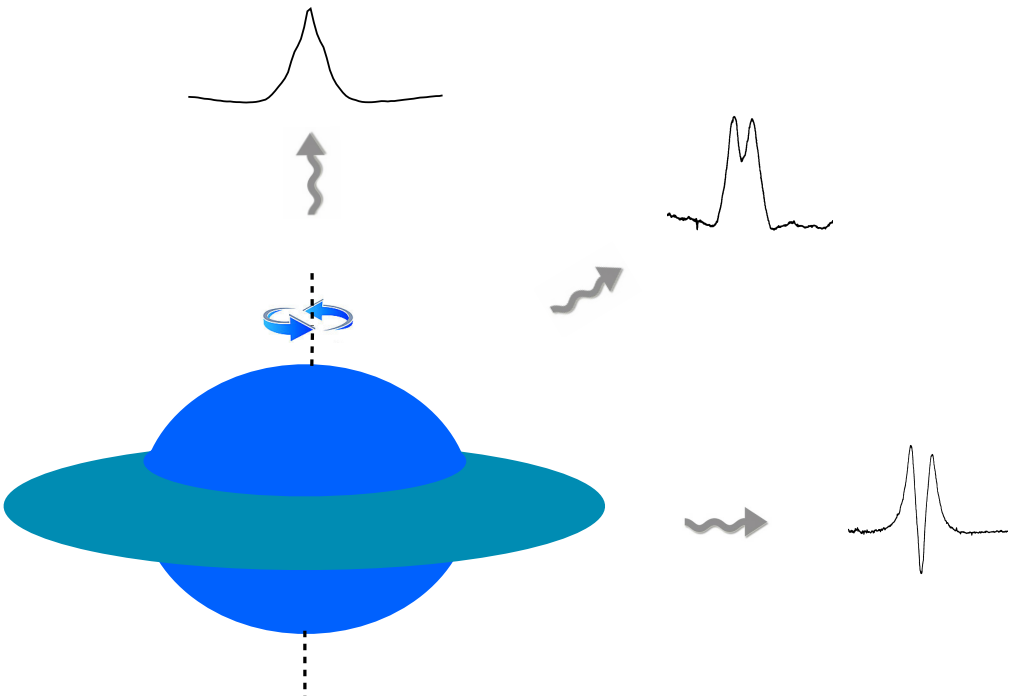

FIGURE 1.5: Schematic view of a Be star. With example of spectral profiles from pole-on to shell Be stars .

suggested the existence of strong magnetic fields on the surface of Be stars by analyzing short-term variabilities in B, V bands, line emissions, and X-ray fluxes. Several theoritical models for magnetic winds and disks are proposed, generally based on the oblique rotator scheme with dipole-like magnetic fields ,(Brown & Cassinelli (2005), Maheswaran (2005), ud-Doula & Blondin (2005)). Cassinelli & Neiner (2005) presented a broad discussion on the origin and dissipation of magnetic fields in Be stars. On the origin, two possible mechanisms were proposed: one is the dynamo action in the convection core and its transportation to the surface and envelope, and the other is that the fossil fields remained from the initial stage of star formation.

1.2.2 The BeSS database

The Be Star Spectra (BeSS) database was created a few years ago to have centralized information on all known Be stars via an up-to-date catalog (http://basebe.obspm.fr/basebe/). BeSS was based mostly in the old Be star catalog of Jaschek & Egret

(1982) and all the new CBe stars that were regularly being discovered since then. The total population of the known Be stars in the catalog are 2265 galactic, Small and Large Magelanic clouds, with more than 123000 spectra of professional and amateur observers of various spectral targets. The catalog and its funcions are explained in Neiner et al. (2011).

1.3 The BCD classification system

The BCD (Barbier-Chalonge-Divan) classification system was developed first by Barbier and Chalonge (1941), and later by Chalonge and Divan (1952). The system is based upon measurable parameters around the Balmer discontinuity (BD) (3200-4600Å). The basic parameters that describe the energy destribution around BD are: D, the Balmer jump depth, given in dex, which is an effective temperature indicator. λ_1, the average position of the Balmer discontinuity, given as the difference $\lambda_1 - 3700$ Å, which is very sensitive to log g, Φ_b, the color gradient which can be written as a function of the $(B-V)$ color of the UBV photometric system (Moujtahid et al., 1998). The BD is a well visible spectral characteristic for stars ranging from early O to late F spectral types. The advantages of the system, compared to other spectroscopic systems, are well described by Zorec et al. (2009). However, in this section we are going to make an overview to the BCD parameters and the calibrations of the system since we are based on its full formalization to develop our automatic program.

1.3.1 The BCD parameters

The parameters D and λ_1 were first introduced in Barbier & Chalonge (1939b) and Barbier & Chalonge (1939a). In their works they show the conection of the different spectral types with their first calibration (Barbier and Chalonge, 1940). The first calibration scheme with (D, λ_1) came in Chalonge & Divan 1952 but for our work we used the calibration scheme of Zorec et al. (2009) which also includes the B supergiants luminosity class, that is missing from previus works. Φ_b, which is the continium gradient at $4000-4600$Å, was introduced in 1955 in the BCD system to distinguish F-type stars from B-type stars having the same (D, λ_1) pairs. This parameter also has been used as a third BCD quantity related to the metal abundance of late type stars, in particular to the abundance ratio $[Fe/H]$

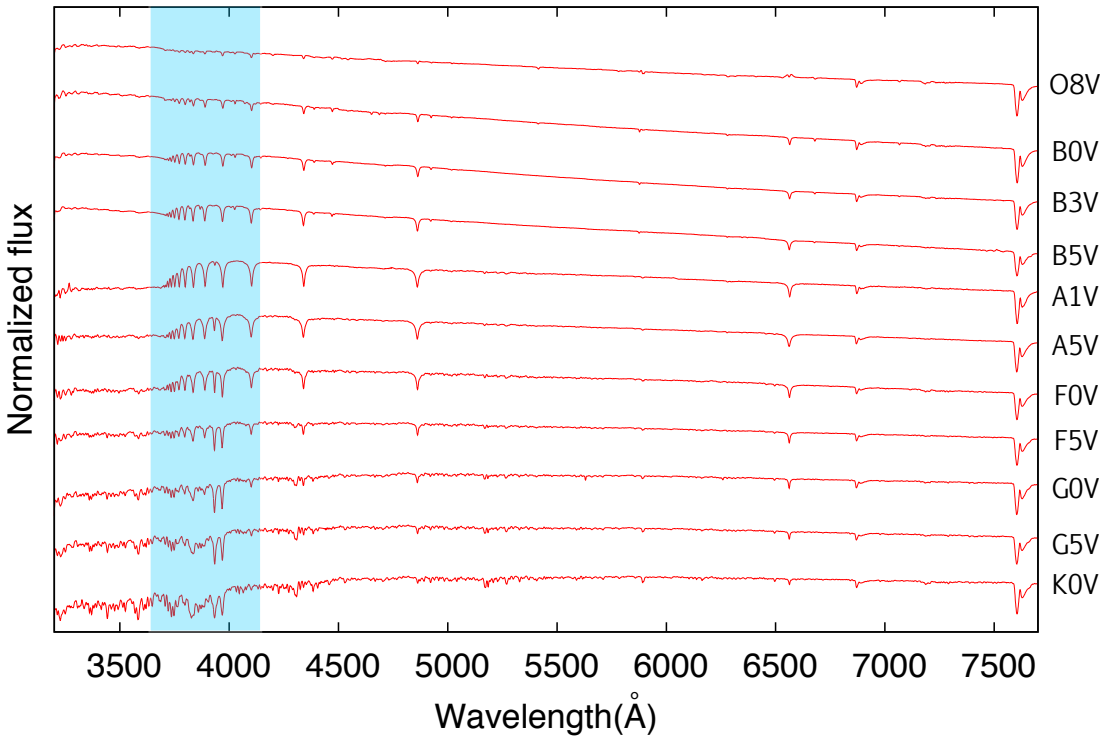

FIGURE 1.6: The Balmer disconinuity across the different spectra types.

(Chalonge & Divan, 1977). For our work we are going to use Φ_b to calculate the color excess as the relation in the BCD and UBV systems due to the ISM reddening (Chalonge & Divan, 1973):

$$A_\nu = 3.1E(B-V) = 1.7(\Phi_{rb} - \Phi^0_{rb}) = 2.1(\Phi_b - \Phi^0_b)mag \tag{1.1}$$

where Φ_{rb} is the continium gradient at $4000-4800$Å, Φ_{uv} at $3500-3700$Å and Φ^0_{rb} is the stellar intrinsic color gradient from calibration defined at Chalonge (1975) and the coeficient 2.1 redefined from 1.9 by Aidelman et al. (2012). It is also possible to estimate the absolute magnitude in V band from the (D,λ_1) parameters as defined from the calibration that had been done in Zorec & Briot (1991).

The value of D is calculated at $\lambda \simeq 3700$Å, as D= $log_{10}F_{3700^+}/F_{3700^-}$, where F_{3700^+} is the Paschen side of the flux and F_{3700^-} is the flux on the ultra violet continuum, Φ_{uv}. To obtain F_{3700^+} we extrapolate the Paschen side continuum up to $\lambda = 3700$Å, for which a relation such as $logF_\lambda/B_\lambda = p \times (1/\lambda) + q$ were B_λ can be the flux of a comparison star or the Planck function of a higher effective

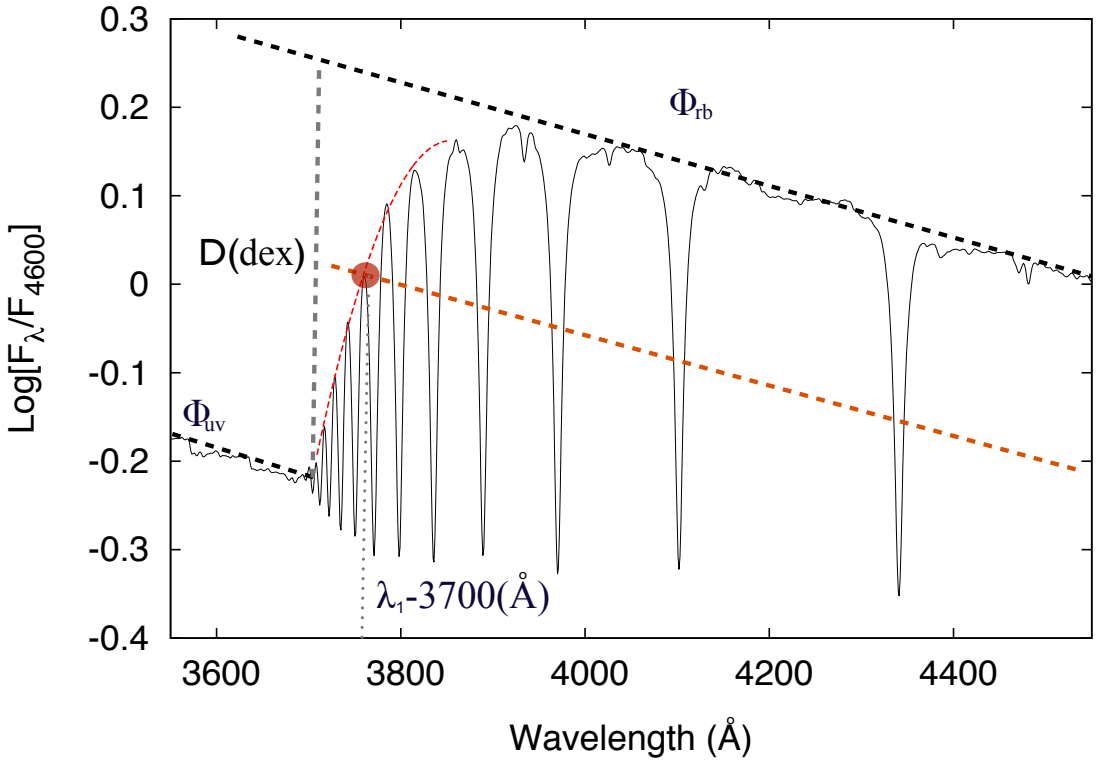

FIGURE 1.7: Explanation of the BCD(D,λ_1, $\Phi_r b$, Φ_{uv}) parameters for non-emission line stars.

temperature than that expected for the studied star. In our procedure we adopted the Planck fuction as advised in Zorec et al. 2009, so that D is:

$$D = \log[\frac{F_{3700^+}/B_{3700}}{F_{3700^-}/B_{3700}}]dex. \tag{1.2}$$

For the average spectral position of the BD we use the point of intersection between the curve continuum of the spectrum and the average of the two continuum fluxes. To calculate the line that represents the average of the fluxes (Φ_{rb} and Φ_{uv} is determined by the points $logF_\lambda - D/2$, for the Paschen side with $\lambda = 4000, 4150, 4300$Å and $)logF_{3700} + D/2$ for the UV side.)

Φ_b ,which is the flux gradient for $\lambda = 4000 - 4600$Å, was introduced first in 1955 to distinguish B-type from F-type stars with the same (D, λ_1) pairs. In present the work we use Φ_b to calculate the Paschen gradient and to estimate ISM reddening as we show in equation (1). To obtain color gradients we worked as it is defined from (Allen 1976):

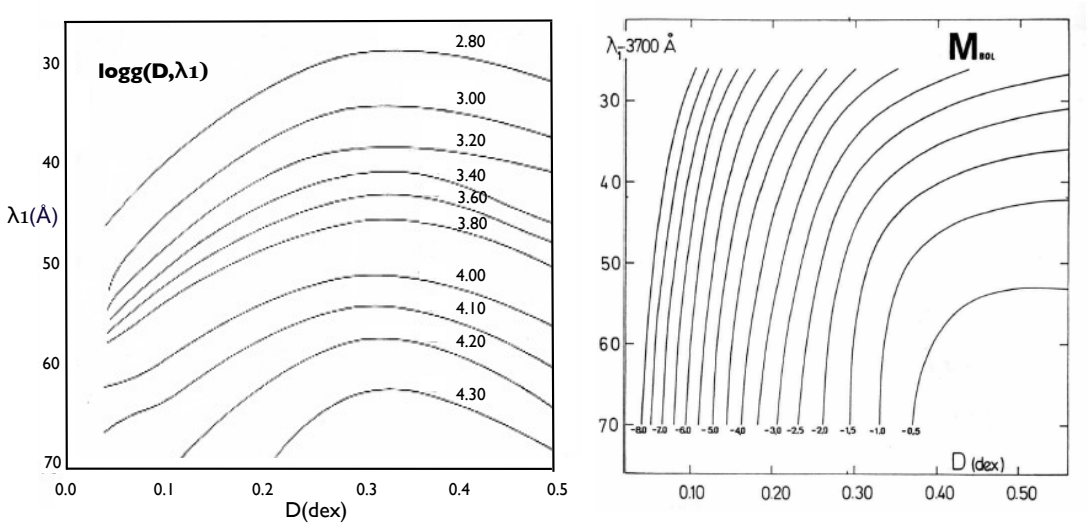

FIGURE 1.8: Calibrations from Zorec (1986) conecting the (D,λ_1) pair parameters with the bolometric absolute magnitude and log g.

$$\Phi = 5\lambda - \frac{dlnF_\lambda}{d(1/\lambda)} \tag{1.3}$$

Which for a black body at temperature T, becomes:

$$\Phi(T) = (C_2/T)(1 - e^{-c_2/\lambda T}), \tag{1.4}$$

And finally for the energy range at $\lambda = 4000 - 4600$Å we have:

$$\Phi_b = 2.144 - 7.064(\log F_{0.4} - \log F_{0.46}). \tag{1.5}$$

The Φ_b^0, which is the intrinsic color gradient for a specific pair of (D,λ_1) parameters, we extract it from Chalonge and Divan (1975).

1.3.2 The BCD system for emission line stars

BCD system, to determine the Balmer discontinuity depth is, however, in general not applicable to CBe stars. Due to the lower pressure of the circumstellar disc, a second Balmer jump exists for these objects in the ultraviolet region of the spectrum, which is either in emission or absorption (Kaiser, 1989). In that case, we extract the flux at F_{3700-} as the point where the bottom of the higher order Balmer line series merges into the continuum.

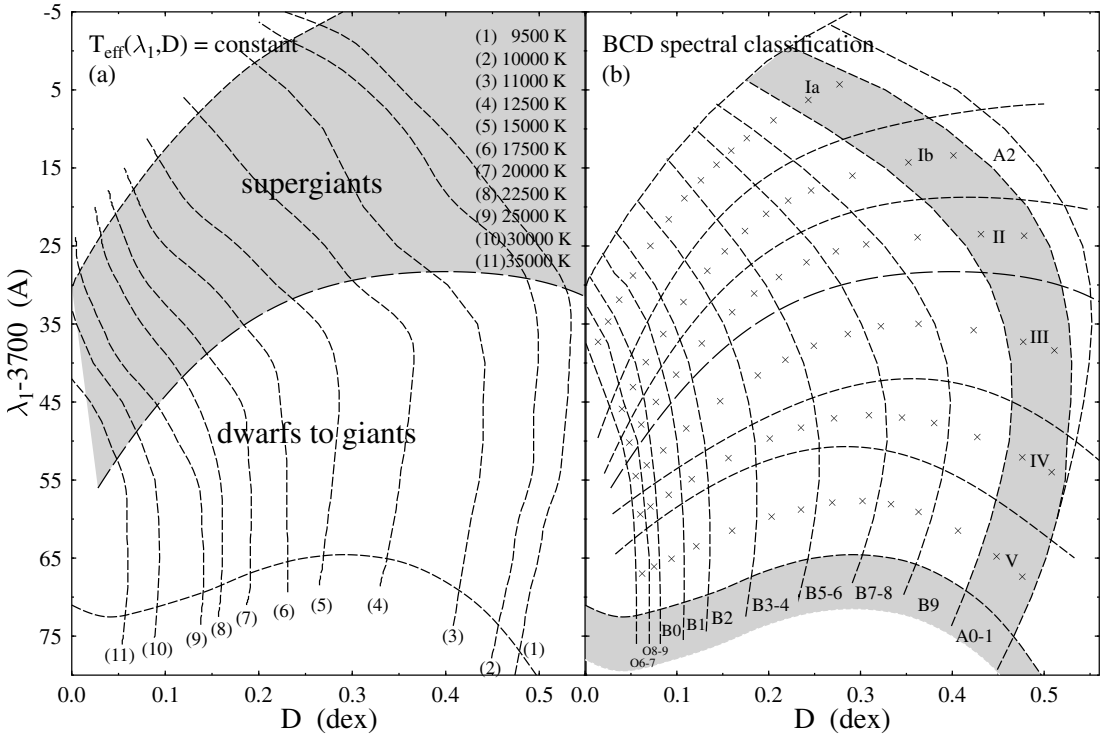

FIGURE 1.9: Figure from (Zorec et al. 2009). a): spline-smoothed $T_{eff}(\lambda_1, D) = const.$ curves for the values of effective temperature given in the box at right-top; b) the curvilinear- quadrilateral $BCD(\lambda_1,\ D)$ spectral classification diagram, where the corresponding 2D MK spectral types (bottom shaded strip) and the luminosity classes (left shaded strip) are indicated. The crossmarks indicate the mid-point of each MK spectral type-luminosity class box where the $T_{eff}(\lambda_1, D)$ values given in Table 3 of (Zorec et al. 2009).

In Fig. 1.10(b) we illustrate this last procedure. To obtain the flux at F_{3700^-} , instead of using the extrapolated Balmer continuum Φ_{uv}, we extrapolate the line traced through the bottom of the higher Balmer lines, which is labeled $\Phi_{Balmerlines}$. In the case of non emission-line stars, both methods lead to the same D values, as shown in Figs. 1.10(a) and 2.10, and in columns 6 and 7 of Table 2.2. The mean of the residuals between the two different measurement procedures is 0.010 ± 0.007 dex, significantly smaller than the characteristic error of 0.015 dex associated to the measure of the D parameter in the BCD system.

In the case of CBe stars, the value of D obtained in this way is the true photospheric value (from now on we are going to symbolise the photospheric value of the BD as D_*) , is not affected by circumstellar emission or absorption in the Balmer and Paschen continua. The validity of this statement is fundamental for the applicability of the BCD system to the determination of the physical parameters of CBe stars.

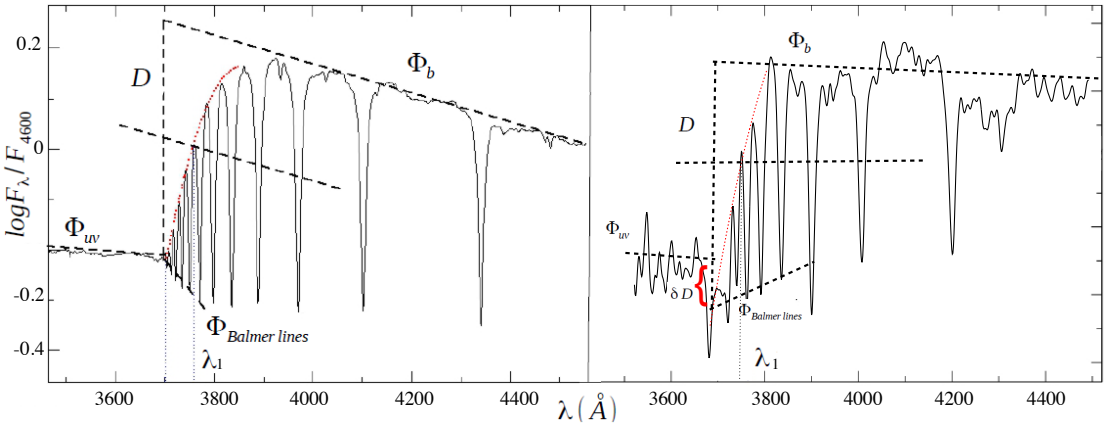

FIGURE 1.10: a) Graphical explanation of the BCD($D, \lambda_1, \Phi_b, \Phi_{uv}$) parameters in the spectrum of the B9.5V star HR4468; (b) determination of the BCD parameters of the emission line star IPHAS J193420.54+262349.9, with B4Ve spectral type. $\Phi_{Balmerlines}$is the line connecting the bottom of the higher Balmer lines, and δ_D is the difference between the values of D obtained from $\Phi_{Balmerlines}$ and Φ_{uv}.

No changes have been detected in the value of the first component of the BD (D_*) within the limits of uncertainties that characterize the BCD system ($0.015dex$ in D and $1-2$Å in λ_1). This has been proved, in particular, in some iconic CBe stars in the Northern Hemisphere as X Per (O9.5Ve, HD 24534), Pleione (B8IV-Ve, HD 23862), ζ Tau (B2IIIe, HD 37202), 48 Lib (B3-4IVe, HD 142983), 88 Her (B6IVe, HD 162732), χ Oph (B0Ve, HD 148184), 59 Cyg (B1Ve, HD 200120) (De Loore et al. (1979); Divan et al. (1983); Zorec (1986); Zorec et al. (1989); Divan & Zorec (1982)b,a; Zorec & Briot (1991)), but also in some frequently observed CBe stars in the South hemisphere, in particular α Eri (B5III3, HD 10144) (Vinicius et al. (2006); Cochetti et al. (2013)). The constancy of D_* has also been proved in stars that underwent Be⇌B⇌Be-shell-phase changes as γ Cas, Pleione, 88 Her and 59 Cyg. A more detailed description is also given at Gkouvelis et al. (2016)

1.3.3 The BCD calibrations

The BCD system has developed various calibrations over the years up to now. Effective temperature, log g, bolometric and V-band absolute magnitudes are among the calibrations we based our analysis procedure. At figure 1.9 it is shown the calibrations of the pair parameters D, λ_1 with effective temperature and spectral classification. It is important to note at this point that the BCD system follows the arithmetic order of the MK classification system for reasons of convenience.

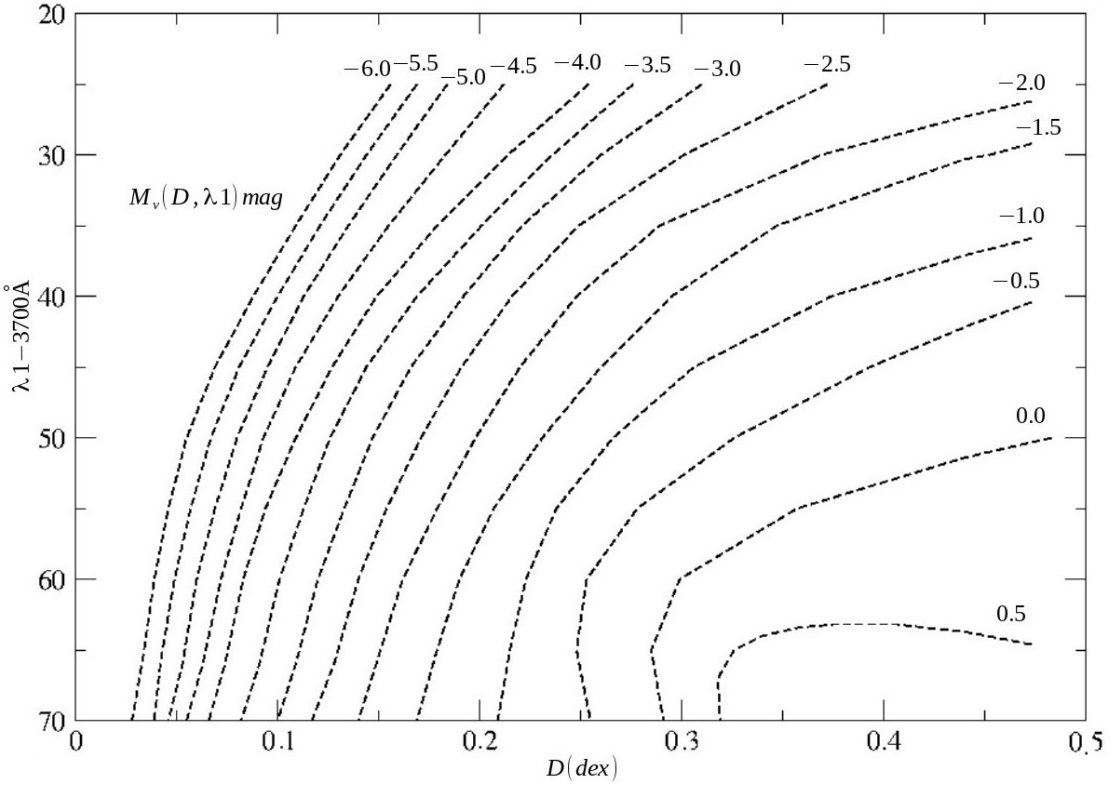

FIGURE 1.11: Calibration from (Zorec 1991) conecting the (D,λ_1) pair parameters for B-type stars with the absolute magnitude in V band.

The classification it is not have to agree in exact. The typical difference between BCD and MK systems are of the order of one sub-type.

For the estimations of the bolometric absolute magnitude we follow the works of Divan & Zorec (1982), Zorec (1986) and the absolute magnitude in V band from Zorec & Briot (1991) displayed in Fig. 1.11.

1.4 Scientific objective

Our scientific objective was to make adavantage of the IPHAS spectroscopic follow-up of the emission line objects. From their analysis we extracted the CBe star spectra. We wanted to give a catalogue of those objects in the depth of $V = 13-16$ mag and obtain their physical parameters and study statisticaly their properties and evolutionary status. Finaly, since our catalogue is distributed in the whole North Galactic Plane we wanted to use CBe stars as tracers of the Galactic spiral structure.

In chapter 2 we explain step by step the development of a semi-automatic technique for spectral analysis and we compare it with other methods applied at the

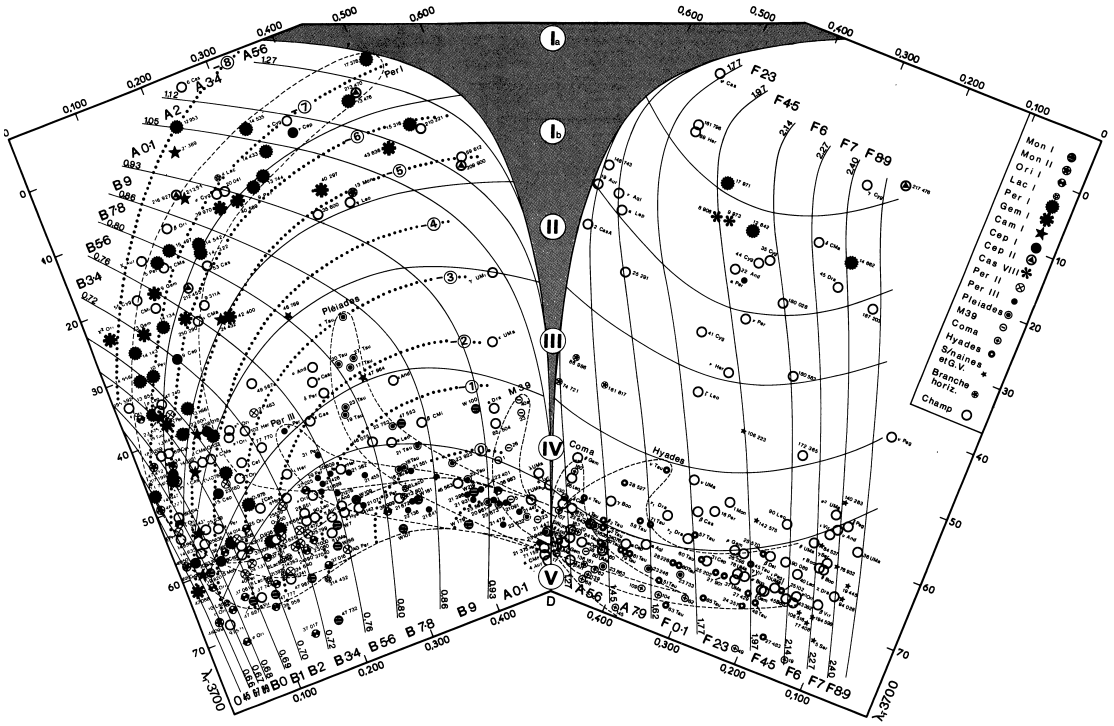

FIGURE 1.12: A twin-diagram (D, λ_1). For any given spectral type, the visible gradient Φ_b remains practically constant (independent of luminosity class, within ± 0.10 (Chalonge & Divan, 1973).

same sub-sample of our total population.

In chapter 3 we present a full catalogue of the discovered CBe stars. 732 that passed the quality test of our method and succesfully analyzed, plus 276 that spectroscopically confirmed as B-type emission line stars but with our methodology we were unable to extract spectral classification and physical parameters.

Furthermore, we want to study the evolution status of the CBe stars and we construct the HR diagram based on evolutionary models for non-rotating stars. From their mass and age were possible to interpolate.

Since CBe stars are fast-rotators, and as it is generally believed that one of the basic reasons of the formation of decreation disc is the fast rotation, we calculate the projected rotational velocity *vsini* of about 50% of our sample. We present the distribution of the projected rotational velocity and as well a comparison to the critical velocity of each star. By measurements of the Hα separation-peak we will study the disc rotation law in which we find as expected the case of a Keplerian disc rotation.

Finally, in this work we examine the anti-center part of the milky way, taking advandage of the regions that the IPHAS has been observing. The anti-centrer

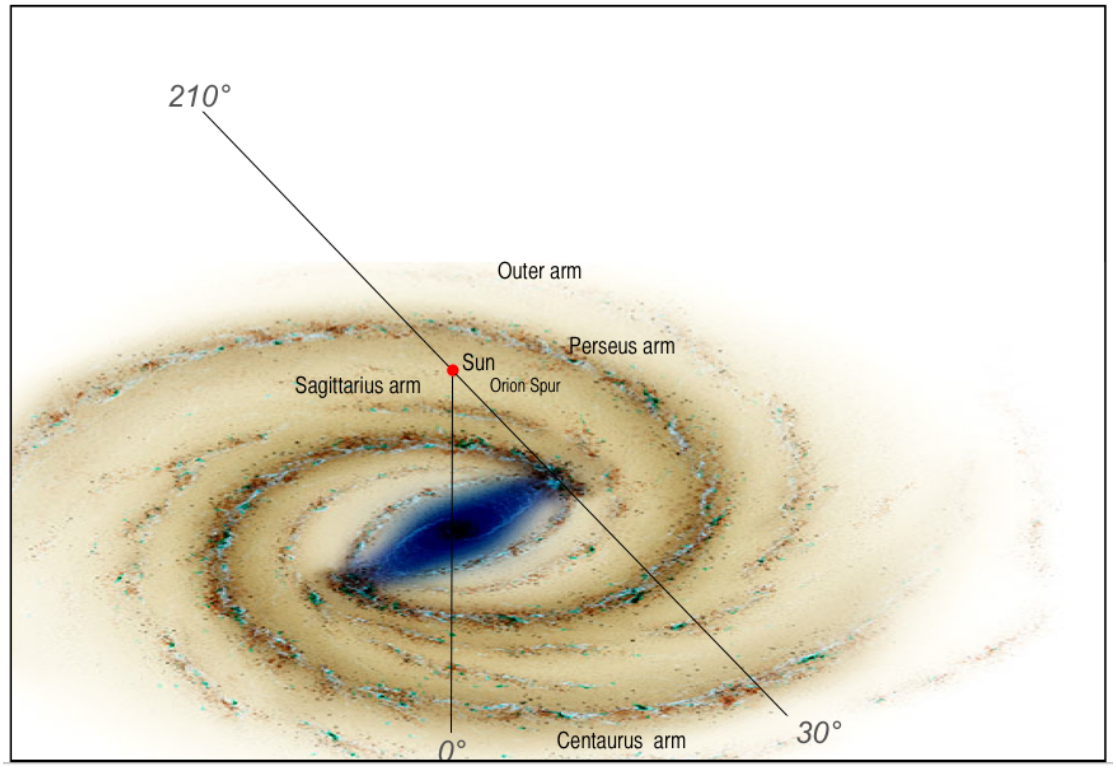

FIGURE 1.13: The Galactic structrure as was presented at Churchwell et al. (2009) from an artistic point of view and in an attempt to summarize and conclude in scientific observations of the SPITZER space telescope in the infrared wavelenghts.We draw on it the names each spiral arm and the limits $(30^o - 210^o)$ of the north Galactic plane in terms of Galactic longitude.

Galactic plane, or the North Galactic plane, is the region of the Galactic disk that it is visible from the Northern Hemisphere. It is the smallest part of of the disk and it is what we find outwards from the position of the sun. The CBe stars are young and bright stars that did not have much time to move away from their birth-places. This makes them a pottential Galactic structure indicator, at least for the spiral arms. We present a spatial distribution of our sample and we compare it with other works.

Chapter 2

Analysis

In this chapter we present a semi-automatic procedure to obtain fundamental physical parameters and distances of classical Be (CBe) stars, based on the Barbier-Chalonge-Divan (BCD) spectrophotometric system. Our aim is to apply this procedure to the whole sample of CBe stars detected by the IPHAS photometric survey, to determine their fundamental physical parameters and to explore their suitability as galactic structure tracers. We present our results in the next chapter. In this one we describe mainly the methodology used and the validation of the procedure by comparing our results with those obtained from different independent astrophysical techniques for subsamples of stars in common with other studies. We also present a test case study of the galactic structure in the direction of the Perseus Galactic Arm, in order to compare our results with others recently obtained with different techniques and the same sample of stars. We did not find any significant clustering of stars at the expected positions of the Perseus and Outer Galactic Arms, in agreement with the reference study (Raddi et al. 2013) used for verification.

2.1 Setting the spectral resolution

As explained in the previous chapter, we will employ the BCD spectrophotometric system and its calibrations to obtain the physical parameters the IPHAS Be star sample. The original calibration of the stellar parameters in the BCD system was made empirically from spectra with mean resolution of $\Delta\lambda \approx 8$Å at the BD. Although the D parameter is independent of the resolution, the mean position of the BD, and hence the λ_1 parameter, varies with the spectral resolution. This

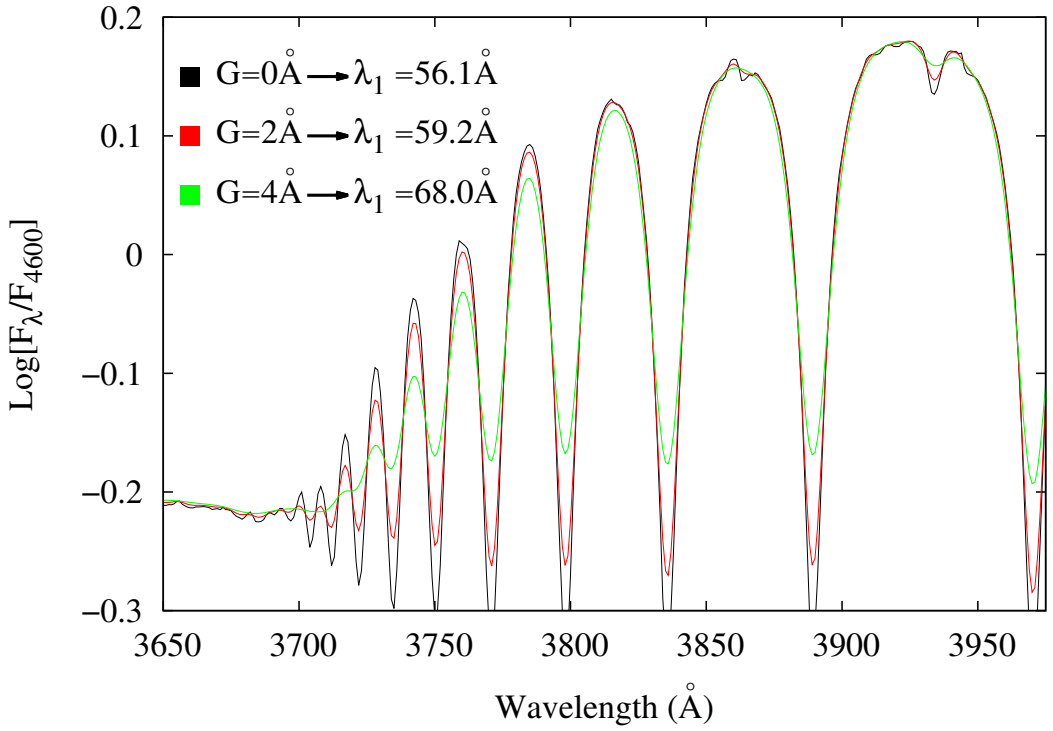

FIGURE 2.1: The region around the BD area of the standard B-type star HR4468. The black line represents the original spectrum, and red and green lines the spectrum convolved with gaussian filters of 2Å and 4Å respectively.

effect is illustrated in fig. 2.1, were we present the spectrum of the B-type star HR4486 at different resolutions.

Because the determination of astrophysical fundamental parameters proceeds with calibrations obtained with the original BCD parameters, to measure λ_1 we have to reduce the resolution of our spectra to the characteristic resolution of the original BCD spectrophotometric system. This is done by convolving the spectra with a gaussian filter of the adequate width, so that the resolution to apply the BCD formalism is obtained by

$$R_F = \sqrt{R_I^2 + G^2} \tag{2.1}$$

were R_F is the resolution to be used, R_I is the initial resolution of the spectra, and G is the width of the gaussian filter.

The setting of the correct spectral resolution is a complex issue, and depends on the available set of data. In Sect. 2.3.4 we explain how we have selected the adequate resolution for the spectra analysed in this project.

2.2 Absolute magnitudes and distances

Absolute magnitudes in the Johnson V band (M_V) are directly obtained from the D and λ_1 parameters by means of the calibration given in Table 3 of Zorec & Briot (1991).We already presented this calibration in the BCD system's description. They are converted to absolute IPHAS r, M_r, magnitudes using the intrinsic $(V - R_C)$ colours for dwarfs and giants supplied by Fabregat (in preparation), and assuming that Cousins R_C and IPHAS r magnitudes in the Vega system are identical within the errors involved in our procedure.

Distances are obtained by means of the standard spectroscopic parallax techniques, by comparing the absolute M_r magnitudes with the observed r magnitudes supplied in the IPHAS Second Data Release (IPHAS DR2, Barentsen et al. 2014), corrected for the interstellar absorption and the circumstellar excess originated by the added flux of the disk emission as follows:

$$d(pc) = 10^{\frac{r+\Delta r-A_r+5-M_r}{5}} \tag{2.2}$$

Intrinsic r magnitudes corrected for interstellar absorption were computed using the relationship $A_r = 0.84A_v$, from Fiorucci & Munari (2003).
Δr corresponts to the correction we apply in r magnitude for circumstellar emission. To correct for CBe circumstellar continuum emission we followed the method described in Sect. 3.3 of Raddi et al. (2013), which follows earlier work of Dachs et al. (1988) aimed to investigate the correlation between $EW(\mathrm{H}\alpha)$ and the circumstellar colour excess $E^{cs}(B - V)$. The relations adopted in this work are:

$$E^{cs}(B - V) \approx 0.02\frac{EW(H\alpha)}{-10\mathring{A}} \tag{2.3}$$

$$f_D = \frac{F_D}{F_D + F^*} \approx 0.1\frac{EW(H\alpha)}{-30\mathring{A}}, \tag{2.4}$$

From these values we obtain the circumstellar emission in the r band, Δr, by interpolating in Table 5 of Raddi et al. (2013). The Δr correction applied for each source is given in Table 4.2. The interpolation is presented grafically in figure 2.2.

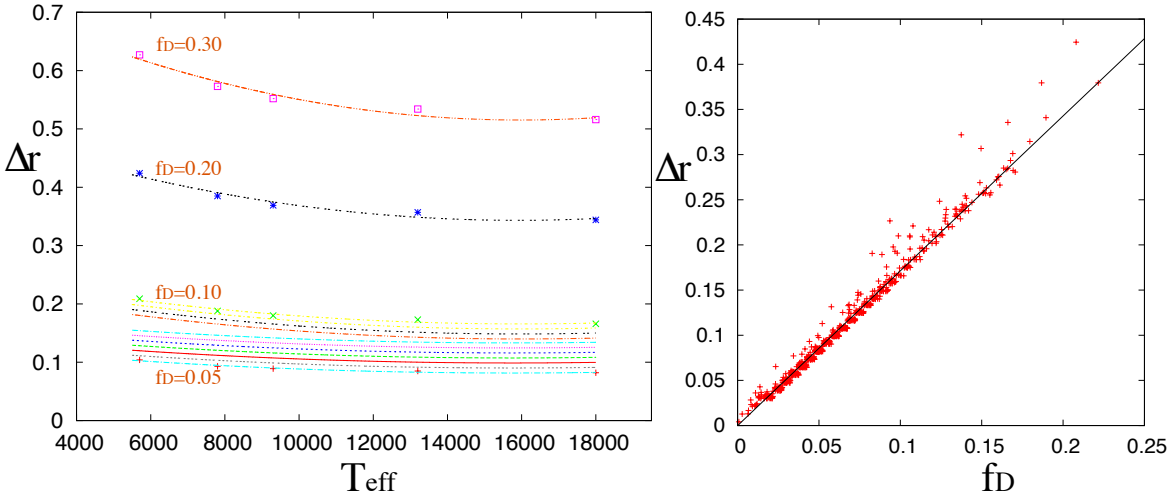

FIGURE 2.2: The interpolation from the table 5 of Raddi et al. (2013). On the left side we show the fits we did for every column which represents a value of f_D and in the inner space we interpolated parabola to reach the error of the calculations. On the right part we plot the result of the total population in this work. we note that the black line is a trend line fit to the data.

2.3 Observations and selection of the data

2.3.1 IPHAS bright sample with FLWO/FAST

Follow-up spectroscopy of the emission line objects photometrically detected by IPHAS Witham et al. (2008) was performed during 2005-2012 at the 1.5m Fred Laurence Whipple Observatory (FLWO) Tillinghast Telescope on Mount Hopkins in Arizona, using the FAST spectrograph Fabricant et al. (1998). The data were taken with the 300 lines mm^{-1}grating, and a projected slit width of 3". The data span a wavelength range from 3500 to 7500 Å at a spectral resolution of $\Delta\lambda \simeq 6$ Å. The data were processed at the Telescope Data Center at the Smithsonian Astrophysical Observatory. The spectra were delivered without relative flux calibration. As explained in the previus chapter, the BCD method requires at least an accurate relative flux calibration, especially in the blue and near ultraviolet part of the spectrum, around the Balmer discontinuity. This spectral region is very hard to observe in a flux-calibrated way, due to the weakness of incandescent flat field calibration lamps, CCD efficiency and optical coating properties. For this reason we took special care in performing the flux calibration.

For each different night we selected calibration spectra from the FAST archive, to ensure that all spectra were calibrated with flux standards observed the same

night. The calibration has been done using standard IRAF routines. Further explanation on the reduction of the data is given in the Appendix A.
The slit is kept at a fixed position, and hence it was not placed at the paralactic angle. We made checks to ensure that there are no chromaticity effects induced by differential atmospheric dispersion. First, we note that all spectra were obtained at airmasses lower than 1.5. For stars with more than one spectra (32 stars), we made plots of the measured flux ratios at 3600 and 4000 Å, after the normalisation at 4600 Å, against the difference in airmass, and no correlation was apparent. See Fig. 2.3. For 32 stars we have two spectra obtained at different epochs, and for one, three spectra. We estimate the mean error of the flux calibration as the difference between the individual values of the flux divided by the mean value. The mean error in the flux of the calibrated and normalised spectra amounts to $5.1 \pm 4.5\%$ at 4000 Å, and to $15 \pm 14\%$ at 3600 Å. The last value in the ultraviolet continuum is significantly larger, as expected. However, to obtain the lower limit of the Balmer discontinuity of the CBe stars we don't use the extrapolated ultraviolet continuum, but instead the bottom of the higher Balmer lines. Hence, even large errors in the flux calibration short of the Balmer discontinuity, which eventually could lead to an inaccurate determination of the slope or the position of the Balmer continuum, will not have any impact in the determination of the CBe stars physical parameters used through this work.

The mean difference between the measured D and λ_1 parameters from different spectra of the same star are 0.032 *dex* and 7.3Å respectively. These differences are of the same order as the ranges in D and λ_1 spanned by one spectral subtype and one luminosity class respectively, as can be seen in Fig. 10 of Zorec et al. (2009). For this work we selected the sources with spectral features characteristic of OB-type stars, manually. Among them we selected the spectra having S/N$\geq$30 around the Balmer discontinuity ($\sim$ 3700Å), where the BCD parameters are measured. Finally, we rejected the spectra in which the continuum around the BD is not well defined. This rejection was applied automatically each time that the χ^2 of a parabolic fit to the pseudo-continuum drawn in the BD region is larger than 3σ as compared to the average of fits obtained for the entire stellar sample. We considered that in those cases we could not derive a reliable λ_1 parameter. We examined an initial sample sample of 612 FAST spectra in the Perseus Arm region. After rejecting the spectra whose characteristics didn't correspond to an OB-type star, and those not meeting the criteria presented in the previous paragraph, we kept a final sample of 257 spectra for further analysis for the first part of this project, which was the evaluation of the analysis procedure. We selected for the

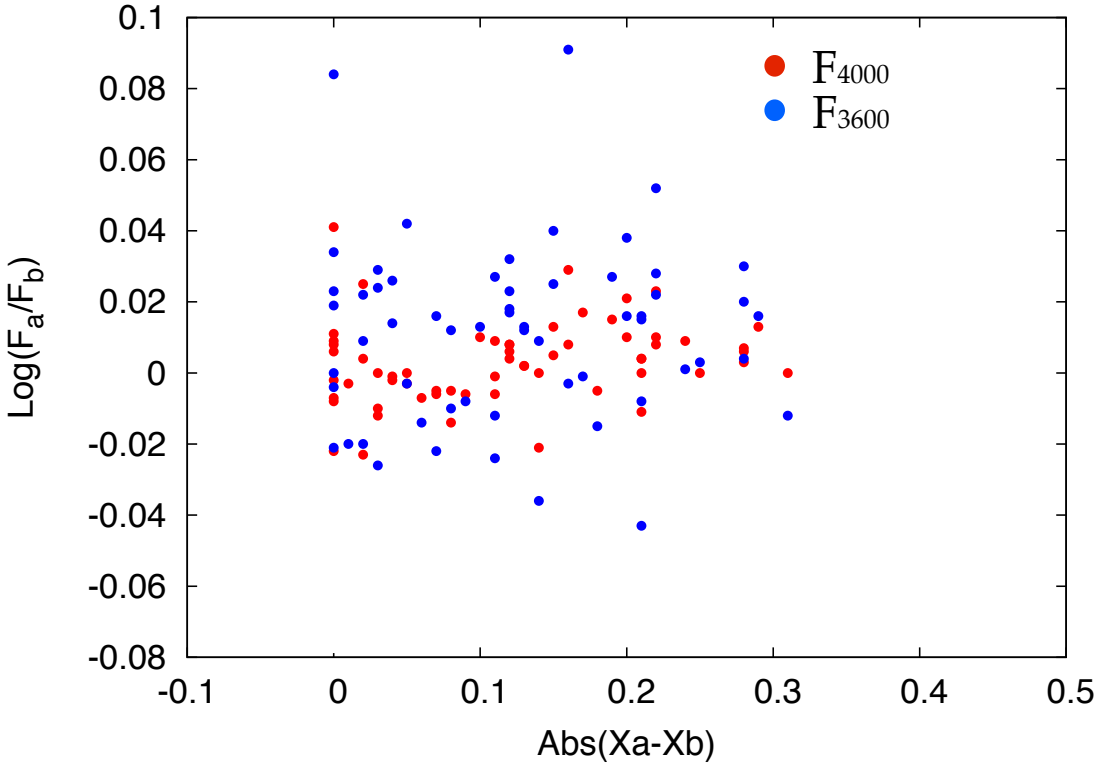

FIGURE 2.3: Flux ratios at 3600 and 4000 Å, after the normalisation at 4600 Å, against the difference in airmass for 32 stars we have double spectra in different epochs. No correlation is apparent.

evaluation to work with the stars that belong to the Perseus arm region ($120^o < l < 140^o$) for the reason that this was the investigation region from (Raddi et al. 2013) work with a part of the same objects. In that case we are able to compare our works and evaluate our methodology.

In chapter 3, the same selection criteria was applied to the rest of 2047 spectra. Finally, we came up with a sample of 823 spectra for 732 CBe stars. For 69 of them we have two spectra and for 1 we have three spectra.

2.3.2 Evaluation of the flux calibration of the FLWO/FAST spectra

The determination of reliable physical parameters of stars by means of the BCD system methods requires the spectra to have at least an accurate relative flux calibration. In this section we present an evaluation of the flux calibration of the FLWO/FAST sample, by comparing different spectra of the same objects. In the discussion below we only analyse the spectral region between 3700 and 4600 Å, where the BCD parameters are measured. For some spectra drops in the signal

to noise and large differences in the flux calibrations at shorter wavelengths are apparent. However, as explained in previous sections, they don't have any impact in the determination of the physical parameters of the stars.

For 31 stars we have two spectra obtained at different epochs, and for one more, star 181, three spectra. All these spectra are presented in Figs. 2.4 to 2.7. For each object we present two panels. In the upper one we overplot the two -or three- flux calibrated and normalised spectra in a logarithmic scale. In the bottom panel we represent the difference between the normalised flux as a function of the wavelength.

From the comparison between the spectra we can divide the object sample into three groups. Group A is composed by the stars for which the two calibrated spectra overlap, indicating that the flux calibrations applied to each spectrum are consistent. It includes 14 objects, namely stars 23, 56, 68, 110, 118, 124, 161, 170, 171, 179, 181, 210, 219 and 223. Group B is composed by the stars displaying differences between the spectra, which imply differences between the flux calibrations, but the difference is a lineal function of the wavelength, as shown in the bottom panel for each star. Group B includes 16 objects, namely stars 109, 116, 127, 130, 153, 154, 164, 169, 172, 183, 185, 188, 211, 214, 217 and 218. Finally, Group C is composed by two more objects, stars 204 and 207, which present differences in the flux calibration which are not a lineal function of the wavelength. The differences in the flux calibration present in the stars of the group B do not have any effect in the determination of the D and λ_1 parameters. If the difference between the two spectra increases linearly with the decreasing wavelength, the variation of the Paschen continuum extrapolated at 3700 Å exactly compensates the variation of the bottom of the Balmer discontinuity at the same wavelength, and the position of the discontinuity is not affected. The mean differences between the D and λ_1 parameters for stars of Group A are 28 $\pm$24 dex and 7.0 $\pm$ 6.0 Å respectively, while for stars of Group B are 31 $\pm$ 22 dex and 7.4 $\pm$ 5.4 Å respectively.

These differences do affect, however, the determination of the interstellar reddening. The reddening value is derived from the Φ_b parameter, which measures the slope of the Paschen continuum. This slope is sensitive to differences in the relative flux calibration. The mean difference in the determination of $E(B-V)$ for stars in the group A is 0.06 $\pm$ 0.04 $mag.$, while for stars in group B amounts 0.15 $\pm$ 0.10 $mag.$ This last figure is consistent with the standard deviation obtained when comparing our $E(B-V)$ values with values in the literature for the same stars presented in the next section , and can be considered as the mean error of our $E(B-V)$ determination.

For stars in Group C the flux calibrations are not consistent. This represent up

to four spectra out of 65 analysed in this section. In addition, it should be noted that the differences between the calibrations are small, and translate into mean differences of the parameters determined from them well within 3σ of the mean errors considered through the work.

2.3.3 INT and NOT spectra

Mid-resolution (2 - 4.8 Å) and high S/N (30-100 at 3700 Å) spectra of 67 classical Be stars were obtained at the Roque de los Muchachos Observatory in La Palma, Canary Islands, Spain. The telescopes and instruments used were the Isaac Newton Telescope (INT) equipped with the Intermediate Dispersion Spectrograph (IDS), and the Nordic Optical Telescope (NOT), using the Andalucia Faint Object Spectrograph and Camera (ALFOSC). A sample of spectrophotometric standard stars, for relative flux calibration, and MK standard stars, were also observed. A complete description of this data sample is given in Sect. 2.3 of Raddi et al. (2013). In this work we will use them in the procedure to determine the value of G, the width of the gaussian filter required for the FLWO/FAST spectra, as described in the next subsection, and to compare the results of our analysis with those obtained by Raddi et al. (2013) via energy distribution fitting to appropriate model atmospheres.

2.3.4 Gaussian filtering

In the introduction we mention that the BCD system is based on observational calibrations that have been made with $\Delta\lambda \sim 8$ Å, spectra. As it is shown in figure 2.1 , spectral resolution can affect the average position of the BD (λ_1) as it is defined by the BDC system. To transform the resolution of our spectra at the BCD resolution, we used the Gaussian filtering technique. Mathematically, a Gaussian filter modifies the input signal by convolution with a Gaussian function where the fit applies to a spectral area ,$\Delta\lambda \sim$ Gaussian width, around a central wavelength λ. As larger the width,the spectra goes smoothest so that can simulate the lower resolutions until we can achieve the requested BCD resolution. The Gaussian filtering funcion can be described as:

$$G(\lambda) = \frac{1}{\sqrt{2\pi\sigma_u^2(\lambda)}} e^{\frac{-c^2}{2\sigma_u^2(\lambda)}} \tag{2.5}$$

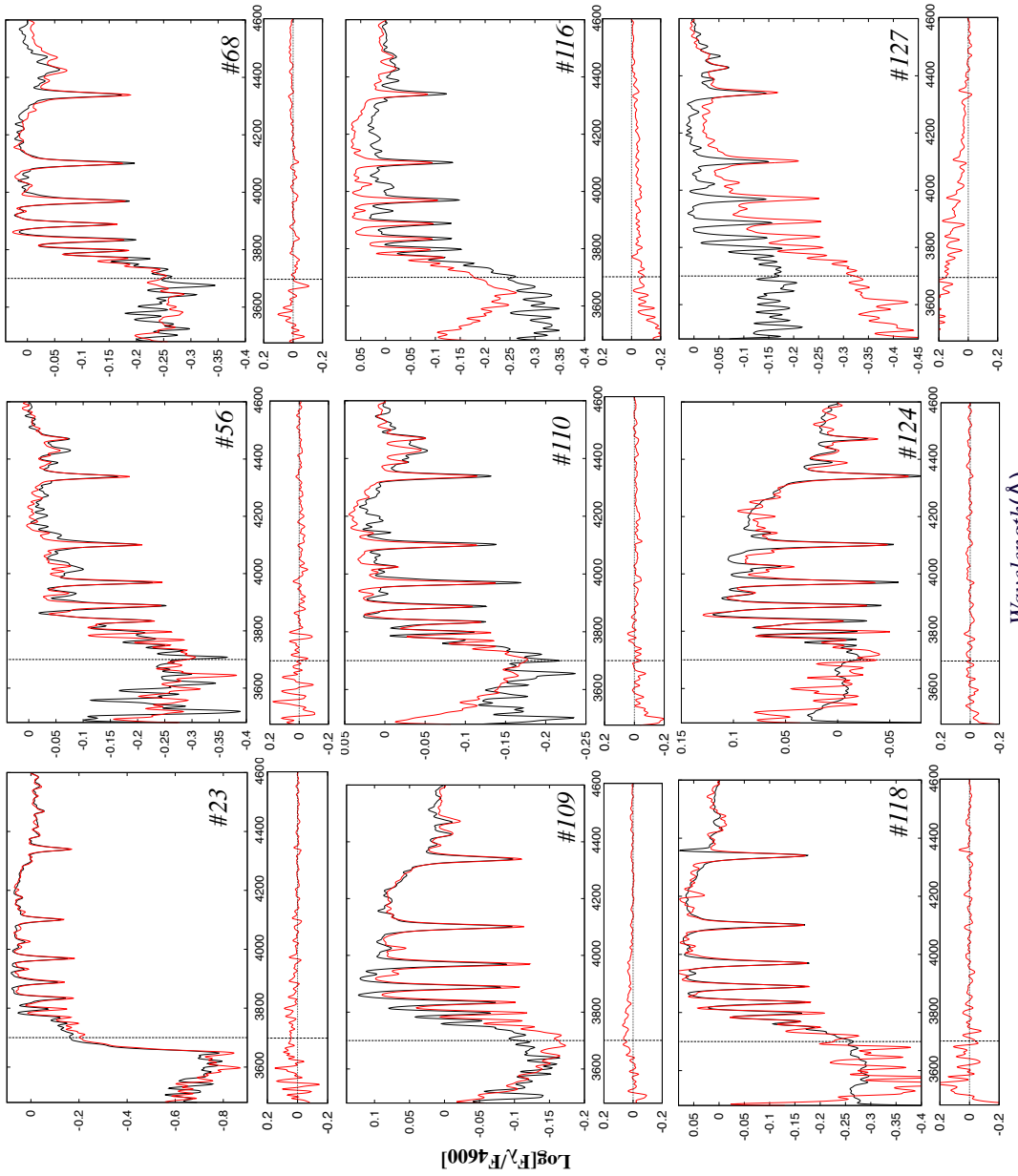

FIGURE 2.4: Stars with two or more spectra. For each object the upper panel represents the overplot of the spectra and the lower panel the difference between the two spectra.

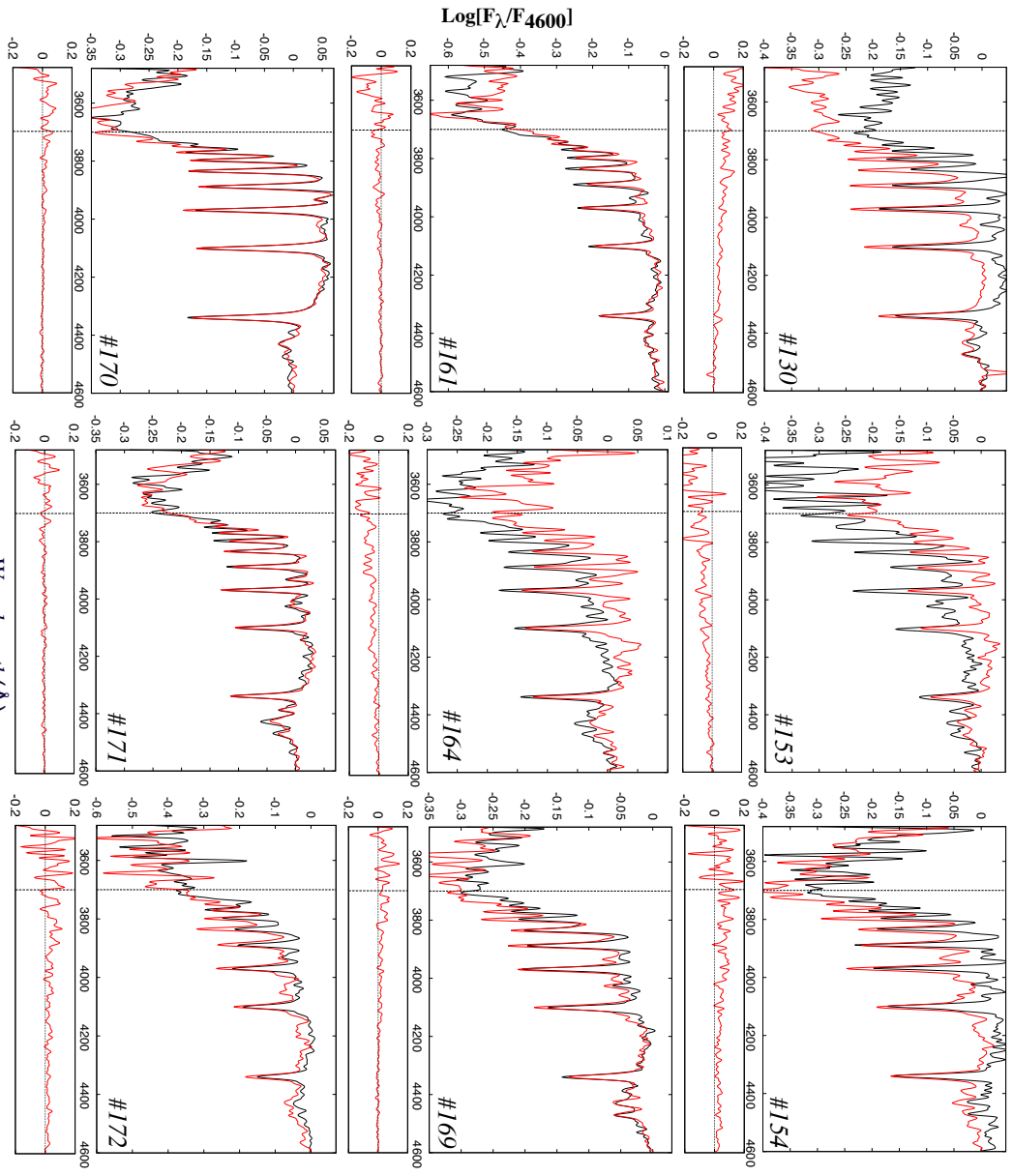

FIGURE 2.5: Same as Fig. 2.4

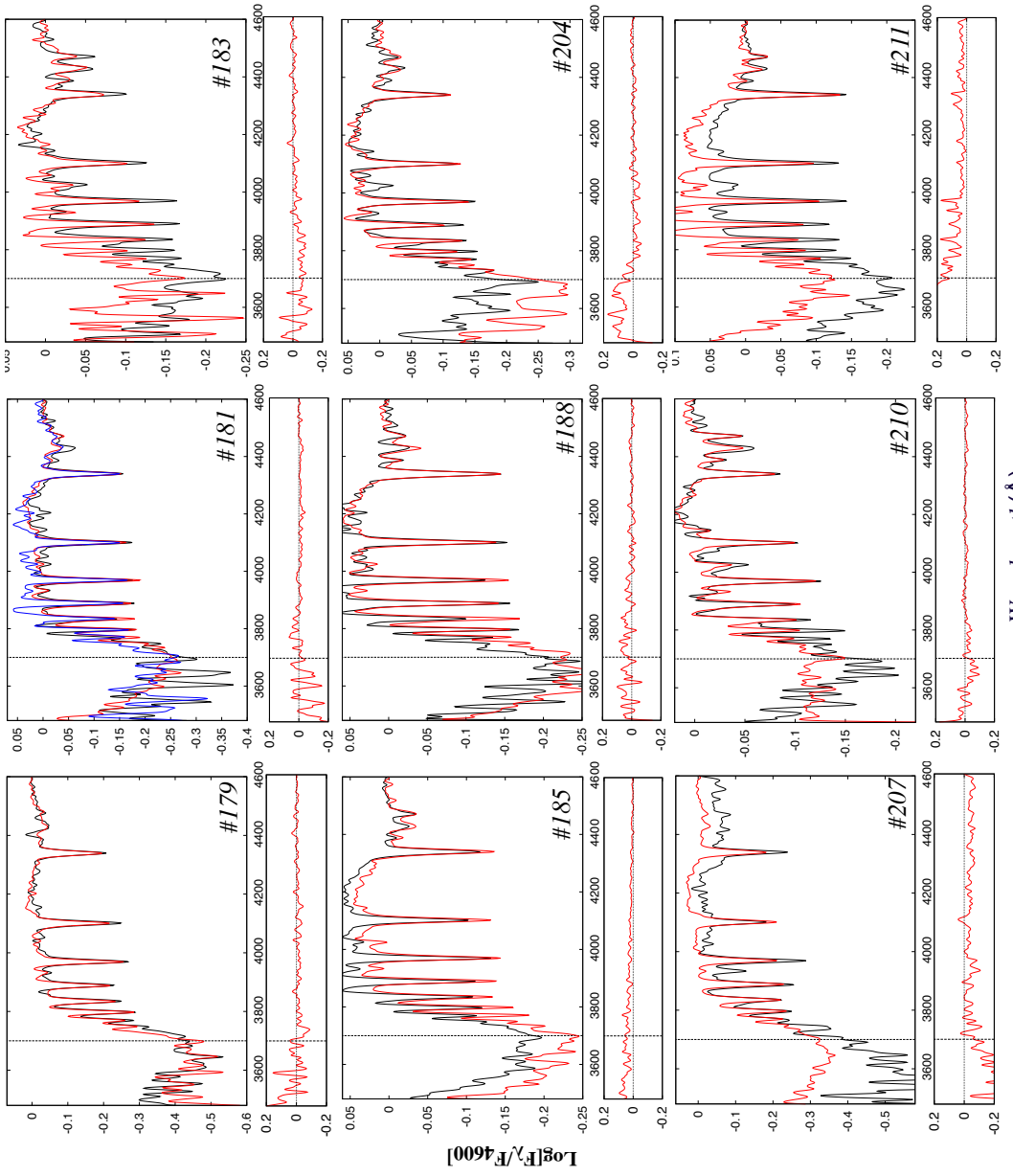

FIGURE 2.6: Same as Fig. 2.4

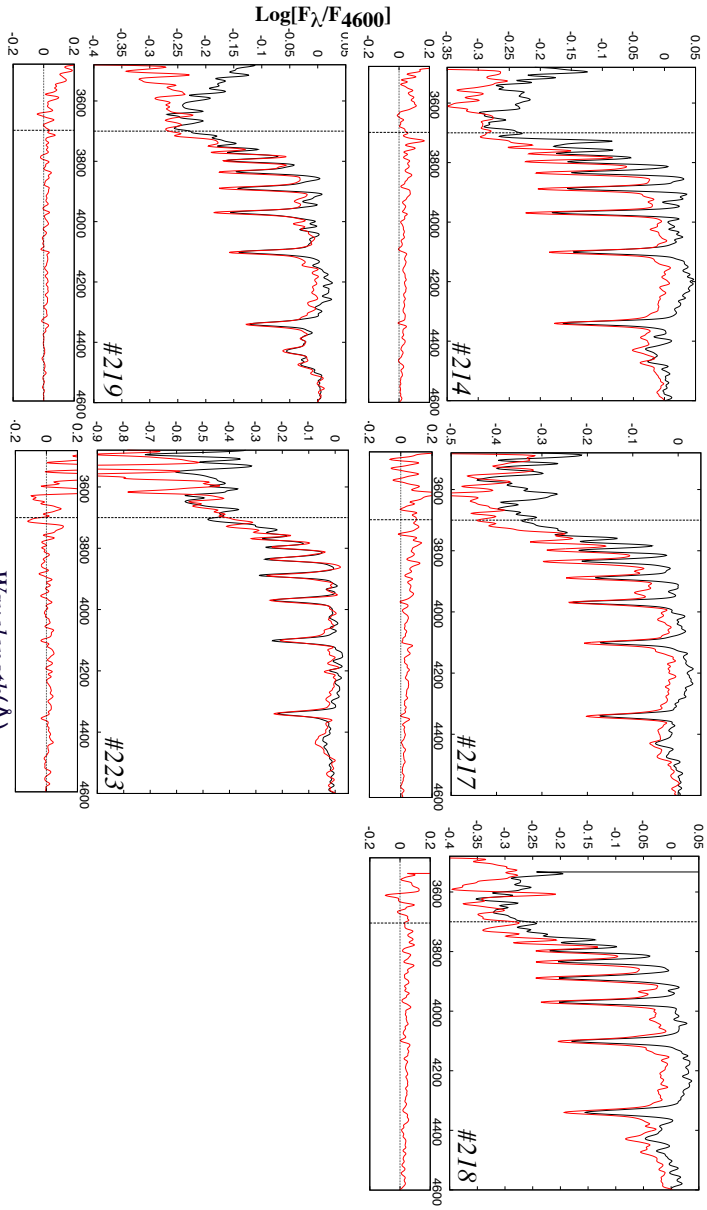

FIGURE 2.7: Same as Fig. 2.4

with $\sigma_u = \frac{\Delta\lambda c}{\lambda}$ were $\Delta\lambda$ is the width of the Gaussian convolution in each wavelength step. The differences at the BD depth ,$D(dex)$, due to the resolution changes are negligible.

In figure 2.1 we have an example of a stadard B-type star convolved by equation 2.5 for Gaussian widths of $2-4$ Å and they are compared with the original spectra which is at resolution of $\Delta\lambda \pm 2$ Å. It is clear that the spectral resolution affects the position of the continuum and finally gives differences at λ_1.

For every dataset, with different resolution, we must find the appropriate Gaussian width with which to convolve the spectra in order to achieve the desired BCD resolution. The best way of doing this is to observe BCD standard stars with the same instrumental configuration as the programme stars. A list of BCD standards, i.e. a sample of stars for which standard values of the D and λ_1 parameters are know, is given by Zorec & Briot (1991). No BCD standards were observed with the FAST spectrograph, and only two were obtained at the INT and two more at the NOT. In order to determine the value of G (Eq. 2.1) and correct the resolution for all spectra we take the following steps:
1. As a starting point we used the INT and NOT spectra of the stars for which the standard D and λ_1 are known. For each star we computed the BCD parameters using gaussian filters of different width, and compared the obtained values with the standard ones. The best agreement for each star was obtained with the gaussian widths presented in Table 2.1 .
2. We obtained the BCD parameters of all MK standard stars observed with the INT and NOT, using the widths in Table 2.1 . From the BCD parameters we obtained the spectral types and luminosity classes, and compared them with the standard MK ones. This comparison is presented in Table 2.2 . The agreement between the MK and BCD classification is fairly good, within two spectral subtypes and one luminosity class for most of the stars. When comparing the classification of stars in both systems, we have to keep in mind that the MK system assigns discrete spectral types, where each encompasses comparatively large intervals of (D, λ_1) parameters. Obvious differences can then appear when interpreting continuous runs of BCD parameters with discrete MK assignments.
From the above procedure, we find $G = 4.8, 4.0$ and 3.5 Å as the widths of the gaussian filters to reduce the resolution of the INT (with two different instrumental configurations) and NOT spectra, respectively. We subsequently applied gaussian filters of these widths to the whole sample of INT and NOT spectra, and computed the BCD parameters for all of them.

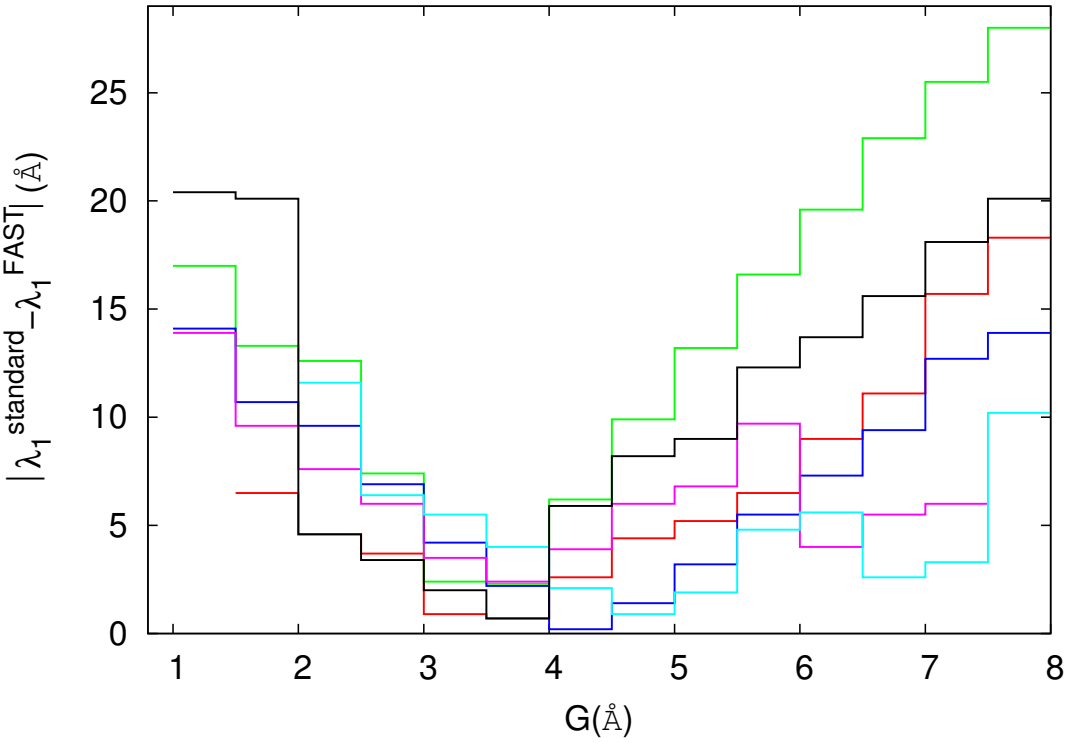

FIGURE 2.8: Differences in the λ_1 parameter obtained with the INT/NOT spectra and the FAST spectra convolved with different gaussian widths ranging from 1.5 to 8 Å, with 0.5 Å step, for a subset of the stars in common between the two samples. Every colour represents a spectrum and the minimum of the $\Delta\lambda_1$ difference corresponds to the convolution that best fits the INT/NOT spectrum.

TABLE 2.1: BCD standard stars observed with the INT and NOT telescopes. The different $\Delta\lambda$ and dispersion values for the two stars observed at the INT are due to different instrumental configurations. The last column lists the width of the gaussian filter used to reproduce the standard BCD parameters from each spectra.

NAME	Telescope	Sp/LC$_{\rm MK}$	Sp/LC$_{\rm BCD}$	$\lambda_1(\AA)$	$D(dex)$	$\Delta\lambda(\AA)$	Disp.$(\AA/pix)$	$G(\AA)$
HR 533	INT	B2 V	B2 V	65	0.144	4.8	1.85	4.8
HR 1122	NOT	B5 III	B5-6 III	42	0.286	2.0	0.72	3.5
HR 2347	NOT	B9 V	B9 V	64	0.422	2.0	0.72	3.5
HR 2461	INT	B8 III	B7 III	41	0.340	3.2	1.40	4.0

3. The final step is to set the resolution for the FAST spectra. The way we proceed is described graphically in Fig. 2.8. We convolved the FAST spectra, one by one, starting from a gaussian width of 1.5 Å up to 8 Å, with a 0.5 Å step. For all the stars in common between the INT/NOT and FAST samples we plot the difference $\mid \lambda_1, INT/NOT - \lambda_1, FAST \mid$ versus the gaussian width. The minimum difference is found at $G = 4.25$ Å, and we assume this value as the gaussian width, G, with which to convolve all the FAST spectra prior to the determination of the BCD parameters from them.

2.4 The semi-automatic pipeline

2.4.1 Code principles

In order to analyse a large sample of spectra in a reasonable amount of time we have developed a semi-automatic procedure, only requiring user interaction to evaluate output diagrams at some important steps during the treatment of each spectrum. The basic input of the programme are the observed spectra, with the wavelength scale in Å and flux in erg s^{-1} cm^{-2}, and a list with the names of the files containing each spectrum.
The pipeline used to treat each spectrum requires a series of inputs that the user provides as the analysis goes along. The first step of the procedure is to ask the user the width G, in Å, of the gaussian filter that the spectra require in order to transform their resolution to the original resolution of the BCD system, and the dispersion of the spectra. This first step is valid for the whole run and applies to all the spectra in the list. The next step is the analysis of the spectra one by one. As each spectrum is presented for analysis, it is first thoroughly checked to establish its wavelength range and to detect possible recording flaws.
One of the steps which require user interaction is the wavelength scale, whose possible variations , caused either by errors in the wavelength calibration or by the radial velocity of the star, may affect the position of the Balmer discontinuity and the determination of BCD parameters. The largest shifts in the wavelength calibration were found to range from 3 to 10 Å.

A flux normalization is applied at λ4600 Å, and the spectral coordinates transformed to $1/\lambda - \log(F/F_{4600})$, to be consistent with the definition of colour gradient (Allen, 1973). This enables a first estimate of the BD depth, $D_1(dex)$, which is considered preliminary as the Paschen continuum cannot be well represented by a straight line in these coordinates. D_1 is used to derive an approximate value of the stellar effective temperature. The spectrum is subsequently divided by a Planck function at this temperature. The Paschen continuum in the normalised spectrum closely approach to a straight line, and can be extrapolated without ambiguity. The determination of D as the ratio of fluxes at 3700Å removes the contribution of the Plank function.
To measure the mean spectral position of the BD we calculate the line determined by the points $logF_\lambda - D/2$ at $\lambda = 3700, 4000, 4150$ and 4300 Å, where F_λ is the

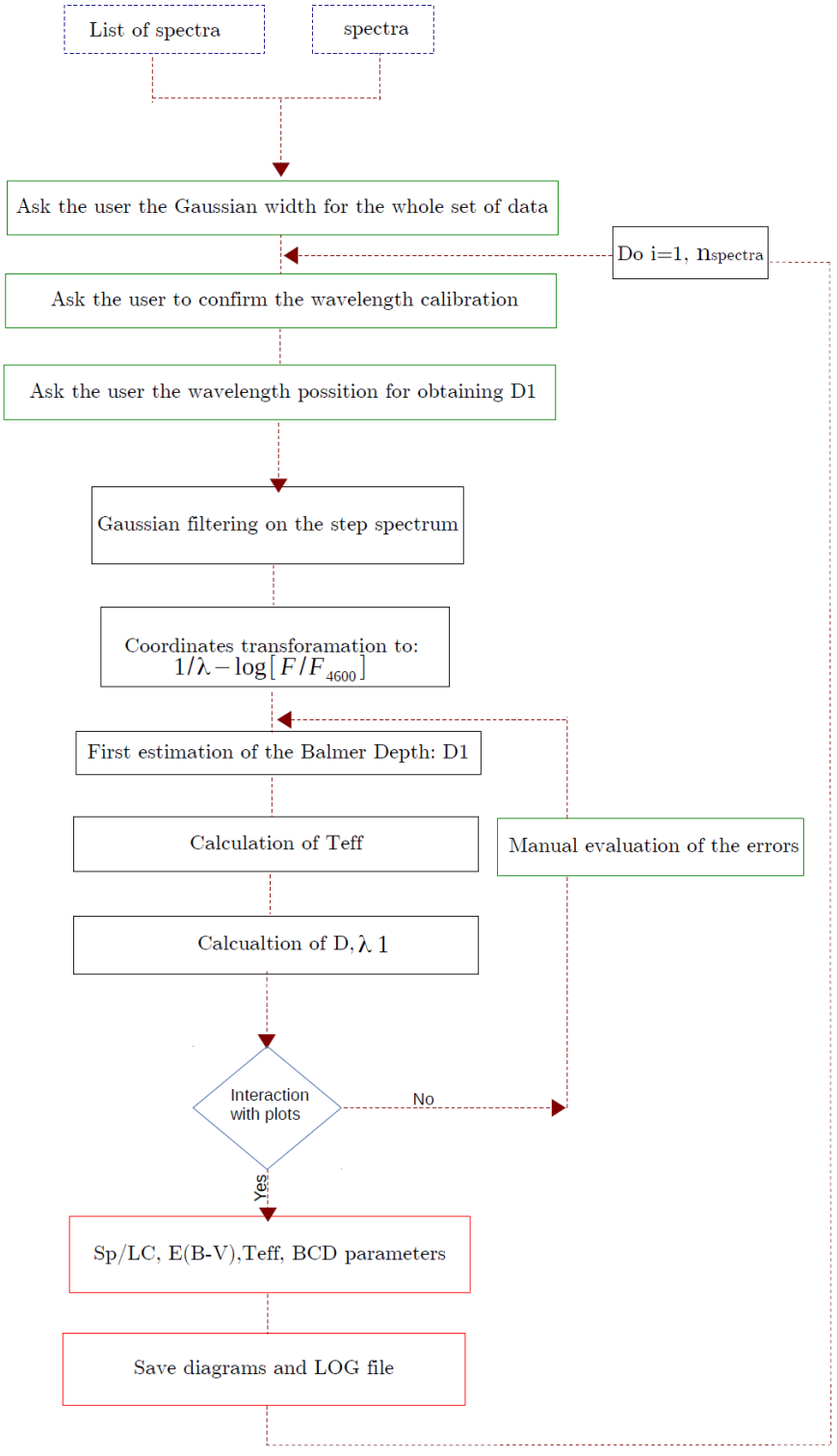

FIGURE 2.9: Simplified block diagram of the spectral analysis pipeline based on the BCD classification system presented in this work.

flux of the extrapolated Paschen continuum. We characterise the spectral continuum as a parabolic fit to the pseudo-continuum in the $3700 - 3850$Å region. The intersection between these two lines determines the value of the λ_1 parameter. This procedure allows the precise determination of the BCD(D, λ_1) parameters as described in Sect 1.3. For each spectrum, a series of diagrams are constructed, with which the user can interact to control the progress of the analysis. The steps in the algorithm are shown in Fig. 2.9. The output of the program is a log file containing the parameters calculated for each spectrum: name, BCD(D, λ_1), T_{eff}, spectral type and luminosity class, Φ_b, Φ_b^0, $E(B-V)$ and M_V .

2.5 Evaluation of the procedure

We now validate the described procedure , by comparing our results with results from literature obtained for the same stars with different astrophysical techniques and analysing spectra for B-type stars observed from INT, NOT and spectral libraries. For the comparison, we used the results obtained from spectroscopic data analysis by Raddi et al. (2013), and from Strömgren photometry calibration of data presented by Fabregat & Capilla (2005) and Monguió et al. (2013).

2.5.1 Validation against previous spectroscopic analyses

2.5.1.1 Standard B-type stars

As a first step of the developing of the automatic analysis procedure we test it's the valiability by analysing standard B-type stars, of all sub-types. We analyzed spectra from the STELIB stellar spectrum library (STELIB/Laboratoire Astrophysique de Toulouse) and INT, NOT spectra that delivered reduced. The whole catalogue of standard B-type stars are presented in table 2.2. Together with the MK standard classification, the BCD classification that our procedure did, and the BCD parameters. Especialy the BD depth, $D(dex)$, for which, as we explained above, we used two different ways and only with the non-emission star spectra we can confirm their agreement.
Our classification results agree with the standard MK classification with the typical difference of one sub-type, which actually is the normal difference between the BCD and the MK systems.

TABLE 2.2: A sample of 46 normal B-type stars, covering almost all the B sub-types. We present the here the calculations of $D(dex)$, calculated automatically with our program, in both sides of the BD and comparison between the classification.

NAME	Source	Sp/LC	Sp/LC_{BCD}	$D_{uv}(dex)$	$D_{B.l.}(dex)$	$\mid D_{uv} - D_{B.l.} \mid$
HR 718	STELIB	B9 III	A0 V	0.501	0.499	0.002
HR 2422	STELIB	O8 V	O6-7 IV	0.048	0.035	0.013
HR 3454	STELIB	B3 V	B3 V	0.175	0.198	0.023
HR 3982	STELIB	B7 V	B7 IV	0.363	0.369	0.006
HR 4468	STELIB	B9.5 V	A0 V	0.467	0.464	0.003
HR 7001	STELIB	A0 V	A0-1 V	0.531	0.523	0.008
HD34816	STELIB	B0.5 IV	B1 III	0.065	0.089	0.024
HD35497	STELIB	B7 III	B6 IV	0.299	0.306	0.007
HD43153	STELIB	B7 V	B8 V	0.323	0.334	0.011
HD40111	STELIB	B0.5 II	O8-9 III	0.018	0.042	0.024
HD53929	STELIB	B9.5 III	B5-6 V	0.294	0.301	0.007
HD77350	STELIB	A0 III	A0-1 V	0.479	0.478	0.001
HD78316	STELIB	B8 III	B5 V	0.278	0.294	0.016
HD79158	STELIB	B8 III	B5 V	0.291	0.302	0.011
HD91316	STELIB	B1 Ib	B0 IV	0.046	0.064	0.018
HD123299	STELIB	A0 III	A2	0.522	0.509	0.013
HD144206	STELIB	B9 III	B9 IV	0.378	0.379	0.001
HD147394	STELIB	B5 IV	B5-6 V	0.249	0.264	0.015
HD149121	STELIB	B9.5 V	A0 V	0.448	0.453	0.005
HD164353	STELIB	B5 Ib	B2 IV	0.157	0.158	0.001
HD268623	STELIB	B2 Ia	B2 Ia	0.030	0.041	0.011
HD268749	STELIB	B7 Ia-Ib	B2 Ia	0.115	0.097	0.018
HD271163	STELIB	B3 Ia	B0 Ia	0.038	0.042	0.004
HD365112	STELIB	B0 V	B0 V	0.071	0.098	0.027
HR 1497	INT	B3 V	B7-8 V	0.294	0.297	0.003
HR 1860	NOT	B6 V	B6 V	0.317	0.301	0.016
HR 2490	NOT	B3 IV	B3 IV	0.242	0.227	0.015
HR 1576	INT	B9 V	B7 V	0.283	0.288	0.005
HR 1863	NOT	B2.5 V	B4 V	0.222	0.210	0.012
HR 2116	NOT	B8 V	B7-8 V	0.355	0.340	0.015
HR 1399	INT	B5-6 V	B6 V	0.287	0.295	0.008
HR 1595	NOT	B2 V	B1 V	0.126	0.116	0.010
HR533	INT	B2 V	B2 V	0.162	0.149	0.013
HR927	INT	B8 V	B7-8 V	0.346	0.345	0.001
HR1760	INT	A3V	>A2	0.545	0.528	0.017
HR1808	NOT	B5 V	B4 V	0.260	0.248	0.012
HR1820	NOT	B2 V	B3 V	0.189	0.193	0.004
HR1892	NOT	B1 V	B0 V	0.104	0.105	0.001
HR2010	NOT	B9 IV	A0-1 V	0.483	0.464	0.019
HR2161	NOT	B3 V	B3 V	0.205	0.213	0.008
HR2344	INT	B2 V	B3 IV	0.183	0.182	0.001
HR2347	NOT	B9 V	A0 V	0.473	0.453	0.020
HR2461	INT	B8 III	B7-8 IV	0.349	0.351	0.002
HR2840	INT	B6 IV	B7 IV	0.336	0.351	0.015
HR7996	INT	B3 III	B3-4 IV	0.270	0.252	0.018
HR8403	INT	B5 III	B5 V	0.331	0.313	0.018

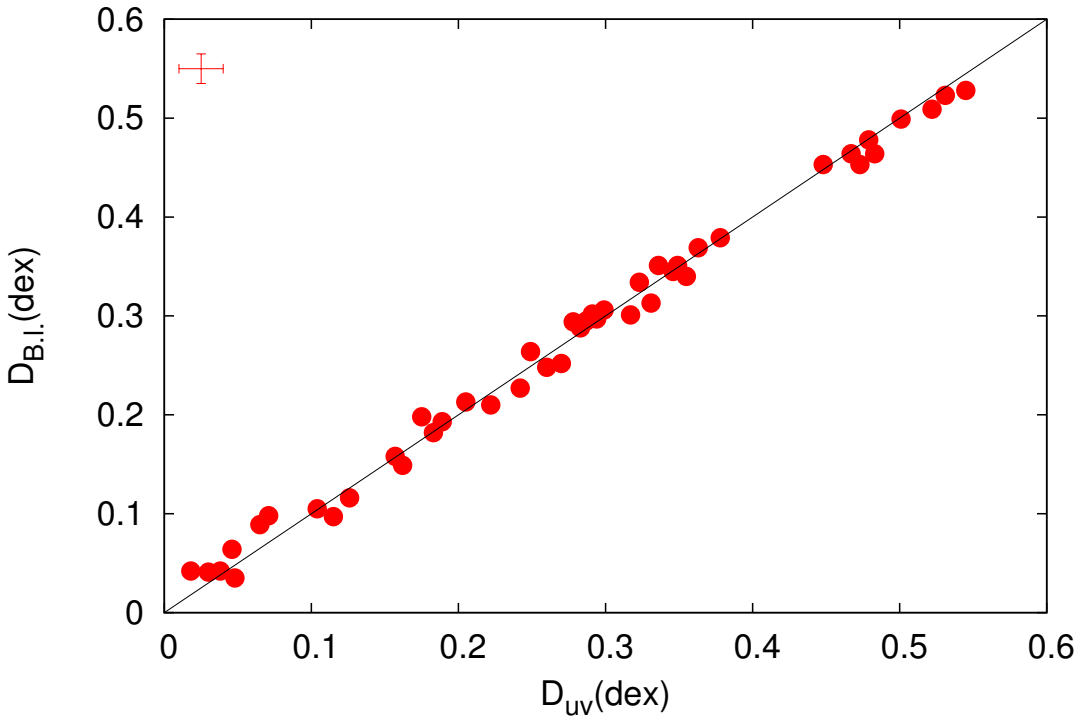

FIGURE 2.10: Comparison of the Balmer jump depth calculated for 46 absorption-line B-type stars, using both the ultraviolet continuum and the Balmer lines limit as explained in the text. At the left upper part it is shown the typical error in the determination of D, 0.015 dex

2.5.1.2 INT and NOT Be stars spectra

Raddi et al. (2013) studied a group of 67 candidate CBe stars in the region of the Perseus Arm, by analysing the mid resolution spectra obtained with the INT and NOT telescopes at La Palma described in Sect. 2.3.2. They determined their spectral types and measured their colour excess via spectral energy distribution fitting to appropriate model atmospheres in the blue part of the spectrum (3800-5000 Å). For the present comparison we use 35 spectra which meet the selection criteria described in Sect. 2.3. The results are presented in Table 2.3 . To provide an additional element of comparison, in Table 2.3 we also present spectral types and luminosity classes obtained from the INT/NOT spectra by means of the standard MK classification procedures, using only the strength and widths of the spectral lines, and the ratios between lines, as temperature and luminosity criteria, as described for instance by Gray & Corbally (2009). From Table 2.3 we can see a general good agreement within the three classification systems. When comparing our results with those of Raddi et al. (2013) we find that 29 of the 35 stars agree within one or two spectral subtypes. In the remaining six stars, however, there

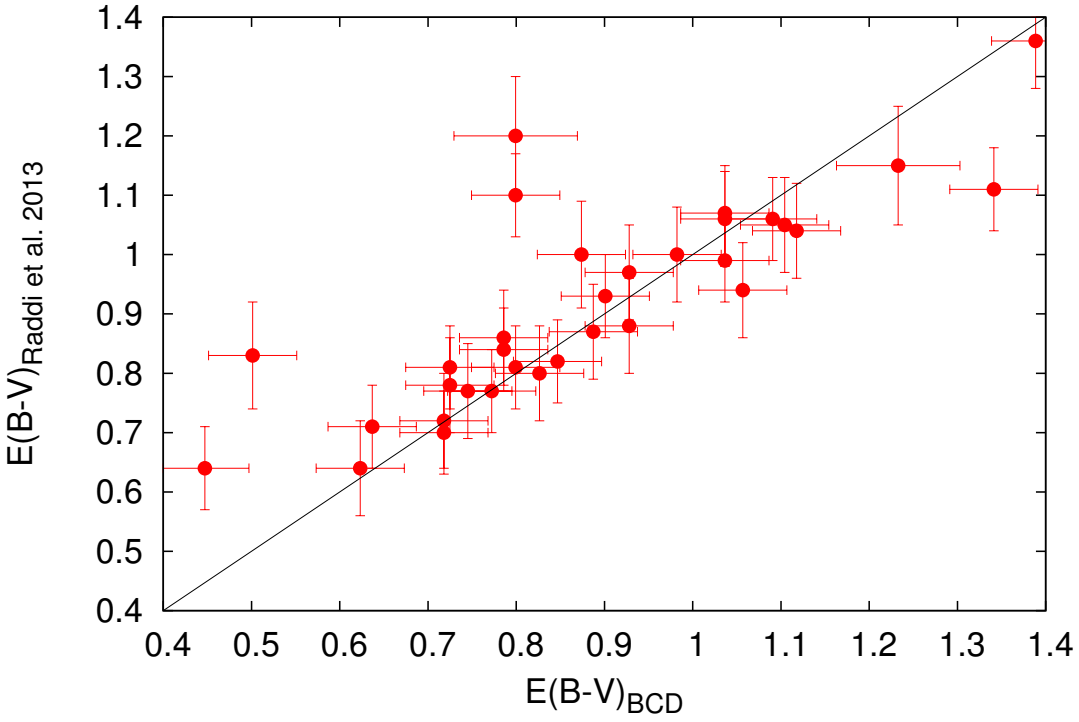

FIGURE 2.11: Comparison between the colour excesses obtained by the procedure described in this work and the values given by Raddi et al. (2013).

are large differences so we did a more carefoul and also an MK classification at those stars (five out of six, that have good quality and we could apply the MK system) and we present it at figure 2.12. Better agreement, with differences not larger than two sub-spectral types, is found between the BCD results and the MK classification applied to the same spectra.

In the last two columns we present the $E(B-V)$ obtained from the measured BCD parameters by means of Eq. 1.1, and the absolute magnitudes in the scale defined by Zorec & Briot (1991). We estimate a mean error of 0.05 mag. for the $E(B-V)$ determination, obtained from the standard propagation of the errors through Eq. 1.1, considering the characteristics uncertainties of the BCD parameters involved. The mean uncertainty of the M_V values amounts to 0.15 mag. Zorec & Briot (1991).

In Fig. 2.11 we present the comparison between the $E(B-V)$ obtained by Raddi et al. (2013) and our procedure. A mean error of $0.05 mag.$ for our determination of the $E(B-V)$ is assumed, as stated above. For the values of Raddi et al. (2013) we used the errors quoted by these authors. Both sets of data show a good agreement, with a mean difference of 0.04 ± 0.15 mag.

TABLE 2.3: BCD parameters and classification of 35 IPHAS CBe stars with INT/NOT spectroscopy, and comparison with MK classification and spectral classification given by Raddi et al. (2013).

NAME	D (dex)	λ_1(Å)	Φ_b	Φ_b^0	Sp/LC$_{\rm BCD}$	Sp/LC$_{\rm MK}$	Raddi et al.	$E(B-V)$	M_V
$J002441.73+642137.5$	0.291	36.5	2.85	0.80	B5-6III	B5III	B5III	1.25	−1.9
$J002926.93+630450.2$	0.355	72.3	1.51	0.85	B9V	B5-8V	B7V	0.40	1.0
$J004014.19+651644.0$	0.174	79.4	2.26	0.73	B3V	B2-3V	B2V	0.93	−1.5
$J005029.25+653330.8$	0.280	53.5	2.41	0.78	B5-6V	B3-4V	B7IV	0.99	−0.8
$J005436.84+630549.9$	0.195	63.3	2.10	0.73	B3V	B3V	B2-3V	0.83	−1.4
$J005611.62+630350.5$	0.280	69.9	1.53	0.79	B7V	B5-6V	B5V	0.45	−0.1
$J005619.50+625824.0$	0.288	70.2	1.07	0.80	B7V	B3-5V	B5V	0.16	−0.1
$J010707.68+625117.0$	0.291	60.8	2.40	0.79	B5V	B6-7Ia	B5V	0.98	−0.1
$J012405.42+660059.9$	0.246	54.8	1.94	0.76	B4V	B2-3V	B6IV	0.72	−1.0
$J012751.29+655104.0$	0.201	63.5	2.02	0.73	B3V	B3V	B7V	0.78	−1.3
$J014458.14+633244.0$	0.346	63.9	1.92	0.82	B7-8V	B3-4V	B7IV	0.63	0.6
$J014620.44+644802.5$	0.315	54.8	2.02	0.80	B6V	B5V	B7V	0.68	−0.4
$J014905.18+624912.3$	0.111	34.5	2.98	0.70	B2Ib	B2IV-III	B3IV	1.39	−5.6
$J015037.67+644446.9$	0.203	64.1	1.87	0.73	B3-4V	B3-5V	B4V	0.54	−1.1
$J015246.27+630315.0$	0.403	55.9	2.02	0.86	B9V	B8-9V	B8-9III	0.70	0.1
$J015613.22+635623.8$	0.165	68.8	1.64	0.72	B2V	B2V	B3V	0.56	−2.0
$J015918.32+654955.8$	0.321	69.0	2.22	0.85	B8V	B7-8V	B6IV	0.85	0.5
$J015922.53+635829.3$	0.234	57.1	1.91	0.75	B4V	B2-3V	B2-3V	0.70	−0.9
$J022337.05+601602.8$	0.185	52.9	2.26	0.73	B3-4IV	B3-4V	B7IV	0.93	−2.2
$J023031.39+594127.1$	0.268	50.0	1.95	0.77	B5-6V	B6-7V	B9V	0.71	−1.0
$J023404.70+605914.4$	0.184	60.5	2.71	0.73	B3-4V	B2V	B3IV	1.21	−1.5
$J023642.66+614714.9$	0.209	47.2	1.82	0.75	B3-4IV	B1-3V	B5V	0.65	−2.0
$J023744.52+605352.8$	0.142	43.6	2.52	0.70	B2III	–	B8	1.11	−3.7
$J024054.96+630009.7$	0.214	50.3	1.99	0.74	B3-4IV	B1-3V	B6	0.76	−1.6
$J024146.74+602532.2$	0.176	52.4	2.37	0.72	B2IV	B3III	B7V	1.01	−2.2
$J024159.21+600106.0$	0.197	57.6	2.18	0.73	B3-4V	B5V	B5V	0.88	−1.6
$J024317.68+603205.5$	0.120	44.2	2.26	0.70	B1III	B1.5-3III	B7V	0.95	−4.3
$J024504.86+612502.0$	0.257	43.4	2.09	0.78	B5-6IV	B6	B7IV	0.79	−1.8
$J024618.12+613514.7$	0.171	59.8	1.79	0.72	B2V	B2V	B3V	0.65	−1.9
$J025016.66+624435.6$	0.345	44.4	1.77	0.83	B7-8IV	B8-9V	B8-9III	0.57	−0.9
$J025059.14+615648.7$	0.147	62.7	1.76	0.70	B2V	B3V	B3-4V	0.64	−1.9
$J025233.25+615902.2$	0.244	40.7	1.83	0.77	B5-6III	B4V	B7V	0.64	−2.1
$J025448.85+605832.1$	0.296	59.5	1.97	0.79	B5-6V	B6-7V	B6V	0.71	−0.2
$J025610.40+580629.6$	0.161	55.2	2.04	0.71	B2V	B3-4V	B5V	0.81	−2.4
$J025700.49+575742.8$	0.152	47.1	2.24	0.71	B2III	B3-4V	B4V	0.93	−3.2

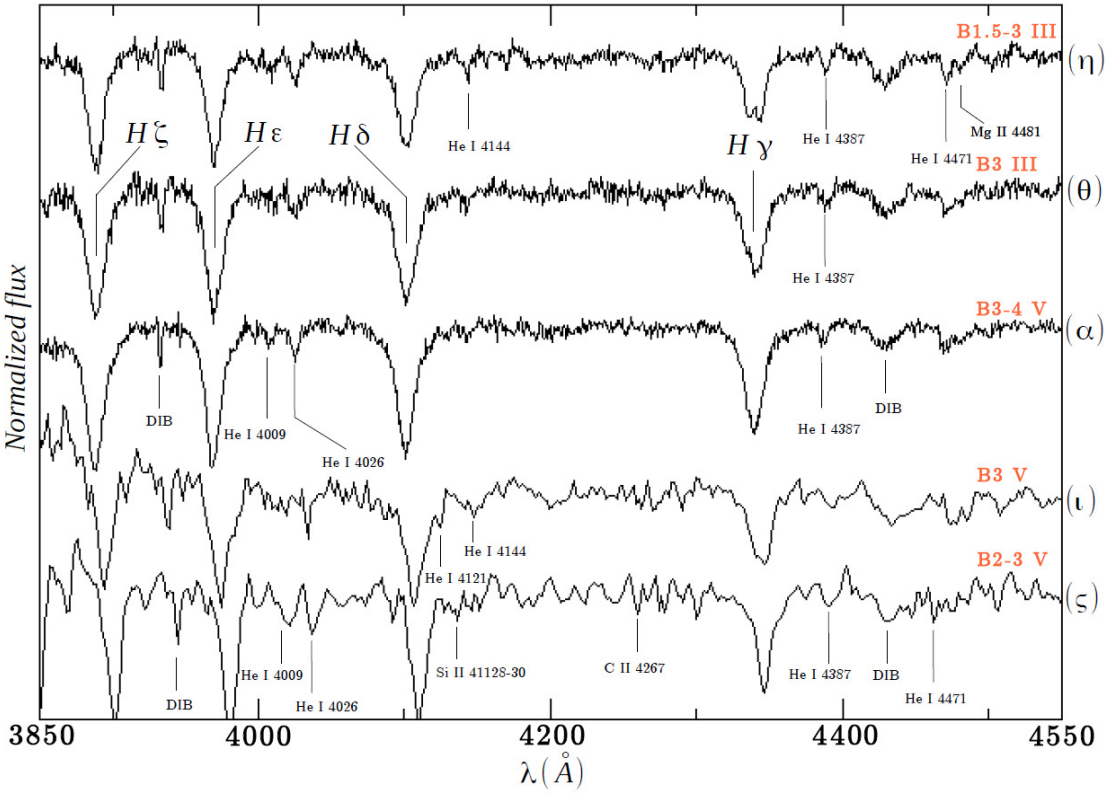

FIGURE 2.12: Five CBe stars that we have, the classification with Raddi et al. (2013), outside of the typical error. Shown here are the lines to estimate the MK spectral types. At table 2 for the detailed comparison between the systems and the spectra.

2.5.2 Validation with *uvbyβ* photometry

In Monguió et al. (2013) it is presented a catalogue of *uvbyβ* Strömgren- Crawford photometry for 35974 stars in the galactic anticenter direction. Thirteen classical Be stars for which we have FLWO/FAST spectroscopy have photometric data in this catalogue. In addition, two more CBe stars in the area of the galactic open cluster NGC 663, with available spectroscopy, have *uvbyβ* photometry published by Fabregat & Capilla (2005).

For these stars we have obtained the interstellar reddening, spectral classification and absolute magnitude, using the *uvbyβ* photometry calibrations given by Crawford (1978), Balona & Shobbrook (1984) and Moon (1986). We have followed the procedures described by Fabregat & Torrejon (1998) to apply the above calibrations to classical Be stars, for which the circumstellar emission in the Balmer and Paschen continua and in the H_β line have large effects on the photometric indices. The measurments we extracted from the above works was: V(mag), the magnitude transformed to the standard Johnson V magnitude. (b-y), Strömgren color

index in mag, c_1 index in mag, m_1 index in mag and Hβ index in mag. Where the indices can described as:

$$\begin{aligned} m_1 &= (v-b)-(b-y) \\ c_1 &= (u-v)-(v-b) \\ H\beta &= \beta_{narrow}-\beta_{wide} \end{aligned} \tag{2.6}$$

The estimation of spectral classification of Strömgren photometry can been done using the work of Crawford (1978) and Moon (1986). However, we know that our sources are Be stars and the measurments we have, are contamineted with emission from the circumstellar emvelope. Combining the works of (Fabregat & Torrejon (1998) and Crawford (1978) we summarize the iteration procedure of inproving the $uvby\beta$ photometrical indices for Be stars produced by continuum circumstellar emission:
We start by determine the quantities:

$$\Delta\beta = \beta - 2.63 \tag{2.7}$$

so that we can define the starting values for the excess in color inidices as follows:

$$E^{cs}(b-y) = -0.339\Delta\beta \qquad E^{cs}(c_1) = 0.661\Delta\beta \tag{2.8}$$

And we can then continue with the measured indices, which we correct from circumstellar excess as:

$$(b-y) = (b-y) - E^{cs}(b-y) \qquad c_1 = c_1 - E^{cs}(c_1) \tag{2.9}$$

Having the values from equation (5) we start an inner iteration as follows:

$$
\begin{aligned}
(b-y)_0 &= -0.1154 + 7.879 \cdot 10^{-2} c_1 + 9.787 \cdot 10^{-2} c_1^2 \\
&\quad +0.1681 c_1^3 - 0.6404 c_1^4 + 0.3915 c_1^5 \\
E(b-y) &= (b-y) - (b-y)_0 \\
E(c_1) &= 0.2 E(b-y) \\
c_0 &= c_1 - E(c_1)
\end{aligned}
\tag{2.10}
$$

We solve the system iteratively, c_0 taking the place of c_1 until convergence and make a better estimation for β as:

$$\beta_\star = 2.60 + 0.2517 c_0 - 0.1400 c_0^2 + 0.1704 c_0^3 \tag{2.11}$$

$$\Delta\beta = \beta - \beta_\star \tag{2.12}$$

and we continue the iteration untill $\Delta\beta$ reach convergence. The accuracy we want to reach is up to the third digit.
Having the excesses for the indices, from equations (2.9) and (2.12), we can now go back and by interpolation of table 2 in Crawford 1978 values, we can make an estimation for the CBe stars spectral type. We present our results at table 2.4 and besides spectral classification we estimated the absolute values in V band, with our procedure and for $uvby\beta$ photometry following the work of Balona & Shobbrook (1984).
The error in the spectral classification between the two methods is maximum ± 1 sub-type, as it is between the BCD system and the MK classification system. For the luminosity class, as we already explain at previus sections, we are more confident for the BCD system results, eventhough the only estimation we could do from (Crawford 1978) was between V and III luminosity classes while the BCD procedures allow a more precise separation of classes V, IV and III. We had also two sources, $J184043.19-023456.9$ and $J044010.16+475038.6$, that using $uvby\beta$ photometrical estimation had spectral types earlier than O9 and with our procedure were out of range. This is expected because we adopted to our program the limits for spectral types O8 to A2.

In Fig. 2.13 we compare the values of $E(B-V)$ obtained with the BCD and Strömgren photometry techniques. For our determination we consider an error of

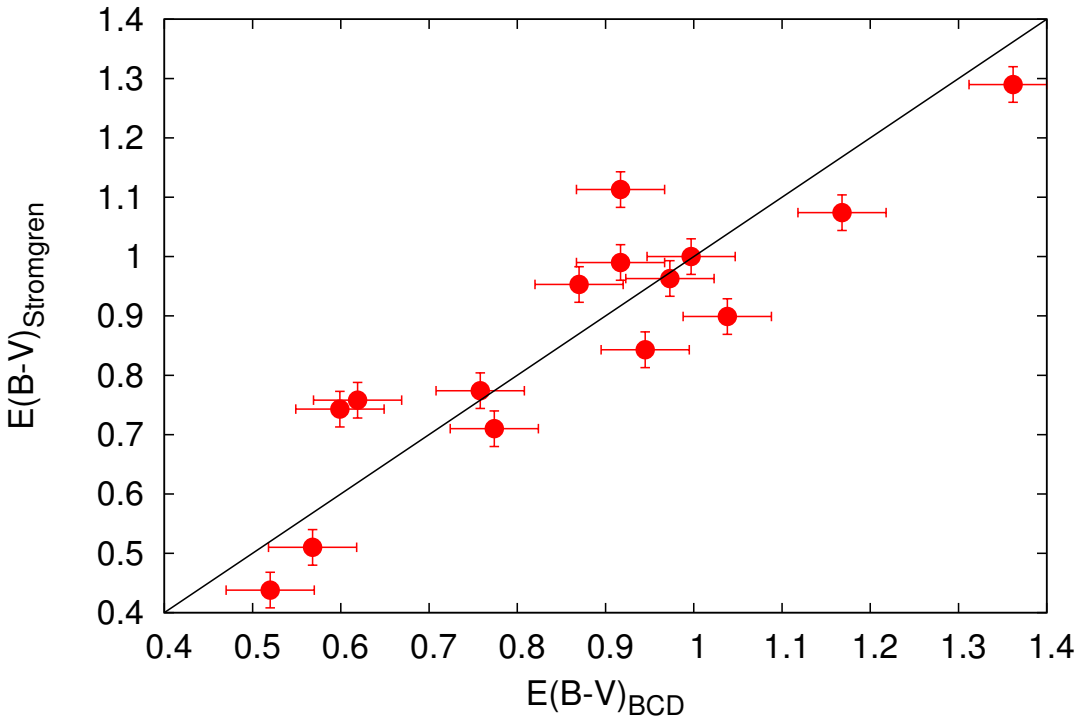

FIGURE 2.13: Comparison between the colour excess obtained from the FAST spectra with our procedure and those obtained with Strömgren photometry techniques.

0.05 mag. as in the previous subsection. For the $uvby\beta$ calibration we use the error of 0.03 mag. quoted in Fabregat & Torrejon (1998). The agreement is very good, with a mean difference of 0.00 ± 0.10 mag. In both the $uvby\beta$ calibrations and the BCD system the intrinsic colours of the stars are determined mainly from the depth of the Balmer discontinuity, measured through the c_1 index in the $uvby\beta$ photometric system and through the D parameter in the BCD system. Both determinations are consistent and lead to similar results.

2.6 Analysis of the Perseus Arm area

As a further evaluation of our procedure, in this section we present the analysis of a sample of IPHAS follow-up spectra obtained with the FLWO/FAST spectrograph. We have selected the stars located in the Perseus Arm region ($-1^o < b < 4^o, 120^o < l < 140^o$). The population of CBe stars in this area has been investigated by Raddi et al. (2013), who analysed the INT and NOT spectra described in Sect. 2.3.2, and by Raddi et al. (2015) also using a sample of FAST spectra. In both papers the spectral classification was performed by comparison with standard templates, complemented with the application of standard

TABLE 2.4: Comparison between the spectral classification and physical parameters obtained for 15 CBe stars and those obtained from Strömgren-Crawford photometry calibrations.

NAME	$D(dex)$	$\lambda_1(\mathring{A})$	Sp/LC$_{\rm BCD}$	Sp/LC$_{uvby\beta}$	$E(B-V)_{\rm BCD}$	$E(B-V)_{uvby\beta}$	$M_{V,BCD}$	$M_{V,uvby\beta}$
$J014602.11+611502.2$	0.191	67.2	B4V	B5-6V	0.917	1.113	-0.3	-0.5
$J014624.42+611037.3$	0.225	68.2	B5V	B5III	0.758	0.774	-0.7	-2.3
$J053237.14+260107.3$	0.290	47.9	B5-6V	B4V	0.917	0.990	-1.4	-1.6
$J053513.10+295912.4$	0.246	31.8	B3-4III	B3III	1.168	1.074	-2.7	-2.5
$J053554.13+295756.4$	0.221	77.9	B5V	B5V	1.362	1.290	-1.4	-0.8
$J053654.85+301757.8$	0.273	66.1	B5-6V	B5V	0.870	0.953	-0.2	-0.4
$J054033.87+274552.4$	0.398	65.4	B8V	B8V	0.619	0.758	0.5	0.2
$J054115.07+274803.2$	0.139	68.4	B2V	B3V	0.997	1.000	-1.7	-0.7
$J054159.24+274038.1$	0.254	74.6	B5-6V	B5V	0.774	0.710	-0.4	-0.4
$J054200.54+304956.6$	0.355	44.4	B7IV	B7V	0.599	0.743	-0.0	-0.1
$J054450.31+290754.5$	0.319	68.7	B7V	B7V	0.568	0.510	0.2	0.0
$J054603.64+272729.5$	0.211	48.9	B3IV	B2.5V	0.973	0.963	-1.1	-1.9
$J054837.64+281710.3$	0.179	63.4	B3V	B2V	0.945	0.843	-1.4	-0.9
$J054848.26+283547.8$	0.159	60.7	B2V	B1.5-2V	1.038	0.899	-1.5	-2.2
$J054937.88+281123.3$	0.329	70.3	B7V	B8V	0.520	0.438	0.2	0.2

procedures of the MK classification system. Both works stress the difficulty of assigning luminosity classes, due to the fact that the profiles of the Balmer lines, which provide the main luminosity indicators in the considered spectral range, are contaminated by the circumstellar emission characteristic of classical Be stars.

In the BCD system, luminosities are derived from the λ_1 parameter, which is not affected by emission. As distance determination with the spectroscopic parallax technique heavily relies on the luminosity class of the objects, it is worthwhile to reproduce the above studies with reddenings and distances computed with the techniques described in this work, in order to compare the results. Our analysis, for the first half part of this work, was done with 257 FAST spectra of 224 stars, which meet the criteria presented in Sect. 2.3. From each spectrum we determined the BCD (D, λ_1) parameters, the effective temperature, spectral type and luminosity class, interstellar and circumstellar colour excesses, absolute magnitude and distance. Results are presented in Tables 1 and 2. It took on average 2- 3 minutes of work to analyse each star by means of our semi-automatic procedure.
For 31 stars we have two spectra obtained at different epochs, and for one more, #181, three spectra. The comparison between the values of the BCD and astrophysical parameters obtained from different spectra of the same star allows us to estimate the errors involved in their determination. The mean difference between the measured D and λ_1 parameters are 0.032 dex and 7.3Å respectively. These differences are of the same order as the ranges in D and λ_1 spanned by one spectral subtype and one luminosity class respectively, as can be seen in Fig. 10 of Zorec et al. (2009). The main contribution to these errors are the differences in the relative flux calibration of the spectra from one observing run to another, or from one night to another within the same observing run.

We estimate the internal relative error in the determination of the effective temperature and distance as the difference between the individual values divided by the mean value. The mean errors measured in this way amount to 8% in T_{eff} and 24% in distance. Regarding the spectral classification, we found all sub-types from O8−9 up to A2. We found one Oe star, #66, with type O8−9IVe. The presence of visible $HeII$ lines in its spectrum confirms this classification. In Fig. 2.15 we present the histogram of the CBe star sample distribution as a function of the spectral types.
The spatial distribution found for the CBe star sample is presented in Fig. 2.16, where the 224 stars with distances listed in Table 2 are plotted. For stars with

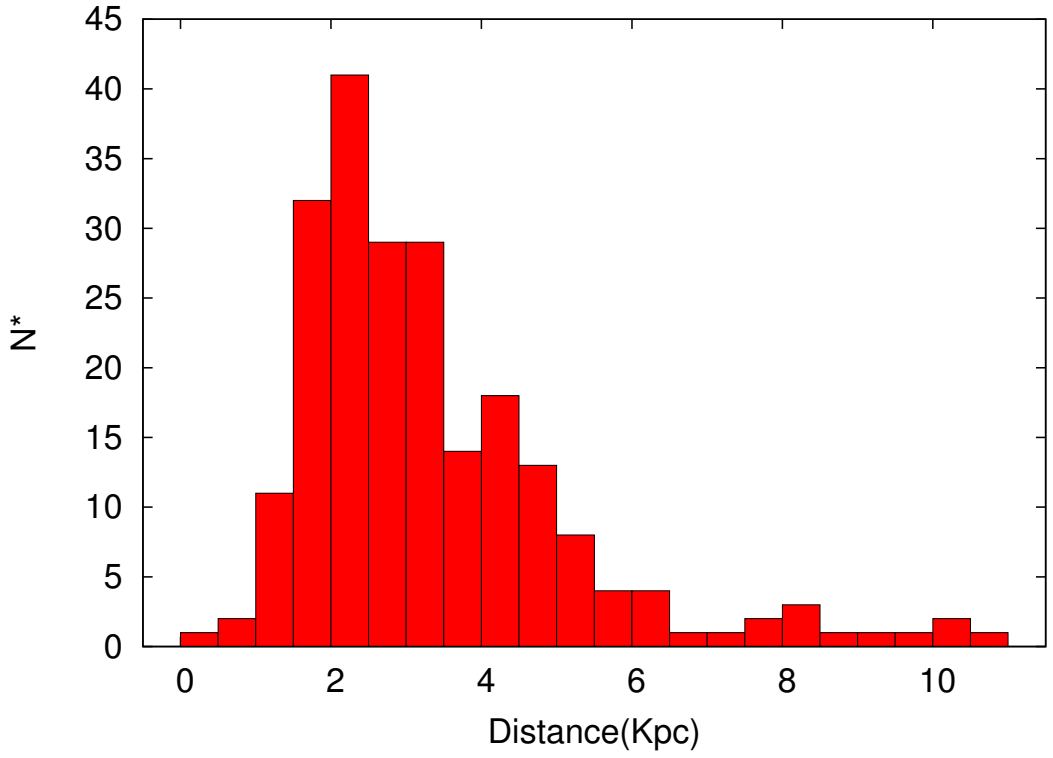

FIGURE 2.14: Histogram distribution of the distances. Most of the stars are placed between 1.5 and 3.5 kpc, where the Perseus Arm is expected to be.

more than one spectrum we used the mean value of the distance determinations. The locations of the Perseus and Outer Galactic arms are marked with dotted lines, following the range of distances given by Russeil et al. (2007). In blue it is the Perseus Arm at $\sim 2-3.5$ kpc. and in green the Outer Arm at $\sim 6-7$ kpc. The distribution of the stars does not present an apparent clustering in or around these two structures. Instead, they appear scattered along the two arms and the space in between, with some stars spreaded along larger distances, beyond the expected location of the Outer Arm. In Fig. 2.14 we present an histogram of the measured distances.These results are consistent with the findings of Raddi et al. (2013).

For ten stars we found distances in excess of 9 kpc., well beyond the expected location of the Outer Galactic Arm. Five of them have distances larger than 11 kpc and hence they are out of the scale of Fig. 2.14. These distances can be due in some cases to large errors in the absolute magnitude or the spectral classification of the stars. A detailed discussion on the uncertainties and possible biasses in distance determination based on absolute magnitudes was given in Raddi et al. (2013). We are however studying in detail a few stars in which the large distance seems to be consistently derived from high signal to noise spectra, in order to use them as tracers of the stellar population in the outskirts of the galactic plane.

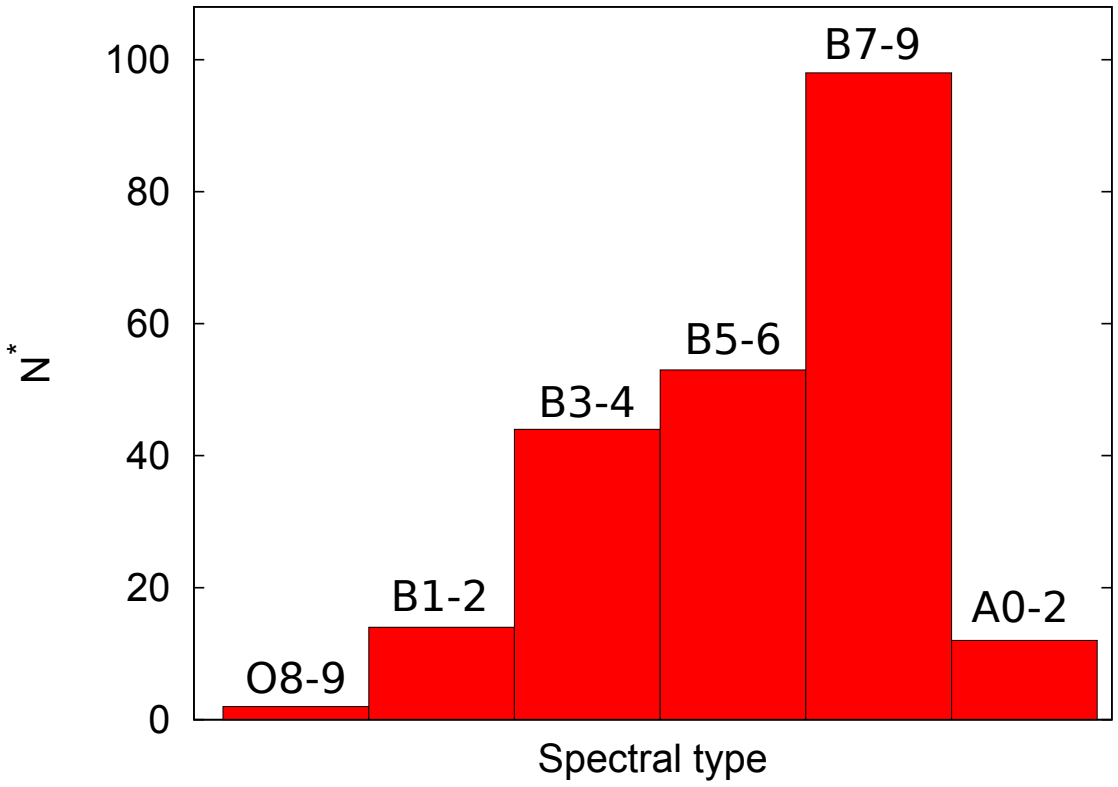

FIGURE 2.15: Histogram distribution of the spectral types.

2.6.1 Conclusions

This chapter we presented a study of a part of the population of CBe stars photometrically detected by the IPHAS survey, and use them as galactic structure tracers. The study will be based on the analysis of follow-up spectroscopy obtained at the FLWO telescope with the FAST spectrograph.

In this chapter we have presented the method devised to obtain the spectral classification and the astrophysical parameters of the stars from the FLWO/FAST spectra. For this purpose we have developed a semi-automatic procedure based on the BCD (Barbier-Chalonge-Divan) spectrophotometric system. We have validated the method by comparing its results for two samples of CBe stars with independent results for the same stars obtained with different astrophysical techniques. In particular, we compared our results with those obtained with spectral template fitting and MK classification system standard techniques for one of the samples, and with Strömgren photometry standard calibrations for the other. In both cases we obtained a general good agreement in the spectral classification, within two spectral subtypes and one luminosity class for most of the stars.

We have also analysed a sample of CBe stars in the direction of the Perseus Arm ($-1^o < b < 4^o, 120^o < l < 140^o$). We didn't find any significant clustering of stars

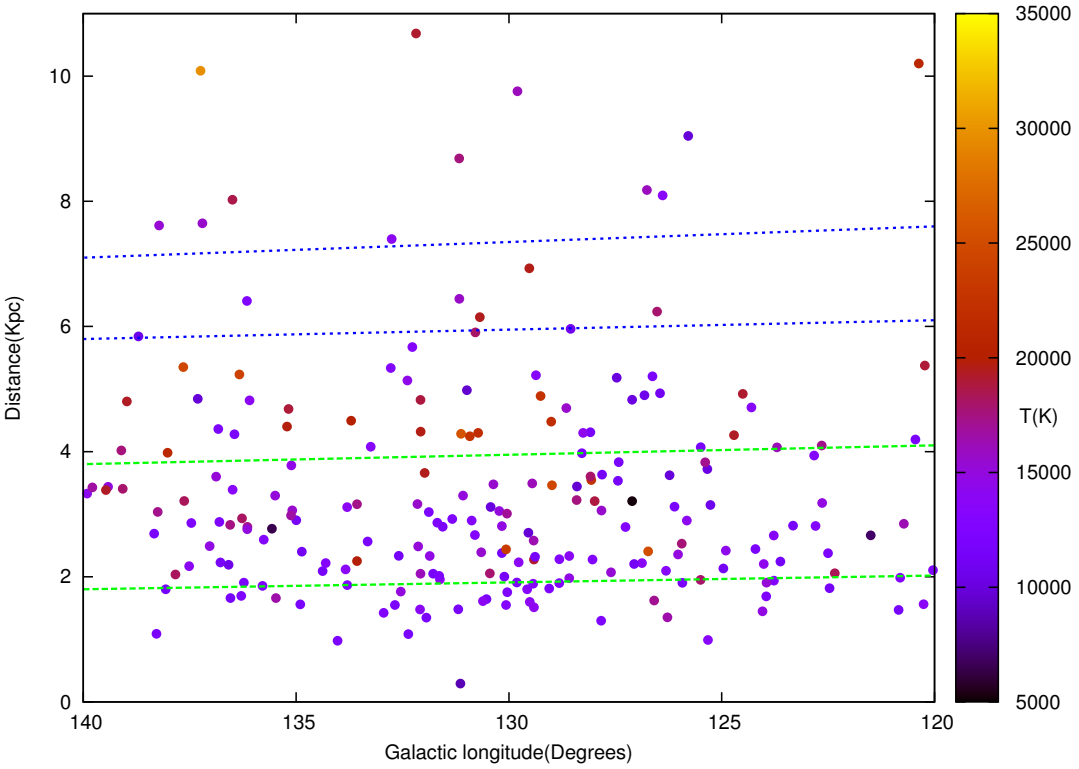

FIGURE 2.16: The distribution of the CBe stars distances as a function of the Galactic longitude. The green and blue dashed lines mark the expected positions of the Perseus and Outer Galactic arms, respectively. Five stars are at distances too long to appear in the diagram. The colour bar at the right represents the effective temperature of the stars.

at the expected distances of the Perseus and Outer Arms. Even with over three times the number of stars considered by Raddi et al. (2013) we obtain the same negative result, indicating that the errors involved in the spectroscopic parallax and absolute magnitude determination blur any hint of Galactic spiral structure, if indeed the CBe stars trace it. In the next chapter we present the analysis of the whole sample of the IPHAS CBe stars for the anticenter-region of the Galactic disc. Together with astrophysical parameters of 732 CBe stars and the study on their nature.

Chapter 3

Overall analysis of FAST spectra.

In the previus chapter we describe in detail the procedure we have developed to obtain CBe stars astrophysical parameters from low resolution spectra. We have analysed a subsample of the stars presented here, and validated the method employed by comparing our results with independent results for the same stars obtained with different astrophysical techniques. We also present a discussion on the reliability of the relative flux calibration of the spectra, and a detailed evaluation of the errors involved in the measured spectral parameters and in the physical quantities derived from them.

In this chapter we present an overall analysis of the whole sample of FAST spectra (2627 low-resolution specta). We have used these data to study several key issues regarding the physics of the CBe stars as a class, in particular their rotational velocities, evolutionary status and velocity law in the circumstellar disc. In addition, we have used our sample to contribute to the investigation of the spiral structure of the Galaxy in the Northern Hemisphere, using them as tracers and the standard techniques of spectroscopic parallax to measure their distances. These sources are likely to be observed at higher spectral resolution and signal to noise within the framework of the WEAVE surveys (Dalton et al., 2014), and will obtain accurate trigonometric parallaxes from Gaia in the near future. Therefore, their proper characterisation would also aid their future exploitation for more detailed studies of CBe star physics and of Galactic structure.

3.1 IPHAS CBe stars catalogue

For this work we selected by visual inspection the sources with spectral features characteristic of OB-type stars. 1120 spectra were selected for 1026 OB-emission line stars. Among them we selected the spectra having a well defined continuum and a S/N $\geq$ 30 around the Balmer discontinuity at $\approx$ 3700 Å, the spectral region that we will use to measure the BCD spectral parameters. This leads to a final sample of of 823 spectra of 732 stars, whose analysis we present in this section.
The determination of the stellar physical parameters was done by means of the techniques and calibrations of the Barbier-Chalonge-Divan (BCD) spectrophotometric system. The BCD system was developed by Barbier & Chalonge (1941), and later by Chalonge & Divan (1952). It is based upon measurable parameters around the Balmer discontinuity (BD), in the $3200 - 4600$ Å spectral range. The basic parameters that describe the energy distribution around the BD are: D, the Balmer jump depth, given in dex, which is an effective temperature indicator;λ_1, the position of the Balmer discontinuity, given in Å as the difference with respect to 3700 Å, which is sensitive to the surface gravity; Φ_b, a spectral gradient which represent the slope of the Paschen continuum near the BD; and Φ_{uv}, the slope of the Balmer continuum. A modern description of the BCD system, together with a presentation of its advantages compared to other spectroscopic systems, is given by Zorec et al. (2009). In chapter 1 we give a detailed description of how the BCD parameters are measured from the spectra of the normal, absorption-line stars, and the procedures to follow in the case of CBe stars, where, due to the lower pressure of the circumstellar disc, a second Balmer jump arises in the ultraviolet region.

For the analysis of the data and the determination of the astrophysical parameters we have developed a semi-automatic procedure, described in chapter 2. The input of the programme are the observed spectra, with the wavelength scale in Å and the flux in $ergs^{-1}cm^{-2}$. In a first step, the spectral parameters D,λ_1 and Φ_b are measured, with mean errors of $0.032dex, 7.3$Åand 0.16 respectively. From these values we calculate the effective temperature, the spectral type and luminosity class, and the interstellar reddening. The values of all these parameters are given in Tables 1 and 2 .

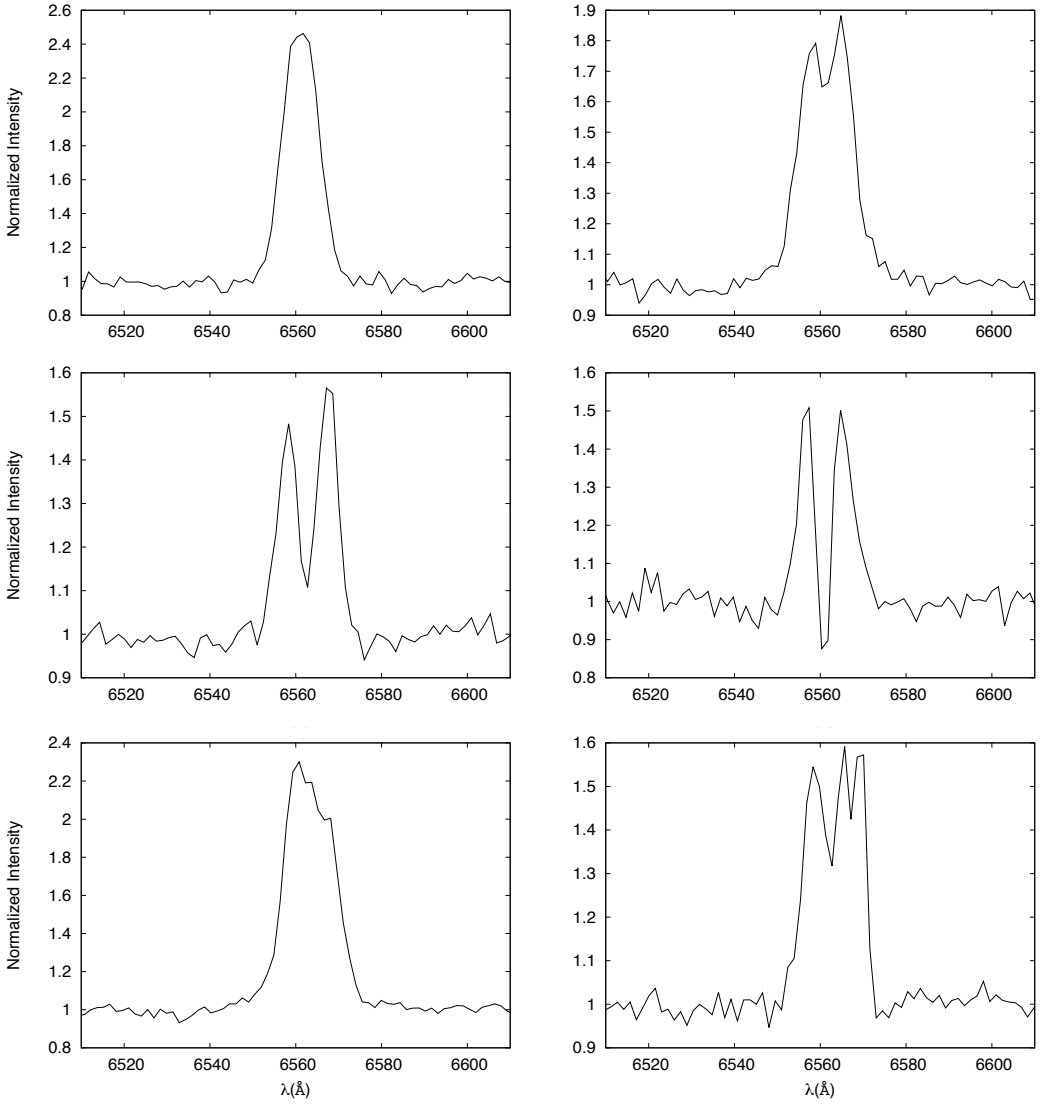

FIGURE 3.1: $H\alpha$ emission line profiles we found out in our sample. Up left we present an example of single-peak profile. Up right, a double peak as the midle left. A shell profile in the midle right figure. On the bottom left a left side peak profile and on the bottom right we have a triple peak or an uncanonical peak profile.

The effective temperature is obtained by means of the calibration given by Zorec et al. (2009). This calibration is applicable in the range $0.0 < D < 0.5$. Stars with $D > 0.5$ appear with a $T_{eff} < 9500K$ in Table 1 . The mean error of our T_{eff} determination is 8%, as discussed in the previus chapter. Spectral type and luminosity class are obtained from the same reference, by interpolating the D and λ_1 values of each star in their Fig. 10b. The distribution of the spectral types is presented in 3.2. Only two stars have been classified as Oe, namely stars #73 and #739 in Tables 1 and 2 , with spectral types O8-9IV and O8-9V respectively. The presence of He II lines at $\lambda\lambda 4200, 4541$ and 4686 Åin the spectra confirms this

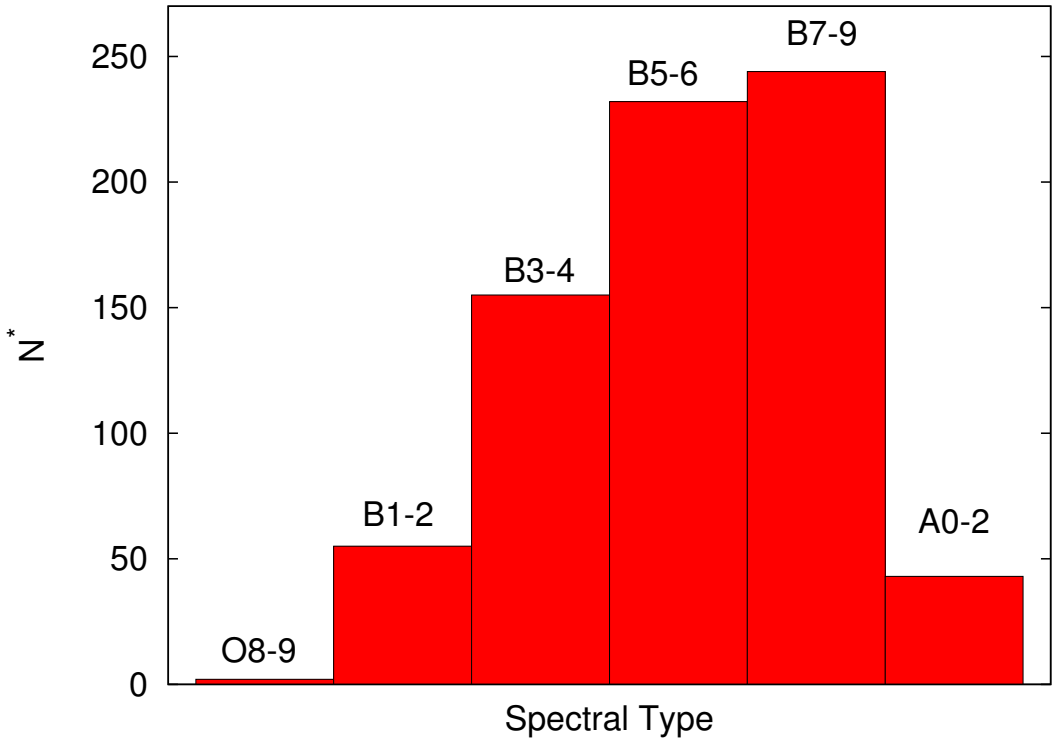

FIGURE 3.2: Histogram distribution of theCBe stars spectral types found in this work.

classification.

Interstellar absorption is calculated by means of the expression 1.1:

$$A_\nu = 3.1E(B-V) = 1.7(\Phi_{rb} - \Phi^0_{rb}) = 2.1(\Phi_b - \Phi^0_b)mag$$

(Aidelman et al. 2012), where Φ^0_b is the intrinsic gradient obtained from D and λ_1 by means of the calibration given in Chalonge & Divan (1973). The mean error of the $E(B-V)$ obtained in this way is 0.012 mag.

Absolute magnitudes in the Johnson V band (M_V) are directly obtained from the D and λ_1 parameters by means of the calibration given in Table 3 of Zorec & Briot (1991). The calibration is constructed for the range $0.0 < D < 0.5dex$ and $30 < \lambda_1 < 70$Å. Stars with spectral indices outside this range have no M_V values in Table 2 . M_V magnitudes are converted to absolute IPHAS r magnitudes using the intrinsic $(V - R_C)$ colours for dwarfs and giants supplied by Fabregat (in preparation), and assuming that Cousins R_C and IPHAS r magnitudes in the Vega system are identical within the errors involved in our procedure.

Distances are obtained by means of the standard spectroscopic parallax techniques, by comparing the absolute M_r magnitudes with the observed r magnitudes supplied in the IPHAS Second Data Release (IPHAS DR2, Barentsen et al. (2014)),

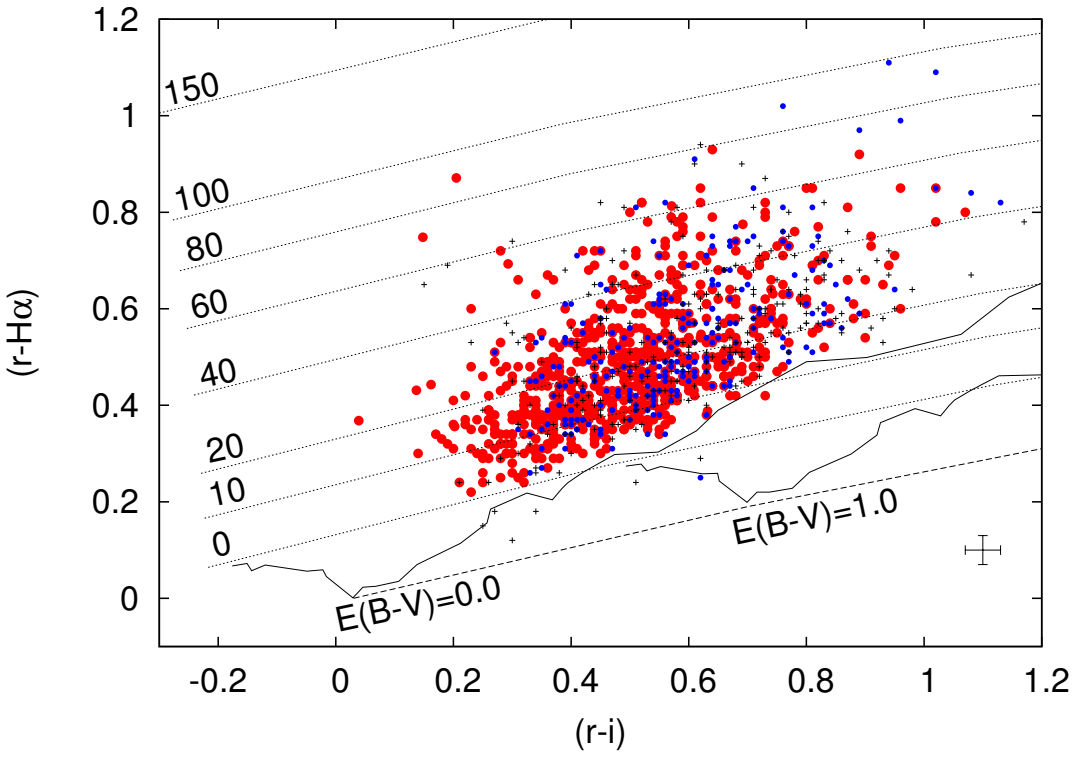

FIGURE 3.3: Colour-colour diagram of the IPHAS CBe star sample. Red dots represent the stars studied in this work, blue dots the stars in Raddi et al. (2015) and black crosses the remaining stars (see text). The black solid curves are synthetic main sequence loci (Drew et al., 2005). The lower dashed curve is the early A reddening line, and the dot-dashed curves are lines of constant Hα emission, whit the corresponding equivalent width indicated on the left-hand side. On the bottom-right side of the figure the mean colour uncertainties are indicated.

corrected for the interstellar absorption and the circumstellar excess due to the added flux of the disc emission. The intrinsic r magnitudes corrected for interstellar absorption were computed using the relationship $A_r = 0.84 A_V$, from Fiorucci & Munari (2003).

To correct for CBe circumstellar continuum emission we used the procedure described in Chapter 1, which follows the method presented in Raddi et al. (2013) and Dachs et al. (1988), based on the correlation between HαEW and the circumstellar colour excess $E^{cs}(B-V)$. From these values we obtain the circumstellar emission in the r band, Δr, by interpolating in Table 5 of Raddi et al. (2013). The Δr correction applied for each source is given in Table 2 .

To obtain the bolometric magnitudes we calculate the bolometric correction as

a function of the effective temperature by means of the relations given by Torres (2010). From them we calculate the stellar radius and luminosity using the following standard formulae:

$$M_{bol} - M_{bol,\odot} = -2.5 \log L/L_{\odot} \tag{3.1}$$

$$M_{bol} = 42.36 - 5 \log R/R_{\odot} - 10 log T_{eff} \tag{3.2}$$

Cox (2000), assuming $M_{bol,\odot} = 4.74 mag$. In 3.6 we plot the HR diagram for our sample of CBe stars, together with the evolutionary tracks computed for stars with and without rotation by Ekström et al. (2012). We finally obtained masses and stellar ages by interpolating in the evolutionary tracks with rotation. All these values are presented in Table 2 .

To derive rotational velocities we applied the methodology that it is described at Steele et al. (1999) in which they follow previus work from Slettebak et al. (1975). We fitted Gaussian profiles at four HeI lines, 4026Å, 4143Å, 4387Å and 4471Å. Due to the high S/N and the weak intensity of the HeI lines, we could reliably fit the Gaussinan profile to less than 50% of the stars. The $vsini$ was calculated from the average of the full width half maximum of the Gaussian fits as:

$$vsini = 41.25 F(4471) km/s \tag{3.3}$$

$$vsini = 42.03 F(4387) km/s \tag{3.4}$$

$$vsini = 44.51 F(4143) km/s \tag{3.5}$$

$$vsini = 45.82 F(4026) km/s \tag{3.6}$$

where $F(\lambda)$ is the full width half maximum in $\mathring{A}$ at a wavelength of $\lambda(\mathring{A})$. The $vsini$ quoted in Table 2 is the mean of those derived from all the four fitted lines for each star, after correcting for the mean instrumental velocity dispersion determined from lines in the FAST HeNeAr wavelength calibration spectra. An histogram showing the rotational velocity distribution of our sample is presented in 3.9.

We have also measured the equivalent width and other parameters of the Hα line for all stars in our sample. The largest measured HαEW are –92, –66 and –62 Å, for stars #144, #445 and #729 respectively. The rest of the stars have EW lower than –60 Å. An histogram of the frequency distribution of the HαEW is presented in Fig.3.5.

In Fig.3.4 we present a comparison between the spectroscopic HαEW and the values estimated from the photometry by interpolating the IPHAS colours between the curves of constant Hα equivalent width computed in Drew et al. (2005). These curves are plotted in Fig. 3.3. From the data in Fig.3.4 we derive a relationship between the photometric and the spectroscopic determinations in the form:

$$\mathrm{H}\alpha EW(photometric) = 1.01\mathrm{H}\alpha EW(spectroscopic) + 2.59 \qquad (3.7)$$

The relation shows a good agreement between both determinations, although the photometric HαEW is systematically larger by a mean value of 2.6 Å with respect to the spectroscopic one. In fig. 3.4 figure we present a comparison between the spectroscopic equivalent width versus the photometric estimations that have been made by means of interpolation of the theoritical models of Drew et al. (2005).

The spectra of twenty stars, representing 2.7% of the sample, display the Hα line in absorption; their photometric colours, however, place them in the region occupied for the emission line stars in the IPHAS colour-colour diagram (Fig.3.3). Conversely, the six stars below the line of 0 Å equivalent width in Fig.3.3, belonging to the Raddi et al. (2015) and the additional samples described is Sect. 2, whose photometry indicates they are absorption-line stars, display the Hα line in emission in their spectra. We interpret these differences as due to phase transitions from emission to absorption or vice versa, originated for the well known variability of the Be phenomenon, in the interval between the acquisition of the photometric and spectroscopic data. The fact that more stars change from emission to absorption than the opposite is a selection effect. Most of the stars selected for spectroscopic observations present photometric colours characteristic of emission line stars, while few objects with normal absorption-line star colours were followed-up spectroscopically. The referred to variability of the Be phenomenon is also responsible of most of the scatter in the relationship presented in Fig. 3.4.

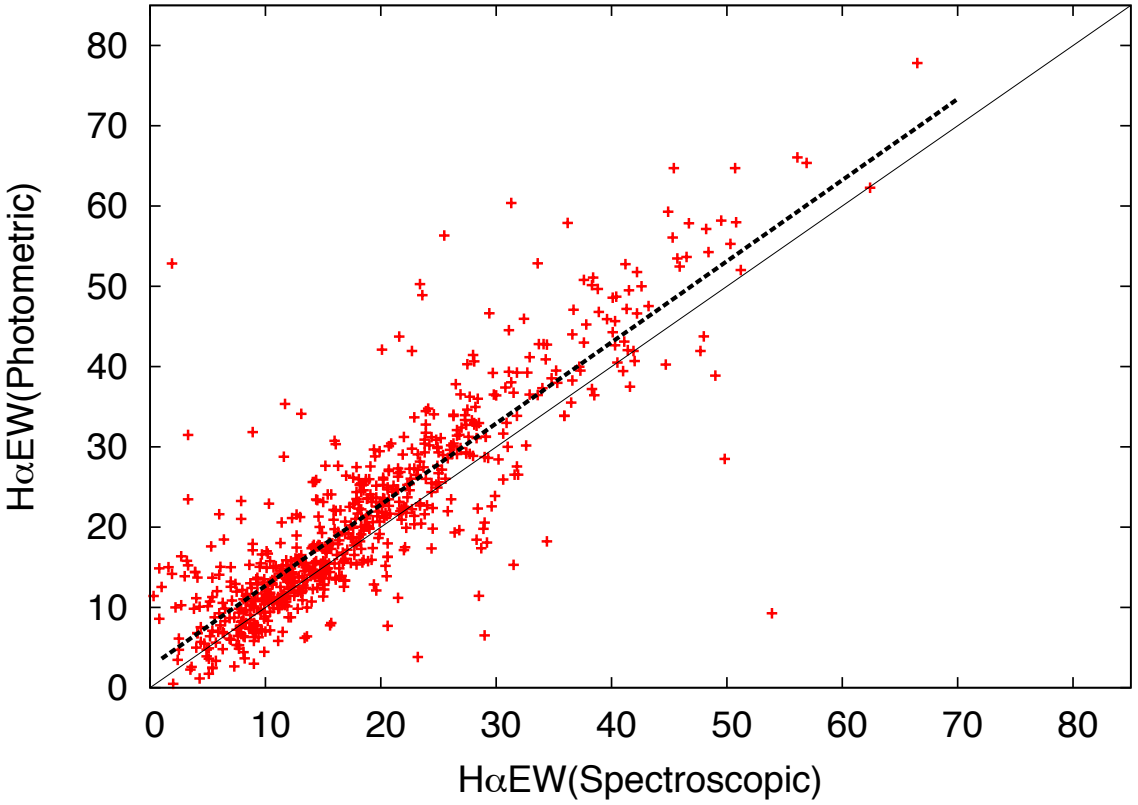

FIGURE 3.4: Comparison of the HαEW(Å) between the spectroscopic measurments and the photometric. The photometric estimations have been made by means of interpolation of the dot-dashed curves lines of constant Hα emission (corresponding equivalent widths are indicated on the left-hand-side of the right colour-colour diagram) Drew et al. (2005).

In 108 stars the Hα line in emission presents a double-peaked profile. For these objects we have measured the peak separation in kms^{-1} and the V/R ratio, defined as the ratio between the peak intensities of the violet and red components of the line. The obtained values, together with the measured HαEW for all the stars, are presented in Table 1 .

3.2 Evolutionary status-HR diagram

It has been proposed that the Be-phenomenon is an evolutionary effect which appears during the second half of a B star main sequence lifetime Fabregat & Torrejón (2000). Zorec et al. (2005) found a similar result for late-type CBe stars, but propose that early-type CBe stars appear mainly in the first half of the main

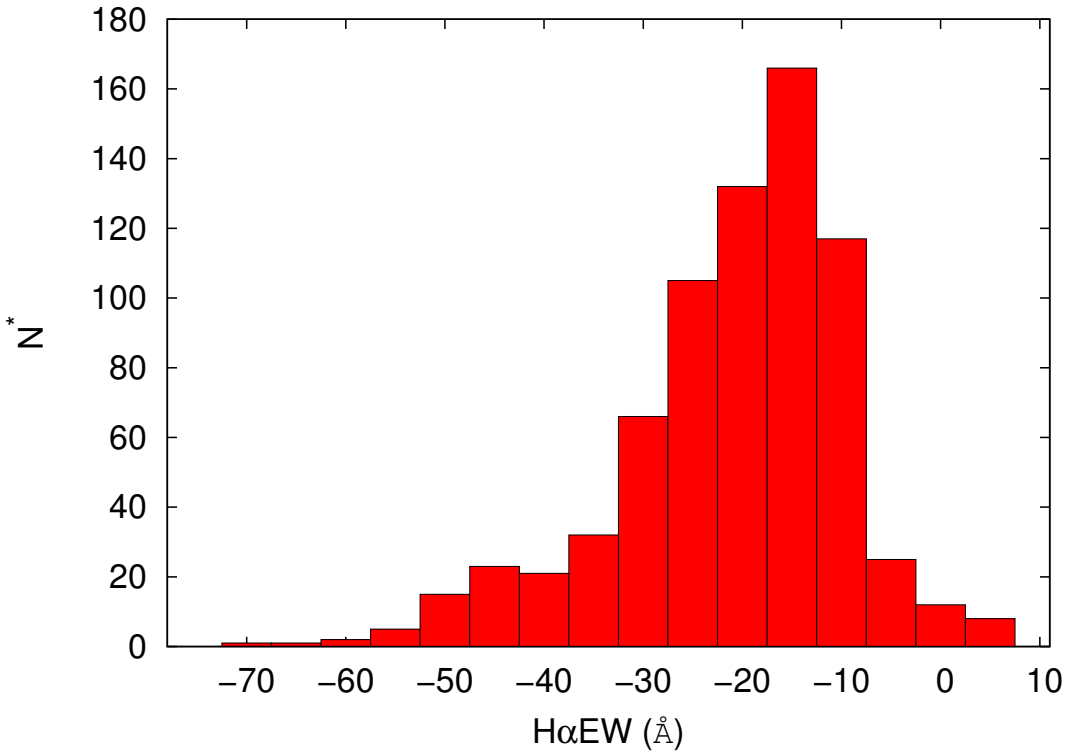

FIGURE 3.5: Histrogram of the measured HαEW.

sequence. However, Martayan et al. (2007) found a significant number of CBe stars at the ZAMS, rotating faster than young B stars in general. This would imply that the CBe nature is innate, and not an acquired characteristic of a fraction of B stars. In the recent literature many other authors have addressed these issues with different, often contradictory conclusions.

In 3.6 we represent the distribution of the ages obtained for the stars in our sample, normalised to the time the star will spend in the main sequence according to the models for rotating stars by Ekström et al. (2012). In the left panel we present the distribution of the normalised ages with respect to the effective temperature. The stars appear distributed along all the diagram, with a larger concentration below the normalised age of 0.5 for the later spectral types. The histogram presented in 3.7, right panel, also show that there are more CBe stars in the first half of the main sequence lifetime than in the second. Hence, our results do not support the claim of an evolutionary nature of the Be phenomenon. Another feature in the left panel is the apparent lack of CBe stars in or near the ZAMS in the $4.2 < \log T_{eff} < 4.4$ interval, although, due to the errors involved in our physical parameters determination, we do not consider this feature as significative.

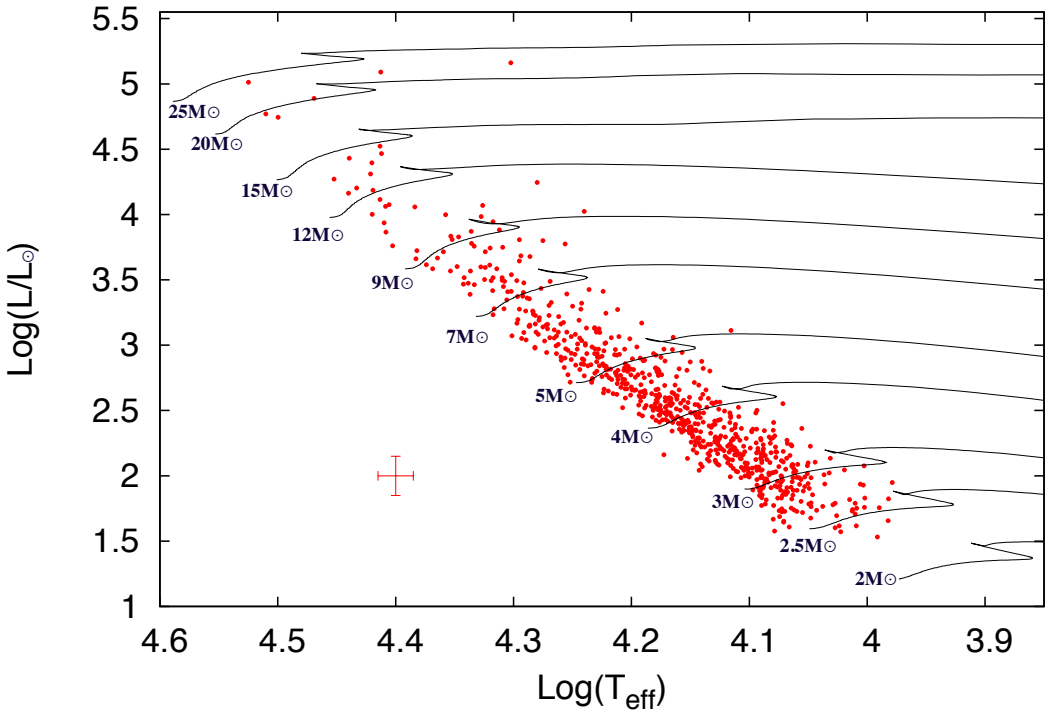

FIGURE 3.6: Distribution in the HR diagram of the IPHAS CBe stars. The evolutionary tracks are fromEkström et al. (2012), without rotation effect.

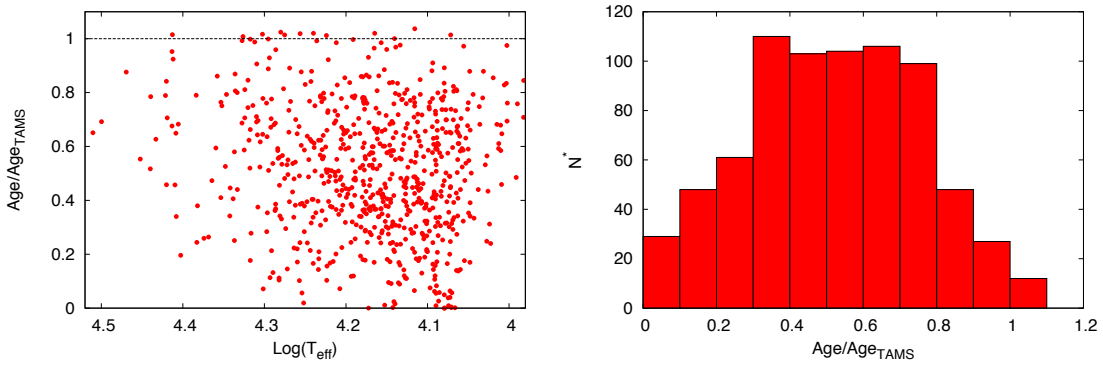

FIGURE 3.7: The distribusion of the Ages normalized with the TAMS of each star.

3.3 Rotational Velocities

It is now well established that CBe stars as a class are fast rotators, with a wide distribution of rotational velocities between about 75% and 100% of the critical value (the velocity at which material will escape from the equator due to the centrifugal force). To obtain the mean rotational velocity of our sample, we have computed for each star the ratio between the measured velocity and the critical one, which we label as Υ following the notation proposed by Rivinius et al. (2013):

$$\Upsilon = \frac{v_{rot}}{v_{crit}} \tag{3.8}$$

Where

$$v_{crit} = \sqrt{\frac{2}{3}\frac{GM}{R}} \tag{3.9}$$

M and R are the mass and radius of the star derived in the previous section. We assume that the obtained radii are representative of the polar radius of each star as, due to gravity darkening, for near critical rotators a large fraction of the photospheric light used to derive the radiative parameters come for the polar regions. With this assumption, the factor 2/3 in eq. 3.9 comes from the oblateness of $R_{eq} = 3/2R_{pole}$ for critical solid body rotation. In 3.8 we present the distribution of the Υ values for our sample.

The mean value of the distribution is $\overline{\Upsilon \sin i} = 0.65 \pm 0.23$. To derive the mean rotational velocity we used the relation given by Chandrasekhar & Münch (1950):

$$\frac{\overline{\Upsilon}}{\overline{\Upsilon \sin i}} = \frac{4}{\pi} = 1.27 \tag{3.10}$$

We obtain $\Upsilon = 0.82 \pm 0.17$, where the quoted error is the root mean square deviation, also computed following the above reference. This indicates that the CBe stars in our sample rotate with a mean value of 82% of their critical velocity. This value is in good agreement with other previous determinations from different CBe star samples in the recent literature, for instance $\Upsilon = 0.83 \pm 0.03$ Chauville et al. (2001), $\Upsilon = 0.81 \pm 0.12$ Rivinius et al. (2006) and $\Upsilon = 0.82 \pm 0.08$ Meilland et al. (2012).

Yudin (2001) and Cranmer (2005) found a strong dependence of the rotational velocity on the spectral type, with a mean value of $\Upsilon \approx 0.5$ for the early-type (O7e–B2e) stars and an increase as T_{eff} decreases which reach up to $\Upsilon \approx 1.0$ for

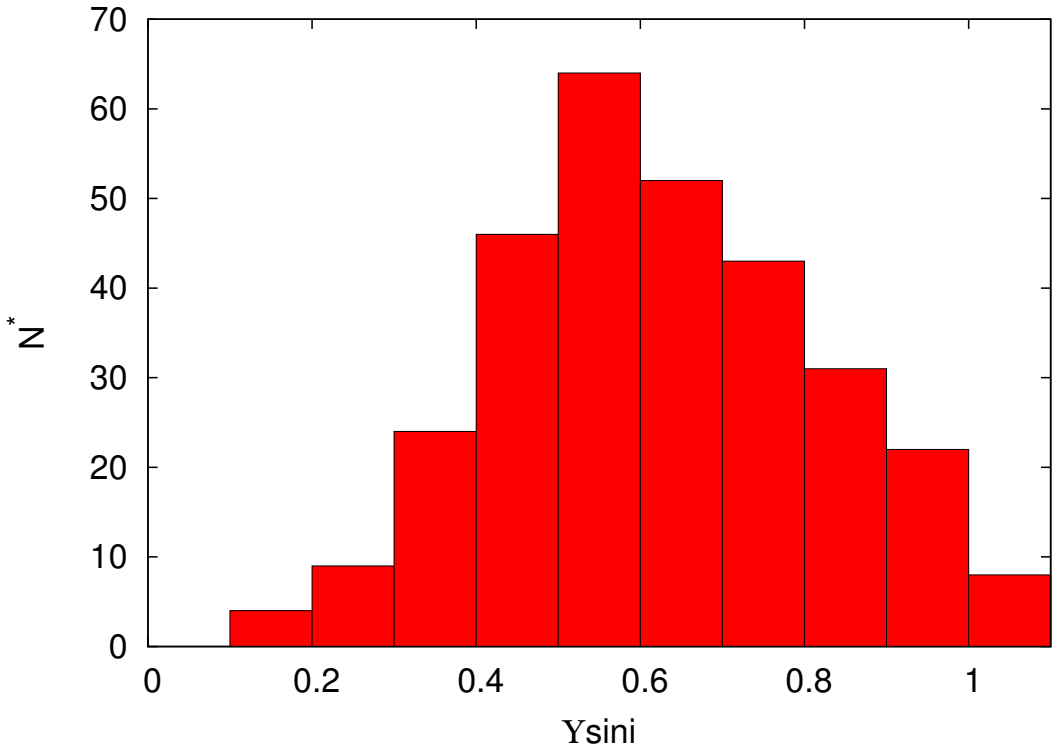

FIGURE 3.8: Υ histrogram distribution.

the coolest CBe stars. However, other authors (e.g. Chauville et al. (2001) ; Rivinius et al. (2006) ; Meilland et al. (2012)) did not found any significant trend of the rotational velocity with T_{eff} . Howarth (2007) notes that the catalog of *vsini* data used by the former authors shows systematic differences with other sources, and it is not homogeneous in itself.

To contribute to this discussion we have divided our data in three subsamples sorted by spectral type, and calculate the mean rotational velocity for each of them. We obtain $\Upsilon = 0.88 \pm 0.10$ for the O9e-B4e interval, $\Upsilon = 0.80 \pm 0.12$ for B5e-B6e, and $\Upsilon = 0.82 \pm 0.25$ for the late B7e-A0e stars. Hence our data do not show any trend of variation of the rotational velocity with the spectral type.

3.4 Disc rotation

The rotational velocity law of the particles in the circumstellar disc can be approximated by a power law,

$$v_{rot} = v_0 (r/R_{eq})^{-j} \tag{3.11}$$

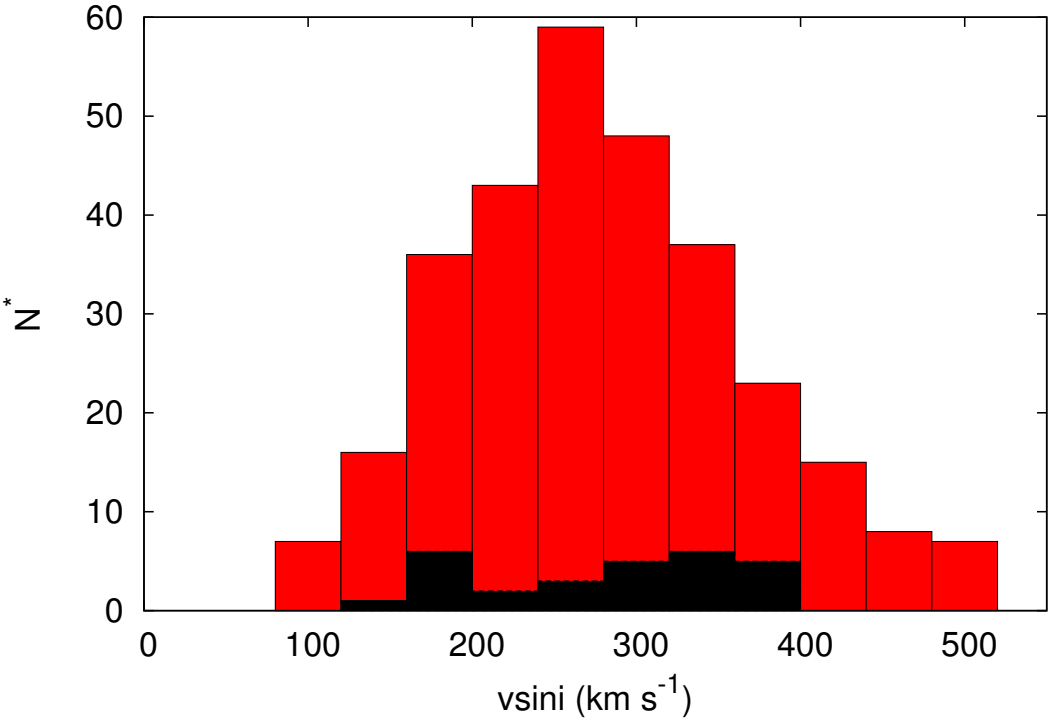

FIGURE 3.9: Histogram of the rotational velocities. In red we show the luminosity class V and in black the classes IV and III

where R_{eq} is the equatorial stellar radius and $v_0 = v_{rot}(R_{eq})$ (Dachs et al., 1992). Three distinct idealized cases for the disc kinematics have been considered for the support of the disc, depending of the choice of the exponent j: i) $j = 1$ when the dominant force on the material is the radially directed radiation pressure that does not exert any torque, and hence the specific angular momentum of the material is conserved; ii): $j = -1$ corresponds to rigid rotation, as in the case of plasma trapped by a strong magnetic field and forced to corotate with the star; iii): $j = 1/2$ in the case of a Keplerian velocity field, in which the disc is rotationally supported. Recent theoretical developments and observational evidence eventually confirmed the case of Keplerian rotation (see Rivinius et al. (2013) for references), which is nowadays generally accepted. From our data we can independently derive the type of rotational velocity law, by means of the relationship between the peak separation in double-peaked profile lines, ΔV, and the equivalent width HαEW of these lines for a sample of stars, derived by Hanuschik (1988)

$$\log(\frac{\Delta V}{2V sini}) = -\alpha \log[-H_\alpha(EQW)] + b \tag{3.12}$$

where $a = j/2$, and b is related to the electron density in the disc. We calculated this relationship for a sample of 91 CBe stars for which we have both ΔV and $vsini$,

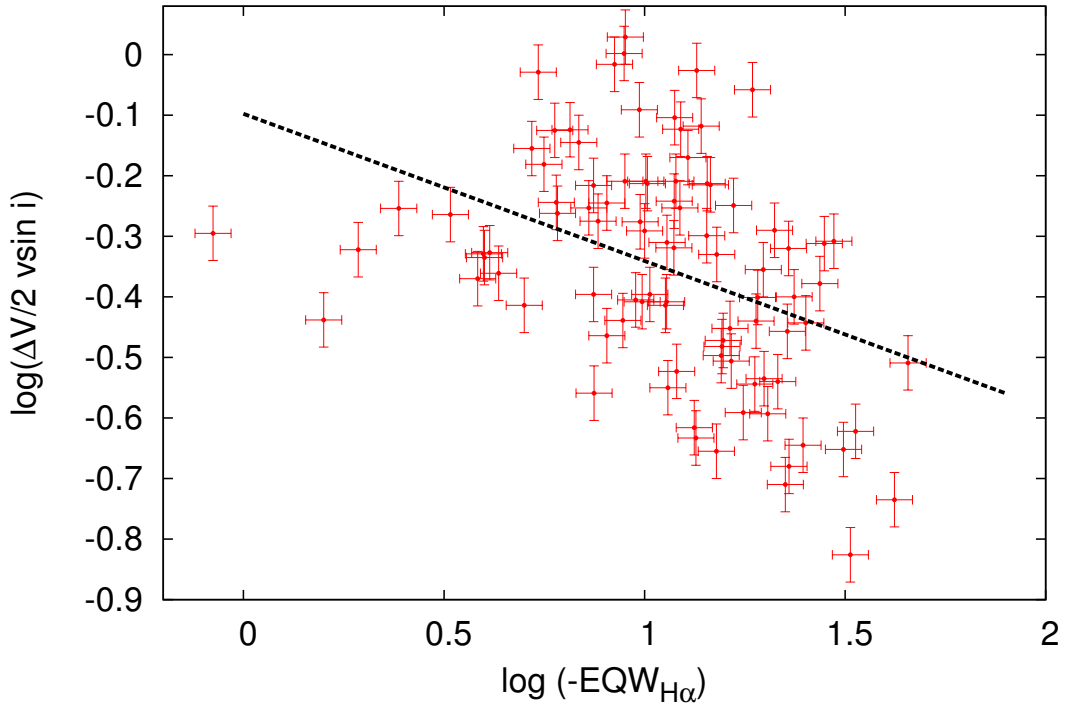

FIGURE 3.10: Fit (black dashed line) in the $\log[-H_\alpha(EQW)]$(Å) versus $log(\Delta V/2v\sin i)$ from 91 CBe stars that we could measure the $V\sin i$ and also found with a double peak profile in the Hα emission line.

obtaining $a = 0.24$ and $b = -0.09$. The a value translates into $j = 0.48$, in very good agreement with the value of $j = 0.5$ expected in the case of a Keplerian disc. In 3.10 we represent the relation between the peak separation and the equivalent width of the Hα line.

3.5 Spatial distribution

In Fig. 3.12 we present the distribution in the sky of the CBe stars discussed in this work, along the strip $-5^o < b < 5^o$, $29^o < l < 215^o$ covered by the IPHAS survey. An uneven distribution along galactic longitude is apparent, with larger densities in the region $110^o < l < 140^o$ and low populated areas around $l = 40^o$ and 80^o. This distribution is related with the variation of the interstellar extinction along the Galactic plane, being the regions of low density of stars coincident with the high extinction directions. In 3.13 we compare the spatial distribution of CBe stars in the Galactic plane with with the extiction map at $b = 0$ from Sale et al. (2014) to illustrate this correlation.

A remarkable feature is the apparent lack of stars at positive galactic latitudes in

TABLE 3.1: 22 GHz water mazer sources

NAME	Arm	longitude(degrees)	Reference
G135.27+02.79	Outer	135.00	Hachisuka et al. (2009)
G075.29+01.32	Outer	75.30	Sanna et al. (2012)
G160.14+03.15	Interarm	160.14	Reid et al. (2014)
G211.59+01.05	Interarm	211.59	Reid et al. (2014)
G196.45-01.67	Interarm	196.45	Asaki et al. (2014)
G097.53+03.18	Outer	97.53	Hachisuka et al. (2015)
G168.06+00.82	Outer	168.06	Hachisuka et al. (2015)
G182.67-03.26	Outer	182.67	Hachisuka et al. (2015)
W3OH	Perseus	133.94	Xu et al. (2006),Hachisuka et al. (2006)
G14.33-0.64	Sagittarius	10.33	Sato et al. (2010)

the anticenter direction. Very few stars appear at $l > 190^o$ and $b > 0^o$, in a region of very low extinction according the Sale et al. (2014) maps depicted in 3.11. This low stellar density could be related with the warping of the Galactic disk in the anticenter direction proposed by Momany et al. (2006).

In 3.12 we plot the spatial distribution of the 732 CBe stars for which we have been able to estimate distances through the spectroscopic parallax method. The sample is spread across the whole Northern Galactic plane for $\mid b \mid < 5^o$. We overplot for reference ten 22GHz water maser sources, with accurate distances measured with VLBI astrometry, listed in 3.1. In the background we drawn an estimation of the Galactic Arm structure, following Georgelin & Georgelin (1976), Taylor & Cordes (1993) and Vallée (2008). The solar galactocentric distance $R_0 = 8.3$ Kpc from Brunthaler et al. (2011) is assumed.

The distribution of the stars does not present an apparent clustering in or around the arms which define the Galactic structure. Instead, they appear scattered along them and the space in between, with some stars spread along larger distances, beyond the expected location of the Outer Arm.

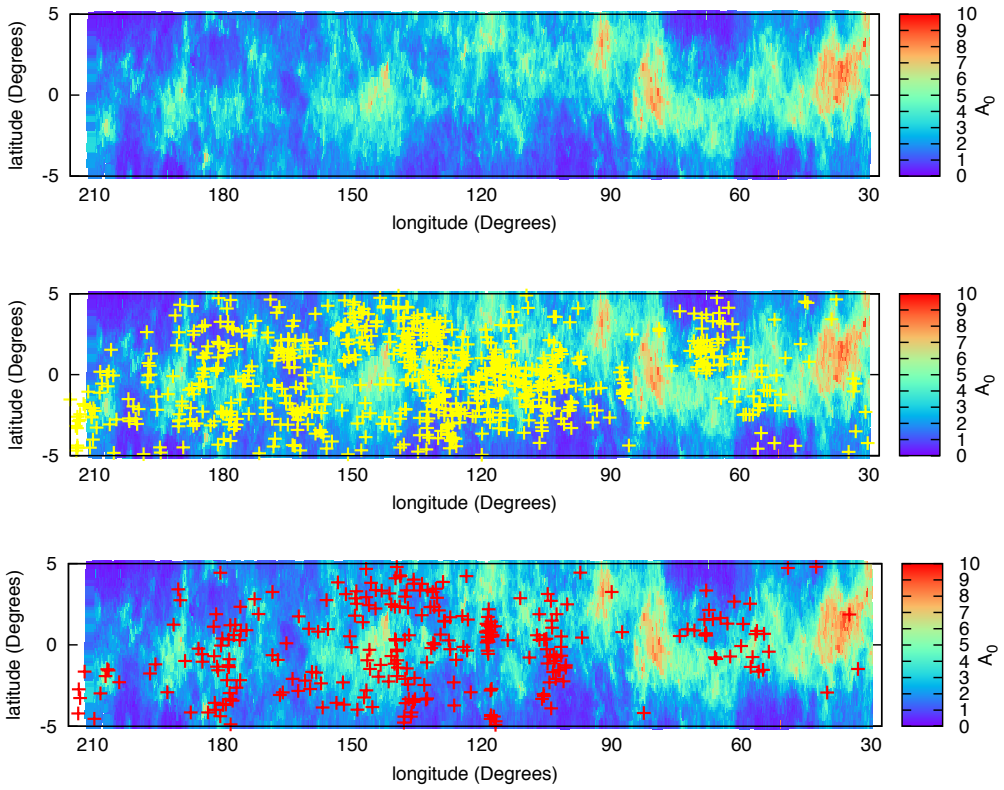

FIGURE 3.11: The IPHAS scanned region of the north Galactic plane with the CBe stars. Comparing with the 3D extincion maps of the (Sale et al. 2014), at 3.5 kpc, we find low density areas at the high extinction regions except of the outer part of the third galactic quadrant, $l > 190°$, where probably the warping effect of the outer parts of the disk Momany et al. (2006) starts.

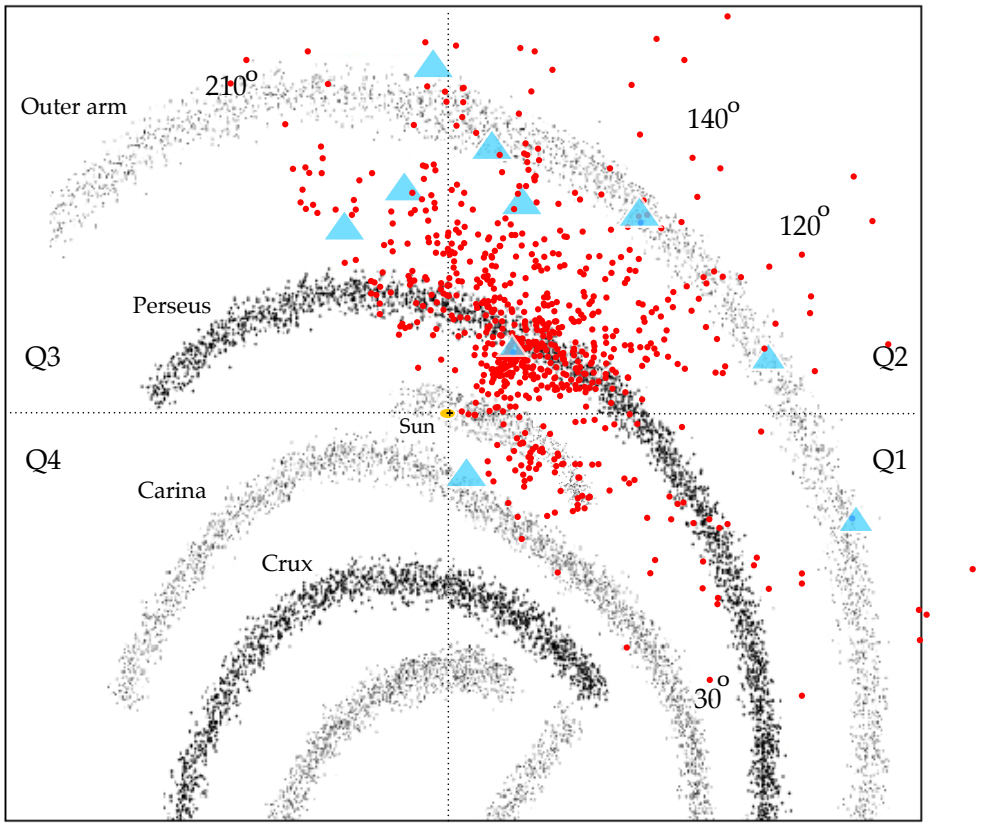

FIGURE 3.12: The spatial distribution of the total sample of the IHPAS CBe stars in the anti-centric region of the Galaxy for $\mid b \mid < 5°$. Red dots represent the stars studied in this work between the longitudes $120° < l < 140°$. The light blue tringles are the 22 GHz water maser regions studied by references in table 1. In the backround we draw the galactic arms across the four quadrants following the Georgelin & Georgelin (1976) ;Taylor & Cordes (1993) in combination of Vallée (2008). The $R_0 = 8.3$ kpc from Branthler et al. (2011) is assumed.

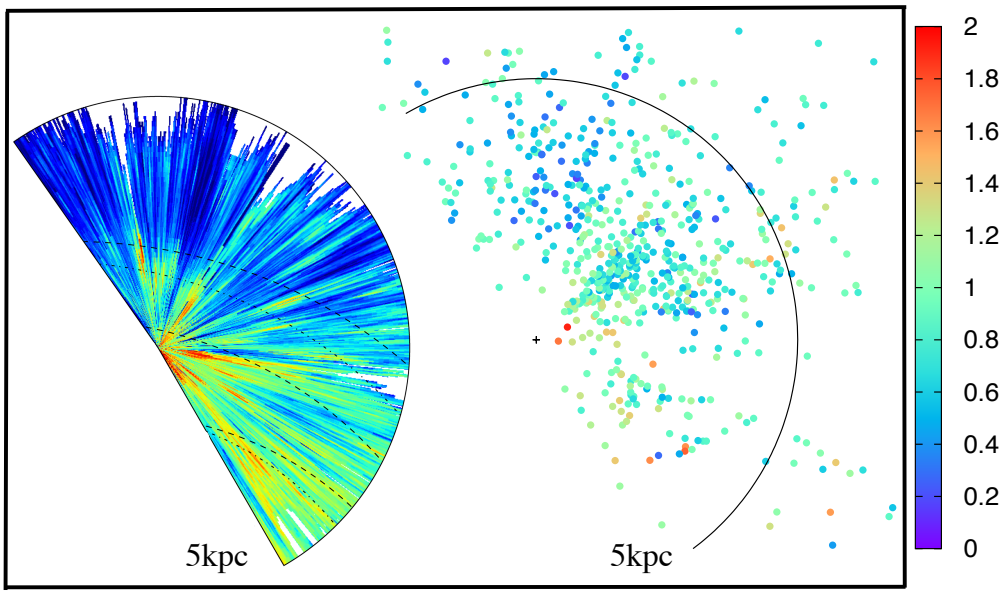

FIGURE 3.13: Distribution of the star positions in the Northern Galactic Plane (right side), and comparison with the extinction map at $b = 0$ Perseus arms of Vallée (2013). Note the non-physical 'fingers of God' - discontinuities in the azimuthal direction. from Sale et al. (2014) (left side). Note that the colour scale in the right indicates the $E(B-V)$ of the stars in mags and in the left it is the 3D map in ΔA_0/kpc.

Chapter 4

Conclusions & future work

In this work we have developed a semi-automatic method for the analysis of spectra from late O to early A type stars, with or without emission lines. Our method is based on the BCD spectrophotometric system. The spectra to be analysed have to meet the following two conditions:

- Flux calibration. At least an accurate relative flux calibration for which spectroscopic standard observations are required.
- Balmer discontinuity spectral range. As we prove also in this work, spectral ranges at least starting from 3700 Å are necessary for the extracion of the BCD parameters.

We have discusted already the advantages of our method, especially for low-resolution spectra. We plan to make it public with some minor modifications to make it "user friendly".

From the analysis of follow-up spectroscopy we have determined spectral types and luminosity classes, effective temperatures, projected rotational velocities, interstellar extinction and absolute magnitudes. The combination of the spectroscopic data with the IPHAS photometry (Barentsen et al. 2014) allowed us to determine the circumstellar continuum emission, the distance by means of the spectroscopic parallax technique, the bolometric magnitude and the luminosity. Finally, we obtained the stellar masses and ages by interpolating in the Ekström et al. (2012) evolutionry tracks. The catalogue presented in Tables 2 and 3 constitutes the largest sample of homogeneous data for CBe stars yet assembled, and a significant

increase of the number of about two thousands of these objects previously known in the Galaxy and the Magellanic Clouds (Neiner et al. 2011).
More particular, in the recent work of Raddi et al. (2015) they analysed a sample of 248 photometrically selected and spectroscopically confirmed CBe stars in the direction of the Perseus Arm. There are 102 stars in common between this sample and the present work. In addition, there are another 211 stars with CBe spectral characteristics which doesn't met the selection criteria presented in the above paragraph and are not included in the Raddi et al. (2015) sample. This results in a total of 1089 faint CBe stars photometrically detected by the IPHAS survey with available follow up spectroscopy. In Fig. 3.3 we plot their position in the IPHAS colour-colour plane.

The IPHAS CBe star sample almost doubles the number of CBe stars known in the Galaxy. The all-sky Be Star Spectra database (BeSS, Neiner et al., 2011) list, at the time of writing this work, 2265 known Be stars. After removing the stars in the Magellanic Clouds and the stars listed by Raddi et al. (2015) which have been recently added, the total number of CBe stars previously known in the Galaxy amounted to 1679 stars. There are only four stars in common between the BeSS and the IPHAS samples.

In Fig. 4.1 we show the distribution in V magnitudes of the BeSS and IPHAS CBe stars sample. For the sake of comparison we have computed the V magnitudes of the IPHAS CBe stars from IPHAS r and i magnitudes, by means of the empirical relationship

$$V = r + 0.024(r - i) + 0.201\,(\sigma = 0.076\,mag.) \tag{4.1}$$

This relation has been obtained from a sample of 461 B and CBe stars in the fields of the open clusters NGC 663, 869 and 884, with available IPHAS photometry (Barentsen et al., 2014) and V magnitudes in Capilla & Fabregat (2002) and Fabregat & Capilla (2005).

We have used the data in the catalogue to address a number of key issues regarding the physics of the CBe stars a a class. We have determined a mean rotational velocity of $82 \pm 17\%$ of the critical velocity, in agreement with the results of several recent studies. We have shown that there is not any trend of variation of the rotational velocity with the spectral type. Our data also confirm that the matter in the circumstellar disc follows a Keplerian rotational velocity law.
We have analysed the age distribution of the stars in our sample. We found CBe

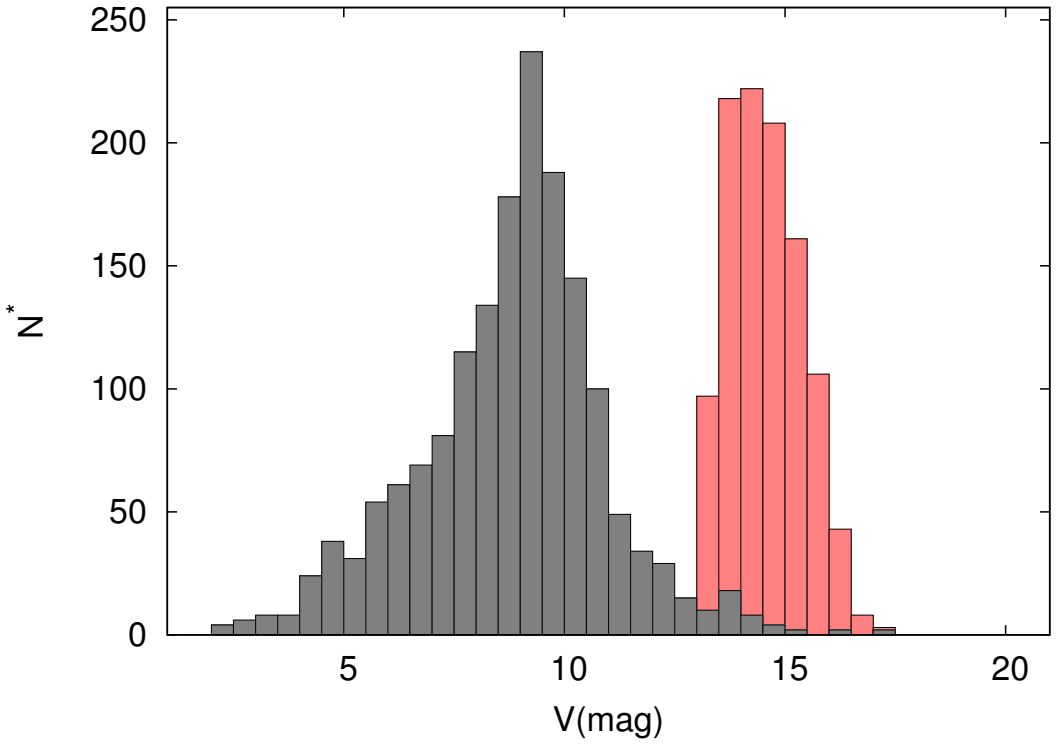

FIGURE 4.1: V magnitude distribution of the galactic CBe stars in the BeSS database (grey) and the IPHAS CBe star sample (red).

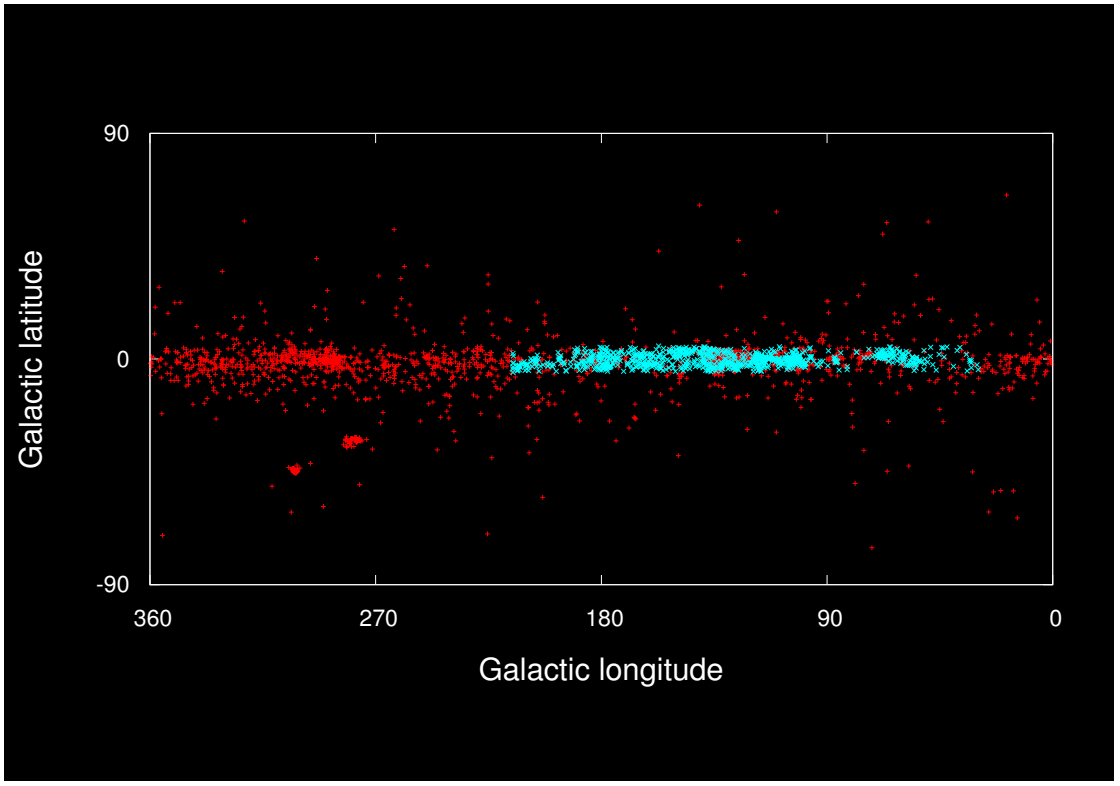

FIGURE 4.2: Full sky map of the known CBe stars. In red we plot the whole BeSS catalogue and in light blue our 649 stars we provide the analisis and an extra sample of 276 CBe stars that we confirm spectroscopically.

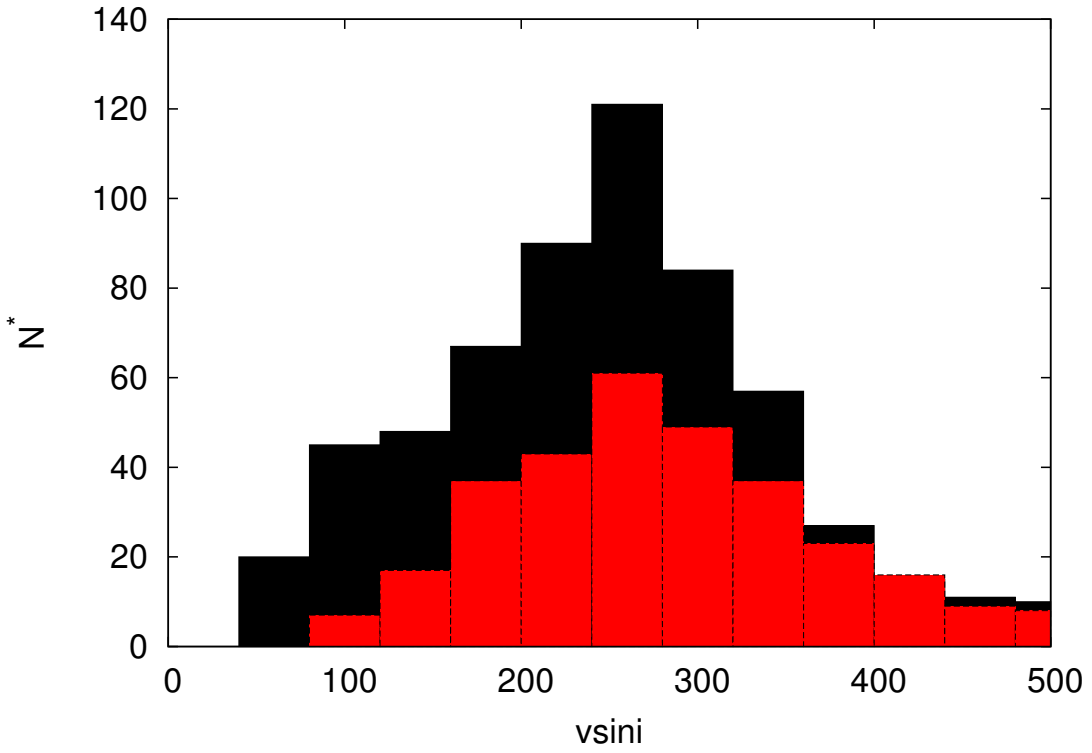

FIGURE 4.3: Comparison of the *vsini* distributions of our sample and the total sample of the BeSS database.

stars of all ages evenly distributed between the ZAMS and the TAMS, and a few of them slightly more evolved. Our results do not support the claims of an evolutionary nature of the Be phenomenon.

Finally, we have studied the distribution of the star positions along the Galactic plane. The distribution of the stars does not present any apparent clustering in or around the arms which define the Galactic structure. Instead, they appear scatered along them and the space in between, with some stars spreaded along larger distances, beyond the expected location of the Outer Arm.

4.1 Variability of Be stars

All the targets were first detected from IPHAS colour-colour diagrams as strong Hα emitters. However, the spectra of 20 stars ($\approx$ 2.7% of the sample) displayed the Hα line in absorption. One of the interpratations of this fact is that are covered by the error of the IPHAS photometry. We present the colour-colour diagram of the non-emitters as they were detected by Witham et al. (2008) and from the

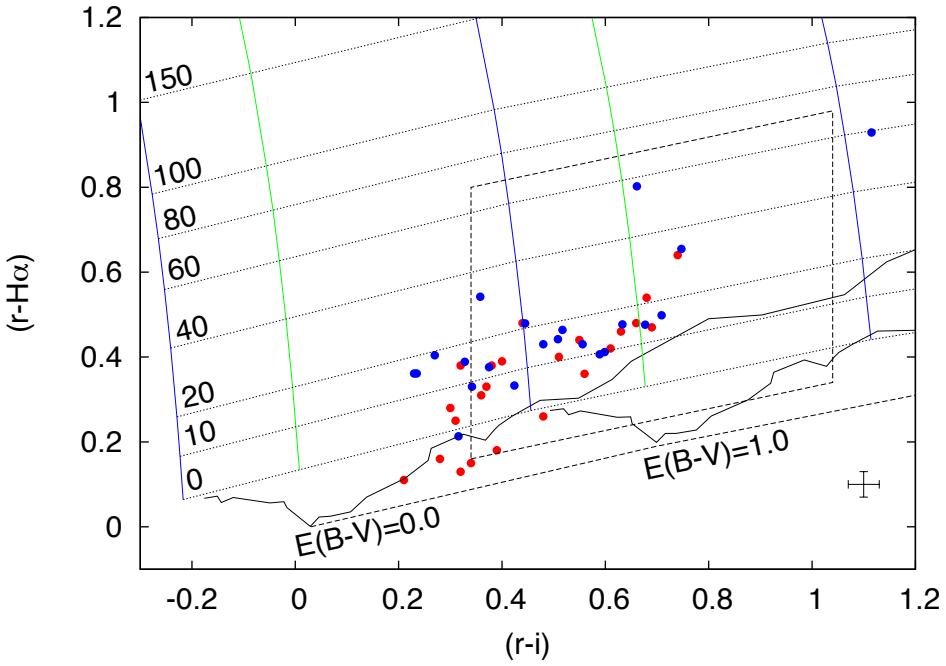

FIGURE 4.4: Colour-colour diagram of the stars we found in absorption phase but they were detected photometrically as bright emitters. Blue dots represent the first IPHAS release by Witham et al. (2008) and the red dots the second IPHAS release by Barentsen et al. (2014). It is clear that colour diagrams detect those objects as bright emitters.

IPHAS DR2 Barentsen et al. (2014) in fig. 4.4. It is clear that colour diagrams detect those objects as bright emitters. This could explained as the phase transition from emission to absorption in the Hα line. The change was produced during the interval between the photometric and spectroscopic data acquisition, which ranges from two to five years. This is compatible with the known timescales of this kind of phase transitions in CBe stars, between four and fifteen years. For three of these stars we have two spectra at different epochs, in which the gradual transition from line emission to absorption can be traced, confirming the proposed scenario. The large amount of CBe stars showing the transition to a disk loss phase represents an opportunity to study the frequency of this phenomenon in CBe stars and its characteristic timescales. Especially the stars that are in the transition phase at this period.

4.2 Future prospects

4.2.1 WEAVE project

WEAVE is the next-generation wide-field survey facility for the William Herschel Telescope. WEAVE will provide the instrument required for full scientific exploitation of the Gaia, LOFAR, and APERTIF surveys in the Northern Hemisphere. WEAVE is a multi- object and multi-integral-field-unit (IFU) facility utilizing a large, new 2^o diameter prime focus corrector at the WHT with a pick-and-place fibre positioner system hosting 1000 multi-object fibres or 20 mini-IFUs for each observation, or a single wide-field IFU. The fibres are fed into a dual-beam spectrograph located in the GHRIL enclosure on the telescope's Nasmyth platform. The spectrograph measures 1000 spectra simultaneously at a spectral resolution of $R \approx 5000$ over an instantaneous wavelength range 370-1000 nm. In high-resolution mode this is $R \approx 20000$ over two more limited wavelength regions.
As part of the WEAVE project, we are going to choose the targets and analyse the spectra of the Be stars candidates in the north Galactic plane, mostly in the uncover population in the magnitude range $16 < r < 19$ that is so far unexplored. The scientific target is to discover thousants of new CBe stars and their physical parameters, study the evolutionary status of the Be stars and to understand the stellar physics relevant to the upper main sequence and using them as tracers of the north Galactic plane structure.

Six surveys will be carried out with WEAVE over a period of 5-7 years, producing more than 30 million spectra of nearly 10 million objects: a survey of the Milky Way Galaxy, providing radial velocities and stellar abundances for stars too faint for these quantities to be measured by Gaia, and probing stellar evolution in the crowded Galactic Plane; a survey probing the evolution of galaxies as a function of environment, from the cores of rich clusters to their exciting suburbs, concentrating on the smallest members, to the field at cosmological distances; a survey of the stellar and gaseous kinematics and physical properties of gas-rich galaxies out to cosmological distances, providing a necessary optical complement to APERTIF's neutral hydrogen surveys of the local Universe; a survey probing galaxy evolution over cosmic time, providing the needed redshifts and galaxy properties of LOFAR's sources; and a survey of quasar absorption using large scale structures as a cosmic ruler to probe the expansion of the Universe itself, which also extends the study

of gaseous environments to larger scales and earlier epochs.

In particular, the following key issues regarding CBe stars physics can be addressed with WEAVE data:

- Rotational velocities It is now well established that CBe stars as a class are fast rotators, with a wide distribution of rotational velocities between about 75% and 100% of the critical value (the velocity at which material would escape from the equator due to the centrifugal force). Once a B star rotates above that threshold it can become a CBe star. This threshold does not depend on the spectral subtype. What is not known is whether there is a threshold above which a star must become a CBe star, i.e., no more non-emission B stars are found. According to Huang et al. (2010 ApJ 772 605) this is such a threshold, and it depends on the spectral subtype. This would mean that, at the origin of the Be-phenomenon, there are either several processes which are differently weighted with the spectral subtype, or only one that decreases in efficiency as a function of the temperature.

- Evolutionary status It has been proposed that the Be-phenomenon is an evolutionary effect which appears during the second half of a B star's main sequence lifetime (Fabregat & Torrejon 2000). Zorec et al. (2005) found a similar result for late-type CBe stars, but propose that early-type CBe stars appear mainly in the first half of the main sequence. However, Martayan et al. (2007) found a significant number of CBe stars at the ZAMS, rotating faster than B stars in general. This would imply that CBe nature is innate, and not an acquired characteristic of a fraction of B stars. In the recent literature many other authors have addressed these issues with different, contradictory conclusions. WEAVE will observe a large number of CBe stars within the OBA selection, yielding the accurate physical parameters needed to place them in the HR diagram and settle this long-standing issue.

- Stellar structural consequences WEAVE data on CBe stars will provide stringent tests of predictions in recent evolutionary models of massive stars taking account of high rotational velocity. The basic effects of fast stellar rotation in massive stars are well known (Maeder & Meynet 2012): for example, the rotationally reduced equatorial gravity lowers the effective temperature from pole to equator. This causes a breakdown of thermal equilibrium that sets up a

meridional circulation, while differential rotation adds horizontal turbulence and shear. This has a number of consequences, including changes to surface abundances. For instance, the models for initially rapidly rotating stars by Granada et al. (2013) predict enhancement of the N/C abundance ratio by x20 or more at the end of the main sequence, for a solar metallicity early B star. The few available studies so far have found negative results. These same models predict an angular momentum transfer from core to envelope and a speed-up within the main sequence lifetime: if there are fast-rotating Be stars on the ZAMS, they will become super-critical rotators before reaching TAMS. The lack of detection of these, together with the absence of observed surface abundance enhancement, imply either that there are no Be stars at the ZAMS, or that Be stars are not fast rotators. Both conclusions contradict the well established observational facts presented above.

A first search for emission line stars from IPHAS photometry produced a list of 4853 objects Witham et al. (2008). This figure represents just a lower limit, as the selection at that time was conservative and the survey was incomplete. Currently, with the survey almost complete and a new globally calibrated photometric catalogue recently published (Barentsen et al. 2014), a refreshed comprehensive selection for emission line stars is now being undertaken. This appears set to increase the number of detected emission line stars by a factor of two, at least. From the work already carried out on the basis of the Witham catalogue, we know that around 70% of the emission line stars are CBe stars. This implies a sample of more than 7000 CBe stars distributed over the 1800 deg^2 of the Northern Galactic Plane ($>$ 12 CBe stars per WEAVE FOV, see, e.g., Raddi et al. 2015). The CBe star sky surface density is highly variable along the Galactic Plane, typically peaking in regions of recent active stellar formation and in regions of low/moderate interstellar absorption. Accordingly, for practical reasons, they will be selected either as candidate OB stars via the u-g, g-r diagram, or as emission line stars via r-Hα, $r - i$ colours. The main focus will be to uncover the population in the magnitude range $16 < r < 19$ that is so far practically unexplored.

4.2.2 Distant CBe stars

We found that a significant number of stars are detected at distances larger than 9 kpc up to 11 kpc and eight stars in distances larger than 15 kpc. Current models

predict that the extension of the galactic disk in the anticenter direction is around, 8 kpc., where the Outer Arm is supposed to end. We are investigating the farther targets one by one in order to examine at which level our results for each one is trustful, with the aim to study the outer limits of the galactic disk, the structure and if massive stars such as CBe stars with sort lifes can be found at such distances.
Studing the same populations with a better quality spectra will give us the advantage of estimating the physical parameters with bigger precision allowing us to be more precise in the distance calculation. We can study this way the north Galactic spiral stracture and if Be stars can be found out of the Galactic limits.

4.2.3 GAIA

Gaia is an astrometric mission to chart a three-dimensional map of our Galaxy, the Milky Way, in the process revealing the composition, formation and evolution of the Galaxy. Gaia will provide unprecedented positional and radial velocity measurements with the accuracies needed to produce a stereoscopic and kinematic census of about one billion stars in our Galaxy and throughout the Local Group. This amounts to about 1 per cent of the Galactic stellar population. Gaia will return accurate luminosities, surface temperatures, chemical abundances, masses, and determinations of the extinction of stellar light by the interstellar medium for all types of stars and hence for the full range covered in the Hertzsprung-Russel diagram. All the sources that we studied in this work and the ones we will descover by the WEAVE survey are likely to be observed with GAIA and will obtain accurate trigonometric parallaxes in the near future. Therefore, their proper characterisation would also aid their future exploitation for more detailed studies of CBe star physics and of Galactic structure.

Bibliography

Aidelman Y., Cidale L. S., Zorec J., Arias M. L., 2012, Astronomy and Astrophysics, 544, A64

Alexander S., 1852, Astronomical Journal, 2, 95

Allen C. W., 1973, Astrophysical quantities

Allen C. W., 1976, Astrophysical Quantities

Asaki Y., Imai H., Sobolev A. M., Parfenov S. Y., 2014, Astrophysical Journal, 787, 54

Balona L. A., Shobbrook R. R., 1984, Monthly Notices of the RAS, 211, 375

Barbier D., 1948, Annales d'Astrophysique, 11, 13

Barbier D., Chalonge D., 1939a, Astrophysical Journal, 90, 627

Barbier D., Chalonge D., 1939b, Annales d'Astrophysique, 2, 254

Barbier D., Chalonge D., 1941, Annales d'Astrophysique, 4, 30

Barentsen G., Farnhill H. J., Drew J. E. e. a., 2014, Monthly Notices of the RAS, 444, 3230

Becker W., Fenkart R., 1971, Astronomy and Astrophysics, Supplement, 4, 241

Becker W., Fenkart R. B., 1970, in Becker W., Kontopoulos G. I., eds, The Spiral Structure of our Galaxy Vol. 38 of IAU Symposium, Galactic Clusters and H II Regions. p. 205

Brown J. C., Cassinelli J. P., 2005, in Ignace R., Gayley K. G., eds, The Nature and Evolution of Disks Around Hot Stars Vol. 337 of Astronomical Society of the Pacific Conference Series, Effects of Magnetic Fields on Winds and Disks. p. 88

Brunthaler A., Reid M. J., Menten K. M., Zheng X.-W., Bartkiewicz A., Choi Y. K., Dame T., Hachisuka K., Immer K., Moellenbrock G., Moscadelli L., Rygl K. L. J., Sanna A., Sato M., Wu Y., Xu Y., Zhang B., 2011, Astronomische Nachrichten, 332, 461

Capilla G., Fabregat J., 2002, Astronomy and Astrophysics, 394, 479

Carciofi A. C., Okazaki A. T., Le Bouquin J.-B., Štefl S., Rivinius T., Baade D., Bjorkman J. E., Hummel C. A., 2009, Astronomy and Astrophysics, 504, 915

Cassinelli J. P., Neiner C., 2005, in Ignace R., Gayley K. G., eds, The Nature and Evolution of Disks Around Hot Stars Vol. 337 of Astronomical Society of the Pacific Conference Series, Magnetic Fields and Be Stars. p. 43

Chalonge D., 1975, L'Astronomie, 89, 118

Chalonge D., Divan L., 1952, Annales d'Astrophysique, 15, 201

Chalonge D., Divan L., 1973, Astronomy and Astrophysics, 23, 69

Chalonge D., Divan L., 1977, Astronomy and Astrophysics, 55, 117

Chandrasekhar S., Münch G., 1950, Astrophysical Journal, 111, 142

Chauville J., Zorec J., Ballereau D., Morrell N., Cidale L., Garcia A., 2001, Astronomy and Astrophysics, 378, 861

Choi Y. K., Hachisuka K., Reid M. J., Xu Y., Brunthaler A., Menten K. M., Dame T. M., 2014, Astrophysical Journal, 790, 99

Churchwell E., Babler B. L., Meade M. R., Whitney B. A., Benjamin R., Indebetouw R., Cyganowski C., Robitaille T. P., Povich M., Watson C., Bracker S., 2009, Publications of the ASP, 121, 213

Cochetti Y. R., Arias M. L., Cidale L., Zorec J., 2013, Boletin de la Asociacion Argentina de Astronomia La Plata Argentina, 56, 207

Cook K. H., Alcock C., Allsman H. A., Axelrod T. S., Freeman K. C., Peterson B. A., Quinn P. J., Rodgers A. W., Bennett D. P., Reimann J., Griest K., Marshall S. L., Pratt M. R., Stubbs C. W., Sutherland W., Welch D. L., 1995, in Stobie R. S., Whitelock P. A., eds, IAU Colloq. 155: Astrophysical Applications of Stellar Pulsation Vol. 83 of Astronomical Society of the Pacific Conference Series, Variable Stars in the MACHO Collaboration Database. p. 221

Corradi R. L. M., Rodríguez-Flores E. R., Mampaso A., Greimel R., Viironen K., Drew J. E., Lennon D. J., Mikolajewska J., Sabin L., Sokoloski J. L., 2008, Astronomy and Astrophysics, 480, 409

Cox A. N., 2000, Allen's astrophysical quantities

Cranmer S. R., 2005, Astrophysical Journal, 634, 585

Crawford D. L., 1978, in Reiz A., Andersen T., eds, Astronomical Papers Dedicated to Bengt Stromgren Comparison of the uvby, beta photometric systems with the MK classification system and with UBV photometry. pp 3–17

Dachs J., Hummel W., Hanuschik R. W., 1992, Astronomy and Astrophysics, Supplement, 95, 437

Dachs J., Kiehling R., Engels D., 1988, Astronomy and Astrophysics, 194, 167

Dalton G., Trager S., Abrams D. C., et al. 2014, in Ground-based and Airborne Instrumentation for Astronomy V Vol. 9147 of Proceedings of the SPIE, Project overview and update on WEAVE: the next generation wide-field spectroscopy facility for the William Herschel Telescope. p. 91470L

Dame T. M., 1983, PhD thesis, Columbia Univ., New York, NY.

Dame T. M., Hartmann D., Thaddeus P., 2001, Astrophysical Journal, 547, 792

Dame T. M., Thaddeus P., 2011, Astrophysical Journal, Letters, 734, L24

De Loore C., Hensberge H., Sterken C., Altamore A., Baratta G. B., Bunner A. N., Divan L., Doazan V., Viotti R., 1979, Astronomy and Astrophysics, 78, 287

de Wit W. J., Lamers H. J. G. L. M., Marquette J. B., Beaulieu J. P., 2006, Astronomy and Astrophysics, 456, 1027

Dias W. S., Lépine J. R. D., 2005, Astrophysical Journal, 629, 825

Divan L., 1954, Annales d'Astrophysique, 17, 456

Divan L., Zorec J., 1982, in Perryman M. A. C., Guyenne T. D., eds, The Scientific Aspects of the Hipparcos Space Astrometry Mission Vol. 177 of ESA Special Publication, Absolute magnitudes and other basic parameters of O and B stars. pp 101–104

Divan L., Zorec J., Andrillat Y., 1983, Astronomy and Astrophysics, 126, L8

Dolidze M. V., 1980, Soviet Astronomy Letters, 6, 394

Domiciano de Souza A., Zorec J., Vakili F., 2012, in Boissier S., de Laverny P., Nardetto N., Samadi R., Valls-Gabaud D., Wozniak H., eds, SF2A-2012: Proceedings of the Annual meeting of the French Society of Astronomy and Astrophysics CHARRON: Code for High Angular Resolution of Rotating Objects in Nature. pp 321–324

Downes D., Wilson T. L., Bieging J., Wink J., 1980, Astronomy and Astrophysics, Supplement, 40, 379

Drew J. E., Greimel R., Irwin M. J., et al. 2005, Monthly Notices of the RAS, 362, 753

Ekström S., Georgy C., Eggenberger P., Meynet G., Mowlavi N., Wyttenbach A., Granada A., Decressin T., Hirschi R., Frischknecht U., Charbonnel C., Maeder A., 2012, Astronomy and Astrophysics, 537, A146

Fabregat J., Capilla G., 2005, Monthly Notices of the RAS, 358, 66

Fabregat J., Torrejon J. M., 1998, Astronomy and Astrophysics, 332, 643

Fabregat J., Torrejón J. M., 2000, Astronomy and Astrophysics, 357, 451

Fabricant D., Cheimets P., Caldwell N., Geary J., 1998, Publications of the ASP, 110, 79

Fenkart R. P., 1979, in Burton W. B., ed., The Large-Scale Characteristics of the Galaxy Vol. 84 of IAU Symposium, The galactic distribution of 60 young open clusters. pp 101–104

Fiorucci M., Munari U., 2003, Astronomy and Astrophysics, 401, 781

Frémat Y., Zorec J., Hubert A.-M., Floquet M., 2005, Astronomy and Astrophysics, 440, 305

Georgelin Y. M., Georgelin Y. P., 1976, Astronomy and Astrophysics, 49, 57

Gies D. R., Bagnuolo J. e. a., 2007, Astrophysical Journal, 654, 527

Gkouvelis L., Fabregat J., IPHAS Consortium 2016, in Sigut T. A. A., Jones C. E., eds, Bright Emissaries: Be Stars as Messengers of Star-Disk Physics Vol. 506 of Astronomical Society of the Pacific Conference Series, North Galactic Plane Structure with IPHAS Be Stars.. p. 187

Gkouvelis L., Fabregat J., Zorec J., Steeghs D., Drew J. E., Raddi R., Wright N. J., Drake J. J., 2016, Astronomy and Astrophysics, 591, A140

Gray R. O., Corbally J. C., 2009, Stellar Spectral Classification

Grundstrom E. D., Gies D. R., 2006, Astrophysical Journal, Letters, 651, L53

Hachisuka K., Brunthaler A., Menten K. M., Reid M. J., Hagiwara Y., Mochizuki N., 2009, Astrophysical Journal, 696, 1981

Hachisuka K., Brunthaler A., Menten K. M., Reid M. J., Imai H., Hagiwara Y., Miyoshi M., Horiuchi S., Sasao T., 2006, Astrophysical Journal, 645, 337

Hachisuka K., Choi Y. K., Reid M. J., Brunthaler A., Menten K. M., Sanna A., Dame T. M., 2015, Astrophysical Journal, 800, 2

Hanuschik R. W., 1988, Astronomy and Astrophysics, 190, 187

Hayes D. S., Latham D. W., 1975, Astrophysical Journal, 197, 593

Howarth I. D., 2007, in Okazaki A. T., Owocki S. P., Stefl S., eds, Active OB-Stars: Laboratories for Stellare and Circumstellar Physics Vol. 361 of Astronomical Society of the Pacific Conference Series, Rotation and the Circumstellar Environment. p. 15

Hubert A. M., Floquet M., 1998, Astronomy and Astrophysics, 335, 565

Hubert A. M., Floquet M., Zorec J., 2000, in Smith M. A., Henrichs H. F., Fabregat J., eds, IAU Colloq. 175: The Be Phenomenon in Early-Type Stars Vol. 214 of Astronomical Society of the Pacific Conference Series, Short-lived and Long-lived Outbursts in B and Be Stars from Hipparcos Photometry and Modelling. p. 348

Hummer D. G., Mihalas D., 1988, Astrophysical Journal, 331, 794

Jackson P. D., Sewall J. R., 1982, in Roger R. S., Dewdney P. E., eds, Regions of Recent Star Formation Vol. 93 of Astrophysics and Space Science Library, Dynamics of CO clouds around HII regions in the outer Galaxy. pp 221–230

Jaschek M., Egret D., 1982, in Jaschek M., Groth H.-G., eds, Be Stars Vol. 98 of IAU Symposium, A Catalogue of Be-Stars. p. 261

Kaiser D., 1989, Astronomy and Astrophysics, 222, 187

Keller S. C., Bessell M. S., Cook K. H., Geha M., Syphers D., 2002, Astronomical Journal, 124, 2039

Kerr F. J., 1962, Monthly Notices of the RAS, 123, 327

Kervella P., Domiciano de Souza A., 2006, Astronomy and Astrophysics, 453, 1059

Kilkenny D., Hill P. W., Schmidt-Kaler T., 1975, Monthly Notices of the RAS, 171, 353

Kurucz R., 1993, ATLAS9 Stellar Atmosphere Programs and 2 km/s grid. Kurucz CD-ROM No. 13. Cambridge, Mass.: Smithsonian Astrophysical Observatory, 1993., 13

Laine J., Laurikainen E., Salo H. e. a., 2014, Monthly Notices of the RAS, 441, 1992

Lang K. R., 1992, Astrophysical Data I. Planets and Stars.

Levine E. S., Blitz L., Heiles C., 2006, Science, 312, 1773

Liszt H. S., 1985, in van Woerden H., Allen R. J., Burton W. B., eds, The Milky Way Galaxy Vol. 106 of IAU Symposium, Determination of galactic spiral structure at radiofrequencies. pp 283–297

Maheswaran M., 2005, in Ignace R., Gayley K. G., eds, The Nature and Evolution of Disks Around Hot Stars Vol. 337 of Astronomical Society of the Pacific Conference Series, A Magnetic Rotator Wind-Disk Model for Be Stars. p. 259

Martayan C., Frémat Y., Hubert A.-M., Floquet M., Zorec J., Neiner C., 2007, Astronomy and Astrophysics, 462, 683

McClure-Griffiths N. M., Dickey J. M., Gaensler B. M., Green A. J., 2004, Astrophysical Journal, Letters, 607, L127

McCuskey S. W., 1970, in Becker W., Kontopoulos G. I., eds, The Spiral Structure of our Galaxy Vol. 38 of IAU Symposium, Local Stellar Distribution and Galactic Spiral Structure. p. 189

Meilland A., Millour F., Kanaan S., Stee P., Petrov R., Hofmann K.-H., Natta A., Perraut K., 2012, Astronomy and Astrophysics, 538, A110

Meilland A., Stee P., Zorec J., Kanaan S., 2006, Astronomy and Astrophysics, 455, 953

Mennickent R. E., Pietrzyński G., Gieren W., Szewczyk O., 2002, Astronomy and Astrophysics, 393, 887

Momany Y., Zaggia S., Gilmore G., Piotto G., Carraro G., Bedin L. R., de Angeli F., 2006, Astronomy and Astrophysics, 451, 515

Monguió M., Figueras F., Grosbøl P., 2013, Astronomy and Astrophysics, 549, A78

Moon T., 1986, Astrophysics and Space Science, 122, 173

Morgan W. W., Sharpless S., Osterbrock D., 1952, Astronomical Journal, 57, 3

Moujtahid A., Zorec J., Hubert A. M., 1999, Astronomy and Astrophysics, 349, 151

Moujtahid A., Zorec J., Hubert A. M., 2000a, in Smith M. A., Henrichs H. F., Fabregat J., eds, IAU Colloq. 175: The Be Phenomenon in Early-Type Stars Vol. 214 of Astronomical Society of the Pacific Conference Series, On the Characteristics of Circumstellar Envelopes in Be Stars near the Central Object. p. 506

Moujtahid A., Zorec J., Hubert A. M., 2000b, in Smith M. A., Henrichs H. F., Fabregat J., eds, IAU Colloq. 175: The Be Phenomenon in Early-Type Stars Vol. 214 of Astronomical Society of the Pacific Conference Series, Physical Properties of Circumstellar Envelopes in Be Stars Derived from their Long-term Spectrophotometric Variations. p. 510

Moujtahid A., Zorec J., Hubert A. M., 2000c, in Smith M. A., Henrichs H. F., Fabregat J., eds, IAU Colloq. 175: The Be Phenomenon in Early-Type Stars Vol. 214 of Astronomical Society of the Pacific Conference Series, Physical Properties of Circumstellar Envelopes in Be Stars Derived from their Long-term Spectrophotometric Variations. p. 510

Moujtahid A., Zorec J., Hubert A. M., Garcia A., Burki G., 1998, Astronomy and Astrophysics, Supplement, 129, 289

Nakanishi H., Sofue Y., 2006, Publications of the ASJ, 58, 847

Neiner C., de Batz B., Cochard F., Floquet M., Mekkas A., Desnoux V., 2011, Astronomical Journal, 142, 149

Neiner C., Henrichs H. F., Hubert A.-M., 2001, in Mathys G., Solanki S. K., Wickramasinghe D. T., eds, Magnetic Fields Across the Hertzsprung-Russell Diagram Vol. 248 of Astronomical Society of the Pacific Conference Series, Search for Magnetic Fields in Be Stars Using the Spectropolarimeter MUSICOS at TBL. p. 419

Neiner C., Hubert A. M., 2005, in Ignace R., Gayley K. G., eds, The Nature and Evolution of Disks Around Hot Stars Vol. 337 of Astronomical Society of the Pacific Conference Series, Magnetic fields in Be stars. p. 275

Oke J. B., Gunn J. E., 1983, Astrophysical Journal, 266, 713

Raddi R., Drew J. E., Fabregat J., Steeghs D., Wright N. J., Sale S. E., Farnhill H. J., Barlow M. J., Greimel R., Sabin L., Corradi R. M. L., Drake J. J., 2013, Monthly Notices of the RAS, 430, 2169

Raddi R., Drew J. E., Steeghs D., Wright N. J., Drake J. J., Barentsen G., Fabregat J., Sale S. E., 2015, Monthly Notices of the RAS, 446, 274

Reid M. J., Menten K. M., Brunthaler A., Zheng X. W., Dame T. M., Xu Y., Wu Y., Zhang B., Sanna A., Sato M., Hachisuka K., Choi Y. K., Immer K., Moscadelli L., Rygl K. L. J., Bartkiewicz A., 2014, Astrophysical Journal, 783, 130

Reig P., Nersesian A., Zezas A., Gkouvelis L., Coe M. J., 2016, ArXiv e-prints

Rivinius T., 2005, in Ignace R., Gayley K. G., eds, The Nature and Evolution of Disks Around Hot Stars Vol. 337 of Astronomical Society of the Pacific Conference Series, Links Between Hot Stars and Their Disks. p. 178

Rivinius T., Carciofi A. C., Martayan C., 2013, Astronomy and Astrophysics Reviews, 21, 69

Rivinius T., Štefl S., Baade D., 2006, Astronomy and Astrophysics, 459, 137

Robertson T. H., Jordan T. M., 1989, Astronomical Journal, 98, 1354

Rohrmann R. D., Zorec J., 2006, Physical Review E, 74, 041120

Russeil D., 2003, Astronomy and Astrophysics, 397, 133

Russeil D., Adami C., Georgelin Y. M., 2007, Astronomy and Astrophysics, 470, 161

Sale S. E., Drew J. E., Barentsen G., Farnhill H. J., Raddi R., Barlow M. J., Eislöffel J., Vink J. S., Rodríguez-Gil P., Wright N. J., 2014, Monthly Notices of the RAS, 443, 2907

Sanna A., Reid M. J., Dame T. M., Menten K. M., Brunthaler A., Moscadelli L., Zheng X. W., Xu Y., 2012, Astrophysical Journal, 745, 82

Sato M., Hirota T., Reid M. J., Honma M., Kobayashi H., Iwadate K., Miyaji T., Shibata K. M., 2010, Publications of the ASJ, 62, 287

Shapley H., 1918, Publications of the ASP, 30, 42

Slettebak A., Collins II G. W., Parkinson T. D., Boyce P. B., White N. M., 1975, Astrophysical Journal, Supplement, 29, 137

Smith L. F., 1968, Monthly Notices of the RAS, 141, 317

Smith M. A., Balona L., 2006, Astrophysical Journal, 640, 491

Stee P., Meilland A., Berger D., Gies D., 2005, in Ignace R., Gayley K. G., eds, The Nature and Evolution of Disks Around Hot Stars Vol. 337 of Astronomical Society of the Pacific Conference Series, Interferometric Studies of Hot Star Disks. p. 211

Steele I. A., Negueruela I., Clark J. S., 1999, Astronomy and Astrophysics, Supplement, 137, 147

Taylor J. H., Cordes J. M., 1993, Astrophysical Journal, 411, 674

Torres G., 2010, Astronomical Journal, 140, 1158

Tycner C., Gilbreath G. C., Armstrong J. T., Benson J. A., Hajian A. R., Hutter D. J., Jones C. E., Pauls T. A., White N. M., Zavala R. T., 2005, in American Astronomical Society Meeting Abstracts Vol. 37 of Bulletin of the American Astronomical Society, Narrowband Hα Interferometry with the NPOI. p. 1306

Tycner C., Gilbreath G. C., Zavala R. T., Armstrong J. T., Benson J. A., Hajian A. R., Hutter D. J., Jones C. E., Pauls T. A., White N. M., 2006, Astronomical Journal, 131, 2710

ud-Doula A., Blondin J., 2005, in American Astronomical Society Meeting Abstracts #206 Vol. 37 of Bulletin of the American Astronomical Society, The Effects of Rotation on Spherical Accretion Shock Instability. p. 500

Vallée J. P., 2005, Astronomical Journal, 130, 569

Vallée J. P., 2008, Astronomical Journal, 135, 1301

Vallée J. P., 2013, International Journal of Astronomy and Astrophysics, 3, 20

van Belle G. T., 2012, Astronomy and Astrophysics Reviews, 20, 51

Vázquez R. A., May J., Carraro G., Bronfman L., Moitinho A., Baume G., 2008, Astrophysical Journal, 672, 930

Vinicius M. M. F., Zorec J., Leister N. V., Levenhagen R. S., 2006, Astronomy and Astrophysics, 446, 643

Vogt N., Moffat A. F. J., 1975, Astronomy and Astrophysics, 39, 477

Walborn N. R., Fitzpatrick E. L., 1990, Publications of the ASP, 102, 379

Wenger M., Ochsenbein F., Egret D., Dubois P., Bonnarel F., Borde S., Genova F., Jasniewicz G., Laloë S., Lesteven S., Monier R., 2000, Astronomy and Astrophysics, Supplement, 143, 9

Witham A. R., Knigge C., Drew J. E., Greimel R., Steeghs D., Gänsicke B. T., Groot P. J., Mampaso A., 2008, Monthly Notices of the RAS, 384, 1277

Witham A. R., Knigge C., Gänsicke B. T., Aungwerojwit A., Corradi R. L. M., Drew J. E., Greimel R., Groot P. J., Morales-Rueda L., Rodriguez-Flores E. R., Rodriguez-Gil P., Steeghs D., 2006, Monthly Notices of the RAS, 369, 581

Xu Y., Li J. J., Reid M. J., Menten K. M., Zheng X. W., Brunthaler A., Moscadelli L., Dame T. M., Zhang B., 2013, Astrophysical Journal, 769, 15

Xu Y., Reid M. J., Zheng X. W., Menten K. M., 2006, Science, 311, 54

Yudin R. V., 2001, Astronomy and Astrophysics, 368, 912

Zorec J., 1986, Structure et rotation differentielle dans le etoiles B avec et sans emission

Zorec J., Arias M. L., Cidale L., Ringuelet A. E., 2007, Astronomy and Astrophysics, 470, 239

Zorec J., Briot D., 1991, Astronomy and Astrophysics, 245, 150

Zorec J., Briot D., 1997, Astronomy and Astrophysics, 318, 443

Zorec J., Cidale L., Arias M. L., Frémat Y., Muratore M. F., Torres A. F., Martayan C., 2009, Astronomy and Astrophysics, 501, 297

Zorec J., Divan L., Hoeflich P., 1989, Astronomy and Astrophysics, 210, 279

Zorec J., Frémat Y., Cidale L., 2005, Astronomy and Astrophysics, 441, 235

Appendix A

Data reduction

The data that we worked with in this project, as we already gave in detail in chapter 2, are mainly one-slit spectra from the FAST follow-up and an extra sample of

67 spectra from INT/NOT telescopes in the La Palma island.
The spectra of La Palma were delivered reduced in physical units and a flux calibration using spectroscopic standard stars of each night of observation. To make the spectra of the FAST follow-up potential for analysis with the BCD method we had to make at least an reliable relative flux calibration. FAST spectra were delivered with a time-averaged flux calibration based on the spectrophotometric Oke standard BD28+4211. This calibration was not sufficiently accurate especially in the blue part of the spectral range , were the BD is. Althought the survey is varying in observational days from 2005 up to 2012, and each observing has from one spectrum up to eight, we performed the flux calibration of each spectrum from spectroscopic standard star spectra observed the same night of the studied spectrum. Many times from an average of more than one spectroscpic standard spectra of each night. In several occasions, for three nights, that there was not performed spectroscopic stadard observavion,we performed the flux calibration with the previus night or the next one.
We worked with IRAF standard methods and for this purpose, with the **kpnoslit** package inside the **imred**. The directory **onedstds$** houses several subdirectories containing the standard star calibrations. The calibrations of the spectroscopic files comes from Hayes & Latham (1975) and Oke & Gunn (1983). Each standard star has its own subdirectory which specifies it with wavelength, width of bandpasses and the magnitude of the star.
To make the correlation between the library calibrated standard stars with our own observed standards we will follow the above procedure. We begin by running **setairmass** task. The subdirectory for the calibration data is **onedstds$irscal/** and also is already set to the **onedstds$kpnoextinct.dat** file to use for extinction correction of our data. The next step is to run the **standard** task. This routines takes a single observation of a spectroscopic flux standard and asks you to give the version of its name listed in the calibration subdirectory. The stadard routine then integrades your data over the appropriate bandpasses, divides by the exposure time, and outputs a single file containing an observation-by-observation listing of the observed counts within each bandpass along with the standard star fluxes.

We continue with creation of the sensitivity function. The **sensfunc** task allow us also interactively fit sensitivity funcion as a function of wavelength using the output file from **standard**. Extincion corrections using the standard extincion table you adopted will be used, or you can try to choose to determine the extincion of your

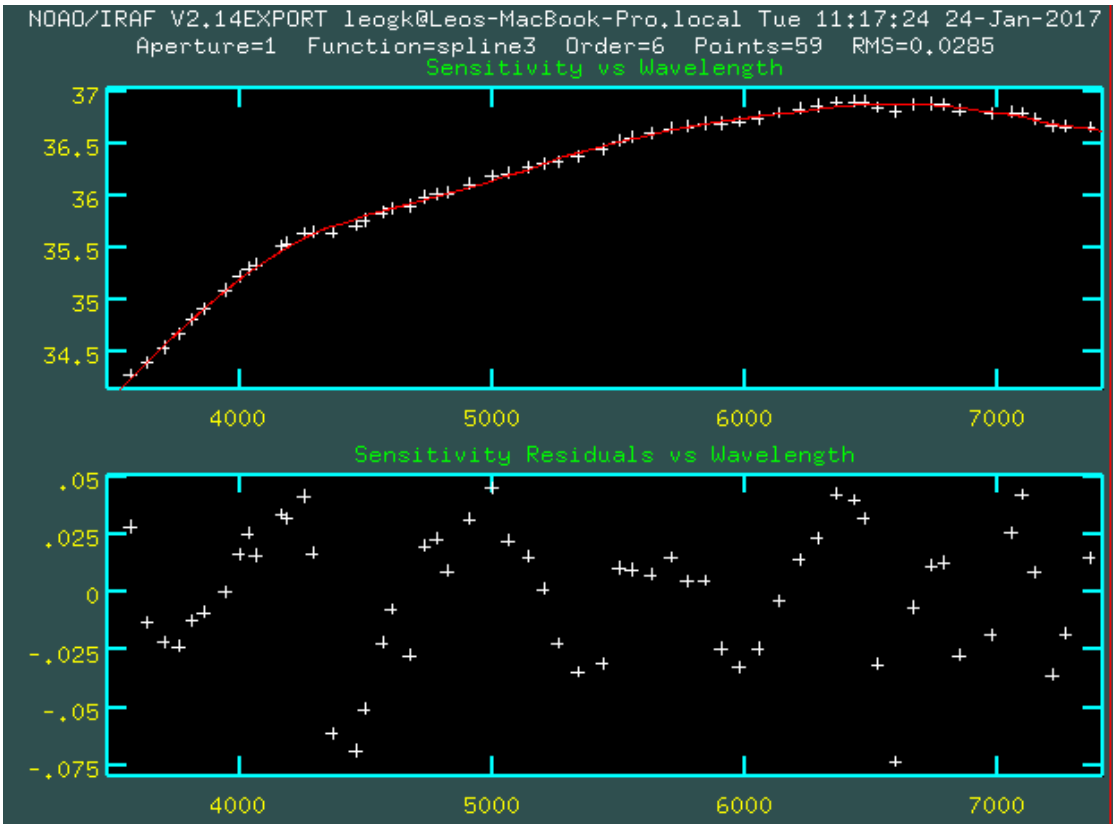

FIGURE 5: Extracion of the sensitivity funcion.

data. Finally, with the task **calibrate** we can apply the sentitivity funcion in our data. In our case we produce at least a sensitivity funcion per night and we applied it to the spectra stars for that night. So we end up with our spectra corrected from atmospheric extincion, divided by the exposure time and transformed using the sensitivity curve.

Appendix B

Spectral continuum energy fits

To follow the continuum distribution of the spectra and extract parameters we used the least-squares method, for line and parabola, above we explain the formalization of the adopted algoriths.

Linear least squares

We extract from the desired spectral range n data points $\{(x_i, y_i), i = 1, ..., n\}$. With the funcion that describes x and y is : $y_i = \alpha + \beta x_i + \epsilon_i$. The goal is to find equation of the straight line $y = \alpha + \beta x$, which would provide a "best" fit for the data points. Here the "best" will be understood as in the least-squares approach: a line that minimizes the sum of squared residuals of the linear regression model. In other words, α(the y-intercept) and β (the slope) solve the following minimization problem:
$min_{\alpha,\beta}Q(\alpha, \beta)$, for $Q(\alpha, \beta) = \sum_{i=1}^{n} \epsilon_i^2 = \sum_{i=1}^{n}(y_i - \alpha - \beta x_i)^2$
By using either calculus, the geometry of inner product spaces, or simply expanding to get a quadratic expression in α and β, it can be shown that the values of α andβ that minimize the objective function Q are:
$\hat{\beta} = \frac{\sum_{i=1}^{n}(x_i - \bar{x})(y_i - \bar{y})}{\sum_{i=1}^{n}(x_i - \bar{x})^2} = \frac{\sum_{i=1}^{n} x_i y_i - \frac{1}{n}\sum_{i=1}^{n} x_i \sum_{j=1}^{n} y_i}{\sum_{i=1}^{n} x_i^2 - \frac{1}{n}(\sum_{i=1}^{n} x_i)^2} = \frac{\bar{xy} - \bar{x}\bar{y}}{\bar{x^2} - \bar{x}^2} = \frac{Cov[x,y]}{Var[x]} = r_{xy}\frac{S_y}{S_x}$,

$\hat{\alpha} = \bar{y} - \hat{\beta}\bar{x}$,
where r_{xy} is the sample correlation coefficient between x and y; s_x is the standard deviation of x; and s_y is correspondingly the standard deviation of y.

Parabolic least squares

The least-squares parabola uses a second degree curve $y = \alpha + bx + cx^2$ to approximate the given set of data, $(x_1, y_1), (x_2, y_2), ..., (x_n, y_n)$, where $n \geq 3$. the best fitting curve $f(x)$ has the least square error, i.e. ,

$$\Pi = \sum_{i=1}^{n}[y_i - f(x_i)]^2 = \sum_{i=1}^{n}[y_i - (\alpha + bx_i + cx_i^2)]^2 = min.$$

note that a, b and c are unknown coefficients while all x_i and y_i are extracted from the spectra. To obtain the least-square error, the unknown coefficients a, b and c must yield zero first derivatives.
$\frac{\partial \Pi}{\partial \alpha} = 2\sum_{i=1}^{n}[y_i - (\alpha + bx_i + cx_i^2)] = 0$
$\frac{\partial \Pi}{\partial b} = 2\sum_{i=1}^{n}[y_i - (\alpha + bx_i + cx_i^2)] = 0$
$\frac{\partial \Pi}{\partial c} = 2\sum_{i=1}^{n}[y_i - (\alpha + bx_i + cx_i^2)] = 0$

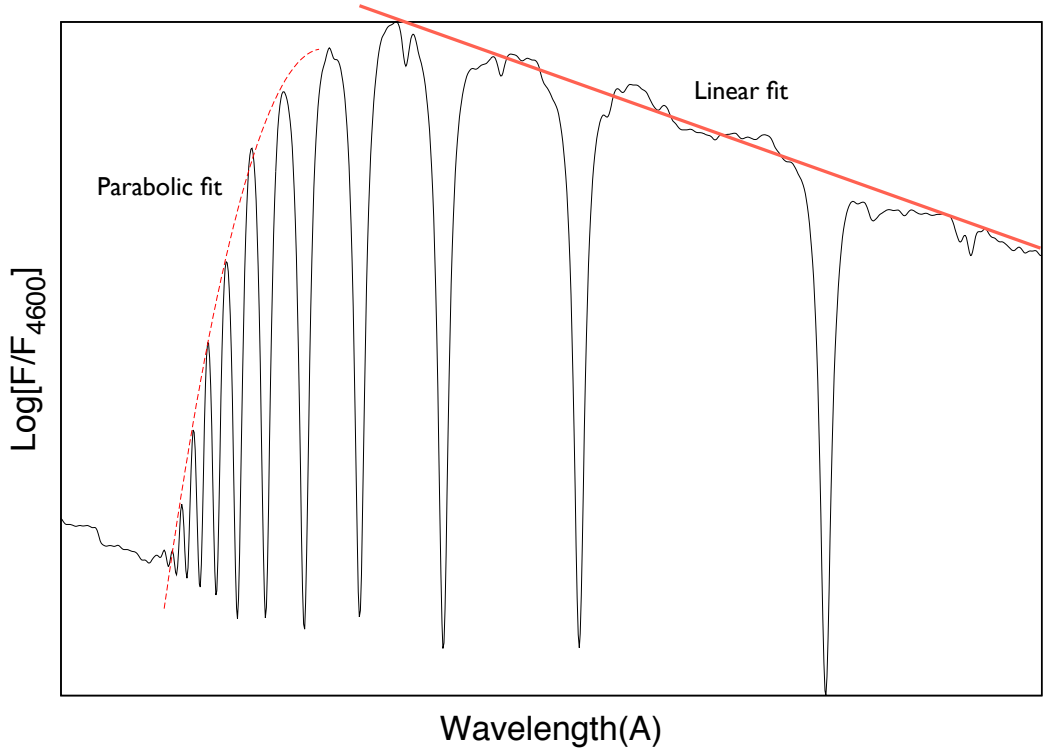

FIGURE 6: The linear and parabolic least-squares fits as we applied them in the data spectra.

Expanding the above equations, we have:

$$\sum_{i=1}^{n} y_i = \alpha \sum_{i=1}^{n} 1 + b \sum_{i=1}^{n} x_i + c \sum_{i=1}^{n} x_i^2$$
$$\sum_{i=1}^{n} x_i y_i = \alpha \sum_{i=1}^{n} x_i + b \sum_{i=1}^{n} x_i^2 + c \sum_{i=1}^{n} x_i^3$$
$$\sum_{i=1}^{n} x_i^2 y_i = \alpha \sum_{i=1}^{n} x_i^2 + b \sum_{i=1}^{n} x_i^3 + c \sum_{i=1}^{n} x_i^4$$

The unknown coefficients a, b and c can hence be obtained by solving the above linear equations.

TABLE 1: Photometric r magnitudes, $H\alpha$HW, BCD parameters, effective temperatures and spectral classification for the stars studied in this work.† stars that we have two spectra. ⋆ stars that we have tree spectra.

#	IPHAS NAME	$l(deg)$	$b(deg)$	$r(mag)$	$H\alpha(eqw)$	ΔV	V/R	$D(dex)$	$\lambda 1(\AA)$	$T_{eff}(K)$	M_v	M_{Bol}	SpT/LC
1	$J000039.05+623316.6$	117.12	0.26	13.13	-21.7	-	-	0.315	58.8	13309	0.010	-1.021	B5-6V
2	$J000220.16+594538.7$	116.78	-2.52	14.51	-8.7	-	-	0.235	51.2	17028	-1.359	-3.077	B3-4 IV
3	$J000523.94+642621.3$	117.99	2.01	14.17	-12.4	-	-	0.268	65.6	14859	-0.127	-1.464	B6 V
4	$J000645.44+644608.9$	118.19	2.31	14.60	-42.0	-	-	0.160	66.7	22566	-1.755	-4.175	B2 V
5	$J000730.07+595614.1$	117.45	-2.47	14.13	-4.0	128.0	1.02	0.308	60.9	13458	0.084	-0.977	B5-6 V
6	$J000749.49+610314.1$	117.68	-1.37	14.50	-20.6	-	-	0.531	61.1	9450	-	-	A2
7	$J000806.97+592804.8$	117.45	-2.94	13.43	-4.1	437.0	1.34	0.149	71.3	23662	-1.772	-4.298	B2 V
8	$J000823.00+651622.5$	118.45	2.78	14.23	-13.9	256.0	1.00	0.301	44.8	14223	-1.067	-2.281	B5-6 IV
9	$J001026.29+602051.1$	117.88	-2.12	13.18	-0.3	278.8	2.44	0.259	63.2	15463	-0.322	-1.772	B5-6 V
10	$J001051.88+621009.5$	118.22	-0.33	13.59	-12.8	352.0	0.95	0.242	65.2	16557	-0.491	-2.132	B5 V
11	$J001122.29+611615.8$	118.14	-1.23	13.73	-12.4	91.4	1.01	0.134	65.1	25690	-2.392	-5.101	B1 V
12	$J001134.31+614614.8$	118.24	-0.74	15.85	-11.9	256.0	1.00	0.146	71.0	24148	-1.842	-4.414	B2 V
13	$J001224.05+623244.3$	118.45	0.01	14.67	-18.9	137.1	0.99	0.230	52.8	17302	-1.326	-3.088	B3-4 V
14	$J001252.06+595439.8$	118.11	-2.60	14.49	-10.7	-	-	0.348	58.3	12306	0.159	-0.668	B7-8V
15	$J001301.13+625649.0$	118.58	0.40	13.40	-13.9	-	-	0.330	58.7	12730	0.093	-0.820	B7-8V
16	$J001953.39+634043.6$	119.44	1.02	14.75	-40.3	-	-	0.175	56.7	21261	-1.973	-4.255	B2 V
17	$J002043.24+624310.7$	119.42	0.06	14.35	-4.4	-	-	0.316	69.8	12619	0.633	-0.257	B7 V
18	$J002242.11+611223.4$	119.48	-1.47	14.63	-13.6	-	-	0.501	78.1	9450	-	-	A1 V
19	$J002318.30+590153.8$	119.31	-3.64	14.16	-2.5	-	-	0.316	68.3	12724	0.549	-0.363	B7 V
20	$J002450.84+574414.6$	119.38	-4.95	13.98	-9.1	-	-	0.322	61.4	12902	0.212	-0.736	B7-8V
21	$J002540.04+623203.2$	119.97	-0.19	14.46	-11.2	-	-	0.318	58.4	13186	0.002	-1.004	B7-8V
22	$J002754.61+603001.4$	120.04	-2.24	13.66	-11.5	-	-	0.345	57.0	12380	0.062	-0.780	B7-8 V
23	$J002758.97+622906.1$	120.23	-0.26	15.03	-16.4	-	-	0.207	59.4	18966	-1.280	-3.283	B3-4V
24	$J002843.24+615216.2$	120.26	-0.88	14.38	-14.3	-	-	0.295	65.5	13778	0.204	-0.922	B7 V
25	$J003000.79+612238.8$	120.37	-1.39	14.24	-11.7	-	-	0.156	44.6	21195	-3.301	-5.432	B2 III
26	$J003025.04+645500.0$	120.71	2.14	15.95	-28.1	346.0	0.86	0.086	52.7	29473	-4.546	-7.477	B1 IV
27	$J003055.94+610048.8$	120.45	-1.76	15.39	-9.6	-	-	0.377	50.0	11980	-0.260	-1.021	B7-8 IV
28	$J003210.31+623929.2$	120.72	-0.13	13.39	-20.2	-	-	0.246	65.0	16295	-0.423	-2.020	B3-4 V
29	$J003351.33+613743.1$	120.84	-1.17	13.17	-5.1	-	-	0.386	63.9	11576	0.537	-0.143	B9 V
30	$J003421.40+601218.1$	120.81	-2.60	14.21	-12.5	-	-	0.314	63.7	13091	0.273	-0.714	B7-8 V
31	$J003952.40+601719.5$	121.50	-2.55	15.45	-15.0	-	-	0.554	62.2	9450	-	-	A0-1 IV
32	$J004620.80+622503.9$	122.34	-0.45	13.18	-23.4	-	-	0.214	71.7	18352	-0.679	-2.598	B4 V
33	$J004734.28+610833.6$	122.47	-1.73	13.45	-2.0	-	-	0.389	70.4	11381	0.875	0.233	B9 V
34	$J004741.54+624203.3$	122.50	-0.17	14.15	-15.5	-	-	0.350	67.7	12063	0.750	-0.027	B8 V
35	$J004842.93+644411.1$	122.64	1.87	14.74	-8.4	-	-	0.266	69.0	14819	-0.005	-1.335	B6 V
36	$J005011.87+635129.9$	122.80	0.99	13.75	-26.2	-	-	0.296	77.0	13066	0.742	-0.240	B7 V
37	$J005458.91+633913.2$	123.33	0.78	13.90	-12.5	-	-	0.394	51.4	11589	-0.149	-0.832	B7-8 V
38	$J005743.72+640235.6$	123.62	1.18	14.18	-16.8	-	-	0.378	73.8	11474	1.082	0.422	B9 V
39	$J005859.29+632603.4$	123.78	0.57	13.17	-33.6	-	-	0.312	66.6	13007	0.410	-0.560	B7 V
40	$J005926.64+651157.0$	123.77	2.34	13.45	-22.5	-	-	0.319	60.6	13038	0.137	-0.839	B7-8V
41	$J010051.26+641327.3$	123.96	1.37	13.61	-12.0	-	-	0.311	70.4	12173	0.600	-0.200	B7 V
42	$J010107.85+633227.0$	124.01	0.69	13.84	-14.5	-	-	0.279	67.5	14329	0.110	-1.125	B7 V
43	$J010138.04+641349.9$	124.04	1.38	13.32	-31.1	-	-	0.267	66.0	14788	-0.121	-1.445	B6 V
44	$J010150.19+603917.9$	124.21	-2.19	13.26	-3.6	-	-	0.341	63.4	12054	0.463	-0.313	B7-8 V
45	$J010232.39+602615.1$	124.30	-2.40	14.33	-12.2	-	-	0.311	60.3	13365	0.070	-0.972	B5-6 V
46	$J010358.11+595310.9$	124.51	-2.95	13.90	-22.0	-	-	0.197	78.1	19139	-0.690	-2.716	B3-4 V
47	$J010551.90+602737.5$	124.71	-2.36	13.57	-27.4	-	-	0.201	65.9	19329	-1.067	-3.118	B3-4 V
48	$J010733.72+604206.8$	124.90	-2.11	13.07	-18.1	-	-	0.276	69.1	14365	0.149	-1.093	B6 V
49	$J010841.17+615511.8$	124.96	-0.88	13.72	-16.3	-	-	0.403	70.5	11160	0.858	0.259	A0-1 V
50	$J011234.21+630432.5$	125.32	0.30	12.64	-24.4	-	-	0.297	65.5	13580	0.227	-0.859	B7 V
51	$J011402.43+625735.3$	125.50	0.20	12.91	-23.2	-	-	0.217	78.1	17948	-0.335	-2.195	B5-6 V
52	$J011520.26+585002.9$	126.03	-3.89	13.02	-27.9	-	-	0.265	66.5	14958	-0.123	-1.479	B6 V
53	$J011556.37+584812.1$	126.11	-3.92	13.48	-11.9	-	-	0.372	59.9	11886	0.312	-0.430	B7-8V
54	$J011757.12+594045.9$	126.28	-3.02	13.09	-18.7	-	-	0.245	60.4	16507	-0.664	-2.297	B3-4 V
55	$J011918.18+642233.8$	125.94	1.67	13.44	-41.3	-	-	0.225	70.6	17676	-0.558	-2.377	B5 V

Table 1. Continued...

#	IPHAS NAME	$l(deg)$	$b(deg)$	$r(mag)$	$H\alpha(eqw)$	ΔV	V/R	$D(dex)$	$\lambda 1(\AA)$	$T_{eff}(K)$	M_v	M_{Bol}	SpT/LC
56	$J012358.07+652615.4$	126.31	2.78	13.72	-16.9	-	-	0.302	66.2	13443	0.302	-0.756	B7 V
57	$J012416.80+633011.7^{\dagger}$	126.59	0.86	13.10	-12.9	-	-	0.232	71.9	17114	-0.363	-2.095	B5 V
58	$J012540.57+623025.7$	126.87	-0.10	13.42	-24.4	-	-	0.278	79.5	13801	0.697	-0.433	B5-6 V
59	$J012821.12+635754.0$	126.97	1.38	14.63	1.9	-	-	0.070	62.2	33482	-4.435	-7.791	O8-9 IV
60	$J013104.42+602337.3$	127.81	-2.10	14.26	-4.4	-	-	0.403	64.7	11295	0.574	-0.051	B9 V
61	$J013130.51+630914.3$	127.44	0.63	15.08	-49.0	-	-	0.375	73.4	11538	1.068	0.395	B7-8 V
62	$J013213.92+623717.2^{\dagger}$	127.60	0.12	13.32	-10.6	-	-	0.264	68.4	14997	-0.055	-1.418	B5-6 V
63	$J013244.08+595633.6$	128.09	-2.52	14.35	-14.0	-	-	0.379	57.3	11824	0.178	-0.551	B7-8 V
64	$J013328.71+610759.4$	127.99	-1.33	12.68	-23.9	-	-	0.209	68.4	18784	-0.860	-2.839	B4 V
65	$J013402.88+611358.6$	128.04	-1.22	12.92	-19.2	-	-	0.303	74.5	12794	0.703	-0.223	B7-8 V
66	$J013422.61+624459.7$	127.82	0.29	12.92	-31.3	-	-	0.246	69.9	15569	-0.216	-1.685	B5 V
67	$J013539.04+610341.6$	128.26	-1.35	14.46	-23.8	-	-	0.279	67.4	14306	0.105	-1.126	B7 V
68	$J013706.99+585234.3$	128.82	-3.47	13.47	-24.9	-	-	0.308	71.2	12876	0.604	-0.339	B7 V
69	$J013729.25+603806.2$	128.55	-1.73	15.46	-9.9	-	-	0.316	74.2	12500	0.881	0.015	B7-8 V
70	$J013739.40+613258.8$	128.41	-0.83	14.31	-11.3	-	-	0.227	71.4	17533	-0.492	-2.290	B5 V
71	$J013920.80+654338.7$	127.83	3.31	13.64	-14.9	-	-	0.337	65.8	12311	0.606	-0.222	B8 V
72	$J014146.63+581803.4$	129.52	-3.93	15.11	-14.7	-	-	0.194	72.5	19560	-0.917	-2.998	B3 V
73	$J014221.27+645836.1$	128.29	2.64	15.24	-12.8	-	-	0.325	74.8	12292	1.137	0.313	B7-8 V
74	$J014238.73+633753.1$	128.58	1.32	13.18	-6.3	-	-	0.267	69.1	14622	0.015	-1.277	B6 V
75	$J014244.86+623056.2$	128.81	0.23	13.22	-10.7	-	-	0.320	62.1	12925	0.235	-0.718	B7-8V
76	$J014322.19+640118.5$	128.58	1.72	13.29	-21.0	-	-	0.280	74.4	13951	0.463	-0.697	B7-8 V
77	$J014323.30+595307.3$	129.41	-2.33	13.69	-50.8	-	-	0.287	63.5	14165	0.016	-1.187	B5-6 V
78	$J014401.85+640124.5$	128.65	1.74	15.49	-17.9	-	-	0.250	74.4	15613	0.037	-1.440	B5-6 V
79	$J014437.08+603458.0$	129.42	-1.62	13.22	-35.9	-	-	0.244	70.5	16304	-0.221	-1.819	B5 V
80	$J014452.24+604123.3$	129.43	-1.51	13.88	-6.4	-	-	0.294	73.9	13360	0.581	-0.460	B7-8 V
81	$J014539.64+611259.1$	129.41	-0.97	12.45	-21.6	-	-	0.203	67.0	19097	-0.984	-3.005	B3-4 V
82	$J014602.11+611502.2$	129.45	-0.93	13.75	-38.9	-	-	0.243	76.0	16126	0.008	-1.560	B5 V
83	$J014624.42+611037.3$	129.51	-0.99	13.36	-4.1	-	-	0.278	74.2	14051	0.431	-0.749	B7-8 V
84	$J014659.63+611229.6$	129.57	-0.95	13.23	-26.3	-	-	0.293	73.3	13443	0.544	-0.514	B7-8 V
85	$J014807.07+631613.2$	129.25	1.10	13.54	-34.1	-	-	0.158	55.1	22559	-2.420	-4.839	B2 V
86	$J014843.39+642854.4$	129.05	2.29	13.74	-22.3	-	-	0.327	68.9	12398	0.770	-0.075	B8 V
87	$J015022.92+652743.2$	129.01	3.29	13.79	-7.0	-	-	0.169	66.4	21798	-1.605	-3.945	B2 V
88	$J015025.75+602245.2$	130.16	-1.66	14.05	-11.1	-	-	0.364	69.2	11799	0.840	0.116	B9 V
89	$J015105.68+611602.6$	130.04	-0.78	13.71	-9.7	-	-	0.332	73.3	12202	1.088	0.282	B7-8 V
90	$J015123.63+600038.6$	130.36	-1.99	12.76	-27.3	-	-	0.243	76.7	15515	0.057	-1.402	B5-6 V
91	$J015213.08+624813.6$	129.81	0.75	13.04	-11.3	-	-	0.339	62.7	12356	0.409	-0.428	B7-8 V
92	$J015307.22+650110.4$	129.39	2.92	13.97	-10.3	-	-	0.381	66.0	11605	0.651	-0.035	B9 V
93	$J015314.56+620241.5$	130.11	0.04	12.89	-7.0	-	-	0.395	57.5	11560	0.211	-0.466	B9 V
94	$J015329.19+643128.1$	129.54	2.45	13.98	-5.4	-	-	0.469	70.3	9768	0.707	0.353	A0-1 V
95	$J015520.62+611752.8$	130.53	-0.63	13.46	-17.9	-	-	0.361	70.1	11824	0.894	0.165	B9 V
96	$J015538.88+600157.0$	130.88	-1.85	14.31	-18.5	-	-	0.322	58.8	13037	0.049	-0.927	B7-8V
97	$J015627.82+612939.2$	130.61	-0.40	12.70	-15.7	-	-	0.280	71.7	13997	0.330	-0.840	B7 V
98	$J015630.89+630307.5^{\dagger}$	130.23	1.11	13.27	-29.1	-	-	0.289	73.8	13666	0.528	-0.575	B6 V
99	$J015645.78+635259.6$	130.05	1.92	13.11	-19.9	-	-	0.223	69.2	17828	-0.644	-2.486	B4 V
100	$J015716.62+575205.7^{\dagger}$	131.62	-3.89	13.15	-11.6	-	-	0.261	63.5	15572	-0.291	-1.761	B4-5 V
101	$J015804.46+653020.6$	129.77	3.52	13.14	-9.0	-	-	0.301	56.7	13917	-0.242	-1.396	B5-6 V
102	$J015919.69+645053.4$	130.07	2.92	12.78	-16.1	-	-	0.304	70.5	13060	0.524	-0.456	B7 V
103	$J015939.01+643615.4^{\dagger}$	130.17	2.69	13.26	-19.9	-	-	0.281	56.1	14670	-0.435	-1.736	B5-6 V
104	$J020014.86+570017.7$	132.23	-4.62	13.26	-5.4	-	-	0.428	53.4	11069	0.064	-0.518	B9 V
105	$J020048.75+585835.1^{\dagger}$	131.78	-2.70	13.58	-14.1	-	-	0.355	70.4	11907	0.914	0.168	B8-9 V
106	$J020049.45+635943.9$	130.45	2.14	13.91	-28.9	-	-	0.223	58.7	17824	-1.078	-2.920	B3-4V
107	$J020056.02+575529.3^{\dagger}$	132.08	-3.71	14.99	-9.2	-	-	0.229	67.5	17396	-0.617	-2.393	B4 V
108	$J020136.00+613207.6$	131.19	-0.21	13.14	-9.9	-	-	0.385	53.7	11779	-0.008	-0.728	B7-8 V
109	$J020144.86+581930.0$	132.07	-3.29	13.05	-8.2	-	-	0.188	78.4	19640	-0.795	-2.886	B3-4 V
110	$J020252.26+620926.0$	131.17	0.43	15.21	-22.9	-	-	0.225	52.3	17564	-1.430	-3.232	B3-4 IV

Table 1. Continued...

#	IPHAS NAME	$l(deg)$	$b(deg)$	$r(mag)$	$H\alpha(eqw)$	ΔV	V/R	$D(dex)$	$\lambda1(\AA)$	$T_{eff}(K)$	M_v	M_{Bol}	SpT/LC
111	$J020325.84+584145.0$	132.18	-2.88	15.42	-28.1	-	-	0.197	78.3	19138	-0.678	-2.704	B3-4 V
112	$J020326.04+635943.0^{\dagger}$	130.72	2.22	14.40	-16.9	-	-	0.188	78.3	20020	-0.798	-2.936	B2-3 V
113	$J020328.05+624334.0$	131.08	1.00	13.73	-12.9	-	-	0.276	50.5	15041	-0.879	-2.251	B5-6 V
114	$J020407.88+643122.2^{\dagger}$	130.65	2.75	13.94	-14.9	-	-	0.266	65.4	15047	-0.163	-1.536	B6 V
115	$J020421.09+591708.1$	132.13	-2.28	13.50	-13.1	-	-	0.261	67.0	15176	-0.158	-1.555	B6 V
116	$J020422.15+595855.8$	131.94	-1.61	13.42	-9.4	-	-	0.372	62.8	11830	0.476	-0.255	B7-8 V
117	$J020504.17+630216.1$	131.17	1.35	15.07	-4.3	-	-	0.262	47.9	15684	-1.235	-2.725	B5-6 IV
118	$J020547.47+641051.7$	130.92	2.47	12.68	-10.9	-	-	0.161	54.9	22501	-2.370	-4.783	B2 IV
119	$J020618.67+644945.1$	130.79	3.11	14.88	-30.9	-	-	0.217	76.2	18072	-0.452	-2.330	B4 V
120	$J020707.67+612422.7$	131.86	-0.15	13.28	-11.9	-	-	0.280	58.8	14677	-0.304	-1.607	B5-6V
121	$J020753.51+644148.9$	130.99	3.03	15.91	-6.5	-	-	0.502	55.8	9520	0.199	-0.127	A0-1 IV
122	$J020826.27+625745.9$	131.55	1.39	14.37	-18.3	-	-	0.377	46.0	12006	-0.515	-1.278	B7-8 IV
123	$J020826.93+642241.5$	131.14	2.74	12.59	-8.9	-	-	0.485	73.7	9450	-	-	A1 V
124	$J020917.87+613045.2$	132.08	0.03	13.89	-17.2	-	-	0.253	56.7	16086	-0.715	-2.276	B3-4 V
125	$J021057.06+624700.8$	131.88	1.30	14.02	-5.7	-	-	0.354	55.9	12246	0.039	-0.776	B7-8 V
126	$J021128.86+634604.0$	131.64	2.26	13.93	-12.1	-	-	0.340	65.0	12293	0.566	-0.258	B8 V
127	$J021210.42+623242.3$	132.09	1.12	12.20	-18.8	-	-	0.284	70.3	13850	0.307	-0.833	B7 V
128	$J021310.78+572406.7^{\dagger}$	133.80	-3.74	13.20	-12.0	292.5	0.99	0.318	69.6	12592	0.650	-0.235	B8 V
129	$J021320.12+613003.1$	132.54	0.17	12.89	-21.5	-	-	0.234	59.0	15011	-0.889	-2.255	B3-4V
130	$J021331.69+561900.9^{\dagger}$	134.18	-4.75	13.70	-8.6	-	-	0.394	60.4	11523	0.357	-0.313	B9 V
131	$J021336.53+601829.1$	132.94	-0.96	13.75	-5.7	-	-	0.316	67.8	12751	0.521	-0.396	B7 V
132	$J021352.00+642520.3$	131.68	2.96	15.03	-13.2	-	-	0.321	68.9	12398	0.663	-0.182	B8 V
133	$J021544.45+582456.8$	133.80	-2.67	13.33	-17.6	-	-	0.285	67.4	14060	0.179	-1.003	B7 V
134	$J022009.79+643605.9^{\dagger}$	132.27	3.35	15.65	-10.6	-	-	0.369	50.3	12226	-0.310	-1.120	B8-9 V
135	$J022025.02+600114.0$	133.84	-0.95	13.31	6.0	-	-	0.288	69.7	13820	0.323	-0.811	B7 V
136	$J022045.25+631642.8$	132.78	2.13	15.02	-18.8	-	-	0.321	61.2	12953	0.190	-0.769	B7-8V
137	$J022053.65+642835.6$	132.38	3.26	15.91	-14.2	-	-	0.283	59.0	14519	-0.265	-1.537	B5-6V
138	$J022100.28+635435.2$	132.59	2.73	13.09	-10.6	-	-	0.403	56.7	11450	0.181	-0.474	B9 V
139	$J022343.45+603545.6$	134.02	-0.27	12.94	-11.0	-	-	0.278	63.5	12086	-0.097	-0.879	B5-6 V
140	$J022502.72+644947.7^{\dagger}$	132.68	3.74	13.26	-9.3	-	-	0.352	54.1	12303	-0.116	-0.942	B7-8 V
141	$J022823.86+631834.8$	133.57	2.46	12.78	-28.4	-	-	0.189	70.6	19823	-1.060	-3.174	B3 V
142	$J022913.58+633224.5$	133.57	2.71	13.74	-14.7	-	-	0.230	57.3	17341	-1.021	-2.789	B3-4 V
143	$J023150.04+604952.4$	134.86	0.31	13.85	-53.9	-	-	0.395	76.0	11169	1.150	0.549	B9 V
144	$J023410.30+612440.6$	134.90	0.95	13.64	-92.5	-	-	0.337	80.1	11985	1.560	0.798	B8 V
145	$J023411.99+595634.4^{\dagger}$	135.47	-0.40	13.13	-17.0	-	-	0.241	71.8	16429	-0.211	-1.831	B5 V
146	$J023758.12+634635.6^{\dagger}$	134.38	3.30	13.30	-9.1	-	-	0.412	59.3	11242	0.314	-0.301	B9 V
147	$J023809.91+620224.6^{\dagger}$	135.09	1.71	13.20	-14.5	-	-	0.255	50.4	16056	-1.128	-2.684	B4-5 IV
148	$J023841.80+640826.3$	134.30	3.66	14.06	-11.1	-	-	0.326	53.6	13075	-0.294	-1.278	B7-8 V
149	$J023923.67+604247.6$	135.76	0.56	13.33	-25.0	-	-	0.319	61.8	12984	0.208	-0.757	B7-8V
150	$J023948.17+604505.1$	135.79	0.61	13.26	-15.2	-	-	0.329	70.0	12321	0.854	0.024	B8 V
151	$J023950.95+611829.1$	135.57	1.12	13.95	-49.8	-	-	0.546	70.6	9450	-	-	A2
152	$J023952.30+574354.2$	137.02	-2.14	13.51	-18.1	-	-	0.364	67.7	11841	0.753	0.020	B9 V
153	$J024102.49+574015.4$	137.19	-2.13	14.19	-22.1	-	-	0.515	73.6	9450	-	-	A1 V
154	$J024132.66+550235.9^{\star}$	138.34	-4.50	13.22	-9.0	-	-	0.382	59.9	11728	0.322	-0.388	B8 V
155	$J024146.73+602532.5$	136.14	0.42	14.05	-34.4	-	-	0.230	57.9	17340	-0.991	-2.759	B3-4V
156	$J024221.54+593716.4^{\dagger}$	136.54	-0.29	13.38	-14.3	-	-	0.417	54.7	11220	0.105	-0.506	B9 V
157	$J024332.09+632150.2$	135.11	3.17	14.16	-17.4	-	-	0.285	62.0	14339	-0.082	-1.319	B5-6 V
158	$J024504.86+612502.1$	136.09	1.48	15.35	-15.3	-	-	0.299	56.7	13990	-0.256	-1.424	B5-6 V
159	$J024519.12+633755.1$	135.18	3.50	14.04	-35.9	-	-	0.179	54.4	20910	-2.044	-4.287	B2 IV
160	$J024521.28+625416.2$	135.49	2.84	13.59	-14.9	-	-	0.259	68.7	15190	-0.111	-1.511	B5 V
161	$J024540.62+592151.1^{\dagger}$	137.03	-0.34	13.28	-23.8	-	-	0.286	61.9	14289	-0.075	-1.302	B5-6 V
162	$J024618.12+613514.8$	136.15	1.70	15.70	-26.8	-	-	0.334	58.4	12564	0.095	-0.784	B7-8V
163	$J024656.04+563924.7$	138.34	-2.72	13.48	-2.4	425.1	0.78	0.173	64.8	21539	-1.600	-3.913	B2 V
164	$J024728.30+570008.2$	138.26	-2.38	13.31	-9.0	-	-	0.255	61.2	15857	-0.437	-1.958	B5-6 V
165	$J024735.56+615530.9$	136.15	2.07	13.43	-19.8	-	-	0.276	49.8	15049	-0.921	-2.294	B5-6 IV

Table 1. Continued...

#	IPHAS NAME	$l(deg)$	$b(deg)$	$r(mag)$	$H\alpha(eqw)$	ΔV	V/R	$D(dex)$	$\lambda1(\AA)$	$T_{eff}(K)$	M_v	M_{Bol}	SpT/LC
166	$J024748.62+605750.5$	136.59	1.22	13.95	-50.7	-	-	0.420	81.1	10533	1.295	0.812	A0-1 V
167	$J024753.07+613405.8$	136.33	1.76	14.37	-29.4	-	-	0.134	72.7	24101	-2.001	-4.568	B1 V
168	$J024823.01+614728.1$	136.29	1.99	12.91	-19.6	-	-	0.282	63.7	12418	-0.038	-0.887	B5-6 V
169	$J024940.66+621424.8$	136.23	2.46	13.24	-20.5	-	-	0.321	79.9	12012	1.338	0.571	B9 V
170	$J025102.24+615733.8$	136.50	2.28	14.07	-45.4	201.6	1.20	0.206	47.8	18582	-2.031	-3.982	B3-4 IV
171	$J025130.43+621052.2$	136.45	2.50	15.79	-38.3	-	-	0.372	64.1	11797	0.549	-0.175	B7-8 V
172	$J025136.03+601557.5$	137.31	0.79	15.81	-16.9	-	-	0.448	83.6	9799	1.270	0.911	A0-1 V
173	$J025143.40+552742.7$	139.47	-3.50	13.31	-12.2	-	-	0.315	49.2	13638	-0.643	-1.741	B5-6 IV
174	$J025200.23+621145.2$	136.49	2.54	13.85	-16.3	-	-	0.310	60.6	13403	0.080	-0.970	B5-6 V
175	$J025324.54+614622.9$	136.83	2.24	15.46	-20.7	-	-	0.338	68.0	12243	0.757	-0.057	B8 V
176	$J025856.75+633557.7$	136.55	4.15	13.48	-34.8	-	-	0.316	61.6	13135	0.172	-0.824	B7-8V
177	$J025905.15+605404.2$	137.84	1.78	12.91	-45.3	-	-	0.215	72.4	18189	-0.640	-2.535	B4 V
178	$J025935.06+603207.2^{\dagger}$	138.06	1.48	13.88	-18.8	-	-	0.369	64.9	11830	0.593	-0.138	B8-9 V
179	$J030010.30+613223.4$	137.65	2.40	13.73	-13.2	-	-	0.133	59.9	25623	-2.712	-5.415	B1 V
180	$J030056.68+615940.7$	137.51	2.85	13.04	2.5	-	-	0.288	68.4	13892	0.261	-0.888	B7 V
181	$J030121.61+602856.6$	138.28	1.54	13.89	-21.8	-	-	0.360	66.9	11923	0.707	-0.042	B9 V
182	$J030144.24+632853.7^{\dagger}$	136.88	4.20	14.39	-7.8	-	-	0.270	59.5	15047	-0.372	-1.745	B5-6 V
183	$J030218.24+551133.7$	140.93	-3.04	13.89	-28.3	-	-	0.196	52.6	19558	-1.866	-3.947	B3-4 V
184	$J030317.45+583402.0$	139.42	-0.02	14.57	-20.2	-	-	0.281	44.0	14877	-1.337	-2.678	B5-6 IV
185	$J030332.35+623856.9^{\dagger}$	137.46	3.56	14.32	-9.0	-	-	0.375	55.0	11933	0.043	-0.708	B8-9 V
186	$J030422.03+574820.4^{\dagger}$	139.91	-0.62	14.40	-25.8	-	-	0.321	62.2	12895	0.251	-0.696	B7-8 V
187	$J030423.35+622901.1^{\dagger}$	137.63	3.47	13.70	-22.7	-	-	0.218	56.1	18096	-1.308	-3.190	B3-4 V
188	$J030953.64+550346.3$	141.94	-2.62	13.85	-30.8	-	-	0.252	59.8	16064	-0.541	-2.098	B3-4V
189	$J031046.28+593003.7$	139.79	1.27	15.46	-42.6	-	-	0.236	74.3	16734	-0.174	-1.845	B5-6 V
190	$J031140.70+542535.8^{\dagger}$	142.48	-3.03	13.92	-26.6	-	-	0.268	63.0	14979	-0.240	-1.600	B6 V
191	$J031141.77+614848.0^{\dagger}$	138.70	3.31	15.50	-7.8	-	-	0.425	48.1	11175	-0.220	-0.821	B9 V
192	$J031528.59+622715.3$	138.75	4.09	14.63	-7.0	-	-	0.274	46.6	15177	-1.200	-2.597	B5-6 IV
193	$J031744.98+571204.1$	141.76	-0.22	13.34	-24.4	-	-	0.247	70.0	16036	-0.196	-1.748	B5 V
194	$J031903.40+630719.9$	138.74	4.88	15.32	-12.8	-	-	0.381	57.6	11780	0.197	-0.524	B7-8V
195	$J031935.37+594155.3$	140.64	2.02	13.93	-27.5	-	-	0.262	60.4	15444	-0.409	-1.855	B5-6 V
196	$J032323.98+595855.9$	140.88	2.52	14.09	-21.0	-	-	0.223	66.1	17825	-0.764	-2.606	B3-4 V
197	$J032332.68+561452.5$	142.95	-0.60	14.21	-15.1	-	-	0.229	65.1	17441	-0.714	-2.497	B3-4 V
198	$J032415.73+615556.5$	139.90	4.20	13.83	-18.1	-	-	0.234	51.2	17036	-1.375	-3.095	B3-4 IV
199	$J033012.18+532710.0$	145.30	-2.38	15.66	-8.9	406.8	1.03	0.240	57.5	16783	-0.872	-2.551	B3-4 V
200	$J033022.30+513800.8$	146.36	-3.86	13.21	-24.1	-	-	0.226	62.3	17615	-0.870	-2.680	B3-4 V
201	$J033234.83+502346.1^{\dagger}$	147.36	-4.67	13.70	-19.2	-	-	0.256	56.1	15970	-0.717	-2.258	B4-5 V
202	$J033847.22+521508.0^{\dagger}$	147.06	-2.60	13.82	-14.3	310.8	0.98	0.300	57.2	13945	-0.216	-1.375	B5-6 V
203	$J033849.89+531730.8$	146.45	-1.76	13.91	-13.5	329.1	1.30	0.161	38.0	19057	-4.000	-5.873	B3-4 III
204	$J033912.16+604217.8$	142.08	4.23	14.87	-38.8	-	-	0.204	50.9	18907	-1.849	-3.844	B3-4 IV
205	$J033945.90+603323.8$	142.22	4.15	13.85	-20.1	-	-	0.288	51.3	14558	-0.715	-1.995	B5-6 V
206	$J034332.26+511037.8$	148.29	-3.02	13.45	-9.9	201.1	1.02	0.249	65.5	16052	-0.370	-1.925	B5 V
207	$J034441.97+583755.2$	143.88	3.00	14.53	-25.6	-	-	0.312	71.1	12691	0.650	-0.255	B7 V
208	$J034459.92+585906.2$	143.70	3.30	14.69	-9.8	137.1	1.00	0.338	63.0	12361	0.424	-0.414	B7-8 V
209	$J034528.81+585113.7$	143.83	3.23	15.42	-11.4	-	-	0.443	56.6	10772	0.212	-0.314	A0-1 V
210	$J034654.95+482052.3$	150.47	-4.92	15.02	-24.8	-	-	0.279	56.8	14769	-0.417	-1.737	B5-6 V
211	$J034748.25+603321.4$	143.01	4.75	15.05	-13.5	-	-	0.232	73.3	17128	-0.313	-2.047	B5-6 V
212	$J034828.55+562915.4$	145.61	1.62	14.31	-13.1	-	-	0.177	74.1	20769	-1.113	-3.340	B3 V
213	$J034846.85+572614.5$	145.05	2.39	13.47	-24.8	169.1	1.01	0.112	55.9	27510	-3.472	-6.336	B1 IV
214	$J034929.34+532910.8$	147.59	-0.64	14.27	-11.5	-	-	0.400	62.3	11382	0.455	-0.187	B9 V
215	$J035203.44+562347.7$	146.05	1.86	15.87	-11.8	152.2	0.95	0.277	65.9	14462	0.001	-1.260	B7 V
216	$J035754.21+571402.5$	146.13	3.01	16.67	-20.4	-	-	0.557	63.2	9450	-	-	A2
217	$J035837.56+564750.5$	146.49	2.75	15.81	-13.3	192.0	1.01	0.324	65.4	12609	0.493	-0.395	B8 V
218	$J035910.88+580234.5$	145.73	3.74	17.13	-16.4	-	-	0.318	63.5	12958	0.297	-0.663	B7-8 V
219	$J040011.86+555937.8$	147.18	2.28	15.22	-13.6	-	-	0.388	55.8	11706	0.112	-0.594	B7-8 V
220	$J040153.91+552435.8$	147.74	1.99	14.18	-6.3	-	-	0.449	49.8	10749	-0.069	-0.592	B9 IV

Table 1. Continued...

#	IPHAS NAME	$l(deg)$	$b(deg)$	$r(mag)$	$H\alpha(eqw)$	ΔV	V/R	$D(dex)$	$\lambda1(\AA)$	$T_{eff}(K)$	M_v	M_{Bol}	SpT/LC
221	$J040200.19+540003.0$	148.68	0.94	15.21	-33.6	132.6	0.94	0.167	71.8	21717	-1.396	-3.728	B2 V
222	$J040351.67+493255.7$	151.83	-2.21	15.42	-11.8	196.6	0.90	0.295	68.6	13582	0.347	-0.739	B7 V
223	$J040410.12+540420.7$	148.87	1.21	14.84	-10.1	-	-	0.284	39.6	14611	-1.665	-2.908	B5-6 III
224	$J040644.24+463308.0$	154.20	-4.12	14.18	-8.0	-	-	0.407	61.0	11299	0.394	-0.232	B9 V
225	$J040647.46+571507.8$	147.02	3.82	14.51	-29.3	-	-	0.237	57.9	16950	-0.891	-2.597	B3-4V
226	$J040648.01+573436.6$	146.80	4.06	15.04	-26.9	-	-	0.228	68.1	17481	-0.609	-2.399	B5 V
227	$J040851.75+570216.8$	147.37	3.85	13.74	5.1	-	-	0.247	65.7	16176	-0.376	-1.952	B5 V
228	$J040930.07+554107.2$	148.36	2.92	15.01	-27.7	-	-	0.279	78.5	13841	0.656	-0.482	B5-6 V
229	$J041016.15+452322.5$	155.44	-4.56	14.39	-18.3	-	-	0.371	67.8	11720	0.757	0.048	B9 V
230	$J041042.30+530216.9$	150.28	1.09	14.70	-14.7	-	-	0.258	72.5	15109	0.061	-1.323	B5-6 V
231	$J041149.03+564157.2$	147.90	3.88	14.34	-8.1	150.8	1.00	0.305	71.3	12995	0.573	-0.394	B7 V
232	$J041325.25+521559.8$	151.11	0.81	14.37	2.2	-	-	0.122	55.2	26385	-3.262	-6.031	B1 IV
233	$J041340.74+553748.6$	148.83	3.28	14.19	-4.0	265.1	1.00	0.205	59.6	19126	-1.303	-3.328	B3-4V
234	$J041503.65+520945.8$	151.37	0.91	13.39	-6.3	-	-	0.334	63.3	12422	0.424	-0.426	B7-8 V
235	$J041519.45+495124.5$	152.99	-0.73	13.68	-12.3	-	-	0.257	56.7	15866	-0.665	-2.187	B5-6 V
236	$J041539.56+532702.8$	150.54	1.90	13.99	-23.9	-	-	0.250	59.7	16190	-0.598	-2.177	B3-4V
237	$J041544.68+534956.1$	150.28	2.18	13.86	-15.2	-	-	0.306	62.6	13468	0.157	-0.906	B5-6 V
238	$J041617.43+452538.8$	156.18	-3.81	13.05	-17.7	-	-	0.325	63.7	12636	0.397	-0.497	B7-8 V
239	$J041629.72+553617.9$	149.13	3.54	14.54	-14.9	-	-	0.325	72.0	12343	0.951	0.117	B8 V
240	$J041750.14+532526.1$	150.79	2.11	13.33	-48.2	-	-	0.189	61.2	20212	-1.465	-3.627	B3-4 V
241	$J041912.84+451756.8$	156.64	-3.54	13.60	-34.3	-	-	0.275	60.4	14798	-0.264	-1.590	B5-6 V
242	$J042035.09+562307.8$	148.99	4.49	14.76	-18.3	-	-	0.321	63.6	12800	0.337	-0.590	B7-8 V
243	$J042053.25+494407.3$	153.72	-0.19	13.99	-8.7	-	-	0.290	55.6	14399	-0.396	-1.645	B5-6 V
244	$J042100.42+560539.0$	149.24	4.33	14.20	-18.2	-	-	0.207	75.1	18704	-0.650	-2.618	B5 V
245	$J042101.62+450857.9$	156.97	-3.42	13.52	-29.0	-	-	0.291	71.6	13606	0.444	-0.647	B7 V
246	$J042138.79+551330.5$	149.92	3.78	14.23	-33.7	-	-	0.260	54.4	15786	-0.779	-2.287	B5-6 V
247	$J042248.80+470643.6$	155.80	-1.82	13.52	-37.8	-	-	0.248	62.1	16269	-0.510	-2.102	B3-4 V
248	$J042332.36+474409.0$	155.44	-1.29	14.92	-19.0	-	-	0.286	68.5	13985	0.243	-0.924	B7 V
249	$J042353.25+460947.0^{\dagger}$	156.60	-2.36	14.11	-19.3	-	-	0.245	60.7	16588	-0.649	-2.295	B4-5 V
250	$J042413.34+535555.2$	151.10	3.13	15.30	-17.5	-	-	0.174	52.4	21085	-2.282	-4.545	B2 IV
251	$J042420.69+441501.8$	158.03	-3.64	13.29	-41.1	-	-	0.239	72.0	16581	-0.234	-1.879	B5 V
252	$J042533.76+533645.4$	151.47	3.05	15.09	-9.9	214.8	0.97	0.288	53.9	14524	-0.505	-1.778	B5-6 V
253	$J042853.13+483132.5$	155.50	-0.10	15.44	-27.4	-	-	0.500	78.1	9450	-	-	A1 V
254	$J042917.05+523426.3$	152.61	2.74	13.37	-17.3	-	-	0.110	65.4	28334	-3.003	-5.935	B1 V
255	$J043002.27+454748.9^{\dagger}$	157.61	-1.84	15.22	-22.9	-	-	0.233	70.9	17102	-0.393	-2.123	B4-5 V
256	$J043035.52+523659.6$	152.71	2.91	15.45	-51.2	-	-	0.264	63.9	15137	-0.244	-1.634	B5-6 V
257	$J043204.46+545014.9$	151.24	4.59	14.05	-15.0	-	-	0.346	59.6	12311	0.233	-0.595	B7-8V
258	$J043206.08+521521.2$	153.13	2.83	13.36	-39.6	-	-	0.224	43.2	17214	-2.099	-3.823	B3-4 IV
259	$J043225.85+485200.7^{\dagger}$	155.65	0.56	14.00	-37.3	-	-	0.251	66.5	15877	-0.278	-1.802	B5 V
260	$J043242.92+443647.3$	158.80	-2.31	13.85	-9.1	-	-	0.393	49.5	11700	-0.233	-0.938	B7-8 IV
261	$J043324.72+405849.2$	161.55	-4.68	14.98	-4.9	-	-	0.257	64.0	15619	-0.309	-1.787	B5-6 V
262	$J043332.06+432101.0$	159.82	-3.06	13.88	-7.3	-	-	0.398	66.6	11331	0.670	0.038	B9 V
263	$J043623.80+452053.6^{\dagger}$	158.70	-1.33	14.29	-5.4	420.5	1.02	0.272	57.5	15014	-0.445	-1.812	B5-6 V
264	$J043846.94+435224.2^{\dagger}$	160.08	-2.00	14.86	-21.8	-	-	0.236	61.5	16965	-0.735	-2.443	B3-4 V
265	$J043848.81+433446.0$	160.30	-2.19	15.31	-15.5	-	-	0.292	65.6	13883	0.175	-0.972	B7 V
266	$J043850.23+475233.9$	157.10	0.67	14.09	-23.7	-	-	0.212	64.9	18593	-0.948	-2.900	B3-4 V
267	$J043857.76+401339.3^{\dagger}$	162.82	-4.40	14.86	-6.0	192.0	0.92	0.303	57.8	13782	-0.153	-1.280	B5-6 V
268	$J044041.07+412132.4^{\dagger}$	162.19	-3.41	14.70	-9.2	-	-	0.376	69.9	11590	0.871	0.188	B9 V
269	$J044057.63+395223.5^{\dagger}$	163.34	-4.35	16.28	-7.5	232.2	0.96	0.287	74.7	13619	0.550	-0.544	B7-8 V
270	$J044137.04+463330.9^{\dagger}$	158.40	0.15	13.97	-9.3	-	-	0.350	60.6	12284	0.310	-0.512	B7-8V
271	$J044154.56+423021.9^{\dagger}$	161.48	-2.48	13.75	-12.0	-	-	0.268	70.1	15010	0.085	-1.281	B6 V
272	$J044156.94+430450.2^{\dagger}$	161.05	-2.10	14.01	-16.1	-	-	0.323	58.2	12994	0.017	-0.950	B6-7 V
273	$J044257.10+415011.7$	162.11	-2.78	14.99	-13.1	-	-	0.229	72.4	17383	-0.397	-2.171	B5 V
274	$J044311.19+485747.1^{\dagger}$	156.76	1.93	14.29	-7.1	320.0	1.02	0.360	57.9	12248	0.178	-0.637	B8-9 V
275	$J044312.52+485736.7^{\dagger}$	156.77	1.94	14.93	-20.2	-	-	0.307	54.6	13765	-0.336	-1.459	B6-7 V

Table 1. Continued...

#	IPHAS NAME	$l(deg)$	$b(deg)$	$r(mag)$	$H\alpha(eqw)$	ΔV	V/R	$D(dex)$	$\lambda1(\AA)$	$T_{eff}(K)$	M_v	M_{Bol}	SpT/LC
276	J044521.00 + 420717.3	162.19	-2.25	14.70	-17.9	-	-	0.197	56.2	19596	-1.610	-3.696	B3-4 V
277	J044547.89 + 443831.9	160.32	-0.55	14.79	-5.2	438.8	1.04	0.350	75.9	11865	1.259	0.521	B9 V
278	J044557.84 + 414245.7	162.57	-2.43	14.08	-23.9	-	-	0.299	58.9	13915	-0.098	-1.251	B5-6V
279	J044748.62 + 514104.1	155.17	4.26	14.06	-7.5	352.0	0.95	0.291	60.5	14166	-0.081	-1.284	B5-6 V
280	J044812.10 + 411819.2	163.15	-2.38	14.01	-22.2	-	-	0.298	61.1	13844	0.038	-1.101	B5-6 V
281	J044818.02 + 433643.4	161.40	-0.88	14.64	-16.5	347.4	1.10	0.396	64.3	11415	0.556	-0.093	B9 V
282	J044841.84 + 445015.7	160.51	-0.03	14.28	-20.2	-	-	0.275	64.9	14618	-0.071	-1.362	B5-6 V
283	J044847.67 + 464207.3	159.09	1.18	13.54	-8.2	-	-	0.393	60.3	11544	0.351	-0.323	B9 V
284	J044943.82 + 395108.5	164.46	-3.09	13.72	-12.2	-	-	0.319	54.1	13324	-0.300	-1.334	B5-6 V
285	J045000.02 + 411434.2	163.42	-2.16	15.69	-15.0	-	-	0.375	48.3	12025	-0.212	-0.982	B7-8 IV
286	J045251.33 + 424635.6	162.57	-0.77	14.12	-17.4	-	-	0.304	69.7	13129	0.486	-0.509	B7 V
287	J045329.30 + 410220.4	163.99	-1.78	13.57	-11.0	-	-	0.282	64.9	14314	0.021	-1.211	B5-6 V
288	J045339.41 + 462135.3	159.89	1.61	15.62	-14.4	-	-	0.331	71.0	12276	0.929	0.108	B8 V
289	J045414.61 + 452916.8	160.63	1.14	15.36	-10.1	-	-	0.412	43.5	11365	-0.533	-1.166	B9 IV
290	J045457.62 + 462400.1	160.00	1.81	14.59	-13.4	141.7	1.03	0.260	51.3	15816	-0.985	-2.498	B5-6 V
291	J045501.67 + 362602.7	167.77	-4.44	14.45	-26.3	-	-	0.215	60.3	18423	-1.120	-3.049	B3-4 V
292	J045511.25 + 383344.1	166.13	-3.08	16.21	-24.0	-	-	0.240	60.8	16758	-0.725	-2.400	B3-4 V
293	J045552.92 + 370005.5	167.43	-3.95	14.64	-21.1	341.0	1.00	0.286	66.5	14068	0.148	-1.036	B7 V
294	J045625.52 + 402409.5	164.84	-1.75	14.55	-10.4	-	-	0.397	59.5	11491	0.314	-0.349	B9 V
295	J045647.57 + 490802.2	158.06	3.76	14.26	-19.6	-	-	0.216	73.8	18179	-0.575	-2.469	B4 V
296	J045659.27 + 463204.2	160.11	2.16	13.67	-16.6	-	-	0.353	63.7	12107	0.508	-0.278	B7-8 V
297	J045901.33 + 403011.5	165.07	-1.30	14.26	-18.2	-	-	0.273	61.6	14829	-0.238	-1.570	B5-6 V
298	J045917.19 + 431609.2	162.93	0.45	13.34	-9.9	-	-	0.389	62.4	11562	0.458	-0.219	B9 V
299	J045929.27 + 455715.4	160.84	2.14	14.93	-37.6	-	-	0.276	68.3	14432	0.108	-1.147	B6 V
300	J050014.87 + 504256.4	157.15	5.17	13.83	-5.4	141.7	0.95	0.289	53.6	14489	-0.523	-1.789	B5-6 V
301	J050142.31 + 433837.7	162.90	1.03	14.68	-19.8	283.4	1.00	0.296	56.9	14119	-0.273	-1.467	B5-6 V
302	J050239.27 + 371555.8	168.06	-2.73	14.66	-12.9	-	-	0.342	66.7	12218	0.681	-0.128	B8 V
303	J050303.80 + 422144.6	164.07	0.44	15.34	-44.7	-	-	0.479	59.5	10076	0.324	-0.084	A0-1V
304	J050315.37 + 401006.4	165.83	-0.87	14.92	-27.7	-	-	0.225	65.5	17698	-0.758	-2.581	B3-4 V
305	J050325.87 + 333301.9	171.11	-4.86	14.69	-10.4	-	-	0.308	62.9	13390	0.185	-0.863	B5-6 V
306	J050517.54 + 433805.3	163.30	1.54	15.50	-22.7	-	-	0.320	67.6	12614	0.566	-0.323	B8 V
307	J050535.04 + 442648.4	162.69	2.07	13.21	-44.4	-	-	0.235	67.9	17027	-0.501	-2.219	B5 V
308	J050556.75 + 430528.9	163.81	1.31	13.34	-11.9	347.4	1.00	0.369	67.9	11758	0.763	0.047	B9 V
309	J050649.71 + 421532.4	164.57	0.93	13.27	-12.9	-	-	0.309	57.9	13557	-0.102	-1.183	B5-6V
310	J050826.96 + 361342.9	169.59	-2.43	15.81	-15.8	-	-	0.275	49.8	15106	-0.935	-2.319	B5-6 IV
311	J050830.91 + 424234.2	164.40	1.45	13.22	-36.7	-	-	0.313	42.3	13771	-1.204	-2.316	B5-6 IV
312	J050904.06 + 385915.2	167.45	-0.68	14.43	-24.9	-	-	0.308	63.5	13348	0.216	-0.823	B5-6 V
313	J051000.63 + 384938.4	167.68	-0.63	13.78	-13.6	-	-	0.312	60.1	13341	0.065	-0.973	B7-8V
314	J051013.60 + 414158.9	165.40	1.11	13.84	-7.6	-	-	0.375	66.3	11693	0.673	-0.030	B9 V
315	J051014.52 + 362436.4	169.66	-2.03	13.58	-3.5	132.6	0.98	0.306	71.7	12916	0.605	-0.346	B7 V
316	J051051.62 + 432124.7	164.13	2.18	13.65	-42.2	-	-	0.193	67.2	19787	-1.141	-3.251	B3-4 V
317	J051143.01 + 431034.8	164.37	2.20	14.56	-14.1	-	-	0.309	46.9	13897	-0.848	-1.998	B5-6 IV
318	J051206.61 + 442634.5	163.39	3.01	13.50	-13.8	-	-	0.259	61.6	15585	-0.387	-1.859	B5-6 V
319	J051208.12 + 365020.3	169.53	-1.47	13.14	-9.9	-	-	0.276	64.9	14562	-0.058	-1.338	B5-6 V
320	J051226.87 + 445432.3	163.04	3.33	14.46	-25.4	-	-	0.252	61.6	16031	-0.463	-2.014	B5-6 V
321	J051339.97 + 413555.0	165.86	1.57	14.77	-9.0	-	-	0.408	65.1	11202	0.590	-0.017	A0-1 V
322	J051427.19 + 412419.1	166.10	1.57	13.15	-11.8	-	-	0.298	65.6	13643	0.242	-0.857	B7 V
323	J051555.71 + 394846.8	167.56	0.87	14.79	-12.0	-	-	0.347	60.1	12286	0.268	-0.555	B7-8V
324	J051633.27 + 414641.0	166.03	2.11	13.25	-21.7	-	-	0.308	57.7	13619	-0.124	-1.218	B5-6V
325	J051634.39 + 402856.1	167.08	1.36	15.73	-40.1	-	-	0.432	70.0	10645	0.771	0.268	A0-1 V
326	J051703.53 + 405053.4	166.84	1.65	14.34	-38.4	-	-	0.167	65.3	21980	-1.693	-4.053	B2 V
327	J051938.22 + 330302.0	173.51	-2.42	13.76	-7.5	146.3	1.02	0.357	73.6	11815	1.103	0.375	B7-8 V
328	J052340.51 + 345144.5	172.50	-0.70	13.83	-9.0	-	-	0.465	53.3	10457	0.098	-0.374	A0-1 IV
329	J052423.13 + 283541.6	177.77	-4.10	13.26	-8.7	-	-	0.324	48.5	13336	-0.631	-1.668	B5-6 IV
330	J052429.89 + 301950.7	176.34	-3.11	13.63	-14.1	-	-	0.214	63.9	18424	-0.961	-2.890	B3-4 V

Table 1. Continued...

#	IPHAS NAME	$l(deg)$	$b(deg)$	$r(mag)$	$H\alpha(eqw)$	ΔV	V/R	$D(dex)$	$\lambda1(\AA)$	$T_{eff}(K)$	M_v	M_{Bol}	SpT/LC
331	$J052500.42+294250.0$	176.92	-3.36	15.37	-6.5	401.3	0.94	0.327	69.4	12379	0.804	-0.038	B8 V
332	$J052524.19+300543.8$	176.65	-3.08	13.58	-13.6	-	-	0.308	64.2	13292	0.251	-0.777	B5-6 V
333	$J052541.12+303753.8$	176.24	-2.73	14.54	-6.9	-	-	0.395	58.7	11545	0.272	-0.402	B9 V
334	$J052636.70+392052.4$	169.11	2.30	14.63	-28.3	-	-	0.215	67.3	18364	-0.825	-2.745	B3-4 V
335	$J052701.81+423622.7$	166.44	4.18	13.94	-25.8	-	-	0.253	83.8	14871	0.680	-0.660	B7 V
336	$J052717.19+415441.6$	167.05	3.83	13.84	-22.3	-	-	0.275	62.9	14692	-0.161	-1.466	B5-6 V
337	$J052754.29+393100.5$	169.11	2.60	14.76	-31.8	-	-	0.152	71.1	23363	-1.723	-4.221	B2 V
338	$J052824.43+315446.2$	175.50	-1.53	14.51	-6.4	-	-	0.253	60.6	15982	-0.481	-2.024	B5-6 V
339	$J052850.94+272112.1$	179.35	-3.97	14.57	-11.8	-	-	0.369	52.2	12068	-0.187	-0.966	B7-8 V
340	$J052903.87+292609.6^{\dagger}$	177.64	-2.78	15.46	-7.3	196.6	1.02	0.331	57.2	12825	-0.003	-0.936	B6-7 V
341	$J052907.77+285336.1$	178.10	-3.07	15.00	-12.3	346.5	1.06	0.323	62.0	12827	0.260	-0.673	B7-8V
342	$J052919.14+341747.2$	173.62	-0.05	13.41	-49.8	-	-	0.371	72.9	11601	1.045	0.360	B7-8 V
343	$J052926.22+351610.6$	172.82	0.51	13.80	-22.2	-	-	0.525	80.7	9450	-	-	A1 V
344	$J052947.46+332915.5$	174.34	-0.42	14.65	-15.6	292.5	0.80	0.613	71.5	9450	-	-	¿A2
345	$J053015.44+343124.3$	173.53	0.23	13.54	-26.6	-	-	0.224	49.3	17499	-1.650	-3.442	B3-4 IV
346	$J053035.92+292653.4$	177.81	-2.50	13.58	-7.7	-	-	0.352	56.9	12263	0.090	-0.728	B7-8 V
347	$J053040.91+260534.7$	180.64	-4.32	14.71	-7.7	274.3	0.96	0.267	59.0	15231	-0.423	-1.830	B5-6V
348	$J053049.54+294638.8$	177.57	-2.27	15.33	-15.3	-	-	0.353	46.6	12430	-0.608	-1.459	B7-8 IV
349	$J053054.44+331859.1$	174.62	-0.32	13.92	-9.6	-	-	0.173	46.0	20507	-2.799	-4.962	B3-4 IV
350	$J053116.68+330327.9$	174.87	-0.39	14.40	-9.0	-	-	0.371	56.9	11952	0.142	-0.613	B7-8 V
351	$J053304.40+300057.1$	177.63	-1.74	15.41	-14.2	-	-	0.211	52.3	18533	-1.631	-3.575	B3-4 IV
352	$J053307.98+284749.1$	178.66	-2.39	15.63	-15.0	-	-	0.238	59.0	16928	-0.829	-2.531	B3-4V
353	$J053459.32+280743.6$	179.45	-2.41	14.36	-8.1	-	-	0.297	56.8	14094	-0.270	-1.459	B5-6 V
354	$J053506.68+410849.2$	168.49	4.64	14.34	-11.8	-	-	0.315	70.2	12613	0.642	-0.247	B7 V
355	$J053534.92+280437.2$	179.56	-2.33	14.88	-8.3	-	-	0.278	50.8	14935	-0.839	-2.191	B5-6 V
356	$J053635.21+315003.2$	176.51	-0.12	13.88	-29.0	-	-	0.532	76.2	9450	-	-	A2
357	$J053645.74+274624.5^{\dagger}$	179.96	-2.27	13.65	-15.9	-	-	0.203	60.1	19194	-1.311	-3.345	B3-4 V
358	$J053814.48+260619.3$	181.54	-2.88	13.26	-11.3	-	-	0.265	53.6	15509	-0.769	-2.227	B5-6 V
359	$J053857.23+373003.2$	171.98	3.32	14.43	-21.5	-	-	0.514	79.8	9450	-	-	¿A2
360	$J053909.17+354422.7$	173.50	2.42	13.77	-26.0	-	-	0.505	65.2	9450	-	-	A2
361	$J053917.89+251535.9$	182.39	-3.13	14.88	-17.1	-	-	0.335	68.8	12263	0.798	-0.020	B8 V
362	$J053918.09+361716.3$	173.05	2.74	13.78	-26.1	-	-	0.407	73.2	11041	0.982	0.405	A0-1 V
363	$J054252.85+325435.9$	176.31	1.58	13.57	-14.5	-	-	0.338	47.4	12855	-0.632	-1.571	B7-8 IV
364	$J054424.58+342802.8$	175.14	2.67	15.25	-18.4	294.4	1.00	0.428	70.7	10695	0.810	0.298	A0-1 V
365	$J054640.73+240939.5$	184.20	-2.28	15.09	-10.4	-	-	0.375	48.5	12012	-0.363	-1.130	B7-8 IV
366	$J054705.80+223410.0^{\dagger}$	185.62	-3.02	14.88	-17.6	-	-	0.249	52.2	16351	-1.068	-2.674	B3-4 V
367	$J054806.31+302129.0$	179.06	1.20	13.62	-22.2	-	-	0.126	58.3	26254	-2.966	-5.724	B1 V
368	$J054818.58+214945.5$	186.40	-3.16	14.42	-41.5	-	-	0.324	64.0	12692	0.402	-0.503	B7-8 V
369	$J054828.23+304607.8^{\dagger}$	178.75	1.48	13.33	-7.9	-	-	0.309	64.5	13227	0.274	-0.740	B7-8 V
370	$J054828.90+312019.6$	178.27	1.77	14.52	-14.1	-	-	0.311	57.0	13517	-0.153	-1.226	B5-6 V
371	$J054836.10+190733.1$	188.76	-4.49	14.19	-18.5	-	-	0.293	73.8	13403	0.567	-0.483	B7-8 V
372	$J054837.64+281710.3$	180.90	0.23	14.71	-40.3	-	-	0.194	57.6	19804	-1.579	-3.691	B3-4V
373	$J054848.26+283547.8$	180.65	0.42	14.72	-41.4	-	-	0.187	57.8	20353	-1.703	-3.882	B3-4V
374	$J054937.88+281123.3^{\dagger}$	181.09	0.37	13.95	-18.3	-	-	0.325	62.9	12815	0.343	-0.587	B6-7 V
375	$J054955.18+325007.3$	177.14	2.80	15.08	-18.3	-	-	0.242	52.7	16689	-1.128	-2.791	B3-4 V
376	$J055034.99+253827.5$	183.39	-0.76	14.91	-17.9	-	-	0.196	61.6	19723	-1.347	-3.449	B3-4 V
377	$J055046.66+324106.0^{\dagger}$	177.36	2.88	13.93	-9.7	294.8	1.05	0.344	63.1	12276	0.451	-0.370	B7-8V
378	$J055118.77+285657.0$	180.63	1.07	13.37	-16.3	273.8	0.98	0.276	51.6	15035	-0.804	-2.175	B5-6 V
379	$J055125.99+212428.9$	187.13	-2.75	15.64	-15.6	-	-	0.309	60.3	13451	0.059	-1.001	B5-6 V
380	$J055339.80+315112.6$	178.39	2.99	13.65	-26.3	-	-	0.280	70.9	14105	0.291	-0.900	B7 V
381	$J055342.76+215223.3^{\dagger}$	187.00	-2.06	14.41	-15.1	-	-	0.290	66.1	13921	0.175	-0.979	B7 V
382	$J055350.96+293653.1$	180.34	1.89	13.03	-19.3	-	-	0.287	58.5	14404	-0.260	-1.510	B5-6V
383	$J055423.14+242447.7$	184.89	-0.64	15.40	-15.1	-	-	0.238	67.3	16786	-0.475	-2.154	B3-4 V
384	$J055428.68+293310.9$	180.46	1.98	13.27	-12.9	-	-	0.234	56.5	17120	-0.993	-2.726	B3-4 V
385	$J055437.81+252106.1$	184.10	-0.12	13.84	-20.7	-	-	0.251	60.1	16117	-0.539	-2.105	B5-6 V

Table 1. Continued...

#	IPHAS NAME	$l(deg)$	$b(deg)$	$r(mag)$	$H\alpha(eqw)$	ΔV	V/R	$D(dex)$	$\lambda 1(\AA)$	$T_{eff}(K)$	M_v	M_{Bol}	SpT/LC
386	$J055439.93+320300.4$	178.32	3.27	14.06	-6.9	431.5	0.95	0.323	65.8	12621	0.503	-0.388	B8 V
387	$J055508.86+241730.0^{\dagger}$	185.08	-0.55	14.26	-14.6	-	-	0.266	64.6	15009	-0.193	-1.559	B6 V
388	$J055517.56+292036.4$	180.73	2.02	14.59	-15.4	-	-	0.366	61.9	11950	0.419	-0.336	B7-8V
389	$J055524.64+225436.7$	186.30	-1.20	13.95	-37.6	-	-	0.107	33.2	20059	-6.398	-8.163	B2 Ib
390	$J055538.03+255133.6$	183.78	0.33	13.61	-19.6	-	-	0.225	57.0	17680	-1.144	-2.964	B3-4 V
391	$J055538.64+185156.8$	189.83	-3.19	13.68	-8.6	-	-	0.263	59.4	15439	-0.442	-1.887	B5-6V
392	$J055552.55+251714.0$	184.30	0.09	14.60	-32.7	-	-	0.211	61.7	18669	-1.107	-3.070	B3-4 V
393	$J055558.82+254846.4$	183.86	0.38	14.72	-22.5	-	-	0.189	47.3	19674	-2.369	-4.464	B3-4 IV
394	$J055638.79+190355.8$	189.77	-2.88	14.91	-22.9	332.8	1.33	0.169	53.0	21551	-2.336	-4.650	B2 IV
395	$J055650.22+190537.3$	189.77	-2.83	14.80	-16.8	-	-	0.241	61.0	16718	-0.702	-2.370	B3-4 V
396	$J055746.88+224033.2$	186.78	-0.84	15.04	9.8	-	-	0.534	64.5	9450	-	-	A2
397	$J055801.70+192238.7$	189.67	-2.44	15.01	-23.8	-	-	0.171	60.5	21712	-1.848	-4.179	B2 V
398	$J055824.07+142741.8$	193.99	-4.81	13.90	-10.1	-	-	0.329	54.4	12946	-0.219	-1.176	B7-8 V
399	$J055831.49+264236.3$	183.37	1.32	14.50	-41.0	-	-	0.399	71.1	11211	0.894	0.285	B9 V
400	$J055838.98+201108.6$	189.04	-1.91	13.47	-13.4	-	-	0.463	76.0	9597	0.927	0.600	A0-1 V
401	$J055851.85+260054.3$	184.01	1.04	15.11	-43.2	-	-	0.238	59.0	16935	-0.829	-2.532	B3-4V
402	$J055852.97+303000.5^{\dagger}$	180.12	3.27	13.07	-8.1	-	-	0.393	54.4	11633	0.049	-0.642	B8-9 V
403	$J055854.14+220300.2$	187.45	-0.93	14.70	-15.1	182.8	0.95	0.187	66.3	20327	-1.277	-3.452	B3-4 V
404	$J055855.66+331231.3$	177.76	4.62	15.31	-10.1	306.3	1.00	0.345	57.7	12372	0.107	-0.733	B7-8V
405	$J055926.03+271328.8$	183.02	1.75	14.67	-16.7	201.1	0.96	0.380	68.5	11561	0.788	0.111	B9 V
406	$J055931.30+201959.8$	189.01	-1.66	14.68	-15.7	288.4	0.88	0.437	78.9	10214	1.129	0.702	A0-1 V
407	$J055936.06+255150.2$	184.22	1.11	15.16	-14.3	-	-	0.324	57.8	12995	-0.004	-0.971	B7-8V
408	$J055951.57+142840.2$	194.15	-4.49	13.76	-21.6	-	-	0.309	61.9	13392	0.141	-0.907	B5-6 V
409	$J060541.43+305126.3$	180.53	4.73	13.22	-12.8	-	-	0.321	63.7	12797	0.343	-0.584	B7-8 V
410	$J060558.53+105731.7$	197.96	-4.91	14.65	-8.4	400.9	0.99	0.361	62.5	12004	0.449	-0.317	B7-8 V
411	$J060602.06+271527.4$	183.72	3.05	13.93	-20.7	-	-	0.192	77.1	19475	-0.790	-2.860	B4 V
412	$J060705.99+264108.3$	184.33	2.97	14.29	-32.6	114.3	1.07	0.257	67.6	15396	-0.166	-1.604	B5 V
413	$J060729.66+233600.8$	187.08	1.56	13.79	-14.9	-	-	0.281	62.1	14483	-0.124	-1.389	B5-6 V
414	$J060803.63+174100.8$	192.31	-1.20	14.29	-21.1	-	-	0.288	64.7	14074	0.086	-1.099	B5-6 V
415	$J060926.17+244107.9$	186.34	2.47	15.17	-15.2	-	-	0.321	65.8	12681	0.472	-0.431	B8 V
416	$J060934.04+150245.0^{\dagger}$	194.80	-2.17	14.11	-28.3	-	-	0.232	65.7	17153	-0.642	-2.380	B4-5 V
417	$J060943.25+191607.8$	191.12	-0.09	15.05	-45.2	-	-	0.219	70.9	18044	-0.638	-2.512	B4 V
418	$J061009.23+245125.7$	186.27	2.69	14.90	-16.0	-	-	0.312	52.2	13679	-0.460	-1.566	B5-6 V
419	$J061256.09+151534.2$	195.00	-1.35	14.50	-22.6	-	-	0.265	65.5	14966	-0.171	-1.529	B6 V
420	$J061501.84+205722.8$	190.23	1.81	14.79	-22.5	196.6	0.96	0.255	62.7	15766	-0.392	-1.896	B5-6 V
421	$J061535.86+103122.4$	199.48	-3.04	14.22	-19.0	-	-	0.367	51.9	12108	-0.215	-1.002	B7-8 V
422	$J061658.93+251525.9$	186.65	4.24	13.65	-16.2	-	-	0.372	62.9	11821	0.481	-0.248	B7-8 V
423	$J061702.42+214726.7$	189.72	2.62	14.97	-16.0	-	-	0.274	55.2	15049	-0.541	-1.914	B5-6 V
424	$J061720.96+102255.8$	199.80	-2.73	13.34	-16.1	-	-	0.342	53.4	12527	-0.226	-1.098	B7-8 V
425	$J061812.82+111641.8$	199.11	-2.12	14.96	-18.3	-	-	0.317	62.4	13056	0.225	-0.755	B7-8V
426	$J061926.67+045535.8$	204.88	-4.83	13.26	-26.3	-	-	0.200	66.3	19367	-1.065	-3.121	B3-4 V
427	$J061938.87+090115.1$	201.27	-2.87	14.56	-11.5	-	-	0.237	72.4	16722	-0.248	-1.917	B5 V
428	$J062010.01+135204.4$	197.06	-0.47	13.75	-15.5	201.1	0.98	0.315	55.2	13469	-0.242	-1.306	B5-6 V
429	$J062026.19+090100.9$	201.37	-2.70	14.22	-10.4	-	-	0.328	60.3	12701	0.190	-0.717	B7-8V
430	$J062028.45+144418.3$	196.32	0.00	15.19	-22.0	-	-	0.329	51.2	13055	-0.426	-1.405	B5-6 V
431	$J062109.79+101511.5$	200.36	-1.96	14.67	-46.5	-	-	0.251	52.7	16225	-0.999	-2.584	B3-4 V
432	$J062121.82+141413.4$	196.87	-0.04	13.78	-25.2	150.8	1.01	0.280	53.1	14855	-0.650	-1.987	B5-6 V
433	$J062245.04+213111.9$	190.59	3.66	13.72	-29.0	-	-	0.417	79.6	10648	1.242	0.738	A0-1 V
434	$J062252.06+144918.7$	196.52	0.55	13.48	-13.5	-	-	0.267	49.6	15450	-1.023	-2.470	B5-6 IV
435	$J062306.42+224659.8$	189.50	4.32	14.95	-19.4	-	-	0.540	72.3	9450	-	-	¿A2
436	$J062406.11+143614.8$	196.85	0.72	14.37	-32.9	-	-	0.262	55.1	15653	-0.707	-2.191	B5-6 V
437	$J062456.26+092740.0$	201.50	-1.51	15.42	-18.7	-	-	0.241	61.0	16726	-0.702	-2.371	B3-4 V
438	$J062502.16+152610.6$	196.22	1.30	13.37	-15.4	-	-	0.208	62.3	18844	-1.121	-3.108	B3-4 V
439	$J062538.89+062506.5$	204.27	-2.77	14.82	-15.7	-	-	0.334	53.8	12787	-0.238	-1.163	B7-8 V
440	$J062728.07+045458.0$	205.82	-3.07	15.55	-24.8	-	-	0.302	42.8	14127	-1.249	-2.438	B5-6 IV

Table 1. Continued...

#	IPHAS NAME	$l(deg)$	$b(deg)$	$r(mag)$	$H\alpha(equ)$	ΔV	V/R	$D(dex)$	$\lambda1(\AA)$	$T_{eff}(K)$	M_v	M_{Bol}	SpT/LC
441	$J063049.29+001016.3$	210.42	-4.51	15.95	-14.1	237.7	1.03	0.287	62.2	14243	-0.048	-1.266	B5-6 V
442	$J063119.96+010043.1$	209.73	-4.01	14.36	-31.8	-	-	0.135	67.9	25595	-2.222	-4.923	B1 V
443	$J063148.63+151010.0$	197.22	2.63	13.45	-23.1	-	-	0.257	54.4	15950	-0.816	-2.353	B5-6 V
444	$J063224.63+020609.5$	208.89	-3.27	14.61	-10.8	-	-	0.300	55.9	14008	-0.299	-1.471	B5-6 V
445	$J063554.84-024244.8$	213.58	-4.69	13.48	-66.5	-	-	0.232	40.9	16746	-2.180	-3.789	B3-4 III
446	$J063605.85-022556.3$	213.35	-4.52	15.33	-40.5	-	-	0.330	50.1	13075	-0.479	-1.463	B7-8 V
447	$J063637.48-022128.3$	213.34	-4.37	15.28	-37.2	-	-	0.536	76.7	9450	-	-	¿A2
448	$J063639.47+012451.7$	209.99	-2.64	16.45	-41.9	187.0	0.97	0.248	53.9	16378	-0.962	-2.573	B3-4 V
449	$J063642.03+053425.8$	206.29	-0.72	14.07	-22.0	-	-	0.285	53.6	14636	-0.561	-1.856	B5-6 V
450	$J063643.35-042748.3$	215.24	-5.30	13.51	-8.4	-	-	0.445	72.1	10292	0.828	0.387	A0-1 V
451	$J063647.63+070015.6$	205.03	-0.05	15.46	-16.8	-	-	0.354	77.6	11773	1.350	0.631	B9 V
452	$J063651.99+021103.8$	209.32	-2.24	13.57	-20.5	-	-	0.161	53.8	22208	-2.443	-4.826	B2 IV
453	$J063702.88+012047.9^{\dagger}$	210.09	-2.59	13.57	-32.9	-	-	0.250	48.8	16245	-1.331	-2.919	B3-4 IV
454	$J063802.43+015937.0$	209.63	-2.07	13.81	-27.6	-	-	0.302	53.3	13998	-0.454	-1.624	B5-6 V
455	$J063846.25+034325.0$	208.17	-1.11	14.20	-15.5	-	-	0.287	42.8	14634	-1.386	-2.674	B5-6 IV
456	$J063924.49+011917.1$	210.38	-2.07	15.94	-24.9	-	-	0.256	62.0	15719	-0.405	-1.901	B5-6 V
457	$J063933.99+061149.1^{\dagger}$	206.07	0.20	13.90	-13.3	-	-	0.310	61.2	13377	0.111	-0.934	B6-7 V
458	$J063938.71+054049.9$	206.53	-0.02	15.56	-17.8	-	-	0.282	57.8	14634	-0.344	-1.638	B5-6V
459	$J063947.29+042801.1^{\dagger}$	207.63	-0.55	14.34	-19.7	-	-	0.301	67.8	13396	0.369	-0.680	B5-6 V
460	$J064035.03-015647.8$	213.43	-3.30	14.56	-25.0	-	-	0.243	65.2	16474	-0.471	-2.098	B5 V
461	$J064116.51-010740.2$	212.78	-2.78	13.14	-56.9	-	-	0.492	49.2	10061	-0.042	-0.449	A0-1 IV
462	$J064132.01-012549.5$	213.08	-2.86	13.72	-9.9	-	-	0.290	60.2	14203	-0.108	-1.318	B5-6 V
463	$J064132.75-020811.9$	213.71	-3.17	15.48	-23.2	-	-	0.263	66.0	15108	-0.175	-1.559	B6 V
464	$J064137.19-035546.1$	215.32	-3.97	13.03	-14.3	-	-	0.269	65.9	14800	-0.105	-1.431	B6 V
465	$J064203.29+002009.8$	211.56	-1.93	14.39	-29.1	-	-	0.317	50.0	13544	-0.572	-1.651	B5-6 IV
466	$J064222.51-005519.2$	212.72	-2.44	14.92	-12.6	264.2	0.96	0.392	58.2	11589	0.243	-0.440	B9 V
467	$J064257.88-013413.4$	213.36	-2.60	15.75	-14.7	-	-	0.275	81.7	13886	0.782	-0.365	B7-8 V
468	$J064308.21+000513.3$	211.91	-1.81	14.72	-15.1	-	-	0.353	63.2	12118	0.478	-0.311	B7-8 V
469	$J064308.31+042635.8$	208.03	0.18	14.11	-10.0	-	-	0.326	55.4	13031	-0.160	-1.135	B7-8 V
470	$J064322.65+071825.5$	205.51	1.54	14.99	-19.2	-	-	0.263	70.4	14918	0.020	-1.328	B6 V
471	$J064350.82+012411.8$	210.82	-1.05	15.05	-16.4	-	-	0.292	68.5	13735	0.310	-0.807	B7 V
472	$J064944.84-023211.4$	215.00	-1.53	15.13	-12.0	-	-	0.262	69.0	15013	-0.054	-1.420	B6 V
473	$J064949.76-025321.2$	215.32	-1.67	14.25	-26.4	-	-	0.216	61.9	18348	-1.016	-2.934	B3-4 V
474	$J070343.05-010021.2$	215.23	2.27	15.07	-9.3	-	-	0.416	56.0	11243	0.163	-0.452	B9 V
475	$J184213.54+054406.0$	37.00	4.65	15.11	-23.4	-	-	0.191	57.4	20051	-1.647	-3.789	B3-4 V
476	$J184836.27+060954.8$	38.10	3.43	13.93	-47.7	-	-	0.353	57.6	12239	0.137	-0.676	B7-8V
477	$J185235.00-003835.3$	32.49	-0.55	14.57	-13.4	-	-	0.267	72.1	14636	0.180	-1.115	B6 V
478	$J185237.90+000158.2$	33.10	-0.25	13.61	-49.5	-	-	0.189	52.9	20035	-1.967	-4.107	B3-4 V
479	$J185505.84+113353.4$	43.66	4.44	16.61	-17.7	-	-	0.326	61.4	12746	0.254	-0.662	B7-8V
480	$J185510.54-002541.2$	32.98	-1.03	13.90	-18.9	-	-	0.239	58.7	16880	-0.830	-2.524	B3-4V
481	$J185553.90+120723.4$	44.25	4.52	16.21	-12.0	256.9	1.00	0.451	67.8	10346	0.647	0.197	A0-1 V
482	$J190032.98-044849.5$	29.68	-4.22	13.57	-24.6	-	-	0.240	45.5	16661	-1.710	-3.369	B3-4 IV
483	$J190303.43-020008.8$	32.47	-3.50	13.20	-16.7	-	-	0.350	58.0	12278	0.149	-0.672	B7-8V
484	$J190725.36+115121.7$	45.29	1.89	13.54	-18.1	-	-	0.221	58.2	17984	-1.142	-3.007	B3-4V
485	$J190738.21+093533.1$	43.31	0.80	14.47	-22.2	-	-	0.312	32.8	13048	-2.088	-3.038	B7-8 III
486	$J191033.51-010724.9$	34.11	-4.77	15.48	-19.6	-	-	0.288	54.8	14504	-0.452	-1.721	B5-6 V
487	$J191323.23+175527.4$	51.35	3.40	14.97	-38.5	-	-	0.156	64.0	23147	-1.947	-4.424	B2 V
488	$J191713.73+143442.4$	48.81	1.03	14.23	-20.6	-	-	0.294	56.1	14210	-0.338	-1.550	B5-6 V
489	$J192513.62+155452.9$	50.90	-0.04	13.73	-24.5	-	-	0.210	53.6	18621	-1.559	-3.515	B3-4 V
490	$J192717.83+121041.1$	47.85	-2.26	14.27	-22.9	201.1	0.88	0.242	61.7	16647	-0.634	-2.290	B3-4 V
491	$J192735.18+142745.3$	49.89	-1.23	14.03	-21.6	-	-	0.275	50.5	15085	-0.889	-2.269	B5-6 V
492	$J192854.74+240302.9$	58.47	3.07	14.04	-32.4	-	-	0.083	44.9	25871	-5.447	-7.986	B0 II
493	$J192953.87+191435.6$	54.36	0.57	14.82	-14.4	-	-	0.182	61.7	20787	-1.572	-3.801	B2 V
494	$J193142.88+164552.9$	52.39	-1.00	13.07	-19.1	-	-	0.297	53.8	14195	-0.454	-1.663	B5-6 V
495	$J193217.78+095748.5$	46.48	-4.39	13.19	-8.3	114.3	1.00	0.375	53.6	11958	-0.056	-0.812	B7-8 V

Table 1. Continued...

#	IPHAS NAME	$l(deg)$	$b(deg)$	$r(mag)$	$H\alpha(eqw)$	ΔV	V/R	$D(dex)$	$\lambda 1(\AA)$	$T_{eff}(K)$	M_v	M_{Bol}	SpT/LC
496	$J193219.96+274126.1$	62.04	4.13	15.34	-5.9	-	-	0.337	61.0	12434	0.285	-0.568	B7-8V
497	$J193231.66+185254.9$	54.34	-0.15	15.42	-20.7	-	-	0.211	56.6	18618	-1.373	-3.329	B3-4 V
498	$J193232.88+151711.5$	51.19	-1.89	14.16	-56.1	-	-	0.109	50.9	25899	-3.933	-6.567	B1 III
499	$J193304.15+172408.7$	53.10	-0.98	13.53	-26.6	-	-	0.117	53.8	26315	-3.479	-6.242	B1 IV
500	$J193323.02+195848.2$	55.40	0.20	14.28	-41.2	-	-	0.082	62.2	31609	-3.918	-7.119	B0 V
501	$J193420.54+262349.9$	61.12	3.12	15.53	-31.5	-	-	0.217	60.1	18287	-1.099	-3.008	B3-4 V
502	$J193424.63+180101.3$	53.80	-0.96	14.36	-26.8	-	-	0.291	51.9	14436	-0.644	-1.900	B5-6 V
503	$J193431.65+233208.6$	58.64	1.69	14.86	-1.9	274.3	0.99	0.273	64.9	14664	-0.097	-1.397	B5-6 V
504	$J193544.33+302057.8$	64.74	4.75	16.13	-5.6	271.1	0.98	0.436	58.0	10877	0.266	-0.280	B9 V
505	$J193612.44+304319.3$	65.12	4.84	15.28	-44.9	-	-	0.114	71.9	27539	-2.801	-5.667	B1 V
506	$J193820.57+233814.6$	59.15	0.98	14.85	-5.4	-	-	0.263	66.3	15055	-0.154	-1.528	B6 V
507	$J193821.61+292525.3$	64.21	3.81	15.22	-21.9	-	-	0.267	49.8	15488	-1.006	-2.460	B5-6 IV
508	$J193842.60+242349.8$	59.85	1.28	15.12	-11.3	-	-	0.346	72.9	12006	1.079	0.313	B7-8 V
509	$J193859.63+282106.3$	63.34	3.16	15.77	-20.6	-	-	0.259	54.6	15859	-0.778	-2.299	B5-6 V
510	$J193939.56+182919.9$	54.82	-1.82	14.76	-20.1	-	-	0.284	66.5	14149	0.123	-1.077	B7 V
511	$J193959.63+182311.7^{\dagger}$	54.77	-1.94	14.16	-29.8	-	-	0.228	57.4	17465	-1.061	-2.848	B3-4 V
512	$J194011.81+290729.1$	64.14	3.31	15.25	-6.0	409.1	1.00	0.273	57.7	15000	-0.427	-1.791	B5-6V
513	$J194046.54+195524.6$	56.20	-1.34	13.40	-18.0	-	-	0.341	63.4	12309	0.463	-0.364	B7-8 V
514	$J194118.59+141802.9$	51.36	-4.22	13.49	-3.8	265.1	1.04	0.305	53.3	13878	-0.436	-1.582	B5-6 V
515	$J194139.39+183400.4$	55.12	-2.19	13.29	-31.3	139.9	0.99	0.272	55.9	15107	-0.521	-1.905	B5-6 V
516	$J194155.60+250424.1$	60.80	0.98	13.55	-14.6	246.8	0.99	0.187	55.9	20313	-1.810	-3.984	B3-4 V
517	$J194254.42+275201.3$	63.34	2.17	13.81	-23.2	-	-	0.211	59.9	18673	-1.194	-3.157	B3-4V
518	$J194304.40+231848.6$	59.41	-0.12	13.37	-38.3	-	-	0.432	62.2	10861	0.442	-0.101	A0-1 V
519	$J194338.78+302510.1$	65.64	3.30	15.09	-10.2	-	-	0.267	62.0	15069	-0.294	-1.671	B5-6 V
520	$J194519.94+193218.0$	56.39	-2.46	14.27	-10.4	-	-	0.342	53.1	12533	-0.247	-1.120	B7-8 V
521	$J194528.53+171707.2$	54.46	-3.61	14.97	-20.3	-	-	0.337	49.7	12848	-0.458	-1.395	B7-8 IV
522	$J194534.27+285637.5$	64.57	2.20	15.49	-40.4	-	-	0.193	45.9	19324	-2.403	-4.452	B3-4 IV
523	$J194536.66+315906.7$	67.21	3.71	15.32	-26.1	-	-	0.245	42.6	16288	-1.860	-3.439	B5-6 IV
524	$J194602.43+283918.8$	64.37	1.97	15.80	-11.4	301.2	1.01	0.293	56.0	14277	-0.352	-1.577	B5-6 V
525	$J194617.86+230454.0$	59.57	-0.88	14.99	-24.9	-	-	0.167	45.2	20769	-2.967	-5.119	B2 III
526	$J194628.92+243732.1$	60.93	-0.14	15.11	-48.0	-	-	0.360	79.0	11647	1.418	0.724	B9 V
527	$J194700.37+201035.1$	57.14	-2.48	13.31	-10.2	329.1	0.94	0.299	52.1	14150	-0.559	-1.759	B5-6 V
528	$J194731.34+273416.5$	63.59	1.14	13.16	-24.4	-	-	0.294	45.9	14444	-1.051	-2.308	B5-6 IV
529	$J194843.72+205529.5$	57.99	-2.45	14.33	-8.3	-	-	0.365	56.0	12066	0.078	-0.700	B7-8 V
530	$J194854.73+324518.2$	68.23	3.50	14.91	-18.7	-	-	0.236	58.6	17038	-0.876	-2.596	B3-4V
531	$J194905.14+271001.3$	63.42	0.64	14.66	-12.7	-	-	0.281	56.9	14686	-0.398	-1.702	B5-6 V
532	$J195001.05+212312.1$	58.55	-2.48	13.28	-12.7	-	-	0.279	65.4	14436	0.005	-1.251	B7 V
533	$J195035.05+172854.6$	55.24	-4.57	15.47	-40.1	-	-	0.307	66.8	13200	0.373	-0.636	B7 V
534	$J195053.47+274338.7$	64.11	0.58	14.26	-20.6	-	-	0.220	61.6	18077	-0.975	-2.854	B3-4 V
535	$J195126.93+295335.8$	66.03	1.58	13.95	-18.2	-	-	0.341	58.7	12413	0.153	-0.695	B7-8V
536	$J195127.35+233225.0$	60.57	-1.67	14.37	-19.0	227.6	0.97	0.265	49.7	15576	-1.041	-2.511	B5-6 IV
537	$J195131.85+322513.6$	68.22	2.85	15.29	3.0	-	-	0.201	65.4	19335	-1.090	-3.142	B3-4 V
538	$J195132.89+301650.5$	66.38	1.76	14.48	-8.1	324.5	0.96	0.336	71.9	12177	1.009	0.208	B8 V
539	$J195140.83+295020.7$	66.01	1.51	14.05	-5.2	355.6	0.98	0.365	66.3	11858	0.672	-0.064	B9 V
540	$J195144.62+310315.9$	67.06	2.12	14.52	-7.0	-	-	0.120	61.2	27109	-2.933	-5.763	B1 V
541	$J195157.17+290739.5$	65.43	1.09	14.12	-5.0	356.5	0.97	0.343	65.6	12230	0.610	-0.201	B8 V
542	$J195159.86+290706.7$	65.43	1.08	15.55	-18.2	-	-	0.250	53.4	16310	-0.968	-2.567	B3-4 V
543	$J195207.94+342745.3$	70.04	3.78	14.52	-7.7	-	-	0.360	59.5	12097	0.272	-0.512	B7-8V
544	$J195336.43+314424.3$	67.86	2.12	14.37	-12.3	-	-	0.326	50.3	13213	-0.485	-1.497	B5-6 V
545	$J195509.84+305528.0$	67.33	1.42	13.95	-13.0	-	-	0.271	63.9	14788	-0.166	-1.490	B5-6 V
546	$J195536.17+321122.4$	68.46	1.99	14.50	-26.5	-	-	0.231	61.0	17296	-0.835	-2.596	B3-4 V
547	$J195709.69+315756.8$	68.44	1.60	13.63	-8.1	-	-	0.306	47.1	14016	-0.870	-2.043	B5-6 IV
548	$J195724.98+293118.3$	66.38	0.28	14.37	8.7	-	-	0.363	65.0	11922	0.596	-0.153	B8 V
549	$J195727.87+300724.0$	66.90	0.58	13.94	-27.5	-	-	0.150	51.9	22794	-2.814	-5.256	B2 IV
550	$J195734.37+324457.4$	69.15	1.93	13.95	-42.2	-	-	0.166	68.6	22001	-1.563	-3.925	B2 V

Table 1. Continued...

#	IPHAS NAME	$l(deg)$	$b(deg)$	$r(mag)$	$H\alpha(equ)$	ΔV	V/R	$D(dex)$	$\lambda1(\AA)$	$T_{eff}(K)$	M_v	M_{Bol}	SpT/LC
551	$J195738.31+321933.5$	68.80	1.70	14.26	-12.2	-	-	0.320	63.1	12894	0.295	-0.652	B7-8 V
552	$J195755.13+262252.2^{\dagger}$	63.76	-1.46	13.59	1.6	301.7	1.03	0.235	56.7	17013	-0.971	-2.687	B3-4 V
553	$J195833.75+315206.3$	68.51	1.29	13.57	-45.9	-	-	0.203	58.7	19217	-1.378	-3.415	B3-4V
554	$J195855.89+305045.9$	67.68	0.69	13.69	-22.7	278.8	0.99	0.114	52.0	25824	-3.718	-6.419	B1 IV
555	$J195911.59+322726.1$	69.08	1.49	13.27	-10.3	274.3	0.99	0.130	59.3	25895	-2.822	-5.549	B1 V
556	$J195916.79+333713.5^{\dagger}$	70.08	2.08	14.24	-8.8	-	-	0.319	41.6	13599	-1.192	-2.265	B6-7 IV
557	$J195928.14+305311.8$	67.78	0.61	14.53	-28.0	-	-	0.344	52.4	12505	-0.285	-1.152	B7-8 V
558	$J195956.08+372139.5$	73.35	3.92	13.70	-28.7	-	-	0.128	66.0	26304	-2.500	-5.262	B1 V
559	$J195959.94+310352.5$	67.99	0.61	13.58	-19.4	-	-	0.242	54.6	16725	-0.982	-2.651	B3-4 V
560	$J200008.06+300700.5$	67.20	0.08	13.85	-10.6	-	-	0.321	50.7	13368	-0.491	-1.534	B5-6 V
561	$J200017.42+313553.9$	68.48	0.84	13.80	-5.8	-	-	0.311	40.7	13819	-1.339	-2.444	B5-6 IV
562	$J200022.20+324303.8$	69.44	1.41	14.07	-3.3	326.8	1.00	0.215	48.1	17979	-1.871	-3.736	B3-4 IV
563	$J200358.72+320803.4$	69.34	0.46	14.10	-24.2	-	-	0.262	57.7	15559	-0.535	-2.002	B5-6V
564	$J200401.24+340235.1$	70.96	1.47	13.95	-9.5	278.8	0.98	0.217	56.7	18188	-1.270	-3.165	B3-4 V
565	$J200516.96+321046.4$	69.53	0.25	13.05	-19.3	-	-	0.247	60.5	16332	-0.600	-2.203	B3-4 V
566	$J201808.03+405050.4$	78.20	2.84	13.56	-30.6	-	-	0.158	60.2	22883	-2.091	-4.542	B2 V
567	$J201831.97+404247.5$	78.13	2.70	13.64	-16.1	-	-	0.352	74.2	11873	1.149	0.410	B7-8 V
568	$J201924.58+370740.7$	75.26	0.54	13.98	-12.3	325.9	1.06	0.357	66.7	11972	0.694	-0.065	B9 V
569	$J203955.62+454446.8$	84.49	2.49	13.64	4.1	-	-	0.182	54.1	20613	-2.008	-4.217	B3-4 IV
570	$J205432.12+401959.4$	81.95	-2.98	13.66	-11.8	-	-	0.308	50.6	13843	-0.599	-1.738	B5-6 V
571	$J205726.50+461315.3$	86.78	0.43	14.15	-29.7	-	-	0.296	59.5	13996	-0.087	-1.256	B5-6V
572	$J205931.56+443544.5$	85.79	-0.91	13.61	-19.9	204.8	1.01	0.328	70.3	12337	0.870	0.037	B8 V
573	$J205958.73+451656.7$	86.36	-0.52	13.32	-16.3	-	-	0.331	69.1	12318	0.801	-0.028	B8 V
574	$J210019.66+454138.2$	86.71	-0.30	13.93	6.1	-	-	0.279	58.5	14719	-0.331	-1.642	B5-6V
575	$J210029.50+443655.5$	85.92	-1.03	13.58	1.0	-	-	0.277	57.1	14836	-0.419	-1.752	B5-6 V
576	$J210035.96+462506.7$	87.29	0.15	13.67	5.1	-	-	0.231	66.7	17255	-0.608	-2.362	B3-4 V
577	$J210252.23+451005.1$	86.61	-0.98	15.46	-31.5	-	-	0.180	70.2	20720	-1.233	-3.454	B3 V
578	$J210259.03+442947.9$	86.12	-1.44	13.54	-34.0	-	-	0.204	63.2	19121	-1.142	-3.166	B3-4 V
579	$J210323.60+450033.1$	86.55	-1.15	13.38	-14.8	-	-	0.537	73.3	9450	-	-	A2
580	$J210330.04+450104.4$	86.57	-1.16	14.64	-30.0	-	-	0.279	46.3	14958	-1.170	-2.526	B5-6 IV
581	$J210348.39+450316.3$	86.64	-1.18	15.20	-27.4	-	-	0.285	62.6	14288	-0.053	-1.280	B5-6 V
582	$J211120.60+414917.4$	85.17	-4.37	13.92	-8.8	-	-	0.384	66.9	11552	0.697	0.022	B9 V
583	$J212148.79+461357.0$	89.66	-2.65	13.93	-24.5	-	-	0.246	50.2	16483	-1.274	-2.903	B3-4 IV
584	$J212246.10+485845.2$	91.71	-0.82	13.57	-16.0	-	-	0.293	65.1	13883	0.163	-0.984	B7 V
585	$J212448.52+561054.6$	96.98	4.10	13.87	-8.3	164.6	1.02	0.326	66.0	12520	0.568	-0.302	B8 V
586	$J212738.50+494219.4$	92.78	-0.85	13.38	-15.9	-	-	0.395	61.8	11475	0.429	-0.231	B9 V
587	$J213238.74+483601.7$	92.62	-2.21	13.28	-14.4	-	-	0.328	56.1	12932	-0.102	-1.056	B7-8 V
588	$J213534.79+533116.1$	96.28	1.10	13.96	-23.4	-	-	0.349	51.8	12412	-0.299	-1.147	B7-8 V
589	$J213808.05+494645.1$	94.08	-1.94	13.71	-0.8	370.3	1.05	0.260	56.4	15729	-0.647	-2.145	B5-6 V
590	$J213901.74+532301.1$	96.57	0.66	14.65	-28.5	-	-	0.188	41.7	18841	-2.904	-4.760	B3-4 III
591	$J213910.99+565115.2$	98.89	3.24	14.92	-18.5	-	-	0.180	48.5	20387	-2.446	-4.629	B3-4 IV
592	$J213938.16+533454.5$	96.77	0.75	15.07	-11.4	274.3	1.00	0.242	60.2	16649	-0.699	-2.356	B3-4 V
593	$J213956.59+484214.3$	93.58	-2.95	13.45	-10.2	-	-	0.311	49.1	13785	-0.693	-1.820	B5-6 IV
594	$J214010.25+512640.1$	95.42	-0.91	15.30	-16.9	-	-	0.374	67.8	11683	0.756	0.055	B9 V
595	$J214014.93+540011.1$	97.12	1.00	14.65	-12.7	-	-	0.328	64.3	12517	0.462	-0.408	B7-8 V
596	$J214941.64+525925.7$	97.53	-0.68	13.33	-20.9	-	-	0.485	65.0	9593	0.514	0.179	A0-1 V
597	$J215636.84+591153.4$	102.17	3.57	13.41	-31.8	-	-	0.134	58.7	25442	-2.757	-5.445	B1 V
598	$J215713.34+542035.4$	99.25	-0.31	14.74	9.9	-	-	0.401	71.9	11158	0.930	0.331	A0-1 V
599	$J215816.96+523953.2$	98.35	-1.74	15.22	-17.4	-	-	0.247	60.4	16357	-0.625	-2.232	B3-4 V
600	$J215828.17+562855.1$	100.70	1.27	15.21	-10.1	-	-	0.314	47.3	13701	-0.789	-1.899	B5-6 IV
601	$J215856.22+564705.8$	100.93	1.47	13.88	-31.1	-	-	0.238	55.4	16904	-0.983	-2.681	B3-4 V
602	$J215923.75+592919.7$	102.63	3.58	13.80	-13.1	-	-	0.320	55.9	13231	-0.167	-1.182	B5-6 V
603	$J215934.48+525438.6$	98.65	-1.66	14.56	-28.0	-	-	0.199	55.8	19423	-1.598	-3.661	B3-4 V
604	$J215950.24+570056.1$	101.17	1.58	15.12	-18.3	-	-	0.227	57.0	17535	-1.092	-2.890	B3-4 V
605	$J220117.18+541450.7$	99.66	-0.75	13.83	-17.6	-	-	0.163	50.9	21677	-2.608	-4.936	B2 IV

Table 1. Continued...

#	IPHAS NAME	$l(deg)$	$b(deg)$	$r(mag)$	$H\alpha(eqw)$	ΔV	V/R	$D(dex)$	$\lambda 1(\AA)$	$T_{eff}(K)$	M_v	M_{Bol}	SpT/LC
606	$J220215.50+524654.4$	98.90	-2.01	13.24	-9.6	-	-	0.205	67.1	19014	-0.953	-2.963	B3-4 V
607	$J220246.29+523551.3$	98.85	-2.20	13.39	-11.3	256.0	0.95	0.285	63.1	14269	-0.029	-1.252	B5-6 V
608	$J220431.39+565346.0$	101.61	1.10	15.44	-12.4	-	-	0.178	59.7	21125	-1.748	-4.015	B2 V
609	$J220508.23+553036.2$	100.86	-0.07	14.32	-20.4	-	-	0.249	63.0	16135	-0.460	-2.029	B5-6 V
610	$J220531.37+513312.7^{\dagger}$	98.57	-3.29	13.62	-8.0	-	-	0.329	56.7	12887	-0.054	-0.999	B6-7 V
611	$J220547.66+525354.0^{\dagger}$	99.40	-2.23	14.62	-12.5	-	-	0.260	66.9	15252	-0.175	-1.586	B6 V
612	$J220635.01+581158.1$	102.60	1.99	15.53	-29.6	237.7	1.08	0.563	74.1	9450	-	-	¿A2
613	$J220709.48+545425.7$	100.74	-0.72	14.27	-8.9	315.4	1.03	0.324	64.1	12650	0.409	-0.488	B7-8 V
614	$J220724.56+520246.0$	99.10	-3.07	16.06	-14.8	-	-	0.282	46.5	14840	-1.122	-2.456	B5-6 IV
615	$J220750.41+545409.7$	100.82	-0.79	13.79	-7.7	-	-	0.356	54.7	12253	-0.037	-0.853	B7-8 V
616	$J220835.26+570037.4$	102.13	0.87	14.85	-11.4	173.7	1.07	0.216	65.5	18288	-0.866	-2.775	B3-4 V
617	$J220923.01+552821.4$	101.33	-0.45	14.54	-7.4	-	-	0.242	52.6	16670	-1.140	-2.800	B3-4 V
618	$J221150.88+564020.3$	102.30	0.34	13.52	-28.2	-	-	0.236	66.1	16959	-0.553	-2.260	B3-4 V
619	$J221207.58+574516.1$	102.95	1.20	14.38	-14.8	141.7	1.01	0.416	60.7	11160	0.379	-0.220	B9 V
620	$J221214.02+560255.2$	101.98	-0.21	14.66	-9.2	-	-	0.398	51.0	11604	-0.165	-0.851	B7-8 V
621	$J221218.99+554040.5$	101.78	-0.52	15.14	7.9	-	-	0.531	53.8	9450	-	-	A2
622	$J221245.10+571439.9$	102.72	0.74	14.21	4.7	-	-	0.238	51.2	16858	-1.306	-2.997	B3-4 IV
623	$J221252.17+585650.4$	103.70	2.13	15.64	-41.6	-	-	0.285	65.5	14185	0.087	-1.120	B7 V
624	$J221321.11+524315.1$	100.23	-3.04	13.80	-12.6	-	-	0.348	66.2	12138	0.655	-0.138	B8 V
625	$J221557.35+564511.7$	102.81	0.08	13.44	-23.9	-	-	0.275	46.7	15116	-1.181	-2.567	B5-6 IV
626	$J221602.76+532235.5$	100.93	-2.72	13.72	-13.1	-	-	0.307	67.4	13154	0.403	-0.597	B7 V
627	$J222241.88+544700.8$	102.52	-2.08	13.96	-8.9	-	-	0.386	74.2	11344	1.082	0.447	B9 V
628	$J222300.94+573545.8$	104.07	0.26	14.03	-10.0	265.1	0.97	0.304	53.0	13924	-0.460	-1.615	B5-6 V
629	$J222326.76+561736.1$	103.42	-0.87	13.47	-12.5	-	-	0.329	51.8	13060	-0.392	-1.372	B5-6 V
630	$J222453.54+564126.9$	103.80	-0.64	14.63	-16.9	-	-	0.221	65.4	17939	-0.802	-2.661	B3-4 V
631	$J222513.15+580638.1$	104.59	0.54	14.12	-9.3	-	-	0.335	55.9	12669	-0.072	-0.973	B7-8 V
632	$J222554.20+574812.6$	104.51	0.23	13.47	-11.4	-	-	0.318	60.5	13088	0.124	-0.862	B7-8V
633	$J222605.29+584410.6$	105.02	1.01	13.05	-10.7	-	-	0.261	60.5	15504	-0.414	-1.871	B5-6 V
634	$J222706.13+560201.7$	103.71	-1.36	13.88	-9.6	-	-	0.354	77.3	11770	1.332	0.613	B9 V
635	$J222914.63+580019.4$	104.99	0.17	13.27	-31.8	-	-	0.237	50.6	16886	-1.372	-3.067	B3-4 IV
636	$J222916.87+570513.9$	104.52	-0.61	13.90	-20.3	132.6	0.96	0.270	52.7	15294	-0.775	-2.194	B5-6 V
637	$J222949.80+552437.8$	103.72	-2.09	14.26	-16.0	-	-	0.285	61.3	14374	-0.115	-1.359	B5-6 V
638	$J223344.50+582438.4$	105.71	0.22	13.89	-14.3	-	-	0.321	49.2	13428	-0.611	-1.666	B5-6 IV
639	$J223344.77+580959.4$	105.58	0.01	14.05	-11.6	-	-	0.334	64.2	12398	0.485	-0.360	B7-8 V
640	$J223406.67+553734.8$	104.35	-2.21	13.84	-30.2	-	-	0.276	58.6	14834	-0.353	-1.686	B5-6V
641	$J223437.81+574319.4$	105.46	-0.43	15.09	-10.0	-	-	0.258	47.3	15900	-1.350	-2.878	B5-6 IV
642	$J223625.68+560319.6$	104.85	-2.00	13.89	-4.9	-	-	0.291	62.0	14106	-0.005	-1.196	B5-6 V
643	$J223646.32+552828.1$	104.60	-2.53	13.79	-11.7	-	-	0.181	58.6	20838	-1.758	-3.993	B2 V
644	$J223701.42+571847.6$	105.54	-0.95	15.13	-28.4	-	-	0.190	48.5	19733	-2.264	-4.367	B3-4 IV
645	$J223812.36+640543.0$	109.00	4.89	14.99	-16.8	-	-	0.223	47.9	17466	-1.771	-3.558	B3-4 IV
646	$J223824.52+561809.5$	105.21	-1.92	14.40	-9.0	-	-	0.255	69.9	15444	-0.111	-1.557	B5 V
647	$J223825.84+574739.1$	105.94	-0.62	14.63	-2.7	-	-	0.249	58.5	16265	-0.682	-2.274	B3-4V
648	$J223828.77+631340.0$	108.60	4.12	13.59	-36.2	-	-	0.167	53.0	21663	-2.378	-4.704	B2 IV
649	$J223952.52+585813.9$	106.68	0.32	13.17	2.7	-	-	0.274	50.0	15125	-0.930	-2.317	B5-6 V
650	$J224137.35+575256.7^{\dagger}$	106.35	-0.75	13.71	-4.3	269.7	0.98	0.467	66.4	10047	0.571	0.172	A0-1 V
651	$J224230.86+570157.6$	106.05	-1.55	14.76	-8.8	-	-	0.329	71.9	12289	0.983	0.160	B8 V
652	$J224354.23+553146.6$	105.51	-2.97	14.31	-11.3	-	-	0.389	40.2	11792	-0.928	-1.641	B7-8 IV
653	$J224417.37+551406.6$	105.42	-3.25	13.36	-20.2	-	-	0.267	61.4	15098	-0.319	-1.701	B5-6 V
654	$J224435.04+550104.9$	105.36	-3.47	14.54	-19.5	-	-	0.291	48.4	14516	-0.887	-2.158	B5-6 IV
655	$J224640.02+592740.1$	107.67	0.34	14.23	-7.9	-	-	0.199	60.8	19484	-1.339	-3.410	B3-4 V
656	$J225034.82+543719.5$	105.95	-4.21	13.30	-29.9	-	-	0.409	63.3	11222	0.503	-0.108	B9 V
657	$J225249.50+582330.5$	107.90	-0.98	15.01	-10.2	-	-	0.206	60.7	18990	-1.232	-3.239	B3-4 V
658	$J225328.64+572059.3$	107.52	-1.95	13.66	3.9	-	-	0.266	54.6	15460	-0.689	-2.138	B5-6 V
659	$J225328.64+572059.3$	107.52	-1.95	13.66	-3.9	-	-	0.203	59.0	19210	-1.364	-3.400	B3-4V
660	$J225634.71+601111.6$	109.11	0.43	14.38	-3.3	-	-	0.141	54.7	24195	-2.830	-5.406	B2 IV

Table 1. Continued...

#	IPHAS NAME	$l(deg)$	$b(deg)$	$r(mag)$	$H\alpha(eqw)$	ΔV	V/R	$D(dex)$	$\lambda1(\AA)$	$T_{eff}(K)$	M_v	M_{Bol}	SpT/LC
661	$J225709.69+573327.8$	108.06	-1.98	13.79	0.8	-	-	0.230	65.0	17391	-0.703	-2.479	B3-4 V
662	$J225735.47+582555.6$	108.48	-1.21	14.23	-7.9	-	-	0.197	55.2	19577	-1.679	-3.762	B3-4 V
663	$J225851.15+594528.4$	109.19	-0.08	14.19	-35.3	-	-	0.164	62.5	22282	-1.866	-4.257	B2 V
664	$J225851.58+594808.8$	109.21	-0.04	15.46	-35.2	-	-	0.210	60.7	18720	-1.174	-3.144	B3-4 V
665	$J225922.92+582338.4$	108.68	-1.34	13.45	-11.9	-	-	0.374	54.9	11953	0.036	-0.719	B7-8 V
666	$J230004.08+592657.1$	109.20	-0.42	15.35	-31.0	-	-	0.290	63.3	14061	0.044	-1.138	B5-6 V
667	$J230048.21+590638.4$	109.14	-0.77	15.98	-20.6	-	-	0.543	71.7	9450	-	-	¿A2
668	$J230140.68+592154.4$	109.35	-0.58	14.57	-15.2	-	-	0.294	61.9	13974	0.027	-1.138	B5-6 V
669	$J230215.46+565630.8$	108.43	-2.82	13.66	-23.4	-	-	0.253	69.5	15626	-0.133	-1.612	B5 V
670	$J230239.06+592622.3$	109.49	-0.56	14.33	-10.7	-	-	0.393	51.1	11690	-0.174	-0.877	B7-8 V
671	$J230402.62+580707.2$	109.12	-1.84	14.90	-20.7	-	-	0.307	59.5	13576	0.009	-1.076	B5-6V
672	$J230415.70+593106.4$	109.71	-0.57	14.88	-20.6	-	-	0.286	53.7	14590	-0.542	-1.828	B5-6 V
673	$J230424.03+632849.0$	111.32	3.05	15.29	-17.9	-	-	0.261	41.7	15535	-1.746	-3.181	B5-6 III
674	$J230430.93+575918.7$	109.13	-1.99	13.75	-50.3	-	-	0.189	58.4	20184	-1.619	-3.777	B3-4V
675	$J230436.93+584851.0$	109.47	-1.24	15.80	-23.8	-	-	0.197	39.6	18042	-2.948	-4.695	B3-4 III
676	$J230844.57+643516.8$	112.19	3.88	14.35	-11.7	-	-	0.307	64.6	13336	0.263	-0.774	B5-6 V
677	$J231108.53+603503.3$	110.92	0.07	13.84	-31.9	-	-	0.182	57.3	20770	-1.826	-4.053	B3-4 V
678	$J231159.52+564037.6$	109.55	-3.59	14.02	-9.0	347.4	1.00	0.356	58.9	12161	0.228	-0.569	B7-8V
679	$J231220.82+605805.9$	111.20	0.37	14.19	-6.1	395.9	1.04	0.236	51.8	16974	-1.296	-3.006	B3-4 IV
680	$J231229.94+600725.7$	110.90	-0.42	14.41	-25.3	-	-	0.175	50.8	20898	-2.375	-4.617	B2 IV
681	$J231307.09+590247.9$	110.57	-1.45	14.42	-46.7	-	-	0.220	49.8	17779	-1.671	-3.506	B3-4 IV
682	$J231331.30+601727.3$	111.08	-0.31	15.84	-36.6	-	-	0.399	61.8	11418	0.430	-0.219	B9 V
683	$J231529.13+621733.0$	112.03	1.47	13.78	-21.5	-	-	0.267	69.2	14754	0.021	-1.296	B6 V
684	$J231640.52+621539.0$	112.15	1.39	14.38	-45.7	-	-	0.270	79.6	14208	0.624	-0.587	B5-6 V
685	$J231819.36+630345.3$	112.61	2.07	14.00	-28.5	-	-	0.256	72.4	15212	0.021	-1.383	B5 V
686	$J231819.36+630345.3$	112.61	2.07	14.00	-28.1	-	-	0.269	58.8	15114	-0.413	-1.798	B5-6V
687	$J231900.76+610845.1^{\dagger}$	112.02	0.25	13.90	-3.2	-	-	0.276	50.7	15067	-0.866	-2.243	B5-6 V
688	$J231906.01+605909.2^{\dagger}$	111.97	0.09	13.26	-17.6	150.8	1.00	0.185	56.4	20403	-1.816	-4.000	B3-4 V
689	$J231910.81+600917.0^{\dagger}$	111.69	-0.69	13.00	-36.6	-	-	0.241	64.6	16646	-0.532	-2.188	B4-5 V
690	$J231935.58+640610.1$	113.11	3.00	14.85	-31.6	-	-	0.304	55.1	13872	-0.319	-1.464	B5-6 V
691	$J232418.51+620233.3$	112.91	0.88	15.33	-13.2	131.6	0.98	0.356	45.6	12405	-0.670	-1.513	B7-8 IV
692	$J232630.27+612437.2$	112.95	0.20	13.65	-27.0	-	-	0.389	66.6	11470	0.677	0.018	B9 V
693	$J232917.20+610128.9$	113.15	-0.28	13.54	-26.9	-	-	0.254	62.7	15829	-0.387	-1.903	B5-6 V
694	$J232937.11+612749.5$	113.32	0.13	13.76	-18.9	-	-	0.281	64.4	14367	-0.017	-1.259	B5-6 V
695	$J233014.52+613401.9$	113.42	0.20	14.33	-25.0	-	-	0.220	65.4	18026	-0.816	-2.687	B3-4 V
696	$J233036.61+610814.6$	113.33	-0.22	13.81	-11.4	-	-	0.293	54.0	14319	-0.468	-1.701	B5-6 V
697	$J233514.67+644512.5^{\dagger}$	114.92	3.07	13.78	-17.7	-	-	0.249	65.2	15990	-0.382	-1.926	B5 V
698	$J233615.33+620424.2$	114.25	0.48	16.00	-19.1	257.8	1.00	0.295	41.6	14351	-1.396	-2.618	B5-6 IV
699	$J233632.92+620616.3$	114.29	0.50	14.18	-36.5	-	-	0.186	55.3	20406	-1.864	-4.049	B3-4 V
700	$J233650.81+585739.2^{\dagger}$	113.43	-2.53	13.91	-20.1	-	-	0.268	59.3	15425	-0.393	-1.836	B5-6 V
701	$J233702.38+623450.4$	114.48	0.94	14.84	-23.5	-	-	0.189	35.8	17378	-3.661	-5.319	B3-4 III
702	$J233823.06+622325.5$	114.58	0.71	15.57	-25.5	-	-	0.201	55.3	19340	-1.594	-3.647	B3-4 V
703	$J233940.45+580809.0$	113.56	-3.42	15.20	-20.8	-	-	0.238	62.3	16865	-0.671	-2.363	B3-4 V
704	$J233941.46+623050.7$	114.76	0.79	15.29	-34.4	-	-	0.445	74.0	10237	0.903	0.472	A0-1 V
705	$J234255.79+613845.6$	114.89	-0.15	13.70	-48.4	-	-	0.216	54.9	18266	-1.402	-3.308	B3-4 V
706	$J234300.59+604248.4$	114.66	-1.05	15.59	-26.3	233.1	1.02	0.183	44.5	19733	-2.737	-4.776	B3-4 III
707	$J234317.62+603732.6$	114.67	-1.15	14.05	-27.3	224.0	1.03	0.161	46.4	21251	-2.994	-5.223	B2 III
708	$J234323.84+620151.8$	115.05	0.21	14.20	-21.3	-	-	0.303	56.7	13856	-0.228	-1.369	B5-6 V
709	$J234409.27+623943.9$	115.29	0.79	13.78	-14.0	-	-	0.355	57.8	12203	0.158	-0.648	B7-8V
710	$J234656.98+623355.6^{\dagger}$	115.58	0.62	13.83	-21.5	-	-	0.332	53.3	12938	-0.284	-1.240	B5-7 V
711	$J234700.05+605626.6^{\dagger}$	115.19	-0.96	14.14	-41.9	-	-	0.195	52.7	19833	-1.878	-3.993	B2-3 V
712	$J234719.89+612552.4$	115.34	-0.49	14.06	-19.9	-	-	0.290	71.3	13649	0.420	-0.680	B7 V
713	$J234840.20+594117.2$	115.08	-2.22	15.90	-8.8	246.8	0.98	0.318	49.9	13513	-0.569	-1.641	B5-6 IV
714	$J234842.28+592615.0$	115.02	-2.47	15.08	-29.2	-	-	0.314	56.3	13460	-0.180	-1.242	B5-6 V
715	$J234943.12+633603.4$	116.14	1.55	14.60	-12.4	-	-	0.308	67.5	13093	0.417	-0.570	B7 V

Table 1. Continued...

#	IPHAS NAME	$l(deg)$	$b(deg)$	$r(mag)$	$H\alpha(eqw)$	ΔV	V/R	$D(dex)$	$\lambda1(\AA)$	$T_{eff}(K)$	M_v	M_{Bol}	SpT/LC
716	$J234946.77+624236.9$	115.93	0.68	13.30	-15.2	320.0	0.88	0.321	60.8	12972	0.166	-0.797	B7-8V
717	$J234949.64+632526.4^{\star}$	116.11	1.37	14.12	-21.5	257.8	0.83	0.295	72.1	13456	0.508	-0.553	B7 V
718	$J235017.97+604242.7$	115.52	-1.28	14.26	-13.3	-	-	0.353	53.7	12311	-0.144	-0.972	B7-8 V
719	$J235046.75+625007.1$	116.07	0.77	13.92	-9.7	-	-	0.271	54.4	15240	-0.646	-2.055	B5-6 V
720	$J235119.01+591118.6^{\dagger}$	115.29	-2.79	14.03	-18.6	249.1	0.96	0.257	54.8	15954	-0.785	-2.323	B4-5 V
721	$J235300.10+602852.8$	115.79	-1.58	15.05	3.3	-	-	0.078	66.0	32381	-3.916	-7.180	O8-9 V
722	$J235314.34+584234.3$	115.42	-3.31	15.43	-11.1	-	-	0.318	54.5	13380	-0.276	-1.322	B5-6 V
723	$J235424.49+611745.0$	116.14	-0.82	14.94	-12.2	-	-	0.282	64.2	14354	-0.014	-1.254	B5-6 V
724	$J235425.40+620411.0$	116.31	-0.07	13.71	-18.5	-	-	0.226	59.7	17603	-0.969	-2.777	B3-4V
725	$J235443.62+631720.8$	116.61	1.12	13.84	-30.6	-	-	0.247	61.2	16309	-0.568	-2.167	B3-4 V
726	$J235457.41+610350.6$	116.15	-1.06	15.14	-9.6	-	-	0.281	55.9	14716	-0.444	-1.754	B5-6 V
727	$J235509.36+622714.9$	116.48	0.29	13.41	-5.3	-	-	0.294	62.3	13969	0.045	-1.119	B5-6 V
728	$J235546.37+623533.9$	116.58	0.41	14.39	-26.3	-	-	0.255	54.2	16041	-0.854	-2.407	B3-4 V
729	$J235549.00+623626.6$	116.58	0.42	13.33	-62.4	-	-	0.135	72.6	25272	-1.986	-4.659	B1 V
730	$J235647.63+622134.5$	116.64	0.16	14.83	-10.0	-	-	0.394	57.6	11579	0.214	-0.467	B9 V
731	$J235804.33+631458.9^{\dagger}$	116.97	1.00	13.25	-14.3	367.1	1.06	0.177	55.9	21090	-1.983	-4.246	B2-3 V
732	$J235840.45+641332.4$	117.23	1.94	14.28	-23.6	324.5	0.70	0.321	60.9	12959	0.172	-0.788	B7-8V

TABLE 2: Spectroscopic gradient, colour excess, absolute and intrinsic magnitudes and distances for the stars studied in this work.

#	Φ_b	Φ_b^0	$E(B-V)$	A_v	A_r	f_D	$E_{cs}(B-V)$	Δr	$vsini$	$d(kpc)$	$logL/L_\odot$	$logR/R_\odot$	$M/M_\odot$	Age(My)
1	1.344	0.805	0.365	1.132	0.951	0.072	0.043	0.117	392.5	2.81	2.305	0.43	3.63	101.00
2	1.841	0.760	0.732	2.269	1.906	0.029	0.017	0.048	-	6.39	3.128	0.63	5.80	48.90
3	1.932	0.770	0.787	2.440	2.049	0.041	0.025	0.065	106.1	2.86	2.483	0.42	4.13	51.40
4	2.141	0.710	0.969	3.004	2.524	0.140	0.084	0.254	-	6.66	3.567	0.60	8.35	12.40
5	1.697	0.805	0.604	1.872	1.573	0.013	0.008	0.031	138.6	3.10	2.288	0.41	3.63	87.80
6	2.055	0.995	0.718	2.226	1.870	0.069	0.041	0.128	433.9	-	-	-	-	-
7	1.611	0.710	0.611	1.893	1.590	0.014	0.008	0.043	463.7	5.47	3.616	0.58	8.87	7.03
8	2.171	0.810	0.922	2.857	2.400	0.046	0.028	0.073	138.6	3.94	2.809	0.62	4.64	92.20
9	1.532	0.765	0.519	1.610	1.352	0.001	0.001	0.004	398.0	2.66	2.606	0.45	4.44	48.90
10	1.839	0.760	0.731	2.266	1.903	0.043	0.026	0.073	260.4	2.79	2.750	0.46	4.89	34.70
11	2.048	0.695	0.917	2.842	2.387	0.041	0.025	0.085	458.5	5.97	3.937	0.67	10.76	8.54
12	2.851	0.710	1.450	4.496	3.777	0.040	0.024	0.079	223.3	6.40	3.662	0.59	9.19	6.21
13	2.099	0.760	0.907	2.811	2.361	0.063	0.038	0.108	240.1	5.65	3.132	0.61	5.85	45.90
14	2.488	0.820	1.130	3.503	2.943	0.036	0.021	0.058	248.0	1.90	2.164	0.43	3.30	146.00
15	1.796	0.810	0.668	2.070	1.739	0.046	0.028	0.075	235.5	2.09	2.225	0.43	3.44	125.00
16	2.734	0.725	1.361	4.218	3.543	0.134	0.081	0.239	-	4.93	3.599	0.67	8.06	22.00
17	2.473	0.815	1.123	3.481	2.924	0.015	0.009	0.032	69.2	1.42	2.000	0.32	3.13	62.00
18	1.804	1.160	0.437	1.353	1.137	0.045	0.027	0.087	-	-	-	-	2.38	-
19	1.913	0.815	0.744	2.306	1.937	0.008	0.005	0.023	253.8	2.12	2.042	0.34	3.20	69.50
20	1.515	0.815	0.474	1.470	1.235	0.030	0.018	0.049	210.3	3.21	2.191	0.40	3.41	105.00
21	2.216	0.810	0.953	2.953	2.481	0.037	0.022	0.057	-	2.50	2.299	0.43	3.60	108.00
22	2.009	0.825	0.802	2.487	2.089	0.038	0.023	0.067	159.6	2.03	2.209	0.44	3.37	148.00
23	2.431	0.740	1.145	3.551	2.983	0.055	0.033	0.092	-	4.86	3.210	0.57	6.39	28.70
24	2.761	0.800	1.328	4.117	3.458	0.048	0.029	0.082	-	1.41	2.266	0.38	3.65	59.30
25	2.207	0.720	1.008	3.124	2.624	0.039	0.023	0.070	-	10.40	4.070	0.91	9.88	21.90
26	2.251	0.675	1.068	3.310	2.780	0.094	0.056	0.227	355.3	41.58	4.888	1.03	19.80	6.74
27	2.457	0.845	1.092	3.385	2.844	0.032	0.019	0.050	191.7	3.68	2.305	0.52	3.48	174.00
28	1.708	0.755	0.646	2.002	1.682	0.067	0.040	0.107	-	2.77	2.705	0.45	4.76	35.90
29	1.771	0.865	0.614	1.902	1.598	0.017	0.010	0.034	-	1.59	1.954	0.37	2.94	169.00
30	2.230	0.810	0.962	2.982	2.505	0.042	0.025	0.066	-	1.95	2.182	0.38	3.43	86.70
31	2.493	1.020	0.998	3.093	2.598	0.050	0.030	0.098	-	-	-	-	-	-
32	2.174	0.745	0.968	3.001	2.521	0.078	0.047	0.135	286.2	1.96	2.936	0.46	5.65	15.00
33	1.684	0.880	0.545	1.689	1.419	0.007	0.004	0.017	249.9	1.66	1.804	0.31	2.75	131.00
34	1.715	0.845	0.590	1.828	1.535	0.052	0.031	0.084	149.8	2.37	1.908	0.31	2.95	84.50
35	2.215	0.780	0.972	3.014	2.532	0.028	0.017	0.047	119.5	2.78	2.431	0.40	4.05	41.30
36	1.748	0.820	0.629	1.950	1.638	0.087	0.052	0.143	-	1.94	1.993	0.29	3.10	18.20
37	2.012	0.855	0.784	2.429	2.041	0.042	0.025	0.068	-	2.56	2.230	0.51	3.32	196.00
38	1.836	0.878	0.649	2.012	1.690	0.056	0.034	0.094	167.4	1.92	1.728	0.27	2.67	63.10
39	1.440	0.814	0.424	1.315	1.105	0.112	0.067	0.187	-	2.27	2.121	0.36	3.34	73.10
40	2.026	0.810	0.824	2.553	2.145	0.075	0.045	0.126	-	1.78	2.232	0.41	3.49	104.00
41	1.995	0.815	0.800	2.479	2.082	0.040	0.024	0.067	200.4	1.53	1.977	0.34	3.05	103.00
42	2.014	0.785	0.833	2.582	2.169	0.048	0.029	0.082	160.8	2.09	2.347	0.38	3.85	46.70
43	2.218	0.770	0.981	3.042	2.555	0.104	0.062	0.175	-	1.60	2.475	0.42	4.11	53.10
44	1.161	0.830	0.224	0.695	0.583	0.012	0.007	0.024	-	2.73	2.022	0.37	3.08	135.00
45	1.526	0.805	0.489	1.515	1.272	0.041	0.024	0.066	-	4.00	2.286	0.41	3.61	93.60
46	1.751	0.740	0.685	2.123	1.783	0.073	0.044	0.127	-	3.84	2.983	0.45	5.78	6.78
47	1.788	0.740	0.710	2.200	1.848	0.091	0.055	0.153	-	3.88	3.144	0.52	6.33	19.20
48	1.616	0.790	0.560	1.735	1.458	0.060	0.036	0.099	242.6	2.01	2.334	0.38	3.83	41.00
49	1.694	0.890	0.545	1.688	1.418	0.054	0.033	0.095	-	1.96	1.793	0.32	2.71	165.00
50	2.381	0.800	1.071	3.320	2.789	0.081	0.049	0.134	318.5	0.87	2.240	0.38	3.58	66.00
51	2.188	0.745	0.978	3.031	2.546	0.077	0.046	0.126	269.9	1.44	2.775	0.40	5.11	4.48
52	1.515	0.785	0.495	1.533	1.288	0.093	0.056	0.158	265.0	2.49	2.489	0.42	4.16	47.90
53	1.305	0.855	0.305	0.945	0.794	0.040	0.024	0.067	207.0	3.00	2.069	0.41	3.12	164.00
54	2.751	0.755	1.352	4.191	3.520	0.062	0.037	0.099	-	1.16	2.816	0.50	5.00	44.30
55	2.073	0.750	0.896	2.778	2.334	0.138	0.083	0.239	286.2	2.38	2.848	0.45	5.32	18.50
56	1.881	0.805	0.729	2.260	1.898	0.056	0.034	0.091	193.7	2.05	2.199	0.37	3.51	63.40
57	2.350	0.760	1.077	3.339	2.805	0.043	0.026	0.073	172.3	1.38	2.735	0.42	4.98	16.20
58	2.078	0.898	0.799	2.478	2.082	0.081	0.049	0.134	200.8	1.38	2.070	0.28	3.11	3.89
59	2.323	0.670	1.120	3.472	2.917	-0.006	0.000	0.000	-	18.15	5.013	0.98	23.50	4.68
60	1.438	0.880	0.378	1.173	0.985	0.015	0.009	0.034	-	3.42	1.917	0.38	2.87	194.00
61	1.939	0.875	0.721	2.235	1.877	0.163	0.098	0.285	-	2.93	1.739	0.27	2.68	59.60
62	1.995	0.779	0.824	2.553	2.144	0.035	0.021	0.056	-	1.78	2.464	0.40	4.13	40.40
63	1.544	0.850	0.470	1.457	1.224	0.047	0.028	0.076	242.1	3.94	2.117	0.44	3.18	178.00
64	1.440	0.740	0.474	1.471	1.235	0.080	0.048	0.135	292.8	3.07	3.032	0.49	5.95	17.60
65	1.333	0.812	0.353	1.093	0.918	0.064	0.038	0.109	340.7	1.85	1.986	0.30	3.12	37.20

Table 2. Continued...

#	Φ_b	Φ_b^0	$E(B-V)$	A_v	A_r	f_D	$E_{cs}(B-V)$	Δr	$vsini$	$d(kpc)$	$logL/L_\odot$	$logR/R_\odot$	$M/M_\odot$	Age(My)
66	1.517	0.770	0.506	1.569	1.318	0.104	0.063	0.175	260.8	2.47	2.571	0.42	4.40	38.20
67	1.592	0.785	0.546	1.694	1.423	0.079	0.048	0.134	231.7	4.02	2.347	0.39	3.84	48.20
68	1.767	0.810	0.649	2.010	1.689	0.083	0.050	0.144	253.1	1.78	2.032	0.32	3.21	49.70
69	1.405	0.825	0.393	1.217	1.022	0.033	0.020	0.061	-	5.11	1.891	0.28	2.87	24.50
70	2.224	0.755	0.995	3.084	2.591	0.038	0.023	0.065	-	2.83	2.813	0.44	5.21	17.10
71	2.304	0.830	0.998	3.095	2.599	0.050	0.030	0.084	330.0	1.23	1.986	0.34	3.07	90.70
72	1.863	0.735	0.764	2.368	1.990	0.049	0.029	0.085	-	6.67	3.096	0.49	6.28	11.30
73	1.837	0.835	0.679	2.104	1.768	0.043	0.026	0.075	-	2.91	1.772	0.23	2.56	3.36
74	1.927	0.790	0.770	2.387	2.005	0.021	0.013	0.030	270.6	1.70	2.408	0.40	3.98	46.00
75	1.652	0.815	0.567	1.757	1.476	0.036	0.021	0.057	260.0	2.01	2.184	0.39	3.41	101.00
76	1.642	0.795	0.574	1.779	1.495	0.070	0.042	0.117	163.6	1.90	2.176	0.32	3.40	19.00
77	2.556	0.795	1.193	3.698	3.107	0.169	0.102	0.282	151.6	1.45	2.372	0.41	3.85	63.10
78	2.303	0.775	1.035	3.209	2.696	0.060	0.036	0.099	-	3.65	2.473	0.37	4.21	15.50
79	1.793	0.765	0.696	2.158	1.813	0.120	0.072	0.202	356.1	2.29	2.625	0.41	4.63	21.30
80	2.099	0.805	0.877	2.718	2.283	0.021	0.013	0.031	202.6	1.57	2.081	0.31	3.28	26.90
81	1.881	0.740	0.773	2.395	2.012	0.072	0.043	0.118	-	2.03	3.099	0.51	6.17	18.80
82	1.873	0.770	0.747	2.315	1.945	0.130	0.078	0.220	466.1	2.48	2.521	0.37	4.28	8.64
83	2.147	0.795	0.916	2.839	2.385	0.014	0.008	0.031	291.8	1.27	2.197	0.33	3.46	19.30
84	1.840	0.805	0.701	2.173	1.825	0.088	0.053	0.151	-	1.55	2.103	0.32	3.31	28.30
85	2.156	0.705	0.983	3.047	2.559	0.114	0.068	0.209	-	5.42	3.833	0.73	9.28	18.80
86	1.938	0.820	0.757	2.348	1.972	0.074	0.045	0.127	52.9	1.62	1.927	0.30	3.01	51.70
87	2.069	0.710	0.921	2.854	2.397	0.023	0.014	0.046	497.0	4.11	3.475	0.58	7.85	13.70
88	1.667	0.855	0.550	1.706	1.433	0.037	0.022	0.059	-	2.25	1.851	0.31	2.85	90.70
89	1.829	0.835	0.674	2.088	1.754	0.032	0.019	0.058	-	1.47	1.784	0.24	2.61	9.98
90	1.270	0.770	0.338	1.049	0.881	0.091	0.055	0.149	286.2	2.43	2.458	0.37	4.18	16.00
91	1.477	0.820	0.445	1.380	1.159	0.038	0.023	0.067	328.7	1.98	2.068	0.37	3.18	118.00
92	1.628	0.830	0.540	1.675	1.407	0.034	0.021	0.059	326.8	2.40	1.911	0.35	2.90	150.00
93	1.663	0.855	0.547	1.697	1.426	0.023	0.014	0.042	-	1.77	2.083	0.44	3.10	196.00
94	1.567	0.950	0.418	1.295	1.088	0.018	0.011	0.037	346.4	2.69	1.756	0.42	2.54	384.00
95	1.788	0.855	0.632	1.959	1.646	0.060	0.036	0.102	213.5	1.54	1.831	0.29	2.83	74.90
96	1.969	0.810	0.785	2.434	2.044	0.062	0.037	0.100	-	2.85	2.268	0.43	3.54	112.00
97	1.819	0.800	0.691	2.141	1.798	0.052	0.031	0.082	329.3	1.32	2.233	0.35	3.62	33.50
98	1.415	0.808	0.412	1.277	1.072	0.097	0.058	0.159	-	2.26	2.127	0.32	3.32	21.30
99	1.892	0.750	0.774	2.398	2.015	0.066	0.040	0.108	332.9	2.33	2.891	0.47	5.44	20.60
100	1.773	0.772	0.678	2.102	1.766	0.039	0.023	0.064	105.7	2.20	2.601	0.44	4.45	43.90
101	1.914	0.802	0.754	2.336	1.962	0.030	0.018	0.048	228.3	1.94	2.455	0.46	3.94	91.70
102	1.569	0.807	0.517	1.601	1.345	0.054	0.032	0.092	291.8	1.54	2.079	0.33	3.29	51.90
103	1.826	0.785	0.705	2.186	1.836	0.066	0.040	0.108	215.7	2.45	2.591	0.49	4.27	76.40
104	1.336	0.870	0.316	0.979	0.823	0.018	0.011	0.035	-	2.97	2.104	0.49	3.09	232.00
105	1.630	0.855	0.525	1.628	1.368	0.047	0.028	0.076	187.3	1.82	1.830	0.29	2.83	61.60
106	2.733	0.740	1.350	4.186	3.516	0.096	0.058	0.158	-	2.12	3.065	0.55	5.79	36.90
107	2.242	0.755	1.007	3.122	2.623	0.031	0.018	0.048	-	4.01	2.854	0.47	5.26	26.20
108	2.179	0.855	0.897	2.780	2.336	0.033	0.020	0.059	99.5	1.47	2.188	0.48	3.28	186.00
109	1.372	0.740	0.428	1.326	1.114	0.027	0.016	0.042	-	3.57	3.051	0.46	6.01	6.23
110	2.148	0.750	0.947	2.936	2.466	0.076	0.046	0.125	-	7.31	3.190	0.63	6.05	43.70
111	1.711	0.745	0.654	2.028	1.704	0.094	0.056	0.161	-	8.10	2.979	0.45	5.73	6.36
112	2.328	0.735	1.079	3.345	2.810	0.056	0.034	0.094	-	3.13	3.071	0.46	5.89	3.78
113	2.040	0.779	0.854	2.648	2.225	0.043	0.026	0.073	387.6	3.10	2.797	0.57	4.72	76.30
114	2.067	0.783	0.870	2.698	2.267	0.050	0.030	0.082	208.4	2.38	2.511	0.42	4.21	48.60
115	1.816	0.780	0.702	2.176	1.828	0.044	0.026	0.073	264.8	2.37	2.519	0.42	4.25	44.30
116	2.009	0.855	0.782	2.423	2.036	0.031	0.019	0.050	-	1.51	1.999	0.38	3.03	152.00
117	2.124	0.780	0.910	2.822	2.371	0.014	0.009	0.030	-	6.24	2.987	0.63	5.24	65.20
118	1.954	0.715	0.839	2.602	2.186	0.036	0.022	0.065	-	3.96	3.810	0.72	9.16	18.90
119	1.992	0.750	0.841	2.608	2.191	0.103	0.062	0.176	215.7	4.56	2.829	0.42	5.28	7.74
120	1.922	0.785	0.770	2.388	2.006	0.040	0.024	0.065	195.4	2.10	2.539	0.46	4.19	69.80

Table 2. Continued...

#	Φ_b	Φ_b^0	$E(B-V)$	A_v	A_r	f_D	$E_{cs}(B-V)$	Δr	$vsini$	$d(kpc)$	$logL/L_\odot$	$logR/R_\odot$	$M/M_\odot$	Age(My)
121	2.272	0.960	0.889	2.756	2.315	0.022	0.013	0.038	-	4.75	1.948	0.54	2.71	413.00
122	2.377	0.845	1.038	3.217	2.702	0.061	0.037	0.102	-	2.84	2.408	0.57	3.63	173.00
123	3.528	0.970	1.733	5.371	4.512	0.030	0.018	0.057	280.8	-	-	-	-	-
124	2.565	0.775	1.213	3.760	3.158	0.057	0.034	0.090	-	2.02	2.807	0.51	4.90	54.00
125	1.768	0.830	0.636	1.970	1.655	0.019	0.011	0.033	211.4	2.91	2.207	0.45	3.35	157.00
126	1.926	0.830	0.742	2.302	1.933	0.040	0.024	0.067	-	1.94	2.000	0.34	3.09	99.20
127	1.592	0.800	0.536	1.663	1.397	0.063	0.038	0.108	360.5	1.29	2.230	0.36	3.61	42.90
128	1.598	0.825	0.524	1.623	1.363	0.040	0.024	0.066	138.6	1.73	1.991	0.32	3.12	60.80
129	2.353	0.750	1.086	3.367	2.828	0.072	0.043	0.116	-	1.63	2.799	0.57	4.72	76.90
130	1.301	0.858	0.301	0.932	0.783	0.029	0.017	0.051	-	3.24	2.022	0.41	3.02	191.00
131	2.236	0.815	0.962	2.983	2.506	0.019	0.011	0.032	-	1.38	2.055	0.34	3.22	72.30
132	2.055	0.817	0.839	2.600	2.184	0.044	0.026	0.075	-	2.74	1.970	0.32	3.07	73.10
133	1.315	0.800	0.349	1.082	0.909	0.059	0.035	0.099	-	2.88	2.298	0.38	3.73	49.70
134	2.163	0.843	0.895	2.773	2.330	0.035	0.021	0.058	-	5.40	2.345	0.52	3.56	162.00
135	1.730	0.800	0.630	1.952	1.640	-0.020	0.000	0.000	-	1.81	2.221	0.35	3.59	42.10
136	1.625	0.815	0.549	1.701	1.429	0.063	0.038	0.109	-	4.92	2.204	0.40	3.44	104.00
137	2.293	0.785	1.022	3.168	2.661	0.047	0.028	0.073	-	5.15	2.512	0.46	4.12	72.40
138	1.599	0.865	0.497	1.541	1.295	0.035	0.021	0.060	-	2.11	2.087	0.45	3.10	205.00
139	2.493	0.774	1.164	3.610	3.032	0.037	0.022	0.059	-	1.01	2.249	0.48	3.40	169.00
140	2.311	0.830	1.003	3.111	2.613	0.031	0.019	0.050	-	1.43	2.274	0.48	3.46	158.00
141	2.072	0.730	0.909	2.819	2.368	0.095	0.057	0.163	-	2.13	3.167	0.51	6.51	13.90
142	2.286	0.750	1.040	3.225	2.709	0.049	0.029	0.082	-	2.68	3.012	0.55	5.57	41.80
143	1.744	0.900	0.572	1.772	1.488	0.180	0.108	0.314	-	1.94	1.677	0.27	2.59	82.10
144	2.363	0.860	1.018	3.157	2.652	0.308	0.185	0.314	-	0.85	1.578	0.16	2.43	0.00
145	2.308	0.763	1.047	3.245	2.726	0.057	0.034	0.090	302.1	1.36	2.629	0.41	4.64	18.10
146	1.601	0.878	0.490	1.519	1.276	0.030	0.018	0.051	-	2.20	2.017	0.43	2.98	218.00
147	1.976	0.774	0.814	2.525	2.121	0.048	0.029	0.082	293.5	2.88	2.970	0.60	5.25	60.30
148	2.309	0.815	1.012	3.137	2.635	0.037	0.022	0.057	-	2.24	2.408	0.49	3.75	126.00
149	1.645	0.855	0.535	1.659	1.394	0.083	0.050	0.143	256.6	2.31	2.200	0.40	3.44	100.00
150	1.649	0.830	0.555	1.719	1.444	0.051	0.030	0.084	428.4	1.56	1.887	0.29	2.89	40.20
151	1.920	1.200	0.488	1.512	1.270	0.166	0.100	0.336	-	-	-	-	-	-
152	1.782	0.855	0.628	1.946	1.635	0.060	0.036	0.102	-	1.70	1.889	0.32	2.90	106.00
153	1.930	1.020	0.616	1.911	1.605	0.074	0.044	0.139	-	-	-	-	-	-
154	1.349	0.852	0.337	1.045	0.878	0.030	0.018	0.051	-	2.53	2.052	0.41	3.08	176.00
155	2.447	0.755	1.146	3.553	2.984	0.115	0.069	0.193	-	2.82	3.000	0.55	5.54	41.10
156	2.208	0.878	0.901	2.793	2.346	0.048	0.029	0.086	-	1.56	2.099	0.47	3.10	222.00
157	1.926	0.795	0.766	2.375	1.995	0.058	0.035	0.099	47.5	2.90	2.424	0.42	3.96	65.30
158	2.213	0.795	0.960	2.977	2.501	0.051	0.031	0.082	-	4.28	2.467	0.47	3.96	89.80
159	2.070	0.725	0.911	2.824	2.372	0.120	0.072	0.211	-	6.22	3.612	0.69	8.02	24.00
160	1.666	0.780	0.600	1.861	1.563	0.050	0.030	0.082	292.6	2.73	2.501	0.41	4.22	39.80
161	1.751	0.795	0.648	2.008	1.687	0.079	0.048	0.134	312.8	2.25	2.418	0.42	3.94	66.60
162	1.840	0.820	0.691	2.142	1.800	0.089	0.054	0.153	-	6.06	2.211	0.43	3.39	135.00
163	1.743	0.725	0.690	2.138	1.796	0.008	0.005	0.028	381.5	4.65	3.462	0.59	7.73	15.20
164	1.967	0.765	0.814	2.524	2.120	0.030	0.018	0.047	-	2.14	2.680	0.46	4.63	46.50
165	1.796	0.785	0.685	2.122	1.783	0.066	0.040	0.107	-	3.43	2.815	0.58	4.76	76.20
166	1.781	0.920	0.583	1.807	1.518	0.169	0.101	0.301	-	1.86	1.572	0.26	2.42	140.00
167	2.299	0.700	1.083	3.358	2.820	0.098	0.059	0.191	-	5.72	3.724	0.62	9.37	9.26
168	1.804	0.778	0.695	2.154	1.809	0.065	0.039	0.110	176.8	1.75	2.252	0.46	3.44	150.00
169	1.579	0.855	0.491	1.521	1.278	0.068	0.041	0.119	170.9	1.35	1.669	0.20	2.50	0.00
170	1.842	0.745	0.743	2.304	1.935	0.151	0.091	0.258	325.5	7.83	3.490	0.73	7.10	36.10
171	1.981	0.855	0.763	2.365	1.987	0.128	0.077	0.226	-	4.82	1.967	0.36	2.98	146.00
172	1.753	0.965	0.534	1.656	1.391	0.056	0.034	0.098	-	4.27	1.532	0.31	2.31	323.00
173	2.458	0.810	1.116	3.461	2.907	0.041	0.024	0.065	-	1.66	2.593	0.55	4.14	109.00
174	1.658	0.805	0.578	1.791	1.504	0.054	0.033	0.091	-	2.90	2.285	0.41	3.61	90.80
175	1.694	0.829	0.586	1.816	1.525	0.069	0.041	0.119	-	4.42	1.920	0.31	2.99	67.10

Table 2. Continued...

#	Φ_b	Φ_b^0	$E(B-V)$	A_v	A_r	f_D	$E_{cs}(B-V)$	Δr	$vsini$	$d(kpc)$	$logL/L_\odot$	$logR/R_\odot$	$M/M_\odot$	Age(My)
176	1.765	0.810	0.647	2.006	1.685	0.116	0.070	0.196	506.7	2.26	2.226	0.40	3.50	95.70
177	2.028	0.745	0.869	2.694	2.263	0.151	0.091	0.258	-	2.02	2.911	0.46	5.56	15.30
178	1.911	0.850	0.719	2.228	1.872	0.063	0.038	0.111	309.8	1.96	1.952	0.35	2.97	136.00
179	2.168	0.705	0.991	3.071	2.580	0.044	0.026	0.093	400.7	6.40	4.063	0.74	11.27	11.00
180	1.729	0.798	0.631	1.955	1.642	-0.008	0.000	0.000	283.4	1.65	2.252	0.36	3.64	47.00
181	2.535	0.853	1.140	3.533	2.968	0.073	0.044	0.128	-	1.13	1.914	0.33	2.94	107.00
182	2.014	0.782	0.834	2.586	2.172	0.026	0.016	0.039	286.7	3.32	2.595	0.47	4.34	63.00
183	2.639	0.740	1.286	3.988	3.350	0.094	0.057	0.162	-	3.32	3.476	0.68	7.26	30.00
184	2.752	0.770	1.343	4.162	3.496	0.067	0.040	0.108	-	3.21	2.968	0.66	5.05	79.10
185	2.142	0.848	0.877	2.718	2.283	0.030	0.018	0.050	-	2.51	2.180	0.46	3.28	176.00
186	2.051	0.813	0.839	2.601	2.185	0.086	0.052	0.144	261.3	2.58	2.175	0.39	3.39	101.00
187	2.215	0.745	0.996	3.086	2.593	0.076	0.045	0.126	-	3.24	3.173	0.59	6.10	37.70
188	2.343	0.765	1.069	3.314	2.784	0.103	0.062	0.175	-	2.25	2.736	0.48	4.77	47.50
189	2.706	0.760	1.319	4.087	3.433	0.142	0.085	0.238	-	3.03	2.635	0.39	4.58	10.40
190	2.598	0.777	1.233	3.823	3.212	0.089	0.053	0.149	-	1.63	2.537	0.44	4.24	56.60
191	2.046	0.878	0.791	2.454	2.061	0.026	0.016	0.043	-	5.42	2.225	0.54	3.27	223.00
192	2.688	0.780	1.292	4.006	3.365	0.023	0.014	0.039	-	3.18	2.936	0.63	5.05	72.60
193	2.478	0.770	1.157	3.586	3.013	0.081	0.049	0.133	204.4	1.33	2.596	0.41	4.53	25.20
194	2.774	0.840	1.310	4.062	3.412	0.043	0.026	0.076	-	2.22	2.106	0.43	3.16	180.00
195	2.106	0.770	0.905	2.805	2.357	0.092	0.055	0.149	242.5	2.64	2.639	0.47	4.49	54.70
196	2.048	0.750	0.879	2.725	2.289	0.070	0.042	0.117	-	3.43	2.939	0.49	5.53	26.50
197	2.765	0.750	1.365	4.232	3.555	0.050	0.030	0.082	-	1.94	2.896	0.49	5.35	30.20
198	2.282	0.760	1.031	3.196	2.684	0.060	0.036	0.099	-	3.37	3.135	0.63	5.82	48.90
199	2.300	0.760	1.043	3.235	2.717	0.030	0.018	0.047	202.7	5.91	2.917	0.53	5.25	46.40
200	2.239	0.750	1.009	3.128	2.627	0.080	0.048	0.134	-	2.07	2.969	0.52	5.54	33.80
201	1.687	0.762	0.627	1.942	1.632	0.064	0.038	0.107	300.6	3.77	2.800	0.52	4.87	56.20
202	2.218	0.792	0.965	2.993	2.514	0.048	0.029	0.082	138.6	2.06	2.447	0.46	3.93	89.30
203	2.578	0.740	1.245	3.859	3.242	0.045	0.027	0.075	174.8	9.43	4.246	1.09	10.87	18.60
204	1.645	0.740	0.613	1.900	1.596	0.129	0.078	0.223	-	11.93	3.435	0.69	7.00	33.70
205	1.680	0.790	0.603	1.869	1.570	0.067	0.040	0.108	-	4.16	2.695	0.54	4.45	85.70
206	2.220	0.760	0.989	3.065	2.575	0.033	0.020	0.056	257.0	1.80	2.667	0.45	4.65	37.80
207	1.967	0.820	0.777	2.409	2.024	0.085	0.051	0.144	-	2.43	1.999	0.32	3.14	53.70
208	1.974	0.820	0.782	2.424	2.036	0.033	0.020	0.058	129.5	2.79	2.062	0.37	3.17	116.00
209	1.881	0.900	0.665	2.061	1.731	0.038	0.023	0.070	-	5.01	2.023	0.47	2.95	258.00
210	1.796	0.775	0.691	2.143	1.800	0.083	0.050	0.140	324.8	5.63	2.592	0.48	4.29	72.90
211	2.098	0.760	0.906	2.810	2.360	0.045	0.027	0.073	-	4.07	2.716	0.41	4.88	12.90
212	2.059	0.727	0.903	2.798	2.351	0.044	0.026	0.078	-	4.29	3.233	0.51	6.91	7.68
213	1.868	0.690	0.798	2.474	2.078	0.083	0.050	0.191	373.1	10.77	4.431	0.86	14.24	9.18
214	2.712	0.870	1.248	3.868	3.249	0.038	0.023	0.068	-	1.30	1.972	0.40	2.94	196.00
215	2.449	0.774	1.134	3.517	2.954	0.039	0.024	0.065	-	3.87	2.401	0.40	3.94	53.10
216	2.229	1.120	0.751	2.329	1.956	0.068	0.041	0.133	-	-	-	-	-	-
217	1.938	0.820	0.757	2.347	1.972	0.044	0.027	0.075	396.5	4.70	2.055	0.35	3.20	86.90
218	2.226	0.810	0.959	2.973	2.497	0.055	0.033	0.092	-	7.50	2.162	0.38	3.38	91.70
219	1.992	0.855	0.770	2.388	2.006	0.045	0.027	0.076	-	4.23	2.134	0.45	3.19	189.00
220	1.981	0.890	0.739	2.292	1.925	0.021	0.013	0.035	-	2.91	2.134	0.53	3.10	257.00
221	2.477	0.722	1.189	3.685	3.095	0.112	0.067	0.196	277.6	5.56	3.388	0.54	7.59	9.06
222	2.448	0.805	1.113	3.450	2.898	0.039	0.024	0.065	204.9	2.74	2.193	0.35	3.52	50.10
223	2.621	0.800	1.233	3.823	3.212	0.034	0.020	0.056	-	4.74	3.060	0.72	5.13	83.40
224	1.738	0.865	0.591	1.833	1.539	0.027	0.016	0.043	258.6	2.80	1.990	0.41	2.95	209.00
225	2.003	0.750	0.849	2.631	2.210	0.098	0.059	0.166	-	4.69	2.936	0.53	5.33	44.30
226	1.725	0.750	0.660	2.047	1.719	0.090	0.054	0.149	90.3	6.50	2.856	0.47	5.29	24.40
227	1.680	0.760	0.623	1.932	1.623	-0.017	0.000	0.000	339.0	3.12	2.678	0.44	4.69	35.40
228	2.120	0.802	0.893	2.768	2.325	0.092	0.055	0.150	-	2.64	2.090	0.29	3.14	5.54
229	1.437	0.860	0.391	1.211	1.018	0.061	0.037	0.102	-	3.38	1.878	0.32	2.87	118.00
230	2.380	0.780	1.084	3.359	2.822	0.049	0.029	0.082	-	2.35	2.426	0.38	4.09	25.80

Table 2. Continued...

#	Φ_b	Φ_b^0	$E(B-V)$	A_v	A_r	f_D	$E_{cs}(B-V)$	Δr	$vsini$	$d(kpc)$	$logL/L_\odot$	$logR/R_\odot$	$M/M_\odot$	Age(My)
231	1.950	0.807	0.774	2.400	2.016	0.027	0.016	0.040	219.3	2.21	2.055	0.32	3.25	47.60
232	2.305	0.695	1.091	3.381	2.840	-0.007	0.000	0.000	-	9.50	4.309	0.84	12.97	10.60
233	2.156	0.740	0.959	2.973	2.497	0.013	0.008	0.032	282.5	4.06	3.228	0.57	6.47	27.60
234	1.875	0.820	0.715	2.215	1.861	0.021	0.013	0.032	-	1.64	2.067	0.37	3.19	111.00
235	2.126	0.765	0.922	2.858	2.401	0.041	0.025	0.064	-	2.51	2.772	0.51	4.79	56.60
236	1.762	0.765	0.675	2.093	1.758	0.080	0.048	0.133	-	3.89	2.768	0.49	4.85	47.60
237	2.109	0.805	0.883	2.739	2.300	0.051	0.030	0.083	183.5	1.94	2.259	0.39	3.59	79.90
238	1.436	0.815	0.420	1.303	1.095	0.059	0.035	0.101	269.1	2.09	2.096	0.37	3.25	99.40
239	2.359	0.835	1.033	3.201	2.689	0.050	0.030	0.084	-	1.52	1.850	0.27	2.74	21.80
240	2.096	0.730	0.925	2.868	2.409	0.161	0.096	0.276	-	3.44	3.348	0.59	7.04	21.60
241	1.668	0.775	0.605	1.875	1.575	0.114	0.069	0.193	-	3.09	2.533	0.45	4.20	63.60
242	1.699	0.815	0.599	1.857	1.560	0.061	0.037	0.101	417.3	3.82	2.133	0.38	3.32	96.50
243	2.270	0.790	1.003	3.109	2.611	0.029	0.017	0.048	-	2.29	2.555	0.48	4.17	82.70
244	2.323	0.740	1.072	3.324	2.792	0.061	0.036	0.101	-	2.69	2.944	0.45	5.69	9.42
245	2.191	0.805	0.939	2.910	2.445	0.097	0.058	0.159	191.8	1.40	2.156	0.33	3.45	35.10
246	2.077	0.765	0.889	2.755	2.314	0.112	0.067	0.184	277.7	3.75	2.812	0.53	4.86	61.20
247	2.321	0.760	1.057	3.278	2.753	0.126	0.076	0.211	-	1.97	2.738	0.47	4.81	41.60
248	2.551	0.800	1.186	3.678	3.090	0.063	0.038	0.108	-	2.13	2.267	0.37	3.68	45.20
249	2.246	0.760	1.006	3.120	2.621	0.064	0.039	0.108	539.6	2.80	2.815	0.49	5.01	42.20
250	2.508	0.730	1.205	3.734	3.137	0.058	0.035	0.105	-	8.34	3.715	0.73	8.45	23.80
251	1.752	0.760	0.672	2.084	1.751	0.137	0.082	0.229	312.1	2.48	2.649	0.41	4.70	16.90
252	2.150	0.780	0.928	2.877	2.416	0.033	0.020	0.056	-	4.40	2.608	0.50	4.28	82.80
253	1.941	1.160	0.529	1.641	1.379	0.091	0.055	0.176	-	-	-	-	-	-
254	2.376	0.680	1.149	3.562	2.992	0.058	0.035	0.132	-	5.25	4.271	0.75	13.48	7.06
255	1.999	0.757	0.841	2.608	2.191	0.076	0.046	0.125	277.7	5.07	2.746	0.43	5.00	18.30
256	2.441	0.770	1.132	3.510	2.948	0.171	0.102	0.281	-	3.98	2.550	0.44	4.29	52.30
257	2.299	0.820	1.002	3.106	2.609	0.050	0.030	0.084	215.2	1.77	2.135	0.41	3.26	140.00
258	2.235	0.760	0.999	3.097	2.602	0.132	0.079	0.220	-	4.22	3.426	0.76	6.55	47.50
259	2.414	0.767	1.116	3.458	2.905	0.124	0.075	0.211	-	2.05	2.618	0.43	4.54	35.30
260	1.934	0.855	0.731	2.266	1.903	0.030	0.018	0.051	-	2.76	2.272	0.52	3.40	188.00
261	1.518	0.765	0.510	1.582	1.329	0.016	0.010	0.030	-	6.20	2.612	0.44	4.48	43.90
262	1.646	0.875	0.522	1.619	1.360	0.024	0.015	0.043	133.9	2.32	1.882	0.36	2.83	177.00
263	2.256	0.780	1.000	3.099	2.603	0.018	0.011	0.030	224.6	2.68	2.622	0.48	4.38	67.50
264	1.868	0.752	0.756	2.342	1.968	0.073	0.044	0.125	-	5.60	2.874	0.50	5.20	39.00
265	1.619	0.800	0.554	1.719	1.444	0.052	0.031	0.082	447.8	5.56	2.286	0.38	3.69	58.00
266	2.584	0.745	1.246	3.862	3.244	0.079	0.047	0.135	-	2.43	3.057	0.51	5.96	23.40
267	1.638	0.805	0.565	1.750	1.470	0.020	0.012	0.031	168.2	5.11	2.409	0.45	3.85	91.80
268	1.632	0.865	0.520	1.611	1.353	0.031	0.018	0.051	-	3.09	1.822	0.31	2.80	107.00
269	1.835	0.803	0.698	2.165	1.819	0.025	0.015	0.040	420.6	5.99	2.114	0.31	3.30	20.50
270	2.347	0.825	1.031	3.195	2.684	0.031	0.019	0.050	-	1.57	2.102	0.40	3.21	135.00
271	1.721	0.785	0.634	1.966	1.652	0.040	0.024	0.064	270.8	2.56	2.409	0.38	4.04	26.30
272	1.910	0.808	0.747	2.314	1.944	0.054	0.032	0.092	557.8	2.63	2.277	0.43	3.54	116.00
273	1.699	0.755	0.639	1.982	1.665	0.044	0.026	0.074	296.9	5.68	2.765	0.43	5.08	14.00
274	2.032	0.833	0.812	2.518	2.115	0.024	0.014	0.041	-	2.50	2.152	0.42	3.27	149.00
275	2.104	0.795	0.887	2.750	2.310	0.067	0.040	0.108	-	4.05	2.481	0.49	3.95	101.00
276	2.559	0.735	1.235	3.830	3.217	0.060	0.036	0.102	-	4.41	3.375	0.63	6.96	28.20
277	1.708	0.870	0.567	1.759	1.477	0.017	0.010	0.033	-	2.50	1.688	0.22	2.53	4.10
278	1.296	0.790	0.343	1.063	0.893	0.080	0.048	0.134	169.2	4.75	2.397	0.44	3.85	82.80
279	1.713	0.790	0.625	1.938	1.628	0.025	0.015	0.039	289.6	3.18	2.410	0.43	3.91	71.70
280	1.373	0.800	0.388	1.204	1.012	0.074	0.044	0.125	255.2	4.06	2.337	0.41	3.75	74.40
281	1.139	0.865	0.186	0.575	0.483	0.055	0.033	0.094	556.6	5.32	1.934	0.38	2.90	183.00
282	1.957	0.774	0.802	2.485	2.087	0.067	0.040	0.108	-	2.93	2.442	0.41	4.03	54.40
283	1.914	0.855	0.717	2.224	1.868	0.027	0.016	0.042	-	1.83	2.026	0.41	3.03	189.00
284	1.482	0.805	0.458	1.421	1.193	0.041	0.024	0.066	-	3.74	2.431	0.49	3.82	116.00
285	1.671	0.850	0.556	1.724	1.449	0.050	0.030	0.084	-	7.96	2.290	0.51	3.45	172.00

Table 2. Continued...

#	Φ_b	Φ_b^0	$E(B-V)$	A_v	A_r	f_D	$E_{cs}(B-V)$	Δr	$vsini$	$d(kpc)$	$logL/L_\odot$	$logR/R_\odot$	$M/M_\odot$	Age(My)
286	1.534	0.807	0.492	1.526	1.282	0.058	0.035	0.100	183.4	3.01	2.100	0.34	3.33	53.90
287	1.289	0.778	0.346	1.072	0.901	0.037	0.022	0.056	-	3.41	2.381	0.40	3.89	56.70
288	1.719	0.830	0.602	1.867	1.568	0.048	0.029	0.084	160.3	4.22	1.854	0.27	2.78	29.10
289	2.033	0.865	0.791	2.453	2.060	0.034	0.020	0.060	-	5.96	2.363	0.59	3.45	215.00
290	1.873	0.770	0.747	2.316	1.945	0.045	0.027	0.073	304.0	5.51	2.896	0.57	5.04	63.30
291	1.896	0.742	0.781	2.423	2.035	0.088	0.053	0.151	-	5.48	3.116	0.55	6.04	30.80
292	1.793	0.760	0.700	2.169	1.822	0.080	0.048	0.133	-	11.15	2.857	0.50	5.13	42.20
293	1.656	0.778	0.594	1.843	1.548	0.070	0.042	0.117	332.1	4.01	2.311	0.38	3.75	53.00
294	1.692	0.860	0.564	1.747	1.468	0.035	0.021	0.060	157.3	3.59	2.037	0.42	3.03	196.00
295	1.742	0.745	0.675	2.094	1.759	0.065	0.039	0.109	259.1	4.30	2.884	0.45	5.49	12.20
296	1.506	0.835	0.455	1.409	1.184	0.055	0.033	0.093	361.9	2.52	2.008	0.36	3.07	124.00
297	1.782	0.774	0.683	2.117	1.778	0.061	0.036	0.099	-	3.61	2.525	0.44	4.19	61.00
298	1.318	0.860	0.310	0.962	0.808	0.033	0.020	0.059	-	2.60	1.985	0.39	2.98	179.00
299	1.859	0.795	0.721	2.234	1.876	0.125	0.075	0.212	-	4.19	2.356	0.38	3.87	43.10
300	1.619	0.780	0.569	1.762	1.480	0.018	0.011	0.030	-	3.78	2.613	0.51	4.28	84.30
301	1.470	0.790	0.461	1.428	1.200	0.066	0.040	0.108	320.6	5.84	2.484	0.47	4.01	86.10
302	1.802	0.835	0.655	2.032	1.707	0.043	0.026	0.076	-	2.86	1.948	0.32	3.02	84.60
303	1.674	0.915	0.514	1.595	1.340	0.149	0.089	0.269	-	6.00	1.930	0.48	2.78	327.00
304	1.589	0.750	0.568	1.762	1.480	0.092	0.055	0.150	-	7.38	2.929	0.49	5.48	28.10
305	1.653	0.805	0.574	1.780	1.495	0.035	0.021	0.057	-	4.02	2.242	0.39	3.55	80.70
306	1.980	0.817	0.788	2.443	2.052	0.076	0.045	0.127	-	3.88	2.026	0.33	3.16	74.30
307	1.480	0.755	0.491	1.522	1.278	0.148	0.089	0.256	233.7	3.42	2.785	0.45	5.05	26.30
308	1.162	0.855	0.208	0.644	0.541	0.040	0.024	0.068	220.6	2.55	1.878	0.32	2.88	112.00
309	1.317	0.805	0.347	1.075	0.903	0.043	0.026	0.074	-	3.17	2.370	0.44	3.76	97.90
310	1.865	0.780	0.735	2.278	1.914	0.053	0.032	0.090	-	9.64	2.824	0.58	4.79	75.20
311	2.054	0.810	0.843	2.613	2.195	0.122	0.073	0.204	305.8	3.08	2.823	0.66	4.55	106.00
312	1.660	0.805	0.579	1.795	1.508	0.083	0.050	0.143	-	3.63	2.226	0.39	3.53	79.40
313	1.371	0.805	0.383	1.188	0.998	0.045	0.027	0.074	202.4	3.54	2.286	0.42	3.61	95.20
314	1.554	0.860	0.470	1.457	1.224	0.025	0.015	0.042	-	2.42	1.909	0.34	2.90	137.00
315	1.747	0.815	0.631	1.956	1.643	0.012	0.007	0.023	-	1.81	2.035	0.32	3.21	46.90
316	1.741	0.735	0.682	2.113	1.775	0.141	0.084	0.243	-	4.50	3.197	0.53	6.57	17.00
317	1.659	0.805	0.579	1.794	1.507	0.047	0.028	0.074	-	6.22	2.696	0.59	4.37	101.00
318	1.329	0.765	0.382	1.184	0.994	0.046	0.028	0.073	383.9	3.88	2.640	0.46	4.52	49.90
319	1.656	0.774	0.598	1.853	1.556	0.033	0.020	0.056	226.7	2.15	2.432	0.41	4.01	55.20
320	1.574	0.765	0.548	1.700	1.428	0.085	0.051	0.140	-	5.28	2.703	0.46	4.70	44.10
321	1.486	0.885	0.407	1.262	1.060	0.876	0.018	0.140	-	4.35	1.904	0.38	2.84	203.00
322	1.054	0.800	0.172	0.532	0.447	0.039	0.024	0.065	261.2	3.13	2.240	0.37	3.59	61.00
323	1.699	0.820	0.595	1.846	1.551	0.040	0.024	0.067	-	3.96	2.119	0.40	3.24	139.00
324	1.307	0.805	0.340	1.055	0.886	0.072	0.043	0.117	258.8	3.27	2.384	0.45	3.79	96.70
325	1.445	0.905	0.366	1.135	0.953	0.134	0.080	0.240	-	6.83	1.790	0.36	2.65	254.00
326	1.685	0.715	0.657	2.037	1.711	0.128	0.077	0.233	-	8.27	3.518	0.60	8.02	14.50
327	1.674	0.860	0.551	1.708	1.435	0.025	0.015	0.042	182.0	1.72	1.747	0.25	2.64	26.90
328	1.526	0.910	0.417	1.293	1.086	0.030	0.018	0.053	-	3.40	2.046	0.51	2.96	281.00
329	1.263	0.815	0.303	0.940	0.790	0.029	0.017	0.048	368.1	4.24	2.564	0.56	4.05	118.00
330	1.431	0.745	0.465	1.441	1.211	0.047	0.028	0.074	-	4.91	3.053	0.52	5.91	26.00
331	1.490	0.820	0.454	1.408	1.182	0.022	0.013	0.032	267.2	4.66	1.912	0.29	2.97	46.20
332	1.520	0.805	0.484	1.502	1.261	0.045	0.027	0.074	-	2.62	2.208	0.38	3.49	78.10
333	1.663	0.855	0.547	1.696	1.425	0.023	0.014	0.042	-	3.69	2.058	0.43	3.07	194.00
334	1.751	0.745	0.681	2.112	1.774	0.094	0.057	0.159	-	5.85	2.995	0.49	5.77	21.50
335	1.553	0.790	0.517	1.603	1.347	0.086	0.052	0.140	127.0	2.49	2.161	0.26	3.00	0.00
336	1.754	0.774	0.664	2.058	1.729	0.074	0.045	0.125	251.4	2.97	2.483	0.43	4.11	59.60
337	1.921	0.715	0.817	2.532	2.127	0.106	0.064	0.196	-	8.27	3.585	0.58	8.68	7.45
338	1.847	0.765	0.733	2.272	1.909	0.021	0.013	0.030	395.5	4.15	2.706	0.47	4.70	46.10
339	1.919	0.835	0.734	2.276	1.912	0.039	0.024	0.067	-	3.77	2.283	0.50	3.45	170.00
340	1.586	0.810	0.526	1.630	1.369	0.024	0.015	0.040	176.1	6.59	2.271	0.44	3.51	127.00

Table 2. Continued...

#	Φ_b	Φ_b^0	$E(B-V)$	A_v	A_r	f_D	$E_{cs}(B-V)$	Δr	$vsini$	$d(kpc)$	$logL/L_\odot$	$logR/R_\odot$	$M/M_\odot$	Age(My)
341	1.780	0.815	0.654	2.027	1.702	0.041	0.025	0.066	229.9	4.08	2.166	0.39	3.37	104.00
342	1.396	0.875	0.353	1.094	0.919	0.166	0.100	0.285	-	2.14	1.753	0.27	2.71	59.10
343	1.435	1.120	0.213	0.661	0.555	0.074	0.044	0.144	-	-	-	-	-	-
344	1.519	1.120	0.270	0.837	0.703	0.052	0.031	0.113	443.6	-	-	-	-	-
345	1.928	0.750	0.798	2.474	2.078	0.089	0.053	0.149	-	4.55	3.274	0.67	6.28	44.10
346	1.891	0.820	0.725	2.248	1.889	0.026	0.015	0.041	-	2.09	2.188	0.44	3.33	153.00
347	2.112	0.770	0.909	2.819	2.368	0.026	0.015	0.039	258.4	3.60	2.629	0.47	4.43	60.80
348	1.861	0.835	0.695	2.154	1.809	0.051	0.031	0.084	-	6.91	2.480	0.57	3.80	152.00
349	2.355	0.730	1.100	3.412	2.866	0.032	0.019	0.052	-	6.26	3.882	0.84	8.80	26.80
350	1.920	0.830	0.739	2.289	1.923	0.030	0.018	0.050	-	2.94	2.142	0.44	3.23	171.00
351	2.367	0.750	1.096	3.397	2.853	0.047	0.028	0.083	-	7.24	3.327	0.65	6.61	36.10
352	2.172	0.750	0.963	2.986	2.508	0.050	0.030	0.082	-	6.39	2.909	0.52	5.27	42.90
353	1.849	0.790	0.717	2.223	1.867	0.027	0.016	0.039	255.0	3.59	2.480	0.47	4.00	86.80
354	1.548	0.817	0.495	1.534	1.289	0.039	0.024	0.066	-	3.03	1.996	0.32	3.13	60.70
355	2.075	0.780	0.878	2.720	2.285	0.028	0.017	0.047	172.0	4.96	2.773	0.56	4.66	78.30
356	1.708	1.250	0.310	0.962	0.808	0.097	0.058	0.193	-	-	-	-	-	-
357	2.064	0.740	0.897	2.780	2.335	0.053	0.032	0.093	-	3.52	3.235	0.57	6.50	27.20
358	1.894	0.770	0.762	2.361	1.984	0.038	0.023	0.056	381.4	2.62	2.788	0.54	4.77	66.20
359	1.735	1.300	0.295	0.914	0.768	0.072	0.043	0.133	-	-	-	-	-	-
360	2.235	0.975	0.853	2.645	2.222	0.087	0.052	0.160	-	-	-	-	-	-
361	1.597	0.830	0.520	1.611	1.354	0.057	0.034	0.093	476.1	3.54	1.905	0.30	2.96	56.50
362	2.576	0.900	1.135	3.520	2.956	0.087	0.052	0.149	-	0.96	1.735	0.30	2.64	153.00
363	1.913	0.820	0.740	2.295	1.928	0.048	0.029	0.083	-	2.94	2.525	0.57	3.93	133.00
364	1.804	0.910	0.605	1.877	1.576	0.061	0.037	0.104	-	3.79	1.778	0.35	2.64	241.00
365	2.058	0.850	0.818	2.537	2.131	0.035	0.021	0.059	-	4.69	2.349	0.54	3.55	170.00
366	2.092	0.762	0.900	2.791	2.344	0.059	0.035	0.099	-	5.52	2.967	0.58	5.29	56.00
367	1.974	0.695	0.867	2.687	2.257	0.074	0.044	0.147	-	8.18	4.186	0.78	12.14	10.50
368	1.399	0.815	0.396	1.227	1.031	0.138	0.083	0.242	-	4.31	2.098	0.37	3.27	94.80
369	1.574	0.805	0.521	1.615	1.357	0.026	0.016	0.040	240.1	2.17	2.193	0.38	3.46	78.80
370	1.476	0.805	0.455	1.410	1.184	0.047	0.028	0.074	299.2	5.08	2.387	0.46	3.78	103.00
371	1.674	0.805	0.589	1.825	1.533	0.062	0.037	0.100	-	2.66	2.090	0.31	3.29	27.00
372	2.027	0.735	0.875	2.713	2.279	0.134	0.081	0.234	-	7.15	3.373	0.62	7.00	26.40
373	2.147	0.730	0.960	2.976	2.499	0.138	0.083	0.245	-	6.92	3.449	0.63	7.36	24.30
374	1.603	0.815	0.534	1.655	1.390	0.061	0.037	0.101	-	2.84	2.132	0.37	3.33	94.70
375	2.631	0.765	1.264	3.918	3.292	0.061	0.037	0.099	-	4.02	3.013	0.59	5.45	51.90
376	2.270	0.735	1.040	3.224	2.708	0.060	0.036	0.102	-	5.41	3.276	0.57	6.73	23.20
377	1.398	0.830	0.385	1.193	1.002	0.032	0.019	0.050	181.7	3.12	2.045	0.37	3.14	118.00
378	1.507	0.780	0.493	1.527	1.283	0.054	0.033	0.090	387.3	3.93	2.767	0.55	4.66	76.10
379	1.696	0.805	0.604	1.871	1.572	0.052	0.031	0.083	-	6.45	2.297	0.41	3.64	90.40
380	1.263	0.800	0.313	0.971	0.816	0.088	0.053	0.150	383.5	3.38	2.257	0.35	3.68	34.10
381	1.557	0.789	0.520	1.611	1.353	0.050	0.030	0.082	321.0	3.83	2.289	0.38	3.70	56.30
382	1.403	0.780	0.422	1.307	1.098	0.064	0.039	0.108	402.0	2.85	2.501	0.46	4.08	75.80
383	2.180	0.760	0.962	2.981	2.504	0.050	0.030	0.082	-	4.86	2.759	0.45	4.95	29.30
384	1.499	0.750	0.507	1.573	1.321	0.043	0.026	0.073	-	4.01	2.987	0.55	5.47	44.20
385	2.052	0.765	0.872	2.703	2.271	0.069	0.041	0.116	-	2.76	2.739	0.48	4.78	46.30
386	1.264	0.820	0.300	0.931	0.782	0.023	0.014	0.041	301.3	3.56	2.052	0.35	3.20	84.40
387	1.763	0.780	0.666	2.064	1.733	0.049	0.029	0.082	-	3.58	2.520	0.43	4.22	52.20
388	1.627	0.840	0.533	1.654	1.389	0.051	0.031	0.085	-	3.65	2.031	0.38	3.08	148.00
389	3.017	0.705	1.566	4.855	4.078	0.125	0.075	0.217	-	22.05	5.162	1.50	21.92	7.03
390	2.198	0.745	0.984	3.051	2.563	0.065	0.039	0.108	-	2.89	3.082	0.57	5.80	39.90
391	1.766	0.770	0.675	2.092	1.757	0.029	0.017	0.047	248.5	3.01	2.652	0.47	4.51	56.60
392	2.450	0.745	1.155	3.581	3.008	0.109	0.065	0.186	-	3.79	3.125	0.54	6.12	27.70
393	2.261	0.735	1.034	3.204	2.691	0.075	0.045	0.128	-	8.26	3.683	0.78	7.94	30.60
394	2.002	0.715	0.872	2.703	2.271	0.076	0.046	0.132	347.4	10.79	3.757	0.74	8.71	22.10
395	2.050	0.760	0.874	2.708	2.275	0.056	0.034	0.090	-	4.58	2.845	0.50	5.09	42.00

Table 2. Continued...

#	Φ_b	Φ_b^0	$E(B-V)$	A_v	A_r	f_D	$E_{cs}(B-V)$	Δr	$vsini$	$d(kpc)$	$logL/L_\odot$	$logR/R_\odot$	$M/M_\odot$	Age(My)
396	1.679	1.000	0.460	1.426	1.198	-0.033	0.000	0.000	-	-	-	-	-	-
397	2.596	0.725	1.268	3.930	3.301	0.079	0.048	0.141	-	5.59	3.569	0.63	8.09	18.50
398	1.490	0.810	0.461	1.429	1.200	0.034	0.020	0.057	214.1	3.88	2.367	0.48	3.67	130.00
399	2.006	0.895	0.752	2.333	1.959	0.137	0.082	0.237	193.0	2.30	1.783	0.32	2.71	150.00
400	2.177	0.965	0.821	2.546	2.139	0.045	0.027	0.081	-	1.21	1.657	0.39	2.41	414.00
401	1.809	0.750	0.717	2.224	1.868	0.144	0.086	0.247	-	7.29	2.910	0.52	5.27	42.70
402	1.218	0.858	0.244	0.757	0.636	0.027	0.016	0.042	315.1	3.00	2.154	0.47	3.21	195.00
403	2.246	0.730	1.027	3.184	2.674	0.050	0.030	0.086	413.4	4.79	3.278	0.55	6.90	16.20
404	1.337	0.815	0.353	1.095	0.920	0.034	0.020	0.058	247.9	7.23	2.190	0.43	3.34	146.00
405	1.873	0.865	0.683	2.117	1.778	0.056	0.033	0.094	178.4	2.66	1.853	0.32	2.83	129.00
406	2.162	0.935	0.832	2.578	2.165	0.052	0.031	0.088	427.7	1.89	1.616	0.31	2.43	265.00
407	1.892	0.810	0.733	2.273	1.909	0.048	0.029	0.083	-	4.57	2.285	0.44	3.56	118.00
408	1.788	0.805	0.666	2.065	1.734	0.072	0.043	0.117	230.5	2.46	2.260	0.40	3.58	85.40
409	1.276	0.815	0.313	0.969	0.814	0.043	0.026	0.075	408.3	2.61	2.130	0.37	3.32	95.90
410	1.094	0.840	0.172	0.533	0.448	0.028	0.017	0.050	208.1	5.61	2.024	0.38	3.08	140.00
411	1.368	0.735	0.429	1.330	1.117	0.069	0.041	0.119	299.0	5.53	3.041	0.47	6.03	7.42
412	1.699	0.780	0.622	1.929	1.621	0.109	0.065	0.184	382.9	3.96	2.538	0.42	4.32	38.70
413	1.339	0.778	0.380	1.177	0.989	0.050	0.030	0.082	404.0	3.93	2.453	0.43	4.02	63.70
414	2.497	0.778	1.165	3.611	3.033	0.070	0.042	0.117	-	1.77	2.336	0.39	3.79	59.70
415	1.458	0.820	0.432	1.340	1.126	0.051	0.030	0.084	207.9	5.24	2.069	0.35	3.23	85.10
416	2.075	0.757	0.892	2.766	2.323	0.094	0.057	0.158	-	3.27	2.849	0.48	5.20	31.70
417	2.249	0.745	1.019	3.159	2.654	0.151	0.090	0.257	459.6	4.53	2.902	0.46	5.51	17.20
418	1.779	0.810	0.656	2.035	1.709	0.053	0.032	0.091	210.9	5.54	2.523	0.51	4.01	107.00
419	2.097	0.770	0.899	2.788	2.342	0.075	0.045	0.125	243.1	3.05	2.508	0.43	4.19	51.70
420	2.380	0.765	1.094	3.391	2.848	0.075	0.045	0.125	504.1	3.07	2.655	0.46	4.58	45.90
421	1.746	0.835	0.617	1.914	1.608	0.063	0.038	0.110	322.7	3.81	2.298	0.51	3.47	168.00
422	1.553	0.855	0.473	1.467	1.232	0.054	0.032	0.093	265.0	2.48	1.996	0.38	3.02	152.00
423	1.968	0.775	0.808	2.504	2.104	0.053	0.032	0.090	-	4.97	2.663	0.50	4.46	70.40
424	1.931	0.815	0.756	2.344	1.969	0.054	0.032	0.092	326.8	2.15	2.336	0.50	3.58	148.00
425	1.809	0.810	0.677	2.097	1.762	0.061	0.037	0.100	-	4.02	2.199	0.39	3.45	94.40
426	1.299	0.735	0.382	1.185	0.995	0.088	0.053	0.153	-	4.99	3.145	0.52	6.34	18.70
427	1.396	0.760	0.431	1.336	1.122	0.038	0.023	0.065	269.9	5.55	2.664	0.41	4.74	15.30
428	1.942	0.805	0.770	2.388	2.006	0.052	0.031	0.083	316.2	2.56	2.419	0.47	3.82	109.00
429	1.390	0.810	0.393	1.218	1.024	0.035	0.021	0.058	-	4.01	2.184	0.41	3.38	119.00
430	2.686	0.810	1.271	3.940	3.310	0.073	0.044	0.126	-	3.03	2.459	0.52	3.83	128.00
431	1.600	0.770	0.562	1.742	1.463	0.155	0.093	0.255	-	7.81	2.930	0.57	5.18	57.20
432	1.933	0.775	0.784	2.431	2.042	0.084	0.050	0.140	209.1	3.18	2.692	0.53	4.48	77.90
433	1.344	0.935	0.277	0.859	0.722	0.097	0.058	0.168	324.9	2.32	1.602	0.27	2.46	138.00
434	1.978	0.775	0.815	2.527	2.122	0.045	0.027	0.073	373.5	3.10	2.885	0.59	4.96	69.30
435	2.202	1.250	0.645	2.000	1.680	0.065	0.039	0.125	-	-	-	-	-	-
436	1.923	0.770	0.781	2.421	2.033	0.110	0.066	0.184	-	4.40	2.773	0.52	4.76	62.10
437	1.626	0.760	0.586	1.818	1.527	0.062	0.037	0.099	-	8.64	2.845	0.50	5.10	41.90
438	1.441	0.740	0.475	1.472	1.237	0.051	0.031	0.084	-	4.67	3.140	0.54	6.20	26.10
439	1.678	0.810	0.588	1.824	1.532	0.052	0.031	0.083	-	5.20	2.362	0.49	3.64	137.00
440	2.427	0.805	1.099	3.406	2.861	0.083	0.050	0.141	-	6.58	2.872	0.66	4.70	96.80
441	1.925	0.778	0.777	2.409	2.024	0.047	0.028	0.073	-	6.34	2.403	0.42	3.91	66.00
442	2.114	0.695	0.961	2.980	2.503	0.106	0.064	0.210	-	7.39	3.866	0.64	10.46	6.74
443	1.907	0.765	0.774	2.399	2.015	0.077	0.046	0.125	-	2.98	2.838	0.54	4.94	59.00
444	2.155	0.790	0.925	2.866	2.408	0.036	0.022	0.056	-	3.21	2.485	0.47	4.00	91.20
445	2.162	0.770	0.943	2.924	2.456	0.222	0.133	0.379	-	5.33	3.412	0.78	6.40	50.90
446	2.121	0.815	0.884	2.742	2.303	0.135	0.081	0.232	-	5.54	2.482	0.53	3.88	127.00
447	1.505	1.350	0.105	0.326	0.274	0.124	0.074	0.248	481.6	-	-	-	-	-
448	2.385	0.760	1.101	3.413	2.867	0.140	0.084	0.238	507.5	9.06	2.926	0.56	5.20	54.40
449	1.506	0.780	0.492	1.525	1.281	0.073	0.044	0.125	-	4.92	2.639	0.51	4.35	81.30
450	2.190	0.935	0.850	2.635	2.214	0.028	0.017	0.053	259.0	1.23	1.742	0.37	2.56	301.00

Table 2. Continued...

#	Φ_b	Φ_b^0	$E(B-V)$	A_v	A_r	f_D	$E_{cs}(B-V)$	Δr	$vsini$	$d(kpc)$	$logL/L_\odot$	$logR/R_\odot$	$M/M_\odot$	Age(My)
451	2.277	0.875	0.950	2.944	2.473	0.056	0.034	0.093	-	2.12	1.645	0.20	2.51	0.92
452	2.203	0.715	1.008	3.125	2.625	0.068	0.041	0.125	-	5.19	3.827	0.74	9.16	20.00
453	2.171	0.767	0.951	2.947	2.476	0.110	0.066	0.184	-	3.35	3.065	0.63	5.52	57.70
454	2.314	0.805	1.022	3.169	2.662	0.092	0.055	0.150	-	2.22	2.546	0.50	4.10	96.70
455	1.798	0.790	0.683	2.117	1.778	0.052	0.031	0.082	-	6.05	2.966	0.68	4.98	84.50
456	2.185	0.765	0.962	2.982	2.505	0.083	0.050	0.140	-	6.19	2.657	0.46	4.57	47.80
457	1.620	0.803	0.554	1.717	1.442	0.044	0.027	0.074	-	2.99	2.270	0.41	3.59	89.20
458	1.897	0.780	0.757	2.346	1.971	0.059	0.036	0.099	-	6.33	2.552	0.47	4.20	73.30
459	2.156	0.810	0.912	2.827	2.374	0.066	0.039	0.109	-	2.14	2.169	0.35	3.46	56.60
460	1.485	0.760	0.491	1.523	1.279	0.083	0.050	0.140	252.5	5.95	2.736	0.46	4.85	35.20
461	1.610	0.940	0.454	1.407	1.182	0.190	0.114	0.341	-	2.89	2.076	0.56	2.92	334.00
462	2.072	0.790	0.868	2.692	2.261	0.033	0.020	0.056	-	2.08	2.424	0.43	3.93	72.50
463	1.351	0.770	0.394	1.221	1.025	0.077	0.046	0.125	431.9	8.80	2.521	0.43	4.24	47.70
464	1.351	0.770	0.394	1.221	1.025	0.048	0.029	0.082	285.2	2.70	2.469	0.42	4.10	51.30
465	1.999	0.810	0.805	2.496	2.097	0.097	0.058	0.159	-	4.00	2.557	0.54	4.06	112.00
466	1.221	0.855	0.248	0.768	0.645	0.042	0.025	0.068	-	6.46	2.073	0.43	3.09	192.00
467	2.201	0.805	0.945	2.931	2.462	0.049	0.029	0.082	-	3.18	2.043	0.26	3.02	0.40
468	1.862	0.835	0.696	2.157	1.812	0.050	0.030	0.084	-	3.10	2.021	0.37	3.09	127.00
469	2.247	0.810	0.973	3.018	2.535	0.033	0.020	0.057	-	2.25	2.351	0.47	3.66	124.00
470	2.109	0.785	0.897	2.781	2.336	0.064	0.038	0.108	-	3.47	2.428	0.39	4.06	35.60
471	1.997	0.800	0.811	2.513	2.111	0.055	0.033	0.091	260.4	3.41	2.220	0.36	3.58	47.80
472	2.010	0.785	0.830	2.572	2.161	0.040	0.024	0.064	289.8	4.07	2.465	0.40	4.14	39.90
473	1.666	0.745	0.624	1.933	1.624	0.088	0.053	0.151	-	5.74	3.070	0.53	5.92	28.80
474	1.543	0.870	0.456	1.414	1.187	0.031	0.019	0.051	-	5.56	2.078	0.46	3.07	221.00
475	2.349	0.735	1.094	3.390	2.848	0.078	0.047	0.137	-	6.53	3.413	0.63	7.18	25.60
476	2.717	0.820	1.285	3.984	3.347	0.159	0.095	0.272	-	1.36	2.167	0.43	3.29	152.00
477	2.566	0.790	1.203	3.729	3.132	0.045	0.027	0.073	-	1.81	2.343	0.36	3.87	27.90
478	2.831	0.735	1.420	4.402	3.698	0.165	0.099	0.284	-	2.76	3.540	0.69	7.58	27.80
479	1.267	0.815	0.306	0.948	0.797	0.059	0.035	0.101	-	13.24	2.162	0.39	3.35	110.00
480	2.419	0.750	1.131	3.505	2.944	0.063	0.038	0.108	-	2.39	2.907	0.52	5.25	43.70
481	1.477	0.925	0.374	1.160	0.974	0.040	0.024	0.070	427.9	8.29	1.818	0.40	2.65	305.00
482	2.412	0.765	1.116	3.459	2.905	0.082	0.049	0.133	-	3.22	3.244	0.70	6.01	53.30
483	1.998	0.820	0.798	2.474	2.078	0.056	0.033	0.093	154.0	1.60	2.166	0.43	3.30	149.00
484	2.422	0.745	1.136	3.522	2.959	0.060	0.036	0.100	-	2.32	3.100	0.56	5.91	36.30
485	3.235	0.830	1.629	5.050	4.242	0.074	0.044	0.126	-	3.15	3.112	0.85	5.10	85.60
486	2.402	0.780	1.099	3.406	2.861	0.065	0.039	0.108	-	4.28	2.585	0.49	4.24	81.70
487	2.646	0.710	1.312	4.067	3.416	0.128	0.077	0.239	-	5.71	3.667	0.63	8.84	12.80
488	2.618	0.790	1.238	3.838	3.224	0.069	0.041	0.116	-	1.94	2.517	0.48	4.08	86.20
489	2.805	0.742	1.398	4.333	3.640	0.082	0.049	0.135	-	2.30	3.303	0.63	6.55	35.10
490	2.610	0.760	1.253	3.885	3.263	0.076	0.046	0.125	481.6	2.24	2.813	0.49	5.02	40.50
491	2.703	0.780	1.303	4.038	3.392	0.072	0.043	0.116	196.3	2.13	2.804	0.57	4.74	75.50
492	2.915	0.678	1.515	4.698	3.946	0.108	0.065	0.221	-	15.50	5.091	1.24	21.15	7.27
493	2.294	0.730	1.059	3.284	2.758	0.048	0.029	0.087	-	5.62	3.417	0.60	7.39	19.60
494	2.213	0.790	0.964	2.987	2.509	0.064	0.038	0.108	405.8	1.66	2.562	0.50	4.15	90.80
495	1.243	0.835	0.276	0.856	0.719	0.028	0.017	0.050	-	3.22	2.222	0.48	3.34	176.00
496	1.696	0.815	0.597	1.850	1.554	0.020	0.012	0.032	748.4	4.97	2.124	0.40	3.26	127.00
497	3.128	0.742	1.616	5.010	4.209	0.069	0.041	0.118	-	3.50	3.228	0.60	6.35	33.50
498	2.725	0.690	1.379	4.275	3.591	0.187	0.112	0.379	-	10.03	4.524	0.96	14.20	11.20
499	3.270	0.690	1.748	5.418	4.551	0.089	0.053	0.189	-	3.55	4.394	0.88	13.58	10.50
500	3.135	0.670	1.670	5.176	4.348	0.137	0.082	0.322	-	7.23	4.744	0.90	18.87	5.66
501	2.030	0.742	0.873	2.705	2.272	0.105	0.063	0.177	-	8.09	3.100	0.55	5.97	31.80
502	2.877	0.800	1.407	4.362	3.664	0.089	0.054	0.149	175.4	1.97	2.657	0.53	4.36	87.90
503	1.989	0.774	0.823	2.552	2.144	0.006	0.004	0.013	287.9	3.61	2.456	0.42	4.06	55.10
504	1.718	0.890	0.561	1.739	1.461	0.019	0.011	0.035	205.7	7.54	2.009	0.45	2.94	250.00
505	1.326	0.686	0.433	1.343	1.128	0.150	0.090	0.307	-	29.35	4.164	0.73	12.53	7.35

Table 2. Continued...

#	Φ_b	Φ_b^0	$E(B-V)$	A_v	A_r	f_D	$E_{cs}(B-V)$	Δr	$vsini$	$d(kpc)$	$logL/L_\odot$	$logR/R_\odot$	$M/M_\odot$	Age(My)
506	2.017	0.770	0.845	2.619	2.200	0.018	0.011	0.030	238.5	3.63	2.508	0.42	4.21	47.60
507	1.359	0.775	0.396	1.227	1.031	0.073	0.044	0.125	227.5	11.60	2.881	0.58	4.96	68.70
508	2.117	0.855	0.855	2.650	2.226	0.038	0.023	0.067	-	2.29	1.772	0.25	2.65	19.60
509	2.049	0.765	0.870	2.696	2.265	0.069	0.041	0.116	270.0	7.56	2.816	0.53	4.88	59.80
510	2.086	0.778	0.886	2.746	2.307	0.067	0.040	0.108	325.4	3.01	2.328	0.39	3.79	52.50
511	2.206	0.748	0.988	3.063	2.573	0.099	0.060	0.167	-	3.66	3.036	0.56	5.65	41.00
512	1.335	0.775	0.379	1.175	0.987	0.020	0.012	0.030	272.8	8.70	2.613	0.48	4.37	67.00
513	2.217	0.830	0.940	2.912	2.446	0.060	0.036	0.101	121.1	1.28	2.043	0.36	3.14	114.00
514	1.492	0.805	0.466	1.444	1.213	0.013	0.008	0.031	310.7	3.50	2.530	0.50	4.05	100.00
515	2.084	0.775	0.887	2.748	2.309	0.104	0.063	0.175	313.7	2.15	2.659	0.49	4.46	68.30
516	2.984	0.730	1.527	4.734	3.977	0.049	0.029	0.086	202.7	2.00	3.490	0.65	7.48	25.60
517	2.225	0.742	1.005	3.115	2.616	0.077	0.046	0.126	-	3.20	3.160	0.56	6.20	29.80
518	2.035	0.900	0.769	2.384	2.002	0.128	0.077	0.230	-	1.66	1.937	0.42	2.85	250.00
519	1.644	0.770	0.592	1.836	1.542	0.034	0.020	0.056	225.1	5.94	2.565	0.45	4.30	57.70
520	1.879	0.815	0.721	2.234	1.877	0.035	0.021	0.058	-	3.42	2.345	0.50	3.59	148.00
521	1.498	0.815	0.463	1.435	1.205	0.068	0.041	0.118	164.0	7.31	2.455	0.53	3.81	135.00
522	2.151	0.740	0.956	2.964	2.490	0.135	0.081	0.233	-	13.79	3.678	0.79	7.81	32.50
523	1.955	0.770	0.803	2.489	2.091	0.087	0.052	0.140	219.2	11.31	3.273	0.74	5.98	57.60
524	2.212	0.790	0.963	2.986	2.508	0.038	0.023	0.065	307.6	5.45	2.528	0.48	4.11	84.70
525	3.045	0.710	1.582	4.903	4.119	0.083	0.050	0.149	-	6.52	3.945	0.86	9.13	25.30
526	2.180	0.880	0.881	2.730	2.293	0.160	0.096	0.275	175.4	2.06	1.607	0.19	2.49	0.32
527	2.003	0.805	0.812	2.516	2.114	0.034	0.020	0.056	268.6	2.28	2.600	0.52	4.21	94.30
528	2.076	0.810	0.858	2.659	2.234	0.081	0.049	0.134	188.6	2.65	2.820	0.61	4.70	86.70
529	1.713	0.830	0.598	1.853	1.557	0.028	0.017	0.050	-	3.47	2.177	0.45	3.29	166.00
530	1.751	0.750	0.678	2.103	1.767	0.062	0.037	0.099	-	6.65	2.935	0.53	5.34	42.50
531	2.231	0.780	0.983	3.046	2.559	0.042	0.025	0.065	251.8	3.22	2.578	0.48	4.25	74.40
532	1.733	0.774	0.650	2.014	1.692	0.042	0.025	0.065	285.3	2.10	2.397	0.40	3.93	53.70
533	1.433	0.810	0.422	1.309	1.099	0.134	0.080	0.232	334.2	6.84	2.151	0.36	3.41	66.90
534	2.091	0.745	0.912	2.827	2.375	0.069	0.041	0.117	-	3.94	3.038	0.53	5.79	30.90
535	1.747	0.815	0.631	1.956	1.643	0.061	0.036	0.101	325.5	2.76	2.175	0.42	3.33	140.00
536	2.693	0.775	1.299	4.028	3.383	0.063	0.038	0.107	313.4	2.68	2.901	0.59	5.02	67.30
537	2.271	0.740	1.037	3.215	2.701	-0.010	0.000	0.000	-	5.46	3.154	0.53	6.35	19.90
538	1.930	0.845	0.735	2.279	1.915	0.027	0.016	0.041	285.5	2.01	1.814	0.26	2.70	21.40
539	1.602	0.855	0.506	1.570	1.318	0.017	0.010	0.033	253.8	2.54	1.923	0.34	2.94	120.00
540	1.986	0.685	0.882	2.733	2.296	0.023	0.014	0.065	-	11.51	4.202	0.76	12.55	8.87
541	1.567	0.835	0.496	1.537	1.291	0.017	0.010	0.033	462.6	2.74	1.977	0.34	3.05	96.70
542	1.863	0.760	0.747	2.316	1.946	0.061	0.036	0.099	-	8.60	2.924	0.56	5.18	55.50
543	1.733	0.825	0.615	1.907	1.602	0.026	0.015	0.041	-	3.37	2.102	0.41	3.19	152.00
544	2.233	0.810	0.964	2.988	2.510	0.041	0.025	0.066	-	3.01	2.496	0.53	3.91	122.00
545	2.135	0.774	0.922	2.857	2.400	0.043	0.026	0.073	305.9	2.24	2.493	0.43	4.14	56.90
546	2.460	0.750	1.158	3.590	3.016	0.088	0.053	0.149	-	3.11	2.935	0.52	5.40	37.30
547	2.494	0.805	1.144	3.547	2.980	0.027	0.016	0.039	286.8	2.05	2.714	0.59	4.42	97.70
548	2.292	0.850	0.977	3.027	2.543	-0.029	0.000	0.000	-	1.71	1.958	0.35	2.99	127.00
549	2.375	0.715	1.125	3.487	2.929	0.092	0.055	0.166	-	6.51	3.999	0.81	10.13	17.90
550	1.963	0.715	0.846	2.621	2.202	0.141	0.084	0.252	-	5.22	3.467	0.57	7.89	11.50
551	2.094	0.810	0.870	2.697	2.266	0.041	0.024	0.066	-	2.20	2.158	0.38	3.37	95.90
552	2.487	0.752	1.175	3.642	3.059	-0.005	0.000	0.000	413.8	2.00	2.972	0.55	5.42	45.20
553	1.914	0.740	0.795	2.466	2.071	0.153	0.092	0.263	-	4.28	3.263	0.59	6.57	28.20
554	2.785	0.690	1.419	4.400	3.696	0.076	0.045	0.146	399.3	6.24	4.465	0.93	13.79	11.30
555	2.129	0.700	0.968	3.002	2.521	0.034	0.021	0.077	341.3	5.56	4.116	0.76	11.63	10.80
556	2.118	0.820	0.879	2.725	2.289	0.029	0.018	0.048	-	4.37	2.803	0.66	4.48	111.00
557	2.931	0.820	1.430	4.434	3.724	0.093	0.056	0.162	-	1.76	2.358	0.51	3.61	150.00
558	1.287	0.695	0.401	1.243	1.045	0.096	0.057	0.198	-	12.12	4.002	0.68	11.27	7.85
559	2.724	0.760	1.331	4.125	3.465	0.065	0.039	0.108	-	1.74	2.957	0.56	5.33	49.60
560	2.337	0.810	1.035	3.208	2.694	0.035	0.021	0.057	-	2.17	2.511	0.53	3.96	117.00

Table 2. Continued...

#	Φ_b	Φ_b^0	$E(B-V)$	A_v	A_r	f_D	$E_{cs}(B-V)$	Δr	$vsini$	$d(kpc)$	$logL/L_\odot$	$logR/R_\odot$	$M/M_\odot$	Age(My)
561	2.577	0.810	1.197	3.711	3.117	0.019	0.012	0.031	170.0	2.59	2.875	0.68	4.63	104.00
562	2.403	0.750	1.120	3.472	2.916	0.011	0.007	0.022	300.4	4.14	3.391	0.71	6.70	40.10
563	2.302	0.770	1.038	3.216	2.702	0.081	0.048	0.133	-	2.57	2.698	0.49	4.61	58.20
564	2.195	0.742	0.984	3.051	2.563	0.032	0.019	0.048	354.4	3.50	3.163	0.59	6.10	36.30
565	2.305	0.760	1.047	3.245	2.726	0.064	0.039	0.107	-	1.60	2.778	0.49	4.89	44.90
566	3.035	0.715	1.571	4.872	4.092	0.102	0.061	0.184	-	2.28	3.714	0.66	8.90	15.80
567	2.029	0.860	0.792	2.455	2.062	0.054	0.032	0.093	-	1.22	1.733	0.24	2.60	16.00
568	2.029	0.845	0.802	2.486	2.088	0.041	0.025	0.067	292.1	1.73	1.923	0.33	2.96	104.00
569	2.427	0.730	1.149	3.563	2.993	-0.014	0.000	0.000	-	3.47	3.584	0.69	7.86	25.20
570	2.335	0.805	1.036	3.213	2.699	0.039	0.024	0.065	245.9	2.10	2.592	0.54	4.16	103.00
571	2.730	0.790	1.314	4.073	3.422	0.099	0.059	0.167	564.3	1.55	2.399	0.43	3.87	78.80
572	3.120	0.825	1.555	4.820	4.049	0.066	0.040	0.110	351.0	0.56	1.882	0.28	2.86	36.00
573	3.325	0.825	1.694	5.250	4.410	0.054	0.033	0.093	383.2	0.42	1.908	0.30	2.96	51.50
574	1.832	0.775	0.716	2.220	1.865	-0.020	0.000	0.000	277.3	2.98	2.554	0.46	4.22	70.00
575	1.759	0.775	0.667	2.067	1.737	-0.003	0.000	0.000	286.2	2.80	2.598	0.48	4.31	71.10
576	1.731	0.755	0.661	2.049	1.721	-0.017	0.000	0.000	-	3.22	2.842	0.47	5.21	28.20
577	2.250	0.730	1.030	3.192	2.682	0.105	0.063	0.183	-	6.94	3.279	0.53	7.02	11.60
578	1.912	0.740	0.794	2.461	2.067	0.113	0.068	0.196	-	3.66	3.163	0.54	6.32	23.80
579	3.132	1.200	1.309	4.056	3.407	0.049	0.030	0.099	157.8	-	-	-	-	-
580	2.152	0.780	0.929	2.881	2.420	0.100	0.060	0.166	182.3	5.16	2.907	0.63	4.95	76.30
581	2.060	0.778	0.869	2.693	2.262	0.091	0.055	0.150	368.2	4.17	2.409	0.42	3.93	64.70
582	3.380	0.865	1.703	5.281	4.436	0.029	0.018	0.051	-	0.57	1.888	0.34	2.86	148.00
583	2.092	0.765	0.899	2.786	2.340	0.082	0.049	0.133	-	4.00	3.058	0.62	5.53	55.00
584	2.549	0.800	1.185	3.673	3.085	0.053	0.032	0.091	276.9	1.18	2.290	0.38	3.70	59.40
585	2.648	0.820	1.238	3.838	3.224	0.028	0.017	0.049	-	1.03	2.018	0.34	3.14	80.90
586	2.704	0.865	1.246	3.863	3.245	0.053	0.032	0.094	-	0.89	1.989	0.40	2.97	189.00
587	1.391	0.810	0.394	1.220	1.025	0.048	0.029	0.083	340.1	3.03	2.319	0.46	3.60	126.00
588	2.925	0.820	1.426	4.420	3.713	0.078	0.047	0.135	410.8	1.35	2.356	0.51	3.60	154.00
589	1.445	0.765	0.460	1.427	1.199	0.003	0.002	0.013	364.9	4.28	2.755	0.51	4.74	58.80
590	2.575	0.740	1.243	3.853	3.237	0.095	0.057	0.160	-	8.16	3.801	0.87	8.16	31.60
591	2.182	0.730	0.983	3.049	2.561	0.062	0.037	0.103	-	9.87	3.748	0.78	8.36	27.10
592	2.377	0.760	1.095	3.396	2.852	0.038	0.023	0.065	486.1	3.93	2.839	0.50	5.07	43.10
593	1.605	0.805	0.542	1.680	1.411	0.034	0.020	0.057	261.8	3.59	2.625	0.56	4.22	105.00
594	2.973	0.860	1.431	4.437	3.727	0.056	0.034	0.094	-	1.47	1.875	0.33	2.87	122.00
595	3.107	0.815	1.553	4.813	4.043	0.042	0.025	0.067	-	1.07	2.060	0.36	3.19	98.40
596	4.191	0.945	2.199	6.816	5.725	0.070	0.042	0.124	-	0.27	1.825	0.47	2.61	394.00
597	2.333	0.700	1.106	3.429	2.881	0.106	0.064	0.209	-	5.18	4.075	0.75	11.27	11.60
598	2.158	0.900	0.853	2.643	2.220	-0.033	0.000	0.000	-	2.00	1.764	0.31	2.68	148.00
599	1.890	0.760	0.766	2.373	1.994	0.058	0.035	0.099	-	6.13	2.790	0.49	4.92	45.50
600	2.183	0.810	0.930	2.883	2.421	0.034	0.020	0.057	-	5.32	2.657	0.58	4.27	106.00
601	2.233	0.750	1.004	3.114	2.616	0.104	0.062	0.175	-	3.05	2.969	0.55	5.39	47.00
602	1.781	0.805	0.661	2.049	1.721	0.044	0.026	0.074	-	2.87	2.370	0.47	3.71	115.00
603	2.134	0.735	0.947	2.937	2.467	0.093	0.056	0.162	-	5.97	3.361	0.63	6.88	29.30
604	2.606	0.745	1.260	3.907	3.282	0.061	0.037	0.099	-	4.05	3.053	0.56	5.70	40.70
605	2.223	0.720	1.018	3.156	2.651	0.059	0.035	0.106	-	6.20	3.871	0.79	9.22	21.60
606	2.027	0.740	0.872	2.703	2.270	0.032	0.019	0.049	-	2.48	3.082	0.51	6.12	18.60
607	1.353	0.778	0.390	1.208	1.015	0.038	0.023	0.056	332.2	3.05	2.398	0.41	3.91	63.30
608	2.439	0.725	1.161	3.599	3.023	0.041	0.025	0.070	-	7.14	3.503	0.63	7.73	20.30
609	2.233	0.760	0.998	3.092	2.598	0.068	0.041	0.116	-	2.85	2.709	0.46	4.74	41.60
610	1.298	0.810	0.331	1.025	0.861	0.027	0.016	0.040	294.3	3.66	2.297	0.45	3.56	126.00
611	2.039	0.767	0.861	2.670	2.243	0.042	0.025	0.064	-	3.29	2.531	0.42	4.28	43.50
612	3.278	1.200	1.408	4.365	3.666	0.099	0.059	0.210	241.6	-	-	-	-	-
613	2.281	0.815	0.993	3.078	2.586	0.030	0.018	0.049	255.1	1.79	2.092	0.37	3.25	96.70
614	1.119	0.790	0.223	0.692	0.581	0.049	0.030	0.082	177.1	21.78	2.879	0.62	4.88	78.70
615	1.668	0.820	0.575	1.781	1.496	0.026	0.015	0.041	-	2.93	2.238	0.47	3.40	159.00

Table 2. Continued...

#	Φ_b	Φ_b^0	$E(B-V)$	A_v	A_r	f_D	$E_{cs}(B-V)$	Δr	$vsini$	$d(kpc)$	$logL/L_\odot$	$logR/R_\odot$	$M/M_\odot$	Age(My)
616	2.574	0.745	1.239	3.841	3.226	0.038	0.023	0.066	222.0	3.24	3.007	0.50	5.78	24.20
617	2.295	0.765	1.037	3.214	2.699	0.025	0.015	0.039	-	4.03	3.017	0.59	5.46	52.20
618	2.068	0.755	0.890	2.758	2.316	0.094	0.056	0.157	-	2.40	2.801	0.47	5.07	30.60
619	2.470	0.870	1.084	3.361	2.823	0.049	0.030	0.086	-	1.74	1.985	0.42	2.93	223.00
620	2.107	0.860	0.845	2.619	2.200	0.031	0.018	0.051	-	3.38	2.237	0.51	3.34	195.00
621	1.927	0.985	0.638	1.978	1.661	-0.026	0.000	0.000	321.5	-	-	-	-	-
622	2.336	0.760	1.068	3.309	2.780	-0.016	0.000	0.000	-	3.55	3.096	0.62	5.69	50.70
623	2.944	0.778	1.467	4.549	3.821	0.139	0.083	0.239	-	2.43	2.345	0.39	3.82	55.00
624	1.205	0.835	0.251	0.777	0.653	0.042	0.025	0.067	-	3.15	1.952	0.33	3.01	96.50
625	2.315	0.780	1.040	3.223	2.708	0.080	0.048	0.133	252.0	2.58	2.924	0.63	5.01	73.70
626	1.475	0.810	0.451	1.397	1.173	0.044	0.026	0.074	-	2.70	2.136	0.35	3.38	65.20
627	1.389	0.880	0.345	1.069	0.898	0.030	0.018	0.051	-	2.45	1.718	0.27	2.65	79.30
628	1.802	0.805	0.675	2.093	1.758	0.033	0.020	0.056	258.9	3.58	2.543	0.51	4.08	99.10
629	1.810	0.810	0.677	2.100	1.764	0.042	0.025	0.066	232.2	2.68	2.446	0.51	3.81	128.00
630	2.054	0.750	0.883	2.739	2.300	0.056	0.034	0.091	-	4.40	2.961	0.50	5.60	26.40
631	2.035	0.810	0.830	2.572	2.160	0.031	0.019	0.049	-	2.56	2.286	0.46	3.51	138.00
632	1.714	0.805	0.615	1.908	1.603	0.038	0.023	0.066	-	2.25	2.242	0.41	3.51	103.00
633	2.199	0.770	0.968	3.001	2.521	0.036	0.021	0.056	-	1.57	2.645	0.47	4.51	53.50
634	1.888	0.875	0.686	2.128	1.787	0.032	0.019	0.050	130.3	1.39	1.652	0.21	2.51	1.66
635	1.878	0.760	0.757	2.347	1.972	0.106	0.064	0.175	-	3.74	3.124	0.63	5.77	50.40
636	1.503	0.775	0.493	1.530	1.285	0.068	0.041	0.116	259.9	5.01	2.774	0.54	4.71	70.60
637	1.647	0.778	0.589	1.825	1.533	0.053	0.032	0.091	301.8	3.80	2.440	0.43	3.99	66.80
638	1.921	0.810	0.753	2.333	1.960	0.048	0.029	0.083	260.4	3.33	2.563	0.55	4.06	115.00
639	1.781	0.820	0.651	2.019	1.696	0.039	0.023	0.067	205.7	2.37	2.041	0.36	3.15	104.00
640	1.895	0.775	0.759	2.351	1.975	0.101	0.060	0.166	326.8	2.96	2.571	0.47	4.27	67.90
641	2.223	0.770	0.984	3.051	2.563	0.033	0.020	0.056	331.4	6.17	3.048	0.64	5.43	61.70
642	2.154	0.800	0.917	2.843	2.388	0.016	0.010	0.031	-	1.99	2.375	0.41	3.85	67.50
643	2.589	0.730	1.259	3.903	3.279	0.039	0.023	0.070	-	2.98	3.494	0.63	7.62	22.10
644	2.443	0.735	1.157	3.587	3.013	0.095	0.057	0.162	-	8.31	3.644	0.76	7.86	29.70
645	2.663	0.750	1.296	4.017	3.374	0.056	0.034	0.091	-	5.04	3.320	0.70	6.40	44.30
646	1.481	0.780	0.475	1.472	1.236	0.030	0.018	0.047	-	4.54	2.520	0.41	4.30	32.70
647	1.850	0.760	0.738	2.289	1.923	0.009	0.005	0.021	-	4.78	2.806	0.50	4.93	49.50
648	2.058	0.725	0.903	2.798	2.351	0.121	0.072	0.214	-	6.00	3.779	0.74	8.83	21.80
649	2.176	0.780	0.946	2.932	2.462	-0.009	0.000	0.000	-	2.13	2.824	0.58	4.79	74.90
650	1.293	0.925	0.250	0.774	0.650	0.014	0.009	0.037	309.6	3.11	1.828	0.43	2.64	343.00
651	1.551	0.835	0.485	1.503	1.262	0.029	0.018	0.050	-	3.14	1.833	0.26	2.71	19.60
652	2.007	0.855	0.780	2.419	2.032	0.038	0.023	0.068	-	4.51	2.553	0.66	3.76	178.00
653	1.636	0.770	0.587	1.819	1.528	0.067	0.040	0.107	-	2.79	2.577	0.45	4.32	58.50
654	1.456	0.800	0.444	1.378	1.157	0.065	0.039	0.108	-	7.50	2.760	0.58	4.58	86.80
655	2.578	0.735	1.249	3.871	3.251	0.026	0.016	0.041	-	2.99	3.261	0.57	6.64	25.10
656	2.228	0.870	0.920	2.851	2.395	0.100	0.060	0.174	-	1.27	1.940	0.39	2.89	209.00
657	1.693	0.740	0.646	2.001	1.681	0.034	0.020	0.058	-	8.44	3.192	0.56	6.35	27.40
658	1.636	0.770	0.587	1.819	1.528	-0.013	0.000	0.000	261.6	3.65	2.752	0.52	4.69	65.50
659	1.693	0.740	0.646	2.001	1.681	0.013	0.008	0.032	-	4.77	3.257	0.58	6.56	28.00
660	2.945	0.705	1.517	4.703	3.951	0.011	0.007	0.036	-	4.73	4.059	0.79	10.82	14.50
661	2.058	0.750	0.886	2.746	2.307	-0.003	0.000	0.000	-	2.72	2.888	0.49	5.33	30.50
662	2.240	0.735	1.019	3.160	2.654	0.026	0.016	0.042	-	4.63	3.402	0.64	7.03	28.90
663	2.818	0.715	1.424	4.415	3.709	0.118	0.071	0.217	-	3.32	3.600	0.63	8.35	15.80
664	2.838	0.742	1.420	4.401	3.697	0.117	0.070	0.205	-	4.27	3.154	0.56	6.20	28.80
665	1.670	0.835	0.565	1.752	1.472	0.040	0.024	0.067	-	2.47	2.185	0.46	3.29	175.00
666	2.673	0.800	1.269	3.932	3.303	0.103	0.062	0.176	-	2.68	2.352	0.40	3.81	64.60
667	2.212	1.250	0.652	2.021	1.697	0.069	0.041	0.134	-	-	-	-	-	-
668	2.059	0.800	0.853	2.644	2.221	0.051	0.030	0.082	103.3	2.97	2.352	0.41	3.80	69.90
669	1.876	0.775	0.746	2.312	1.942	0.078	0.047	0.133	304.1	2.45	2.542	0.41	4.37	29.80
670	2.042	0.855	0.804	2.493	2.095	0.036	0.021	0.059	-	3.07	2.248	0.51	3.36	190.00

Table 2. Continued...

#	Φ_b	Φ_b^0	$E(B-V)$	A_v	A_r	f_D	$E_{cs}(B-V)$	Δr	$vsini$	$d(kpc)$	$logL/L_\odot$	$logR/R_\odot$	$M/M_\odot$	Age(My)
671	1.982	0.805	0.797	2.472	2.076	0.069	0.041	0.117	493.2	3.79	2.327	0.42	3.70	88.90
672	2.423	0.780	1.113	3.450	2.898	0.069	0.041	0.116	-	3.35	2.628	0.51	4.33	82.10
673	3.175	0.790	1.615	5.007	4.206	0.060	0.036	0.099	313.2	3.91	3.169	0.73	5.57	68.00
674	2.111	0.730	0.935	2.900	2.436	0.168	0.101	0.294	-	4.48	3.408	0.62	7.19	24.40
675	2.420	0.755	1.128	3.497	2.937	0.079	0.048	0.134	-	16.06	3.775	0.90	7.92	33.50
676	2.214	0.805	0.954	2.959	2.485	0.039	0.023	0.066	198.2	2.11	2.206	0.38	3.50	74.30
677	2.468	0.730	1.177	3.650	3.066	0.106	0.064	0.183	-	3.66	3.518	0.65	7.68	23.20
678	1.633	0.825	0.547	1.697	1.425	0.030	0.018	0.050	162.4	2.97	2.125	0.42	3.23	151.00
679	2.136	0.760	0.932	2.889	2.427	0.020	0.012	0.030	361.6	4.18	3.099	0.61	5.71	49.40
680	2.670	0.725	1.318	4.084	3.431	0.084	0.051	0.149	-	5.16	3.744	0.76	8.53	24.40
681	2.566	0.745	1.234	3.824	3.213	0.156	0.093	0.258	-	4.30	3.299	0.67	6.40	41.80
682	2.500	0.865	1.108	3.434	2.884	0.122	0.073	0.210	-	3.43	1.985	0.40	2.96	195.00
683	2.811	0.790	1.369	4.244	3.565	0.072	0.043	0.116	313.9	1.13	2.415	0.39	4.01	40.80
684	3.622	0.795	1.915	5.937	4.987	0.152	0.091	0.257	-	0.62	2.132	0.28	3.11	2.35
685	2.026	0.780	0.844	2.616	2.198	0.095	0.057	0.157	-	2.40	2.450	0.38	4.14	26.80
686	2.275	0.770	1.020	3.161	2.655	0.094	0.056	0.157	144.2	2.39	2.616	0.47	4.39	63.30
687	2.630	0.782	1.252	3.880	3.259	0.011	0.006	0.021	173.4	2.02	2.794	0.56	4.72	75.80
688	2.306	0.730	1.068	3.309	2.780	0.059	0.035	0.103	294.0	3.07	3.497	0.65	7.52	25.10
689	1.854	0.757	0.743	2.302	1.934	0.122	0.073	0.202	261.1	2.27	2.772	0.47	4.95	35.30
690	2.353	0.805	1.048	3.250	2.730	0.105	0.063	0.176	277.6	3.29	2.482	0.48	3.97	96.70
691	2.115	0.850	0.857	2.657	2.232	0.044	0.026	0.075	-	5.84	2.502	0.59	3.81	155.00
692	2.334	0.865	0.995	3.085	2.591	0.090	0.054	0.156	354.1	1.24	1.890	0.35	2.86	160.00
693	1.898	0.765	0.768	2.379	1.999	0.090	0.054	0.149	327.9	2.57	2.658	0.45	4.59	44.10
694	1.896	0.778	0.757	2.348	1.972	0.063	0.038	0.108	172.7	2.37	2.401	0.41	3.93	58.40
695	2.204	0.750	0.985	3.053	2.564	0.083	0.050	0.142	-	3.50	2.972	0.50	5.64	25.80
696	1.973	0.790	0.801	2.485	2.087	0.038	0.023	0.065	297.5	2.80	2.577	0.50	4.20	87.50
697	2.292	0.770	1.031	3.196	2.685	0.059	0.035	0.099	-	2.04	2.667	0.45	4.64	40.00
698	2.423	0.805	1.096	3.399	2.855	0.064	0.038	0.108	324.4	8.58	2.944	0.68	4.87	90.80
699	2.651	0.730	1.301	4.033	3.388	0.122	0.073	0.209	-	3.81	3.516	0.66	7.58	25.50
700	2.617	0.782	1.243	3.852	3.236	0.067	0.040	0.107	251.1	1.70	2.631	0.46	4.47	54.30
701	2.842	0.755	1.414	4.383	3.682	0.078	0.047	0.134	-	10.31	4.025	1.06	9.28	25.10
702	2.879	0.740	1.449	4.491	3.772	0.085	0.051	0.144	-	5.16	3.356	0.63	6.85	29.90
703	2.266	0.755	1.024	3.174	2.666	0.069	0.042	0.116	-	4.59	2.842	0.49	5.12	38.10
704	2.641	0.930	1.159	3.592	3.018	0.115	0.069	0.205	-	1.99	1.708	0.36	2.52	303.00
705	2.239	0.742	1.014	3.144	2.641	0.161	0.097	0.266	-	3.54	3.220	0.61	6.26	37.00
706	3.055	0.735	1.571	4.872	4.092	0.088	0.053	0.154	-	7.81	3.807	0.84	8.34	29.90
707	2.633	0.725	1.293	4.007	3.366	0.091	0.055	0.159	267.1	6.09	3.986	0.86	9.42	23.70
708	1.906	0.795	0.752	2.333	1.959	0.071	0.043	0.117	342.2	3.24	2.445	0.46	3.91	93.20
709	1.621	0.820	0.543	1.682	1.413	0.047	0.028	0.076	-	2.80	2.156	0.43	3.27	153.00
710	1.950	0.828	0.760	2.356	1.979	0.072	0.043	0.118	196.2	2.79	2.393	0.50	3.71	131.00
711	2.386	0.740	1.115	3.457	2.904	0.140	0.084	0.243	-	4.78	3.494	0.68	7.38	28.60
712	2.138	0.805	0.903	2.798	2.351	0.066	0.040	0.108	222.2	1.85	2.169	0.34	3.48	36.50
713	2.075	0.810	0.857	2.656	2.231	0.029	0.018	0.048	338.8	7.14	2.553	0.54	4.05	113.00
714	2.489	0.805	1.141	3.537	2.971	0.097	0.058	0.160	-	3.04	2.394	0.46	3.78	106.00
715	2.190	0.810	0.935	2.898	2.435	0.041	0.025	0.066	112.2	2.25	2.125	0.35	3.36	66.70
716	2.665	0.810	1.257	3.896	3.272	0.051	0.030	0.083	342.1	0.95	2.215	0.41	3.46	105.00
717	2.510	0.807	1.153	3.575	3.003	0.072	0.043	0.117	447.4	1.36	2.118	0.32	3.37	32.90
718	2.341	0.820	1.030	3.194	2.683	0.044	0.027	0.075	-	2.25	2.286	0.49	3.47	158.00
719	1.818	0.775	0.707	2.191	1.840	0.032	0.019	0.047	589.2	3.56	2.719	0.52	4.59	69.10
720	1.837	0.765	0.726	2.251	1.891	0.062	0.037	0.099	142.4	4.01	2.826	0.53	4.91	58.30
721	2.062	0.668	0.945	2.928	2.460	-0.011	0.000	0.000	-	21.19	4.769	0.89	19.51	5.12
722	1.960	0.805	0.782	2.425	2.037	0.037	0.022	0.057	-	5.49	2.426	0.48	3.82	113.00
723	1.937	0.778	0.785	2.434	2.045	0.041	0.024	0.065	371.2	3.86	2.398	0.41	3.92	58.60
724	1.709	0.745	0.653	2.024	1.701	0.062	0.037	0.099	-	4.13	3.008	0.54	5.62	37.00
725	1.963	0.760	0.815	2.527	2.123	0.102	0.061	0.166	-	3.07	2.764	0.48	4.86	43.80
726	2.031	0.780	0.847	2.627	2.206	0.032	0.019	0.047	-	4.79	2.598	0.49	4.29	75.50
727	1.574	0.800	0.524	1.625	1.365	0.018	0.011	0.031	329.5	2.50	2.344	0.41	3.78	68.30
728	1.834	0.765	0.724	2.245	1.886	0.088	0.053	0.149	-	5.02	2.860	0.54	5.00	58.10
729	1.622	0.700	0.625	1.937	1.627	0.208	0.125	0.424	-	6.78	3.760	0.60	9.94	4.32
730	2.086	0.855	0.834	2.586	2.172	0.033	0.020	0.059	224.3	3.10	2.084	0.44	3.11	194.00
731	1.752	0.728	0.694	2.152	1.807	0.048	0.029	0.087	365.4	5.14	3.595	0.67	8.01	22.80
732	2.752	0.810	1.316	4.079	3.426	0.079	0.047	0.135	407.2	1.43	2.212	0.40	3.45	106.00

TABLE 3: CBe stars that detected photometrically and follow-up spectroscopy by IPHAS but we could not analyze them with our method. They confirmed as OB emission line stars thought as their spectra have OB type spectroscopic characteristics.

NAME	$l(deg)$	$b(deg)$	r	r-i	r-Hα	V	$EW_{H\alpha}$	Ref.
J000039.05+623316.6	117.12	0.26	13.13	0.29	0.48	13.338	-21.7	1
J000220.16+594538.7	116.78	-2.52	14.51	0.38	0.33	14.720	-8.7	1
J000358.84+643556.6	117.87	2.19	13.44	0.37	0.36	13.650	-8.7	3
J000511.92+625310.1	117.69	0.49	15.16	0.59	0.75	15.375	-42.6	3
J000523.94+642621.3	117.99	2.01	14.17	0.54	0.44	14.384	-12.4	1
J000558.51+631752.0	117.85	0.88	13.55	0.30	0.45	13.758	-17.6	3
J000602.32+640926.0	118.01	1.72	15.36	0.86	0.59	15.582	-15.6	3
J000645.44+644608.9	118.19	2.31	14.60	0.57	0.67	14.815	-42.0	1
J000716.51+623746.5	117.88	0.19	13.50	0.31	0.53	13.708	-9.4	3
J000730.07+595614.1	117.45	-2.47	14.13	0.40	0.31	14.341	-4.0	1
J000749.49+610314.1	117.68	-1.37	14.50	0.54	0.46	14.714	-20.6	1
J000806.97+592804.8	117.45	-2.94	13.43	0.37	0.32	13.640	-4.1	1
J000823.00+651622.5	118.45	2.78	14.23	0.60	0.46	14.445	-13.9	1
J000902.50+625839.8	118.14	0.50	14.70	0.57	0.78	14.915	-46.5	3
J000956.48+620812.2	118.10	-0.35	14.33	0.76	0.56	14.549	-20.2	3
J001026.29+602051.1	117.88	-2.12	13.18	0.28	0.34	13.388	-0.3	1
J001051.88+621009.5	118.22	-0.33	13.59	0.54	0.42	13.804	-12.8	1
J001113.74+624023.4	118.34	0.16	14.15	0.46	0.58	14.362	-31.9	3
J001122.29+611615.8	118.14	-1.23	13.73	0.47	0.41	13.942	-12.4	1
J001134.31+614614.8	118.24	-0.74	15.85	0.73	0.50	16.069	-11.9	1
J001224.05+623244.3	118.45	0.01	14.67	0.49	0.51	14.883	-18.9	1
J001252.06+595439.8	118.11	-2.60	14.49	0.52	0.40	14.703	-10.7	1
J001301.13+625649.0	118.58	0.40	13.40	0.40	0.40	13.611	-13.9	1
J001953.39+634043.6	119.44	1.02	14.75	0.75	0.73	14.969	-40.3	1
J002043.24+624310.7	119.42	0.06	14.35	0.52	0.37	14.563	-4.4	1
J002242.11+611223.4	119.48	-1.47	14.63	0.35	0.31	14.839	-13.6	1
J002318.30+590153.8	119.31	-3.64	14.16	0.41	0.31	14.371	-2.5	1
J002441.72+642137.9	120.04	1.64	14.75	0.83	0.61	14.971	4.4	2
J002450.84+574414.6	119.38	-4.95	13.98	0.30	0.30	14.188	-9.1	1
J002540.04+623203.2	119.97	-0.19	14.46	0.54	0.40	14.674	-11.2	1
J002754.61+603001.4	120.04	-2.24	13.66	0.47	0.39	13.872	-11.5	1
J002758.97+622906.1	120.23	-0.26	15.03	0.59	0.46	15.245	-16.4	1,2
J002843.24+615216.2	120.26	-0.88	14.38	0.48	0.42	14.593	-14.3	1,2
J002926.93+630450.2	120.45	0.32	14.07	0.40	0.36	14.281	-8.4	2
J003000.79+612238.8	120.37	-1.39	14.24	0.58	0.63	14.455	-11.7	1
J003025.04+645500.0	120.71	2.14	15.95	1.02	0.78	16.175	-28.1	1
J003055.94+610048.8	120.45	-1.76	15.39	0.58	0.41	15.605	-9.6	1
J003210.31+623929.2	120.72	-0.13	13.39	0.47	0.51	13.602	-20.2	1,2
J003248.02+664759.6	121.09	3.99	14.41	1.02	0.85	14.635	-22.4	2
J003351.33+613743.1	120.84	-1.17	13.55	0.38	0.29	13.760	-5.1	1
J003421.40+601218.1	120.81	-2.60	14.21	0.56	0.42	14.424	-12.5	1
J003559.27+664503.3	121.40	3.92	15.85	0.71	0.60	16.068	-23.2	2
J003952.40+601719.5	121.50	-2.55	15.45	0.60	0.43	15.665	-15.0	1
J004014.89+651644.0	121.76	2.43	14.82	0.68	0.77	15.037		2
J004121.36+650413.5	121.87	2.22	13.80	0.67	0.50	14.017	-25.6	2
J004353.19+595641.6	121.99	-2.91	15.19	0.47	0.70	15.402	-39.3	3
J004517.05+640124.4	122.26	1.16	15.61	0.95	0.64	15.834	-25.1	2
J004620.80+622503.9	122.34	-0.45	13.18	0.63	0.54	13.396	-23.4	1,2
J004651.68+625914.7	122.41	0.12	14.88	0.60	0.45	15.095	-13.1	2
J004734.28+610833.6	122.47	-1.73	13.45	0.32	0.24	13.659	-2.0	1
J004741.54+624203.3	122.50	-0.17	14.15	0.46	0.43	14.362	-15.5	1,2
J004842.93+644411.1	122.64	1.87	14.74	0.58	0.42	14.955	-8.4	1,2
J004850.12+642533.7	122.65	1.56	15.64	0.86	0.56	15.862	-20.9	2
J005011.87+633526.1	122.79	0.72	15.38	0.64	0.60	15.596	-22.8	2
J010054.58+643729.6	123.95	1.77	13.02	0.61	0.57	13.236	-18.4	2
J010107.85+633227.0	124.01	0.69	13.84	0.57	0.49	14.055	-14.5	1,2
J010138.04+641349.9	124.04	1.38	13.32	0.63	0.71	13.536	-31.1	1,2
J010150.19+603917.9	124.21	-2.19	13.26	0.28	0.25	13.468	-3.6	1
J010232.39+602615.1	124.30	-2.40	14.33	0.30	0.32	14.538	-12.2	1
J010358.11+595310.9	124.51	-2.95	13.90	0.41	0.55	14.111	-22.0	1
J010551.90+602737.5	124.71	-2.36	13.57	0.47	0.55	13.782	-27.4	1
J010707.68+625117.0	124.72	0.04	14.57	0.74	0.58	14.789	-20.6	2
J010733.72+604206.8	124.90	-2.11	13.43	0.36	0.47	13.640	-18.1	1
J010841.17+615511.8	124.96	-0.88	13.72	0.38	0.44	13.930	-16.3	1,2
J010958.80+625229.3	125.04	0.08	14.00	0.85	0.65	14.221	-33.6	2
J011216.30+615051.2	125.39	-0.92	13.56	0.35	0.27	13.769	4.9	2
J011234.21+630432.5	125.32	0.30	12.64	0.67	0.62	12.857	-24.4	1,2
J011352.28+590144.6	125.82	-3.72	13.27	0.32	0.45	13.479	-19.7	3
J011402.43+625735.3	125.50	0.20	12.91	0.56	0.34	13.124	-23.2	1,2
J011520.26+585002.9	126.03	-3.89	13.02	0.35	0.55	13.229	-27.9	1
J011542.33+602558.4	125.92	-2.30	13.33	0.30	0.74	13.538	-51.3	3
J011543.99+660116.2	125.40	3.27	14.21	0.94	1.11	14.434	-70.5	2
J011556.37+584812.1	126.11	-3.92	13.48	0.25	0.35	13.687	-11.9	1
J011604.41+630926.7	125.71	0.42	14.83	0.76	0.54	15.049	-23.9	2
J011757.12+594045.9	126.28	-3.02	13.09	0.50	0.53	13.303	-18.7	1
J011918.18+642233.8	125.94	1.67	13.44	0.55	0.71	13.654	-41.3	1,2
J012158.75+642813.1	126.22	1.79	14.35	0.67	0.74	14.567	-40.5	2
J012320.11+635830.9	126.42	1.32	14.08	0.89	0.97	14.302	-61.7	2
J012325.80+642638.7	126.37	1.79	16.32	0.67	0.57	16.537	-19.2	2
J012339.47+631544.2	126.55	0.62	15.04	0.80	0.61	15.260	-10.2	2
J012339.76+635313.0	126.47	1.24	15.07	0.82	0.75	15.291	-36.6	2
J012358.07+652615.4	126.31	2.78	13.72	0.47	0.47	13.932	-16.9	1,2
J012405.46+660100.0	126.25	3.36	15.09	0.63	0.57	15.306		2
J012416.76+633011.7	126.59	0.86	13.10	0.66	0.49	13.317	-12.9	1,2
J012430.74+622156.5	126.76	-0.26	16.69	0.83	0.82	16.911	-39.3	3
J012540.54+623025.6	126.87	-0.10	13.42	0.48	0.52	13.633	-24.4	1,2
J012609.29+651618.0	126.55	2.64	14.79	0.87	0.62	15.012	-21.6	2
J012634.69+641850.9	126.73	1.70	12.77	0.64	0.55	12.986	-17.9	2
J012703.28+634333.3	126.86	1.13	14.05	0.81	0.81	14.270	-26.9	2
J012745.08+625154.3	127.06	0.28	13.46	0.45	0.58	13.672	-26.2	2
J012751.32+655104.2	126.65	3.24	14.51	0.71	0.75	14.728	-39.8	2
J012821.12+635754.0	126.97	1.38	14.63	0.59	0.76	14.845	1.9	1
J013000.21+631044.6	127.27	0.63	13.76	1.02	1.09	13.985	-60.8	2
J013104.42+602337.3	127.81	-2.10	14.26	0.34	0.30	14.469	-4.4	1
J013130.51+630914.3	127.44	0.63	15.08	0.51	0.64	15.293	-49.0	1
J013213.90+623717.2	127.60	0.12	13.32	0.54	0.43	13.534	-10.6	1,2
J013244.08+595633.6	128.09	-2.52	14.35	0.26	0.39	14.557	-14.0	1
J013245.71+645233.3	127.30	2.36	15.42	0.76	1.02	15.639	-51.0	2
J013328.71+610759.4	127.99	-1.33	12.68	0.33	0.54	12.889	-23.9	1
J013402.88+611358.6	128.04	-1.22	12.92	0.34	0.40	13.129	-19.2	1
J013422.61+624459.7	127.82	0.29	12.92	0.39	0.61	13.130	-31.3	1,2
J013539.04+610341.6	128.26	-1.35	14.46	0.37	0.46	14.670	-23.8	1
J013706.99+585234.3	128.82	-3.47	13.47	0.38	0.49	13.680	-24.9	1
J013729.25+603806.2	128.55	-1.73	15.46	0.34	0.33	15.669	-9.9	1
J013739.40+613258.8	128.41	-0.83	14.31	0.63	0.50	14.526	-11.3	1,2
J013819.58+635306.0	128.06	1.48	12.98	0.61	0.91	13.196	-61.4	2
J013825.56+635008.5	128.08	1.43	13.96	0.53	0.47	14.174	-14.7	2
J013834.27+634841.3	128.10	1.41	15.28	0.65	0.56	15.497	-25.9	2

Table 4.3. Continued...

NAME	$l(deg)$	$b(deg)$	r	r-i	r-Hα	V	$EW_{H\alpha}$	Ref.
J005011.87+635129.9	122.80	0.99	13.75	0.40	0.53	13.961	-26.2	1,2
J005012.69+645621.6	122.80	2.07	14.14	0.56	0.49	14.354	-12.5	2
J005029.22+653331.1	122.83	2.69	14.63	0.70	0.65	14.848	-26.5	2
J005032.31+623155.5	122.83	-0.34	15.43	0.59	0.47	15.645	-13.1	2
J005207.69+670616.5	123.00	4.23	14.43	0.64	0.50	14.646	-18.7	3
J005436.84+630549.8	123.29	0.23	14.91	0.64	0.75	15.126	-35.3	2
J005458.91+633913.2	123.33	0.78	13.90	0.57	0.44	14.115	-12.5	1
J005611.62+630350.5	123.47	0.20	14.40	0.55	0.46	14.614	-15.0	2
J005619.50+625824.0	123.49	0.11	14.63	0.42	0.37	14.841	-9.6	2
J005743.72+640235.6	123.62	1.18	14.18	0.45	0.40	14.392	-16.8	1,2
J005809.86+624412.9	123.70	-0.12	14.67	0.50	0.56	14.883	-25.0	2
J005859.24+632603.0	123.78	0.57	13.18	0.45	0.72	13.392	-33.6	1,2
J005926.64+651157.0	123.77	2.34	13.45	0.49	0.54	13.663	-22.5	1,2
J010045.61+631740.4	123.98	0.44	15.43	0.77	0.63	15.649	-26.7	2
J010051.26+641327.3	123.96	1.37	13.61	0.53	0.42	13.824	-12.0	1,2
J014602.11+611502.2	129.45	-0.93	13.75	0.55	0.71	13.964	-38.9	1,2
J014620.49+644802.5	128.74	2.55	14.41	0.48	0.43	14.623	-15.2	2
J014624.42+611037.3	129.51	-0.99	13.36	0.45	0.34	13.572	-4.1	1,2
J014659.63+611229.6	129.57	-0.95	13.23	0.48	0.56	13.443	-26.3	1
J014807.07+631613.2	129.25	1.10	13.54	0.60	0.69	13.755	-34.1	1,2
J014843.39+642854.4	129.05	2.29	13.74	0.45	0.49	13.952	-22.3	1,2
J014905.20+624912.3	129.46	0.68	13.60	0.81	0.68	13.820	-26.8	2
J015001.17+642219.7	129.21	2.22	15.76	0.56	0.45	15.974	-11.4	2
J015022.92+652743.2	129.01	3.29	13.79	0.51	0.42	14.003	-7.0	1,2
J015025.75+602245.2	130.16	-1.66	14.05	0.44	0.33	14.262	-11.1	1
J015030.72+634132.5	129.42	1.57	15.70	0.60	0.50	15.915	-14.3	2
J015037.70+644447.0	129.19	2.60	14.64	0.40	0.39	14.851	4.6	2
J015105.68+611602.6	130.04	-0.78	13.71	0.50	0.37	13.923	-9.7	1,2
J015109.13+641421.8	129.36	2.12	15.71	0.57	0.48	15.925	-12.4	2
J015123.63+600038.6	130.36	-1.99	12.76	0.28	0.53	12.968	-27.3	1
J015213.08+624813.6	129.81	0.75	13.04	0.31	0.35	13.248	-11.3	1,2
J015221.93+635739.6	129.56	1.88	14.29	0.56	0.61	14.504	-28.6	2
J015246.27+630315.0	129.82	1.00	14.35	0.51	0.40	14.563		2
J015307.22+650110.4	129.39	2.92	13.97	0.41	0.37	14.181	-10.3	1,2
J015314.56+620241.5	130.11	0.04	12.89	0.39	0.31	13.100	-7.0	1,2
J015329.19+643128.1	129.54	2.45	13.98	0.33	0.26	14.189	-5.4	1,2
J015427.15+612204.7	130.41	-0.59	14.38	1.08	0.84	14.607	-39.0	2
J015510.44+632108.5	130.01	1.36	15.85	0.50	0.41	16.063	-10.0	2
J015520.62+611752.8	130.53	-0.63	13.46	0.50	0.43	13.673	-17.9	1,2
J015524.75+615836.1	130.37	0.03	14.98	0.55	0.43	15.194	-9.3	3
J015526.12+625056.4	130.16	0.88	14.34	0.55	0.61	14.554	-32.7	2
J015538.88+600157.0	130.88	-1.85	14.31	0.41	0.42	14.521	-18.5	1
J015601.25+633944.1	130.02	1.68	14.58	0.56	0.46	14.794	-15.0	2
J015613.26+635623.7	129.97	1.96	14.08	0.46	0.64	14.292	-31.6	2

NAME	$l(deg)$	$b(deg)$	r	r-i	r-Hα	V	$EW_{H\alpha}$	Ref.
J013920.80+654338.7	127.83	3.31	13.64	0.61	0.47	13.856	-14.9	1,2
J014146.63+581803.4	129.52	-3.93	15.11	0.56	0.50	15.324	-14.7	1
J014218.76+624733.5	128.71	0.49	14.56	0.60	0.50	14.775	-15.3	2
J014221.27+645836.1	128.29	2.64	15.24	0.40	0.36	15.451	-12.8	1
J014238.73+633753.1	128.58	1.32	13.18	0.40	0.37	13.391	-6.3	1,2
J014244.86+623056.2	128.81	0.23	13.22	0.38	0.40	13.430	-10.7	1,2
J014322.19+640118.5	128.58	1.72	13.29	0.37	0.48	13.500	-21.0	1,2
J014323.30+595307.3	129.41	-2.33	13.69	0.53	0.78	13.904	-50.8	1
J014401.85+640124.5	128.65	1.74	15.49	0.54	0.53	15.704	-17.9	1,2
J014437.08+603458.0	129.42	-1.62	13.22	0.44	0.58	13.432	-35.9	1
J014452.24+604123.3	129.43	-1.51	13.88	0.44	0.34	14.092	-6.4	1
J014458.15+633244.0	128.85	1.29	13.99	0.42	0.43	14.201	-13.5	2
J014458.27+625245.8	128.99	0.64	13.35	0.59	0.61	13.565	-23.2	2
J014519.02+633559.1	128.88	1.35	13.13	0.42	0.55	13.341	-22.5	2
J014539.64+611259.1	129.41	-0.97	12.45	0.76	0.74	12.669	-21.6	1,2
J020734.24+623601.1	131.56	1.01	14.43	0.56	0.46	14.644	-13.1	2
J020753.51+644148.9	130.99	3.03	15.91	0.33	0.34	16.119	-6.5	1,2
J020817.76+614220.1	131.91	0.18	13.43	0.55	0.61	13.644	-26.5	2
J020826.27+625745.9	131.55	1.39	14.37	0.64	0.53	14.586	-18.3	1,2
J020826.93+642241.5	131.14	2.74	12.59	0.65	0.62	12.807	-8.9	1
J020833.88+585547.6	132.75	-2.46	15.93	0.45	0.39	16.142	-9.6	3
J020837.59+652028.2	130.87	3.67	14.74	0.53	0.54	14.954	-19.1	2
J020855.24+631501.1	131.52	1.68	12.72	0.54	0.61	12.934	-2.6	2
J020859.72+635536.1	131.33	2.33	14.94	0.41	0.35	15.151	-8.3	2
J020917.87+613045.2	132.08	0.03	13.89	0.83	0.57	14.111	-17.2	1,2
J021000.05+640838.5	131.37	2.57	12.81	0.35	0.35	13.019	-8.0	2
J021005.63+631100.3	131.67	1.65	15.98	0.51	0.39	16.193	-5.9	2
J021011.09+652230.2	131.02	3.75	13.77	0.61	0.53	13.986	-19.9	2
J021036.32+611444.0	132.31	-0.18	13.09	0.50	0.42	13.303	-10.9	2
J021057.06+624700.8	131.88	1.30	14.02	0.47	0.31	14.232	-5.7	1,2
J021121.67+624707.5	131.92	1.32	15.57	0.57	0.52	15.785	-15.6	2
J021128.86+634604.0	131.64	2.26	13.93	0.48	0.42	14.143	-12.1	1,2
J021159.14+615639.9	132.25	0.54	15.00	0.84	0.69	15.221	-25.4	2
J021202.03+613230.4	132.38	0.16	15.41	0.83	0.59	15.631	-21.4	2
J021210.42+623242.3	132.09	1.12	12.20	0.34	0.45	12.409	-18.8	1,2
J021310.78+572406.7	133.80	-3.74	13.20	0.30	0.37	13.408	-12.0	1
J021320.12+613003.1	132.54	0.17	12.89	0.67	0.57	13.107	-21.5	1,2
J021325.98+622043.1	132.29	0.97	14.51	0.72	0.59	14.728	-17.1	2
J021331.69+561900.9	134.18	-4.75	13.70	0.25	0.29	13.907	-8.6	1
J021336.53+601829.1	132.94	-0.96	13.75	0.63	0.38	13.966	-5.7	1,2
J021352.00+642520.3	131.68	2.96	15.03	0.47	0.39	15.242	-13.2	1,2
J021532.96+623236.9	132.46	1.24	13.20	0.64	0.65	13.416	-13.4	2
J021544.45+582456.8	133.80	-2.67	13.33	0.32	0.42	13.539	-17.6	1
J021647.40+642812.9	131.97	3.11	14.59	0.52	0.46	14.803	-16.6	2

Table 4.3. Continued...

NAME	$l(deg)$	$b(deg)$	r	r-i	r-Hα	V	$EW_{H\alpha}$	Ref.
J015627.82+612939.2	130.61	-0.40	12.70	0.44	0.50	12.912	-15.7	1,2
J015630.87+630307.5	130.23	1.11	13.28	0.27	0.51	13.487	-29.1	1,2
J015644.71+653640.6	129.61	3.59	15.01	0.54	0.40	15.224	-0.5	2
J015645.75+635259.8	130.05	1.92	13.11	0.58	0.53	13.325	-19.9	1,2
J015650.51+645341.1	129.80	2.90	15.43	0.41	0.46	15.641	-17.1	3
J015716.62+575205.7	131.62	-3.89	13.15	0.41	0.53	13.361	-11.6	1
J015741.35+605313.7	130.91	-0.95	14.76	0.71	0.51	14.978	-17.0	2
J015804.46+653020.6	129.77	3.52	13.14	0.39	0.36	13.350	-9.0	1,2
J015809.04+615813.6	130.68	0.11	14.59	0.72	0.60	14.808	-21.8	2
J015918.33+654955.8	129.81	3.87	15.19	0.55	0.54	15.404		2
J015919.69+645053.4	130.07	2.92	12.78	0.34	0.53	12.989	-16.1	1,2
J015922.56+635829.2	130.30	2.08	15.15	0.56	0.82	15.364	-44.3	2
J015938.99+643615.4	130.17	2.69	13.26	0.39	0.53	13.470	-19.9	1,2
J015945.33+630314.9	130.58	1.20	14.63	0.53	0.39	14.844	-9.5	2
J020014.86+570017.7	132.23	-4.62	13.26	0.25	0.24	13.467	-5.4	1
J020037.84+652133.9	130.07	3.45	13.08	0.40	0.34	13.291	2.4	2
J020048.75+585835.1	131.78	-2.70	13.58	0.33	0.38	13.789	-14.1	1
J020049.43+635944.0	130.45	2.14	13.91	0.84	0.57	14.131	-28.9	1,2
J020056.02+575529.3	132.08	-3.71	14.99	0.60	0.45	15.205	-9.2	1
J020105.33+613403.0	131.12	-0.19	14.46	0.67	0.68	14.677	-35.0	2
J020109.65+641219.4	130.43	2.35	14.58	0.44	0.35	14.792	-7.8	3
J020121.79+630117.3	130.77	1.22	13.32	0.45	0.35	13.532	2.2	2
J020136.00+613207.6	131.19	-0.21	13.14	0.47	0.39	13.352	-9.9	1,2
J020144.86+581930.0	132.07	-3.29	13.05	0.21	0.24	13.256	-8.2	1
J020203.16+630213.4	130.84	1.25	13.41	0.77	0.73	13.629	-37.0	2
J020252.26+620926.0	131.17	0.43	15.21	0.60	0.57	15.425	-22.9	1,2
J020325.84+584145.0	132.18	-2.88	15.42	0.33	0.54	15.629	-28.1	1
J020326.01+635943.1	130.72	2.22	14.40	0.54	0.49	14.614	-16.9	1,2
J020328.03+624333.8	131.08	1.00	13.73	0.41	0.42	13.941	-12.9	1,2
J020343.87+581058.2	132.36	-3.36	12.84	0.70	0.53	13.058	-7.0	3
J020407.85+643122.2	130.65	2.75	13.94	0.36	0.39	14.150	-14.9	1,2
J020421.09+591708.1	132.13	-2.28	13.50	0.40	0.38	13.711	-13.1	1
J020422.15+595855.8	131.94	-1.61	13.42	0.32	0.30	13.629	-9.4	1
J020504.17+630216.1	131.17	1.35	15.07	0.57	0.41	15.285	-4.3	1,2
J020547.47+641051.7	130.92	2.47	12.68	0.40	0.41	12.891	-10.9	1,2
J020618.67+644945.1	130.79	3.11	14.88	0.42	0.57	15.091	-30.9	1,2
J020649.26+645826.9	130.80	3.26	14.49	0.57	0.42	14.705	-9.1	3
J020707.67+612422.7	131.86	-0.15	13.28	0.39	0.37	13.490	-11.9	1,2
J020710.67+602546.5	132.15	-1.08	14.40	0.57	0.49	14.615		3
J020717.23+645046.2	130.88	3.15	12.57	0.35	0.54	12.779	-25.8	2
J020731.12+634520.4	131.22	2.12	14.54	0.67	0.45	14.757	-8.5	2
J023948.17+604505.1	135.79	0.61	13.26	0.37	0.42	13.470	-15.2	1,2
J023950.95+611829.1	135.57	1.12	13.95	0.49	0.55	14.163	-49.8	1
J023952.30+574354.2	137.02	-2.14	13.51	0.35	0.49	13.719	-18.1	1
J024021.07+582834.0	136.78	-1.44	13.81	0.49	0.37	14.023	-5.8	3
J024052.88+574400.8	137.14	-2.09	14.40	0.52	0.53	14.613	-20.3	3
J024054.97+630009.8	134.99	2.72	15.69	0.54	0.49	15.904	2.9	2
J024102.49+574015.4	137.19	-2.13	14.19	0.50	0.46	14.403	-22.1	1
J024132.66+550235.9	138.34	-4.50	13.22	0.26	0.29	13.427	-9.0	1
J024146.73+602532.2	136.14	0.42	14.05	0.63	0.71	14.266	-34.4	1,2
J024159.21+600106.0	136.34	0.06	14.55	0.65	0.58	14.767	1.1	2
J024221.54+593716.4	136.54	-0.29	13.38	0.61	0.46	13.596	-14.3	1,2
J024252.56+611953.9	135.89	1.30	15.74	0.64	0.73	15.956	-39.1	2
J024305.60+631614.7	135.10	3.07	14.55	0.55	0.61	14.764	-26.7	2
J024317.68+603205.5	136.27	0.59	13.67	0.66	0.68	13.887	-37.3	2
J024332.05+632150.1	135.11	3.17	14.16	0.46	0.46	14.372	-17.4	1,2
J024405.37+621448.7	135.64	2.19	15.22	0.49	0.48	15.433	-31.5	2
J024454.00+635608.0	135.01	3.76	15.75	0.58	0.51	15.965	-18.0	2

NAME	$l(deg)$	$b(deg)$	r	r-i	r-Hα	V	$EW_{H\alpha}$	Ref.
J021744.41+644335.2	131.98	3.38	13.71	0.56	0.63	13.924	-19.4	2
J021747.84+643419.9	132.04	3.24	14.66	0.57	0.62	14.875	-25.6	2
J022009.76+643605.9	132.27	3.35	15.65	0.55	0.43	15.864	-10.6	1,2
J022025.02+600114.0	133.84	-0.95	13.31	0.44	0.48	13.522	6.0	1
J022033.45+625717.4	132.86	1.81	15.71	0.71	0.85	15.928	-62.9	2
J022045.25+631642.8	132.78	2.13	15.02	0.52	0.49	15.233	-18.8	1,2
J022053.65+642835.6	132.38	3.26	15.91	0.61	0.49	16.126	-14.2	1,2
J022100.28+635435.2	132.59	2.73	13.09	0.40	0.39	13.301	-10.6	1,2
J022107.83+625754.6	132.92	1.85	14.94	0.68	0.57	15.157	-24.6	2
J022222.78+623841.9	133.17	1.59	15.17	0.58	0.43	15.385	-8.1	2
J022227.73+623530.6	133.19	1.55	14.32	0.41	0.71	14.531	-25.3	2
J022337.05+601602.8	134.13	-0.59	14.00	0.58	0.49	14.215	-13.9	2
J022343.45+603545.6	134.02	-0.27	12.94	0.66	0.44	13.157	-11.0	1,2
J022420.68+624842.5	133.32	1.83	13.43	0.60	0.48	13.645	-15.5	2
J022502.69+644947.6	132.68	3.74	13.26	0.53	0.44	13.474	-9.3	1,2
J022558.78+583626.1	134.99	-2.03	15.11	0.51	0.40	15.323	-16.1	3
J022636.00+601401.8	134.49	-0.49	14.50	0.96	0.99	14.724	-56.6	2
J022821.67+641216.0	133.24	3.29	15.84	0.61	0.49	16.056	-13.0	2
J022823.86+631834.8	133.57	2.46	12.78	0.55	0.63	12.994	-28.4	1,2
J022913.58+633224.5	133.57	2.71	13.74	0.72	0.52	13.958	-14.7	1
J022953.81+630742.2	133.79	2.35	14.25	0.67	0.50	14.467	-9.7	2
J023003.21+643829.4	133.25	3.76	15.31	0.56	0.53	15.524	-17.2	2
J023031.38+594127.1	135.14	-0.81	14.48	0.57	0.43	14.695	-10.7	2
J023035.11+610005.9	134.66	0.41	14.56	0.63	0.47	14.776	-10.5	2
J023150.04+604952.4	134.86	0.31	13.85	0.41	0.35	14.061	-53.9	1,2
J023202.89+641033.2	133.62	3.41	16.23	0.67	0.44	16.447		2
J023235.10+640522.7	133.71	3.35	13.53	0.76	0.76	13.749	-38.5	2
J023404.70+605914.4	135.06	0.55	12.90	0.64	0.66	13.116	-35.8	2
J023410.30+612440.6	134.90	0.95	13.64	0.65	1.21	13.857	-92.5	1
J023411.97+595634.2	135.47	-0.40	13.13	0.59	0.56	13.345	-17.0	1,2
J023431.08+601616.5	135.38	-0.08	13.58	1.13	0.82	13.808	-32.2	2
J023439.79+641813.4	133.83	3.64	17.02	0.77	0.49	17.239	-12.9	2
J023536.82+625251.7	134.49	2.37	16.68	0.59	0.46	16.895	-13.3	2
J023629.19+634245.8	134.25	3.17	15.61	0.64	0.60	15.826	-17.1	2
J023642.66+614714.8	135.03	1.41	15.38	0.54	0.41	15.594	-7.5	2
J023744.52+605352.8	135.50	0.65	16.79	0.76	0.52	17.009		2
J023753.78+620410.0	135.05	1.73	13.03	0.58	0.47	13.245	2.3	2
J023758.11+634635.6	134.38	3.30	13.30	0.36	0.36	13.510	-9.1	1,2
J023809.91+620224.6	135.09	1.71	13.21	0.57	0.54	13.425	-14.5	1,2
J023841.80+640826.3	134.30	3.66	14.05	0.64	0.44	14.266	-11.1	1,2
J023923.67+604247.6	135.76	0.56	13.33	0.43	0.54	13.541	-25.0	1
J030144.24+632853.7	136.88	4.20	14.39	0.56	0.38	14.604	-7.8	1
J030218.24+551133.7	140.93	-3.04	13.89	0.81	0.55	14.110	-28.3	1
J030317.45+583402.0	139.42	-0.02	14.57	0.80	0.61	14.790	-20.2	1,2
J030331.33+585234.6	139.29	0.27	14.64	0.77	0.51	14.859	-7.9	2
J030332.31+623856.7	137.46	3.56	14.32	0.55	0.38	14.534	-9.0	1,2
J030422.01+574820.4	139.91	-0.62	14.40	0.65	0.54	14.617	-25.8	1,2
J030423.32+622900.9	137.63	3.47	13.70	0.60	0.59	13.915	-22.7	1,2
J030451.26+594758.8	138.99	1.15	15.09	0.76	0.81	15.309	-43.1	2
J030501.73+585146.8	139.47	0.35	13.46	0.81	0.59	13.680	-16.6	2
J030519.62+555119.3	140.98	-2.25	14.94	0.86	0.55	15.162	-15.1	3
J030539.90+610725.6	138.43	2.36	14.47	0.81	0.73	14.690	-29.7	2
J030625.00+614359.0	138.20	2.93	15.87	0.71	0.58	16.088	-21.0	2
J030655.90+573207.3	140.34	-0.68	15.95	0.80	0.57	16.170	-21.1	3
J030953.64+550346.3	141.94	-2.62	13.85	0.83	0.71	14.071	-30.8	1
J031046.28+593003.7	139.79	1.27	15.46	0.87	0.81	15.682	-42.6	1
J031140.70+542535.8	142.48	-3.03	13.92	0.76	0.65	14.139	-26.6	1
J031141.73+614847.9	138.70	3.31	15.50	0.54	0.38	15.714	-7.8	1,2

Table 4.3. Continued...

NAME	$l(deg)$	$b(deg)$	r	r-i	r-Hα	V	$EW_{H\alpha}$	Ref.
J024504.86+612502.1	136.09	1.48	15.35	0.56	0.47	15.564	-15.3	1,2
J024506.09+611409.1	136.17	1.32	15.97	0.65	0.65	16.187	-33.0	2
J024509.54+612523.5	136.10	1.49	15.11	0.53	0.34	15.324	-27.1	2
J024519.10+633755.1	135.18	3.50	14.04	0.55	0.62	14.254	-35.9	1,2
J024521.28+625416.2	135.49	2.84	13.59	0.44	0.46	13.802	-14.9	1,2
J024540.61+592151.2	137.03	-0.34	13.28	0.47	0.55	13.492	-23.8	1,2
J024553.87+635414.7	135.12	3.77	14.21	0.68	0.53	14.427	-14.4	2
J024618.12+613514.7	136.15	1.70	15.70	0.50	0.47	15.913	-26.8	1,2
J024656.04+563924.7	138.34	-2.72	13.48	0.42	0.30	13.691	-2.4	1
J024728.30+570008.2	138.26	-2.38	13.31	0.50	0.37	13.523	-9.0	1
J024735.56+615530.9	136.15	2.07	13.44	0.39	0.44	13.650	-19.8	1,2
J024737.27+640509.3	135.21	4.02	14.24	0.47	0.33	14.452	-17.7	3
J024748.62+605750.5	136.59	1.22	13.95	0.52	0.82	14.163	-50.7	1
J024753.07+613405.8	136.33	1.76	14.37	0.68	0.74	14.587	-29.4	1,2
J024758.73+630156.8	135.71	3.09	14.66	0.54	0.74	14.874	-39.3	2
J024823.01+614728.1	136.29	1.99	12.91	0.38	0.48	13.120	-19.6	1,2
J024823.69+614107.1	136.34	1.90	14.09	0.40	0.61	14.301	-22.9	2
J024838.04+630153.0	135.77	3.12	15.21	0.45	0.65	15.422	-35.7	2
J024913.93+631042.4	135.77	3.28	13.16	0.39	0.54	13.370	-20.7	2
J024928.47+595248.4	137.24	0.33	13.37	0.83	0.70	13.591	-30.6	2
J024940.66+621424.8	136.23	2.46	13.24	0.33	0.45	13.449	-20.5	1,2
J025016.65+624435.6	136.07	2.94	14.48	0.42	0.37	14.691	-7.2	2
J025059.12+615648.7	136.50	2.26	15.28	0.45	0.58	15.492		2
J025102.21+615733.8	136.50	2.28	14.07	0.51	0.81	14.283	-45.4	1,2
J025130.43+621052.2	136.45	2.50	15.79	0.51	0.72	16.003	-38.3	1
J025136.03+601557.5	137.31	0.79	15.71	0.44	0.45	15.922	-16.9	1,2
J025143.40+552742.7	139.47	-3.50	13.31	0.55	0.39	13.521	-12.2	1
J025200.23+621145.2	136.49	2.54	13.85	0.40	0.45	14.061	-16.3	1,2
J025204.14+583423.4	138.12	-0.70	12.96	0.35	0.46	13.169	-17.2	2
J025233.24+615902.2	136.64	2.38	14.82	0.43	0.36	15.031	-6.5	2
J025324.51+614622.9	136.83	2.24	15.46	0.59	0.58	15.675	-20.7	1,2
J025359.43+570402.9	139.03	-1.92	13.46	0.61	0.53	13.676	-21.2	3
J025442.51+573654.8	138.86	-1.39	14.11	0.76	0.61	14.329	-20.7	3
J025448.83+605832.1	137.34	1.60	16.17	0.80	0.52	16.390		2
J025502.38+605001.9	137.43	1.49	14.52	0.54	0.42	14.734		2
J025610.39+580629.6	138.81	-0.87	13.81	0.62	0.25	14.026	-25.7	2
J025631.47+593648.4	138.16	0.49	15.01	0.70	0.74	15.228	-36.3	2
J025700.47+575742.8	138.98	-0.94	14.26	0.71	0.56	14.478	-22.1	2
J025704.89+584311.6	138.63	-0.27	16.25	0.81	0.51	16.470		2
J025737.78+624703.4	136.80	3.36	14.77	0.51	0.39	14.983	-10.3	2
J025856.75+633557.7	136.55	4.15	13.48	0.52	0.64	13.693	-34.8	1
J025904.88+621459.5	137.20	2.97	15.59	0.39	0.34	15.800	-5.5	2
J025905.15+605404.2	137.84	1.78	12.91	0.58	0.78	13.125	-45.3	1
J025935.04+603207.2	138.06	1.48	13.88	0.43	0.49	14.091	-18.8	1,2
J025950.85+582333.1	139.10	-0.39	14.05	0.62	0.94	14.266	-70.1	3
J025959.45+582929.5	139.07	-0.29	13.31	0.63	0.49	13.526	-13.8	2
J030010.27+613223.2	137.65	2.40	13.73	0.54	0.42	13.944	-13.2	1,2
J030023.60+572849.0	139.60	-1.16	15.29	0.85	0.58	15.511	-17.8	3
J030056.68+615940.7	137.51	2.85	13.04	0.35	0.31	13.249	2.5	1,2
J030120.82+602444.9	138.31	1.48	14.38	0.55	0.48	14.594	-13.7	2
J030121.61+602856.6	138.28	1.54	13.89	0.64	0.54	14.106	-21.8	1
J030124.02+610221.3	138.02	2.03	14.85	0.69	0.64	15.068	-27.9	2
J030133.63+593518.5	138.73	0.77	14.07	0.67	0.73	14.287	-36.6	2
J040140.39+523628.1	149.56	-0.14	14.35	0.87	0.76	14.572	-33.4	3
J040153.91+552435.8	147.74	1.99	14.18	0.55	0.35	14.394	-6.3	1
J040200.19+540003.0	148.68	0.94	15.21	0.82	0.70	15.431	-33.6	1
J040208.47+494029.5	151.54	-2.30	16.30	0.67	0.51	16.517	-13.3	3
J040351.67+493255.7	151.83	-2.21	15.42	0.64	0.44	15.636	-11.8	1
J040357.96+474411.0	153.05	-3.56	15.55	0.63	0.47	15.766	-15.0	3
J040410.12+540420.7	148.87	1.21	14.84	0.76	0.48	15.059	-10.1	1
J040625.91+543402.4	148.79	1.80	15.66	0.82	0.57	15.881	-19.8	3
J040628.52+582709.4	146.18	4.68	16.28	0.70	0.55	16.498	-21.9	3
J040636.07+525022.8	149.96	0.53	14.19	0.77	0.64	14.409	-23.3	3

NAME	$l(deg)$	$b(deg)$	r	r-i	r-Hα	V	$EW_{H\alpha}$	Ref.
J031207.83+625028.3	138.22	4.22	15.96	0.61	0.44	16.176	-7.8	3
J031208.92+605534.5	139.21	2.58	15.11	0.78	0.67	15.330	-13.8	2
J031331.30+624842.2	138.37	4.28	14.78	0.67	0.52	14.997	-10.8	3
J031333.27+603307.1	139.55	2.35	15.74	0.89	0.59	15.962	-16.4	2
J031528.59+622715.3	138.75	4.09	14.63	0.66	0.48	14.847	-7.0	1
J031744.98+571204.1	141.76	-0.22	13.34	0.77	0.53	13.559	-24.4	1
J031903.40+630719.9	138.74	4.88	15.32	0.61	0.43	15.534	-12.8	1
J031935.37+594155.3	140.64	2.02	13.93	0.64	0.64	14.146	-27.5	1
J032001.54+601400.6	140.39	2.50	14.70	0.45	0.41	14.912	-11.5	3
J032019.82+620624.3	139.41	4.10	15.27	0.80	0.59	15.490	-19.7	3
J032025.39+554621.1	142.84	-1.23	13.85	0.89	0.68	14.072	-26.7	3
J032037.05+545407.8	143.33	-1.95	15.07	0.80	0.66	15.290	-21.7	3
J032113.71+625155.4	139.09	4.79	14.81	0.73	0.87	15.029	-50.5	3
J032152.94+523327.9	144.76	-3.82	15.41	0.45	0.52	15.622	-21.0	3
J032323.98+595855.9	140.88	2.52	14.09	0.62	0.55	14.306	-21.0	1
J032332.68+561452.5	142.95	-0.60	14.21	0.83	0.52	14.431	-15.1	1
J032415.73+615556.5	139.90	4.20	13.83	0.64	0.54	14.046	-18.1	1
J032539.17+603425.1	140.79	3.17	13.94	0.68	0.57	14.157	-12.1	3
J033012.18+532710.0	145.30	-2.38	15.66	0.70	0.51	15.878	-8.9	1
J033022.30+513800.8	146.36	-3.86	13.21	0.56	0.62	13.424	-24.1	1
J033234.83+502346.1	147.36	-4.67	13.70	0.36	0.47	13.910	-19.2	1
J033310.88+523754.2	146.14	-2.79	15.07	0.69	0.45	15.288	-10.8	3
J033328.96+541232.3	145.27	-1.48	13.19	0.79	0.63	13.410	-23.0	3
J033422.04+515757.8	146.68	-3.23	14.41	0.53	0.39	14.624	-6.0	3
J033812.67+594141.5	142.58	3.34	15.16	0.52	0.36	15.373	-7.7	3
J033847.22+521508.0	147.06	-2.60	13.82	0.69	0.48	14.038	-14.3	1
J033849.89+531730.8	146.45	-1.76	13.91	0.90	0.54	14.133	-13.5	1
J033907.39+550419.5	145.42	-0.30	15.22	1.33	0.83	15.453	-23.6	3
J033912.16+604217.8	142.08	4.23	14.87	0.56	0.73	15.084	-38.8	1
J033914.34+541555.5	145.92	-0.94	13.56	1.08	0.67	13.787	-32.4	3
J033930.41+502711.3	148.22	-3.98	12.94	0.50	0.46	13.153	-15.1	3
J033945.90+603323.8	142.22	4.15	13.85	0.47	0.49	14.062	-20.1	1
J034158.92+575733.7	144.01	2.24	14.34	0.71	0.68	14.558	-32.1	3
J034332.26+511037.8	148.29	-3.02	13.45	0.60	0.45	13.665	-9.9	1
J034441.97+583755.2	143.88	3.00	14.53	0.49	0.53	14.743	-25.6	1
J034459.92+585906.2	143.70	3.30	14.69	0.50	0.39	14.903	-9.8	1
J034528.81+585113.7	143.83	3.23	15.42	0.52	0.41	15.633	-11.4	1
J034649.15+585327.3	143.94	3.37	13.39	0.69	0.50	13.608	-21.2	3
J034654.95+482052.3	150.47	-4.92	15.02	0.42	0.55	15.231	-24.8	1
J034748.25+603321.4	143.01	4.75	15.05	0.60	0.44	15.265	-13.5	1
J034828.55+562915.4	145.61	1.62	13.47	0.58	0.62	13.685	-13.1	1
J034846.85+572614.5	145.05	2.39	13.37	0.68	0.53	13.588	-24.8	1
J034929.34+532910.8	147.59	-0.64	14.27	0.73	0.42	14.489	-11.5	1
J035147.05+571057.1	145.52	2.44	15.35	0.46	0.55	15.562	-21.6	3
J035203.44+562347.7	146.05	1.86	15.87	0.71	0.46	16.088	-11.8	1
J035447.39+552939.6	146.92	1.40	14.83	0.73	0.53	15.049	-18.5	3
J035529.64+484755.6	151.29	-3.67	14.62	0.67	0.54	14.837	-17.0	3
J035541.79+583157.9	145.06	3.82	14.37	0.56	0.43	14.584	-11.5	3
J035744.18+570938.9	146.16	2.94	14.98	0.38	0.44	15.190	-16.1	3
J035754.21+571402.5	146.13	3.01	16.67	0.47	0.43	16.882	-20.4	1
J035837.56+564750.5	146.49	2.75	15.81	0.43	0.42	16.021	-13.3	1
J035910.88+580234.5	145.73	3.74	17.13	0.59	0.45	17.345	-16.4	1
J040011.86+555937.8	147.18	2.28	15.22	0.53	0.43	15.434	-13.6	1
J044159.16+415752.1	161.90	-2.83	14.58	0.95	0.60	14.804	-16.0	3
J044257.10+415011.7	162.11	-2.78	14.99	0.41	0.42	15.201	-13.1	1
J044311.19+485747.1	156.76	1.93	14.29	0.58	0.42	14.505	-7.1	1
J044312.52+485736.7	156.77	1.94	14.93	0.60	0.54	15.145	-20.2	1
J044521.00+420717.3	162.19	-2.25	14.70	0.71	0.60	14.918	-17.9	1
J044547.89+443831.9	160.32	-0.55	14.79	0.49	0.35	15.003	-5.2	1
J044557.84+414245.7	162.57	-2.43	14.08	0.28	0.47	14.288	-23.9	1
J044748.62+514104.1	155.17	4.26	14.06	0.47	0.40	14.272	-7.5	1
J044812.10+411819.2	163.15	-2.38	14.01	0.33	0.45	14.219	-22.2	1
J044818.02+433643.4	161.40	-0.88	14.64	0.22	0.42	14.846	-16.5	1

Table 4.3. Continued...

NAME	$l(deg)$	$b(deg)$	r	r-i	r-Hα	V	$EW_{H\alpha}$	Ref.
J040644.24+463308.0	154.20	-4.12	14.18	0.42	0.35	14.391	-8.0	1
J040647.46+571507.8	147.02	3.82	14.51	0.56	0.57	14.724	-29.3	1
J040648.01+573436.6	146.80	4.06	15.04	0.47	0.61	15.252	-26.9	1
J040733.30+552427.4	148.34	2.53	14.61	0.57	0.55	14.825	-17.0	3
J040851.75+570216.8	147.37	3.85	13.74	0.31	0.25	13.948	5.1	1
J040930.07+554107.2	148.36	2.92	15.01	0.59	0.64	15.225	-27.7	1
J041016.15+452322.5	155.44	-4.56	14.39	0.33	0.48	14.599	-18.3	1
J041042.30+530216.9	150.28	1.09	14.70	0.64	0.50	14.916	-14.7	1
J041052.79+552531.9	148.68	2.86	14.97	0.72	0.73	15.188	-32.2	3
J041146.03+555508.2	148.43	3.30	15.00	0.50	0.41	15.213	-7.1	3
J041149.03+564157.2	147.90	3.88	14.34	0.46	0.36	14.552	-8.1	1
J041325.25+521559.8	151.11	0.81	14.37	0.61	0.42	14.586	2.2	1
J041340.74+553748.6	148.83	3.28	14.19	0.57	0.42	14.405	-4.0	1
J041503.65+520945.8	151.37	0.91	13.39	0.40	0.33	13.601	-6.3	1
J041519.45+495124.5	152.99	-0.73	13.68	0.57	0.45	13.895	-12.3	1
J041539.56+532702.8	150.54	1.90	13.99	0.43	0.56	14.201	-23.9	1
J041544.68+534956.1	150.28	2.18	13.86	0.54	0.44	14.074	-15.2	1
J041617.43+452538.8	156.18	-3.81	13.05	0.32	0.40	13.259	-17.7	1
J041629.72+553617.9	149.13	3.54	14.54	0.50	0.46	14.753	-14.9	1
J041750.14+532526.1	150.79	2.11	13.33	0.59	0.79	13.545	-48.2	1
J041912.84+451756.8	156.64	-3.54	13.60	0.49	0.65	13.813	-34.3	1
J042035.09+562307.8	148.99	4.49	14.76	0.41	0.45	14.971	-18.3	1
J042053.25+494407.3	153.72	-0.19	13.99	0.67	0.42	14.207	-8.7	1
J042100.42+560539.0	149.24	4.33	14.20	0.44	0.51	14.412	-18.2	1
J042101.62+450857.9	156.97	-3.42	13.52	0.52	0.56	13.733	-29.0	1
J042138.79+551330.5	149.92	3.78	14.23	0.59	0.69	14.445	-33.7	1
J042248.80+470643.6	155.80	-1.82	13.52	0.64	0.72	13.736	-37.8	1
J042302.47+540534.6	150.87	3.12	13.49	0.74	0.55	13.709	-15.3	3
J042332.36+474409.0	155.44	-1.29	14.92	0.72	0.54	15.138	-19.0	1
J042353.25+460947.0	156.60	-2.36	14.11	0.69	0.51	14.328	-19.3	1
J042413.34+535555.2	151.10	3.13	15.30	0.61	0.50	15.516	-17.5	1
J042420.69+441501.8	158.03	-3.64	13.29	0.47	0.66	13.502	-41.1	1
J042533.76+533645.4	151.47	3.05	15.09	0.56	0.41	15.304	-9.9	1
J042853.13+483132.5	155.50	-0.10	15.44	0.73	0.62	15.659	-27.4	1
J042917.05+523426.3	152.61	2.74	13.37	0.75	0.57	13.589	-17.3	1
J043002.27+454748.9	157.61	-1.84	15.22	0.55	0.50	15.434	-22.9	1
J043035.52+523659.6	152.71	2.91	15.45	0.73	0.79	15.669	-51.2	1
J043105.01+454856.8	157.72	-1.70	12.57	0.44	0.48	12.782	-17.9	3
J043135.00+493650.1	155.01	0.97	16.02	0.72	0.46	16.238	-9.9	3
J043204.46+545014.9	151.24	4.59	14.05	0.54	0.52	14.264	-15.0	1
J043206.08+521521.2	153.13	2.83	13.36	0.78	0.76	13.580	-39.6	1
J043220.87+440518.5	159.14	-2.71	15.33	0.68	0.44	15.547	-11.1	3
J043225.85+485200.7	155.65	0.56	14.00	0.72	0.70	14.218	-37.3	1
J043242.92+443647.3	158.80	-2.31	13.85	0.53	0.36	14.064	-9.1	1
J043324.72+405849.2	161.55	-4.68	14.98	0.34	0.29	15.189	-4.9	1
J043332.06+432101.0	159.82	-3.06	13.88	0.45	0.30	14.092	-7.3	1
J043500.15+450714.9	158.70	-1.66	16.28	0.56	0.49	16.494	-5.6	3
J043509.41+531546.5	152.71	3.85	15.03	0.57	0.45	15.245	-16.0	3
J043623.80+452053.6	158.70	-1.33	14.29	0.64	0.44	14.506	-5.4	1
J043846.94+435224.2	160.08	-2.00	14.86	0.57	0.51	15.075	-21.8	1
J043848.81+433446.0	160.30	-2.19	15.31	0.42	0.44	15.521	-15.5	1
J043850.23+475233.9	157.10	0.67	14.09	0.79	0.62	14.310	-23.7	1
J043857.76+401339.3	162.82	-4.40	14.86	0.42	0.36	15.071	-6.0	1
J044010.16+475038.6	157.27	0.82	15.91	0.93	0.58	16.133	-8.0	3
J044041.07+412132.4	162.19	-3.41	14.70	0.36	0.32	14.910	-9.2	1
J044057.63+395223.5	163.34	-4.35	16.28	0.46	0.35	16.492	-7.5	1
J044114.89+503413.2	155.34	2.76	14.03	0.58	0.45	14.245	-16.1	3
J044137.04+463330.9	158.40	0.15	13.97	0.66	0.46	14.187	-9.3	1
J044154.56+423021.9	161.48	-2.48	13.75	0.43	0.38	13.965	-12.0	1
J044156.94+430450.2	161.05	-2.10	14.01	0.52	0.43	14.223	-16.1	1
J044841.84+445015.7	160.51	-0.03	14.28	0.55	0.54	14.494	-20.2	1
J044847.67+464207.3	159.09	1.18	13.54	0.53	0.36	13.754	-8.2	1
J044916.13+461919.0	159.44	1.00	14.04	0.58	0.81	14.255	-5.9	3
J044934.72+412647.6	163.21	-2.09	14.20	0.68	0.51	14.417	-19.0	3
J044943.82+395108.5	164.46	-3.09	13.72	0.41	0.41	13.931	-12.2	1
J045000.02+411434.2	163.42	-2.16	15.69	0.38	0.41	15.900	-15.0	1
J045251.33+424635.6	162.57	-0.77	14.12	0.34	0.44	14.329	-17.4	1
J045329.30+410220.4	163.99	-1.78	13.57	0.30	0.34	13.778	-11.0	1
J045339.41+462135.3	159.89	1.61	15.62	0.45	0.43	15.832	-14.4	1
J045342.48+391109.0	165.46	-2.92	15.34	0.38	0.26	15.550	-51.4	3
J045414.61+452916.8	160.63	1.14	15.36	0.57	0.42	15.575	-10.1	1
J045457.62+462400.1	160.00	1.81	14.59	0.42	0.41	14.801	-13.4	1
J045501.67+362602.7	167.77	-4.44	14.45	0.58	0.59	14.665	-26.3	1
J045511.25+383344.1	166.13	-3.08	16.21	0.59	0.53	16.425	-24.0	1
J045552.92+370005.5	167.43	-3.95	14.64	0.48	0.52	14.853	-21.1	1
J045625.52+402409.5	164.84	-1.75	14.55	0.52	0.39	14.763	-10.4	1
J045647.57+490802.2	158.06	3.76	14.26	0.48	0.52	14.473	-19.6	1
J045659.27+463204.2	160.11	2.16	13.67	0.37	0.39	13.880	-16.6	1
J045901.33+403011.5	165.07	-1.30	14.26	0.37	0.49	14.470	-18.2	1
J045917.19+431609.2	162.93	0.45	13.34	0.28	0.32	13.548	-9.9	1
J045929.27+455715.4	160.84	2.14	14.93	0.51	0.67	15.143	-37.6	1
J050014.87+504256.4	157.15	5.17	13.83	0.50	0.36	14.043	-5.4	1
J050057.33+450010.9	161.75	1.76	14.79	0.75	0.66	15.009	-13.7	3
J050142.31+433837.7	162.90	1.03	14.68	0.36	0.46	14.890	-19.8	1
J050239.27+371555.8	168.06	-2.73	14.66	0.43	0.39	14.871	-12.9	1
J050303.80+422144.6	164.07	0.44	15.34	0.47	0.64	15.552	-44.7	1
J050315.37+401006.4	165.83	-0.87	14.92	0.40	0.53	15.131	-27.7	1
J050325.87+333301.9	171.11	-4.86	14.69	0.41	0.38	14.901	-10.4	1
J050327.55+414217.3	164.63	0.10	13.61	0.45	0.82	13.822	-3.5	3
J050517.54+433805.3	163.30	1.54	15.50	0.53	0.51	15.714	-22.7	1
J050528.18+393124.0	166.60	-0.92	15.21	0.44	0.40	15.422	-21.3	3
J050535.04+442648.4	162.69	2.07	13.21	0.53	0.61	13.422	-44.4	1
J050556.75+430528.9	163.81	1.31	13.34	0.26	0.37	13.547	-11.9	1
J050649.71+421532.4	164.57	0.93	13.27	0.27	0.38	13.477	-12.9	1
J050826.96+361342.9	169.59	-2.43	15.81	0.52	0.47	16.023	-15.8	1
J050830.91+424234.2	164.40	1.45	13.22	0.37	0.66	13.430	-36.7	1
J050904.06+385915.2	167.45	-0.68	14.43	0.56	0.58	14.644	-24.9	1
J051000.63+384938.4	167.68	-0.63	13.78	0.43	0.37	13.991	-13.6	1
J051013.60+414158.9	165.40	1.11	13.84	0.28	0.29	14.048	-7.6	1
J051014.52+362436.4	169.66	-2.03	13.58	0.36	0.27	13.790	-3.5	1
J051027.30+384249.6	167.83	-0.63	13.87	0.47	0.36	14.082	-30.0	3
J051051.62+432124.7	164.13	2.18	13.65	0.58	0.75	13.865	-42.2	1
J051143.01+431034.8	164.37	2.20	14.56	0.38	0.40	14.770	-14.1	1
J051206.61+442634.5	163.39	3.01	13.50	0.31	0.38	13.708	-13.8	1
J051208.12+365020.3	169.53	-1.47	13.14	0.45	0.37	13.352	-9.9	1
J051226.87+445432.3	163.04	3.33	14.46	0.44	0.54	14.672	-25.4	1
J051339.97+413555.0	165.86	1.57	14.77	0.26	0.32	14.977	-9.0	1
J051427.19+412419.1	166.10	1.57	13.15	0.18	0.33	13.355	-11.8	1
J051555.71+394846.8	167.56	0.87	14.79	0.48	0.42	15.003	-12.0	1
J051633.27+414641.0	166.03	2.11	13.25	0.29	0.44	13.458	-21.7	1
J051634.39+402856.1	167.08	1.36	15.73	0.44	0.69	15.942	-40.1	1
J051703.53+405053.4	166.84	1.65	14.34	0.56	0.74	14.554	-38.4	1
J051938.22+330302.0	173.51	-2.42	13.76	0.53	0.35	13.974	-7.5	1
J052050.62+282125.8	177.53	-4.88	14.63	0.41	0.40	14.841	-50.8	3
J052340.51+345144.5	172.50	-0.70	13.83	0.44	0.33	14.042	-9.0	1
J052423.13+283541.6	177.77	-4.10	13.26	0.29	0.32	13.468	-8.7	1
J052429.89+301950.7	176.34	-3.11	13.63	0.36	0.49	13.840	-14.1	1
J052500.42+294250.0	176.92	-3.36	15.37	0.25	0.30	15.577	-6.5	1
J052502.64+293439.1	177.04	-3.43	13.02	0.40	0.56	13.231	-12.6	3
J052524.19+300543.8	176.65	-3.08	13.58	0.30	0.38	13.788	-13.6	1

Table 4.3. Continued...

NAME	$l(deg)$	$b(deg)$	r	r-i	r-Hα	V	$EW_{H\alpha}$	Ref.
J052541.12+303753.8	176.24	-2.73	14.54	0.36	0.31	14.750	-6.9	1
J052550.06+304551.9	176.15	-2.63	14.54	0.44	0.45	14.752	-8.1	3
J052636.70+392052.4	169.11	2.30	14.63	0.55	0.60	14.844	-28.3	1
J052649.17+291056.6	177.58	-3.33	14.50	0.31	0.36	14.708	-9.8	3
J052701.81+423622.7	166.44	4.18	13.94	0.38	0.52	14.150	-25.8	1
J052704.62+405643.6	167.83	3.26	14.32	0.45	0.51	14.532	-28.8	3
J052717.19+415441.6	167.05	3.83	13.84	0.37	0.49	14.050	-22.3	1
J052754.29+393100.5	169.11	2.60	14.76	0.49	0.60	14.975	-31.8	1
J052813.88+280650.4	178.64	-3.66	15.14	0.40	0.30	15.351	-13.2	3
J052824.43+315446.2	175.50	-1.53	14.51	0.54	0.48	14.724	-6.4	1
J052839.81+264017.2	179.90	-4.38	15.75	0.63	0.40	15.966	-13.2	3
J052850.94+272112.1	179.35	-3.97	14.57	0.44	0.38	14.782	-11.8	1
J052903.87+292609.6	177.64	-2.78	15.46	0.37	0.34	15.670	-7.3	1
J052907.77+285336.1	178.10	-3.07	15.00	0.43	0.42	15.211	-12.3	1
J052919.14+341747.2	173.62	-0.05	13.41	0.29	0.69	13.621	-49.8	1
J052926.22+351610.6	172.82	0.51	13.80	0.38	0.47	14.010	-22.2	1
J052941.92+273400.6	179.28	-3.69	15.08	0.52	0.45	15.293	-24.0	3
J052947.46+332915.5	174.34	-0.42	14.65	0.37	0.33	14.860	-15.6	1
J053015.44+343124.3	173.53	0.23	13.54	0.55	0.59	13.754	-26.6	1
J053024.02+373010.3	171.06	1.90	14.48	0.77	0.75	14.699	-4.0	3
J053035.92+292653.4	177.81	-2.50	13.58	0.46	0.33	13.792	-7.7	1
J053040.91+260534.7	180.64	-4.32	14.71	0.47	0.38	14.922	-7.7	1
J053049.54+294638.8	177.57	-2.27	15.33	0.51	0.46	15.543	-15.3	1
J053054.44+331859.1	174.62	-0.32	13.92	0.72	0.50	14.138	-9.6	1
J053116.68+330327.9	174.87	-0.39	14.40	0.47	0.35	14.612	-9.0	1
J053237.14+260107.3	180.94	-3.99	13.38	0.48	0.47	13.593	-7.5	3
J053304.40+300057.1	177.63	-1.74	15.41	0.72	0.50	15.628	-14.2	1
J053307.98+284749.1	178.66	-2.39	15.63	0.66	0.46	15.847	-15.0	1
J053309.05+291103.1	178.34	-2.17	13.78	0.71	0.64	13.998	-13.8	3
J053349.72+343730.5	173.85	0.91	14.25	0.48	0.65	14.463	-33.0	3
J053447.54+260331.9	181.17	-3.56	12.98	0.26	0.24	13.187	-17.2	3
J053459.32+280743.6	179.45	-2.41	14.36	0.49	0.35	14.573	-8.1	1
J053506.68+410849.2	168.49	4.64	14.34	0.36	0.36	14.550	-11.8	1
J053513.10+295912.4	177.91	-1.36	14.21	0.80	0.57	14.430	-45.5	3
J053532.40+325751.0	175.44	0.30	15.20	0.45	0.38	15.412	-37.1	3
J053534.92+280437.2	179.56	-2.33	14.88	0.50	0.37	15.093	-8.3	1
J053554.13+295756.4	178.01	-1.25	16.07	0.93	0.53	16.293	-4.1	3
J053615.78+242607.1	182.72	-4.15	14.56	0.49	0.37	14.773	-15.1	3
J053635.21+315003.2	176.51	-0.12	13.88	0.45	0.34	14.092	-29.0	1
J053645.74+274624.5	179.96	-2.27	13.65	0.57	0.52	13.865	-15.9	1
J053649.42+371342.8	171.99	2.82	15.83	0.61	0.63	16.046	-10.6	3
J053654.85+301757.8	177.84	-0.88	15.67	0.62	0.62	15.886	-11.7	3
J053707.75+333039.8	175.16	0.88	12.97	0.30	0.55	13.178	-9.9	3
J053814.48+260619.3	181.54	-2.88	13.26	0.57	0.42	13.475	-11.3	1
J053857.23+373003.2	171.98	3.32	14.43	0.39	0.37	14.640	-21.5	1
J053909.17+354422.7	173.50	2.42	13.77	0.76	0.63	13.989	-26.0	1
J053917.89+251535.9	182.39	-3.13	14.88	0.51	0.46	15.093	-17.1	1
J053918.09+361716.3	173.05	2.74	13.78	0.72	0.57	13.998	-26.1	1
J054007.76+315904.1	176.79	0.60	15.70	0.67	0.49	15.917	-27.8	3
J054033.87+274552.4	180.41	-1.56	14.11	0.51	0.35	14.323	-29.4	3
J054153.95+323613.1	176.46	1.24	14.43	0.63	0.68	14.646	-26.9	3
J054159.24+274038.1	180.65	-1.34	12.77	0.53	0.46	12.984	-12.8	3
J054200.54+304956.6	177.97	0.33	14.18	0.48	0.36	14.393	-8.9	3
J054252.85+325435.9	176.31	1.58	13.57	0.49	0.41	13.783	-14.5	1
J054326.82+341123.2	175.28	2.35	12.79	0.39	0.68	13.000	-34.7	3
J054424.58+342802.8	175.14	2.67	15.25	0.42	0.42	15.461	-18.4	1
J054436.71+313658.7	177.60	1.21	12.84	0.46	0.60	13.052	-6.0	3
J054450.31+290754.5	179.74	-0.04	12.88	0.37	0.42	13.090	-32.4	3
J054522.53+210213.5	186.72	-4.15	14.84	0.46	0.51	15.052	-32.6	3
J054553.54+293646.4	179.45	0.40	13.95	0.54	0.50	14.164	-17.8	3
J054603.64+272729.5	181.31	-0.69	13.18	0.55	0.39	13.394	-19.5	3
J054937.88+281123.3	181.09	0.37	13.95	0.33	0.41	14.159	-18.3	1
J054955.18+325007.3	177.14	2.80	15.08	0.75	0.55	15.299	-18.3	1
J055034.99+253827.5	183.39	-0.76	14.91	0.67	0.51	15.127	-17.9	1
J055046.66+324106.0	177.36	2.88	13.93	0.29	0.34	14.138	-9.7	1
J055100.21+245735.1	184.03	-1.03	13.30	0.43	0.37	13.511	-19.8	3
J055118.77+285657.0	180.63	1.07	13.37	0.38	0.43	13.580	-16.3	1
J055125.99+212428.9	187.13	-2.75	14.41	0.32	0.38	14.619	-15.6	1
J055257.22+250622.4	184.12	-0.57	14.64	0.68	0.51	14.857	-17.8	3
J055320.45+281656.6	181.43	1.12	12.96	0.25	0.39	13.167	-15.2	3
J055339.80+315112.6	178.39	2.99	13.65	0.16	0.44	13.859	-26.3	1
J055342.76+215223.3	187.00	-2.06	14.91	0.21	0.87	15.112	-15.1	1
J055350.96+293653.1	180.34	1.89	13.03	0.26	0.42	13.237	-19.3	1
J055423.14+242447.7	184.89	-0.64	15.40	0.57	0.43	15.615	-15.1	1
J055428.68+293310.9	180.46	1.98	13.27	0.27	0.36	13.477	-12.9	1
J055437.81+252106.1	184.10	-0.12	13.84	0.53	0.55	14.054	-20.7	1
J055439.93+320300.4	178.32	3.27	14.06	0.27	0.31	14.267	-6.9	1
J055503.24+291001.4	180.86	1.89	13.44	0.15	0.65	13.645	-44.1	3
J055508.86+241730.0	185.08	-0.55	14.26	0.49	0.46	14.473	-14.6	1
J055517.56+292036.4	180.73	2.02	14.59	0.34	0.39	14.799	-15.4	1
J055524.64+225436.7	186.30	-1.20	13.95	1.02	0.85	14.175	-37.6	1
J055538.03+255133.6	183.78	0.33	13.61	0.52	0.51	13.823	-19.6	1
J055538.64+185156.8	189.83	-3.19	13.68	0.43	0.42	13.891	-8.6	1
J055552.55+251714.0	184.30	0.09	14.60	0.65	0.68	14.817	-32.7	1
J055558.82+254846.4	183.86	0.38	14.72	0.57	0.54	14.935	-22.5	1
J055607.14+243347.7	184.96	-0.23	15.46	0.50	0.37	15.673	-9.6	3
J055638.79+190355.8	189.77	-2.88	14.91	0.67	0.64	15.127	-22.9	1
J055650.22+190537.3	189.77	-2.83	14.80	0.52	0.45	15.013	-16.8	1
J055746.88+224033.2	186.78	-0.84	15.04	0.69	0.47	15.258	9.8	1
J055801.70+192238.7	189.67	-2.44	15.01	0.77	0.63	15.229	-23.8	1
J055824.07+142741.8	193.99	-4.81	13.90	0.17	0.34	14.105	-10.1	1
J055831.49+264236.3	183.37	1.32	14.50	0.53	0.65	14.714	-41.0	1
J055838.98+201108.6	189.04	-1.91	13.47	0.57	0.37	13.685	-13.4	1
J055851.85+260054.3	184.01	1.04	15.11	0.43	0.68	15.321	-43.2	1
J055852.97+303000.5	180.12	3.27	13.07	0.25	0.26	13.277	-8.1	1
J055854.14+220300.2	187.45	-0.93	14.70	0.51	0.44	14.913	-15.1	1
J055855.66+331231.3	177.76	4.62	15.31	0.34	0.41	15.519	-10.1	1
J055926.03+271328.8	183.02	1.75	14.67	0.42	0.42	14.881	-16.7	1
J055931.30+201959.8	189.01	-1.66	14.68	0.50	0.37	14.893	-15.7	1
J055936.06+255150.2	184.22	1.11	15.16	0.46	0.42	15.372	-14.3	1
J055951.57+142840.2	194.15	-4.49	13.76	0.20	0.41	13.966	-21.6	1
J055956.97+213011.8	188.05	-0.99	13.35	0.71	0.64	13.568	-26.8	3
J060128.98+165957.4	192.14	-2.91	14.69	0.47	0.46	14.902	-24.3	3
J060302.63+311723.9	179.87	4.44	14.58	0.41	0.45	14.791	-12.7	3
J060541.43+305126.3	180.53	4.73	13.22	0.24	0.37	13.427	-12.8	1
J060558.53+105731.7	197.96	-4.91	14.65	0.14	0.30	14.854	-8.4	1
J060602.06+271527.4	183.72	3.05	13.93	0.34	0.46	14.139	-20.7	1
J060705.99+264108.3	184.33	2.97	14.29	0.37	0.53	14.500	-32.6	1
J060729.66+233600.8	187.08	1.56	13.79	0.14	0.43	13.993	-14.9	1
J060803.63+174100.8	192.31	-1.20	14.29	0.74	0.63	14.509	-21.1	1
J060926.17+244107.9	186.34	2.47	15.17	0.20	0.36	15.378	-15.2	1
J060934.04+150245.0	194.80	-2.17	14.11	0.56	0.59	14.324	-28.3	1
J060943.25+191607.8	191.12	-0.09	15.05	0.46	0.60	15.264	-45.2	1
J061009.23+245125.7	186.27	2.69	14.90	0.39	0.45	15.107	-16.0	1
J061256.09+151534.2	195.00	-1.35	14.50	0.49	0.53	14.713	-22.6	1
J061318.83+152524.7	194.90	-1.19	15.68	0.69	0.90	15.898	-75.3	3
J061341.91+140419.4	196.13	-1.76	13.83	0.68	0.69	14.047	-31.5	3
J061351.59+201709.1	190.69	1.25	13.82	0.71	0.63	14.038	-29.1	3
J061501.84+205722.8	190.23	1.81	14.79	0.66	0.57	15.007	-22.5	1
J061535.86+103122.4	199.48	-3.04	14.22	0.35	0.44	14.429	-19.0	1
J061622.52+222110.0	189.15	2.75	14.07	0.86	0.70	14.292	-29.3	3
J061658.93+251525.9	186.65	4.24	13.65	0.32	0.40	13.859	-16.2	1

Table 4.3. Continued...

NAME	$l(deg)$	$b(deg)$	r	r-i	r-Hα	V	$EW_{H\alpha}$	Ref.
J054640.73+240939.5	184.20	-2.28	15.09	0.51	0.41	15.303	-10.4	1
J054705.80+223410.0	185.62	-3.02	14.88	0.51	0.51	15.093	-17.6	1
J054806.31+302129.0	179.06	1.20	13.62	0.61	0.57	13.838	-22.2	1
J054818.58+214945.5	186.40	-3.16	14.42	0.31	0.66	14.628	-41.5	1
J054828.23+304607.8	178.75	1.48	13.33	0.34	0.31	13.539	-7.9	1
J054828.90+312019.6	178.27	1.77	14.52	0.32	0.36	14.729	-14.1	1
J054836.10+190733.1	188.76	-4.49	14.19	0.36	0.44	14.400	-18.5	1
J054837.64+281710.3	180.90	0.23	14.71	0.59	0.71	14.925	-40.3	1
J054848.26+283547.8	180.65	0.42	14.72	0.61	0.69	14.936	-41.4	1
J062109.79+101511.5	200.36	-1.96	14.67	0.42	0.72	14.881	-46.5	1
J062121.82+141413.4	196.87	-0.04	13.78	0.45	0.56	13.992	-25.2	1
J062245.04+213111.9	190.59	3.66	13.72	0.33	0.44	13.929	-29.0	1
J062252.06+144918.7	196.52	0.55	13.48	0.53	0.45	13.694	-13.5	1
J062306.42+224659.8	189.50	4.32	14.95	0.66	0.46	15.167	-19.4	1
J062406.11+143614.8	196.85	0.72	14.37	0.52	0.66	14.583	-32.9	1
J062456.26+092740.0	201.50	-1.51	15.42	0.35	0.45	15.629	-18.7	1
J062502.16+152610.6	196.22	1.30	13.37	0.30	0.46	13.578	-15.4	1
J062529.35+073117.7	203.28	-2.29	13.64	0.43	0.63	13.851	-32.2	3
J062538.89+062506.5	204.27	-2.77	14.82	0.40	0.43	15.031	-15.7	1
J062728.07+045458.0	205.82	-3.07	15.55	0.74	0.59	15.769	-24.8	1
J062808.68+012343.4	209.02	-4.54	13.78	0.44	0.65	13.992	-34.5	3
J063049.29+001016.3	210.42	-4.51	15.95	0.57	0.48	16.165	-14.1	1
J063103.40+032323.6	207.59	-2.98	14.96	0.65	0.63	15.177	-25.7	3
J063119.96+010043.1	209.73	-4.01	14.36	0.55	0.61	14.574	-31.8	1
J063148.63+151010.0	197.22	2.63	13.45	0.37	0.50	13.660	-23.1	1
J063224.63+020609.5	208.89	-3.27	14.61	0.52	0.43	14.823	-10.8	1
J063238.08+054143.0	205.72	-1.57	14.86	0.69	0.50	15.078	-30.7	3
J063241.75+045338.3	206.44	-1.92	12.57	0.23	0.53	12.777	-30.1	3
J063324.80+052742.4	206.02	-1.50	14.73	0.72	0.50	14.948	-9.9	3
J063554.840024244.8	213.58	-4.69	13.48	0.64	0.93	13.696	-66.5	1
J063605.850022556.3	213.35	-4.52	15.33	0.73	0.71	15.549	-40.5	1
J063607.59-014610.6	212.76	-4.21	14.77	0.66	0.52	14.987	-18.0	3
J063637.480022128.3	213.34	-4.37	15.28	0.91	0.75	15.503	-37.2	1
J063639.47+012451.7	209.99	-2.64	16.45	0.57	0.81	16.668	-41.9	1
J063642.03+053425.8	206.29	-0.72	14.07	0.44	0.44	14.282	-22.0	1
J063643.350042748.3	215.24	-5.30	13.51	0.36	0.35	13.719	-8.4	1
J063647.63+070015.6	205.03	-0.05	15.46	0.68	0.47	15.677	-16.8	1
J063651.99+021103.8	209.32	-2.24	13.57	0.55	0.44	13.784	-20.5	1
J063702.88+012047.9	210.09	-2.59	13.57	0.62	0.65	13.786	-32.9	1
J063802.43+015937.0	209.63	-2.07	13.81	0.63	0.61	14.026	-27.6	1
J063841.53-005657.9	212.32	-3.27	13.32	0.74	0.64	13.539	-28.2	3
J063846.25+034325.0	208.17	-1.11	14.20	0.71	0.48	14.418	-15.5	1
J063924.49+011917.1	210.38	-2.07	15.94	0.59	0.57	16.155	-24.9	1
J063933.99+061149.1	206.07	0.20	13.90	0.41	0.39	14.111	-13.3	1

NAME	$l(deg)$	$b(deg)$	r	r-i	r-Hα	V	$EW_{H\alpha}$	Ref.
J061702.42+214726.7	189.72	2.62	14.97	0.46	0.47	15.182	-16.0	1
J061720.96+102255.8	199.80	-2.73	13.34	0.50	0.50	13.553	-16.1	1
J061812.82+111641.8	199.11	-2.12	14.96	0.43	0.50	15.171	-18.3	1
J061926.67+045535.8	204.88	-4.83	13.26	0.15	0.75	13.467	-26.3	1
J061938.87+090115.1	201.27	-2.87	14.56	0.26	0.37	14.767	-11.5	1
J061950.15+221607.6	189.61	3.42	14.37	0.50	0.48	14.583	-17.4	3
J062010.01+135204.4	197.06	-0.47	13.75	0.59	0.49	13.965	-15.5	1
J062026.19+090100.9	201.37	-2.70	14.22	0.29	0.30	14.428	-10.4	1
J062028.45+144418.3	196.32	0.00	15.19	0.71	0.56	15.408	-22.0	1
J190738.21+093533.1	43.31	0.80	14.47	0.96	0.60	14.694	-22.2	1
J191033.510010724.9	34.11	-4.77	15.48	0.43	0.39	15.691	-19.6	1
J191323.23+175527.4	51.35	3.40	14.97	0.70	0.67	15.188	-38.5	1
J191407.66+043537.8	39.61	-2.93	14.71	0.60	0.41	14.925	-6.4	3
J191713.73+143442.4	48.81	1.03	14.23	0.72	0.58	14.448	-20.6	1
J192513.62+155452.9	50.90	-0.04	13.73	0.88	0.58	13.952	-24.5	1
J192717.83+121041.1	47.85	-2.26	14.27	0.63	0.53	14.486	-22.9	1
J192735.18+142745.3	49.89	-1.23	14.03	0.73	0.57	14.249	-21.6	1
J192848.86+225217.2	57.42	2.53	15.90	0.71	0.52	16.118	-2.4	3
J192854.74+240302.9	58.47	3.07	14.04	0.82	0.77	14.261	-32.4	1
J192909.75+190933.3	54.20	0.68	14.89	0.74	0.72	15.109	-40.0	3
J192953.87+191435.6	54.36	0.57	14.82	0.76	0.58	15.039	-14.4	1
J193058.97+173838.8	53.08	-0.42	14.08	0.79	0.56	14.300	12.5	3
J193142.88+164552.9	52.39	-1.00	13.07	0.63	0.58	13.286	-19.1	1
J193150.00+204105.8	55.84	0.86	15.02	0.94	0.67	15.244	-23.3	3
J193217.78+095748.5	46.48	-4.39	13.19	0.20	0.31	13.396	-8.3	1
J193219.96+274126.1	62.04	4.13	15.34	0.33	0.31	15.549	-5.9	1
J193231.66+185254.9	54.34	-0.15	15.42	0.93	0.65	15.643	-20.7	1
J193232.88+151711.5	51.19	-1.89	14.16	0.89	0.92	14.382	-56.1	1
J193304.15+172408.7	53.10	-0.98	13.53	0.90	0.66	13.753	-26.6	1
J193315.02+205259.9	56.17	0.67	14.48	0.84	0.72	14.701	-30.3	3
J193323.02+195848.2	55.40	0.20	14.28	0.96	0.85	14.504	-41.2	1
J193420.54+262349.9	61.12	3.12	15.53	0.50	0.62	15.743	-31.5	1
J193424.63+180101.3	53.80	-0.96	14.36	0.82	0.66	14.581	-26.8	1
J193431.65+233208.6	58.64	1.69	14.86	0.54	0.44	15.074	-1.9	1
J193544.33+302057.8	64.74	4.75	16.13	0.30	0.32	16.338	-5.6	1
J193601.96+260903.7	61.09	2.67	14.20	0.31	0.30	14.408	-7.1	3
J193612.44+304319.3	65.12	4.84	15.28	0.28	0.72	15.488	-44.9	1
J193656.49+234138.0	59.04	1.29	13.72	0.94	0.72	13.944	-31.3	3
J193746.91+181719.0	54.42	-1.53	13.72	0.77	0.55	13.939	-14.0	3
J193820.57+233814.6	59.15	0.98	14.85	0.52	0.43	15.063	-5.4	1
J193821.61+292525.3	64.21	3.81	15.22	0.23	0.48	15.427	-21.9	1
J193842.60+242349.8	59.85	1.28	15.12	0.49	0.43	15.333	-11.3	1
J193859.63+282106.3	63.34	3.16	15.77	0.45	0.51	15.982	-20.6	1
J193939.56+182919.9	54.82	-1.82	14.76	0.59	0.53	14.975	-20.1	1

Table 4.3. Continued...

NAME	$l(deg)$	$b(deg)$	r	r-i	r-Hα	V	$EW_{H\alpha}$	Ref.
J063938.71+054049.9	206.53	-0.02	15.56	0.53	0.50	15.774	-17.8	1
J063947.29+042801.1	207.63	-0.55	14.34	0.52	0.50	14.553	-19.7	1
J064035.030015647.8	213.43	-3.30	14.56	0.47	0.53	14.772	-25.0	1
J064111.04-005845.7	212.63	-2.73	13.40	0.33	0.40	13.609	-16.9	3
J064116.510010740.2	212.78	-2.78	13.14	0.62	0.85	13.356	-56.9	1
J064132.010012549.5	213.08	-2.86	13.72	0.35	0.29	13.929	-9.9	1
J064132.750020811.9	213.71	-3.17	15.48	0.53	0.55	15.694	-23.2	1
J064137.190035546.1	215.32	-3.97	13.03	0.26	0.39	13.237	-14.3	1
J064203.29+002009.8	211.56	-1.93	14.39	0.63	0.61	14.606	-29.1	1
J064222.510005519.2	212.72	-2.44	14.88	0.04	0.37	15.084	-12.6	1
J064235.23+004321.3	211.28	-1.64	13.62	0.51	0.67	13.833	-34.3	3
J064257.880013413.4	213.36	-2.60	15.75	0.39	0.39	15.960	-14.7	1
J064308.21+000513.3	211.91	-1.81	14.72	0.27	0.35	14.927	-15.1	1
J064308.31+042635.8	208.03	0.18	14.11	0.63	0.39	14.328	-10.0	1
J064322.65+071825.5	205.51	1.54	14.99	0.53	0.47	15.202	-19.2	1
J064350.82+012411.8	210.82	-1.05	15.05	0.40	0.44	15.261	-16.4	1
J064413.11-032821.8	215.20	-3.19	14.46	0.63	0.63	14.676	-29.3	3
J064944.840023211.4	215.00	-1.53	15.13	0.51	0.38	15.343	-12.0	1
J064949.760025321.2	215.32	-1.67	14.25	0.51	0.48	14.463	-26.4	1
J065947.09-011856.4	215.05	1.26	15.00	0.35	0.49	15.209	-22.2	3
J070343.050010021.2	215.23	2.27	15.07	0.27	0.34	15.277	-9.3	1
J184213.54+054406.0	37.00	4.65	15.11	0.62	0.75	15.326	-23.4	1
J184732.64+021206.0	34.45	1.87	15.01	1.17	0.78	15.239	-25.5	3
J184836.27+060954.8	38.10	3.43	13.93	1.07	0.80	14.157	-47.7	1
J185106.38+102410.6	42.17	4.80	15.85	0.91	0.56	16.073	-0.9	3
J185235.000003835.3	32.49	-0.55	14.59	0.73	0.58	14.806	-13.4	1
J185237.90+000158.2	33.10	-0.25	13.61	0.80	0.85	13.830	-49.5	1
J185505.84+113353.4	43.66	4.44	16.61	0.30	0.45	16.818	-17.7	1
J185510.540002541.2	32.98	-1.03	13.92	0.69	0.78	14.140	-18.9	1
J185553.90+120723.4	44.25	4.52	16.21	0.35	0.38	16.419	-12.0	1
J185555.15-010404.7	32.49	-1.48	14.23	0.51	0.48	14.443	-15.4	3
J190032.980044849.5	29.68	-4.22	13.57	0.62	0.63	13.786	-24.6	1
J190303.430020008.8	32.47	-3.50	13.20	0.38	0.42	13.410	-16.7	1
J190322.42+160919.5	48.68	4.73	15.54	0.59	0.67	15.755	-33.6	3
J190725.36+115121.7	45.29	1.89	13.54	0.68	0.52	13.757	-18.1	1
J195127.35+233225.0	60.57	-1.67	14.37	0.68	0.58	14.587	-19.0	1
J195131.85+322513.6	68.22	2.85	15.29	0.55	0.44	15.504	3.0	1
J195132.89+301650.5	66.38	1.76	14.48	0.43	0.38	14.691	-8.1	1
J195140.83+295020.7	66.01	1.51	14.05	0.37	0.36	14.260	-5.2	1
J195144.62+310315.9	67.06	2.12	14.52	0.45	0.40	14.732	-7.0	1
J195157.17+290739.5	65.43	1.09	14.12	0.32	0.34	14.329	-5.0	1
J195159.86+290706.7	65.43	1.08	15.55	0.66	0.51	15.767	-18.2	1
J195207.94+342745.3	70.04	3.78	14.52	0.28	0.32	14.728	-7.7	1
J195336.43+314424.3	67.86	2.12	14.37	0.57	0.45	14.585	-12.3	1
J195509.84+305528.0	67.33	1.42	13.95	0.38	0.46	14.160	-13.0	1
J195536.17+321122.4	68.46	1.99	14.50	0.58	0.65	14.715	-26.5	1
J195609.20+313233.6	67.97	1.56	14.45	0.59	0.48	14.665	-11.4	3
J195709.69+315756.8	68.44	1.60	13.63	0.56	0.40	13.844	-8.1	1
J195724.98+293118.3	66.38	0.28	14.37	0.40	0.39	14.581	8.7	1
J195727.87+300724.0	66.90	0.58	13.94	0.58	0.67	14.155	-27.5	1
J195734.37+324457.4	69.15	1.93	13.95	0.49	0.69	14.163	-42.2	1
J195738.31+321933.5	68.80	1.70	14.26	0.45	0.43	14.472	-12.2	1
J195755.13+262252.2	63.76	-1.46	13.59	0.66	0.48	13.807	1.6	1

NAME	$l(deg)$	$b(deg)$	r	r-i	r-Hα	V	$EW_{H\alpha}$	Ref.
J193959.63+182311.7	54.77	-1.94	14.16	0.62	0.65	14.376	-29.8	1
J194000.25+204730.0	56.86	-0.75	13.90	0.73	0.60	14.119	-18.5	3
J194011.81+290729.1	64.14	3.31	15.25	0.23	0.35	15.457	-6.0	1
J194017.66+190709.6	55.44	-1.64	14.89	0.71	0.58	15.108	-17.7	3
J194046.54+195524.6	56.20	-1.34	13.40	0.51	0.50	13.613	-18.0	1
J194118.59+141802.9	51.36	-4.22	13.49	0.23	0.31	13.697	-3.8	1
J194139.39+183400.4	55.12	-2.19	13.29	0.62	0.82	13.506	-31.3	1
J194155.60+250424.1	60.80	0.98	13.55	0.71	0.55	13.768	-14.6	1
J194254.42+275201.3	63.34	2.17	13.81	0.51	0.56	14.023	-23.2	1
J194304.40+231848.6	59.41	-0.12	13.37	0.45	0.61	13.582	-38.3	1
J194305.24+205057.8	57.27	-1.35	13.67	0.75	0.61	13.889	-22.5	3
J194307.51+232602.9	59.52	-0.07	14.85	0.57	0.54	15.065	-24.5	3
J194338.78+302510.1	65.64	3.30	15.09	0.34	0.37	15.299	-10.2	1
J194448.05+265152.2	62.68	1.31	14.23	0.58	0.51	14.445	-13.5	3
J194519.94+193218.0	56.39	-2.46	14.27	0.45	0.43	14.482	-10.4	1
J194528.53+171707.2	54.46	-3.61	14.97	0.28	0.43	15.178	-20.3	1
J194534.27+285637.5	64.57	2.20	15.49	0.51	0.71	15.703	-40.4	1
J194536.66+315906.7	67.21	3.71	15.32	0.44	0.55	15.532	-26.1	1
J194602.43+283918.8	64.37	1.97	15.80	0.54	0.44	16.014	-11.4	1
J194617.86+230454.0	59.57	-0.88	14.99	0.87	0.66	15.212	-24.9	1
J194628.92+243732.1	60.93	-0.14	15.11	0.68	0.72	15.327	-48.0	1
J194657.96+282340.4	64.24	1.66	15.89	0.71	0.81	16.108	-45.7	3
J194700.37+201035.1	57.14	-2.48	13.31	0.49	0.45	13.523	-10.2	1
J194731.34+273416.5	63.59	1.14	13.16	0.54	0.53	13.374	-24.4	1
J194756.66+320712.0	67.57	3.35	13.92	0.49	0.81	14.133	-25.0	3
J194843.72+205529.5	57.99	-2.45	14.33	0.37	0.35	14.540	-8.3	1
J194854.73+324518.2	68.23	3.50	14.91	0.42	0.51	15.121	-18.7	1
J194905.14+271001.3	63.42	0.64	14.66	0.55	0.51	14.874	-12.7	1
J195001.05+212312.1	58.55	-2.48	13.28	0.38	0.44	13.490	-12.7	1
J195035.05+172854.6	55.24	-4.57	15.47	0.23	0.60	15.677	-40.1	1
J195053.47+274338.7	64.11	0.58	14.26	0.52	0.47	14.473	-20.6	1
J195103.15+251610.4	62.01	-0.71	13.68	0.98	0.64	13.905	-18.4	3
J195119.77+305755.0	66.94	2.15	15.77	0.41	0.45	15.981	-7.0	3
J195124.41+295306.7	66.02	1.58	13.50	0.38	0.42	13.710	-12.4	3
J195126.93+295335.8	66.03	1.58	13.95	0.37	0.49	14.160	-18.2	1
J213938.16+533454.5	96.77	0.75	15.07	0.58	0.51	15.285	-11.4	1
J213956.59+484214.3	93.58	-2.95	13.45	0.34	0.36	13.659	-10.2	1
J214010.25+512640.1	95.42	-0.91	15.30	0.70	0.50	15.518	-16.9	1
J214014.93+540011.1	97.12	1.00	14.65	0.65	0.50	14.867	-12.7	1
J214713.52+564929.8	99.71	2.50	14.76	0.82	0.70	14.981	-26.1	3
J214941.64+525925.7	97.53	-0.68	13.33	0.58	0.59	13.545	-20.9	1
J215636.84+591153.4	102.17	3.57	13.41	0.65	0.68	13.627	-31.8	1
J215713.34+542035.4	99.25	-0.31	14.74	0.51	0.40	14.953	9.9	1
J215816.96+523953.2	98.35	-1.74	15.22	0.53	0.45	15.434	-17.4	1
J215828.17+562855.1	100.70	1.27	15.21	0.64	0.44	15.426	-10.1	1
J215856.22+564705.8	100.93	1.47	13.88	0.57	0.66	14.095	-31.1	1
J215923.75+592919.7	102.63	3.58	13.80	0.44	0.39	14.012	-13.1	1
J215934.48+525438.6	98.65	-1.66	14.56	0.55	0.67	14.774	-28.0	1
J215950.24+570056.1	101.17	1.58	15.12	0.76	0.57	15.339	-18.3	1
J220117.18+541450.7	99.66	-0.75	13.83	0.56	0.55	14.044	-17.6	1
J220215.50+524654.4	98.90	-2.01	13.24	0.48	0.38	13.453	-9.6	1
J220246.29+523551.3	98.85	-2.20	13.39	0.38	0.38	13.600	-11.3	1
J220352.65+560625.5	101.07	0.52	14.25	0.68	0.64	14.467	-20.6	3

Table 4.3. Continued...

NAME	$l(deg)$	$b(deg)$	r	r-i	r-Hα	V	$EW_{H\alpha}$	Ref.
J195833.75+315206.3	68.51	1.29	13.57	0.45	0.72	13.782	-45.9	1
J195837.46+304811.3	67.61	0.72	13.81	0.60	0.61	14.025	-18.1	3
J195855.89+305045.9	67.68	0.69	13.69	0.77	0.73	13.909	-22.7	1
J195904.26+304118.5	67.56	0.58	15.08	0.80	0.64	15.300	-17.2	3
J195908.62+275733.7	65.25	-0.86	15.52	0.83	0.66	15.741	-12.0	3
J195911.59+322726.1	69.08	1.49	13.27	0.51	0.51	13.483	-10.3	1
J195916.79+333713.5	70.08	2.08	14.24	0.53	0.40	14.454	-8.8	1
J195926.59+281542.9	65.54	-0.76	14.28	0.69	0.58	14.498	-22.6	3
J195928.14+305311.8	67.78	0.61	14.53	0.59	0.58	14.745	-28.0	1
J195939.51+305645.9	67.85	0.61	13.69	0.41	0.52	13.901	-23.4	3
J195956.08+372139.5	73.35	3.92	13.70	0.26	0.39	13.907	-28.7	1
J195959.94+310352.5	67.99	0.61	13.58	0.68	0.61	13.797	-19.4	1
J200008.06+300700.5	67.20	0.08	13.85	0.51	0.40	14.063	-10.6	1
J200017.42+313553.9	68.48	0.84	13.80	0.54	0.42	14.014	-5.8	1
J200022.20+324303.8	69.44	1.41	14.07	0.54	0.45	14.284	-3.3	1
J200358.72+320803.4	69.34	0.46	14.10	0.44	0.55	14.312	-24.2	1
J200401.24+340235.1	70.96	1.47	13.95	0.51	0.44	14.163	-9.5	1
J200440.83+331106.3	70.31	0.89	14.60	0.42	0.41	14.811	-8.0	3
J200516.96+321046.4	69.53	0.25	13.05	0.60	0.54	13.265	-19.3	1
J200828.04+343218.8	71.88	0.96	13.21	0.54	0.43	13.424	-12.0	3
J201501.37+355022.1	73.70	0.55	14.71	0.72	0.60	14.928	-21.2	3
J201808.03+405050.4	78.20	2.84	13.56	0.94	0.69	13.784	-30.6	1
J201831.97+404247.5	78.13	2.70	13.64	0.42	0.40	13.851	-16.1	1
J201924.58+370740.7	75.26	0.54	13.98	0.49	0.49	14.193	-12.3	1
J203955.62+454446.8	84.49	2.49	13.64	0.63	0.46	13.856	4.1	1
J205432.12+401959.4	81.95	-2.98	13.66	0.63	0.48	13.876	-11.8	1
J205446.99+500442.6	89.43	3.26	13.47	0.78	0.71	13.690	-39.2	3
J205637.42+463659.9	86.99	0.79	14.32	0.58	0.58	14.535	-17.8	3
J205726.50+461315.3	86.78	0.43	14.15	0.50	0.64	14.363	-29.7	1
J205929.49+393523.3	82.00	-4.19	14.72	0.32	0.54	14.929	-24.7	3
J205931.56+443544.5	85.79	-0.91	13.61	0.59	0.50	13.825	-19.9	1
J205958.73+451656.7	86.36	-0.52	13.32	0.59	0.57	13.535	-16.3	1
J210019.66+454138.2	86.71	-0.30	13.93	0.37	0.33	14.140	6.1	1
J210029.50+443655.5	85.92	-1.03	13.58	0.38	0.38	13.790	1.0	1
J210035.96+462506.7	87.29	0.15	13.67	0.30	0.28	13.878	5.1	1
J210252.23+451005.1	86.61	-0.98	15.46	0.65	0.48	15.677	-31.5	1
J210259.03+442947.9	86.12	-1.44	13.54	0.52	0.63	13.753	-34.0	1
J210323.60+450033.1	86.55	-1.15	13.38	0.31	0.37	13.588	-14.8	1
J210330.04+450104.4	86.57	-1.16	14.64	0.51	0.62	14.853	-30.0	1
J210348.39+450316.3	86.64	-1.18	15.20	0.51	0.59	15.413	-27.4	1
J211120.60+414917.4	85.17	-4.37	13.92	0.51	0.40	14.133	-8.8	1
J212128.76+561218.8	96.67	4.45	13.35	0.79	0.61	13.570	-23.7	3
J212148.79+461357.0	89.66	-2.65	13.93	0.60	0.53	14.145	-24.5	1
J212246.10+485845.2	91.71	-0.82	13.57	0.57	0.59	13.785	-16.0	1
J212448.52+561054.6	96.98	4.10	13.87	0.56	0.42	14.084	-8.3	1
J212738.50+494219.4	92.78	-0.85	13.38	0.57	0.51	13.595	-15.9	1
J213238.74+483601.7	92.62	-2.21	13.28	0.25	0.46	13.487	-14.4	1
J213534.79+533116.1	96.28	1.10	13.96	0.50	0.55	14.173	-23.4	1
J213808.05+494645.1	94.08	-1.94	13.71	0.24	0.30	13.917	-0.8	1
J213828.34+530209.3	96.28	0.45	14.31	0.73	0.59	14.529	-18.4	3
J213901.74+532301.1	96.57	0.66	14.65	0.75	0.47	14.869	-28.5	1
J213910.99+565115.2	98.89	3.24	14.92	0.57	0.54	15.135	-18.5	1

NAME	$l(deg)$	$b(deg)$	r	r-i	r-Hα	V	$EW_{H\alpha}$	Ref.
J220426.56+575143.1	102.17	1.89	15.26	0.50	0.51	15.473	-13.2	3
J220431.39+565346.0	101.61	1.10	15.44	0.63	0.46	15.656	-12.4	1
J220508.23+553036.2	100.86	-0.07	14.32	0.40	0.47	14.531	-20.4	1
J220518.19+540246.8	100.01	-1.26	14.05	0.39	0.40	14.260	-12.5	3
J220531.37+513312.7	98.57	-3.29	13.62	0.19	0.32	13.826	-8.0	1
J220547.66+525354.0	99.40	-2.23	14.62	0.43	0.40	14.831	-12.5	1
J220601.27+535732.1	100.05	-1.40	13.64	0.47	0.65	13.852	-35.2	3
J220635.01+581158.1	102.60	1.99	15.53	0.67	0.55	15.747	-29.6	1
J220646.36+553645.0	101.11	-0.12	14.22	0.36	0.34	14.430	-7.6	3
J220709.48+545425.7	100.74	-0.72	14.27	0.45	0.45	14.482	-8.9	1
J220724.56+520246.0	99.10	-3.07	16.06	0.22	0.36	16.266	-14.8	1
J220750.41+545409.7	100.82	-0.79	13.79	0.44	0.32	14.002	-7.7	1
J220835.26+570037.4	102.13	0.87	14.85	0.63	0.44	15.066	-11.4	1
J220851.62+591752.0	103.48	2.71	15.32	0.63	0.51	15.536	-17.7	3
J220901.08+550946.6	101.10	-0.67	15.35	0.53	0.42	15.564	-14.9	3
J220923.01+552821.4	101.33	-0.45	14.54	0.62	0.45	14.756	-7.4	1
J221135.71+600311.2	104.20	3.13	13.81	0.53	0.49	14.024	-10.5	3
J221150.88+564020.3	102.30	0.34	13.52	0.48	0.60	13.733	-28.2	1
J221158.97+533236.5	100.53	-2.24	13.89	0.34	0.26	14.099	4.0	3
J221207.58+574516.1	102.95	1.20	14.38	0.56	0.45	14.594	-14.8	1
J221214.02+560255.2	101.98	-0.21	14.66	0.51	0.37	14.873	-9.2	1
J221218.99+554040.5	101.78	-0.52	15.14	0.68	0.54	15.357	7.9	1
J221245.10+571439.9	102.72	0.74	14.21	0.56	0.36	14.424	4.7	1
J221247.29+581029.4	103.26	1.50	15.34	0.92	0.70	15.563	-32.3	3
J221252.17+585650.4	103.70	2.13	15.64	0.91	0.73	15.863	-41.6	1
J221321.11+524315.1	100.23	-3.04	13.80	0.20	0.36	14.006	-12.6	1
J221423.13+574724.9	103.21	1.06	14.95	0.65	0.57	15.167	-16.2	3
J221426.75+543806.1	101.44	-1.55	15.73	0.33	0.32	15.939	-7.8	3
J221541.81+554224.2	102.19	-0.76	14.67	0.43	0.42	14.881	-14.0	3
J221557.35+564511.7	102.81	0.08	13.44	0.57	0.62	13.655	-23.9	1
J221602.76+532235.5	100.93	-2.72	13.72	0.22	0.37	13.926	-13.1	1
J221606.05+544827.4	101.74	-1.54	14.94	0.28	0.29	15.148	-3.2	3
J221838.77+561056.8	102.80	-0.60	15.59	0.53	0.42	15.804	-13.6	3
J221909.03+554624.3	102.63	-0.98	15.05	0.58	0.45	15.265	-10.5	3
J222146.00+544138.6	102.36	-2.09	13.09	0.19	0.69	13.296	-43.1	3
J222241.88+544700.8	102.52	-2.08	13.96	0.29	0.30	14.168	-8.9	1
J222300.94+573545.8	104.07	0.26	14.03	0.47	0.40	14.242	-10.0	1
J222326.76+561736.1	103.42	-0.87	13.47	0.37	0.37	13.680	-12.5	1
J222345.10+552206.5	102.96	-1.67	13.72	0.29	0.57	13.928	-29.3	3
J222442.04+563429.7	103.72	-0.72	14.65	0.49	0.72	14.863	-45.5	3
J222453.54+564126.9	103.80	-0.64	14.63	0.46	0.41	14.842	-16.9	1
J222513.15+580638.1	104.59	0.54	14.12	0.44	0.35	14.332	-9.3	1
J222522.96+575546.5	104.51	0.38	13.72	0.41	0.53	13.931	-18.3	3
J222554.20+574812.6	104.51	0.23	13.47	0.35	0.35	13.679	-11.4	1
J222605.29+584410.6	105.02	1.01	13.05	0.54	0.41	13.264	-10.7	1
J222706.13+560201.7	103.71	-1.36	13.88	0.42	0.36	14.091	-9.6	1
J222722.87+572039.7	104.43	-0.26	14.86	0.42	0.39	15.071	-12.7	3
J222845.91+580839.9	105.01	0.33	14.05	0.74	0.64	14.269	-27.5	3
J222914.63+580019.4	104.99	0.17	13.27	0.41	0.52	13.481	-31.8	1
J222916.87+570513.9	104.52	-0.61	13.90	0.35	0.47	14.109	-20.3	1
J222928.54+562914.3	104.23	-1.14	14.90	0.60	0.51	15.115	-14.2	3
J222949.80+552437.8	103.72	-2.09	14.26	0.32	0.39	14.469	-16.0	1

Table 4.3. Continued...

NAME	$l(deg)$	$b(deg)$	r	r-i	r-Hα	V	$EW_{H\alpha}$	Ref.
J223009.30+600422.4	106.16	1.89	13.87	0.62	0.29	14.086	3.2	3
J223112.30+551642.7	103.82	-2.30	15.23	0.45	0.57	15.442	-22.1	3
J223344.50+582438.4	105.71	0.22	13.89	0.42	0.42	14.101	-14.3	1
J223344.77+580959.4	105.58	0.01	14.05	0.34	0.36	14.259	-11.6	1
J223406.67+553734.8	104.35	-2.21	13.84	0.42	0.53	14.051	-30.2	1
J223424.64+534204.3	103.42	-3.90	15.20	0.49	0.44	15.413	-17.1	3
J223437.81+574319.4	105.46	-0.43	15.09	0.54	0.37	15.304	-10.0	1
J223612.77+584154.8	106.13	0.31	13.28	0.83	0.70	13.501	-34.3	3
J223625.68+560319.6	104.85	-2.00	13.89	0.37	0.29	14.100	-4.9	1
J223646.32+552828.1	104.60	-2.53	13.79	0.70	0.45	14.008	-11.7	1
J223701.42+571847.6	105.54	-0.95	15.13	0.64	0.54	15.346	-28.4	1
J223812.36+640543.0	109.00	4.89	14.99	0.72	0.48	15.208	-16.8	1
J223824.52+561809.5	105.21	-1.92	14.40	0.30	0.26	14.608	-9.0	1
J223825.84+574739.1	105.94	-0.62	14.63	0.42	0.37	14.841	-2.7	1
J223828.77+631340.0	108.60	4.12	13.59	0.57	0.79	13.805	-36.2	1
J223854.62+591250.7	106.69	0.59	14.95	0.77	0.80	15.169	-38.4	3
J223952.52+585813.9	106.68	0.32	13.17	0.65	0.49	13.387	2.7	1
J224137.35+575256.7	106.35	-0.75	13.71	0.23	0.22	13.917	-4.3	1
J224153.04+551033.8	105.09	-3.14	13.89	0.34	0.18	14.099	5.7	3
J224201.01+551951.9	105.18	-3.02	15.22	0.25	0.15	15.427	5.0	3
J224230.86+570157.6	106.05	-1.55	14.76	0.35	0.37	14.969	-8.8	1
J224354.23+553146.6	105.51	-2.97	14.31	0.43	0.41	14.521	-11.3	1
J224417.37+551406.6	105.42	-3.25	13.36	0.31	0.48	13.568	-20.2	1
J224435.04+550104.9	105.36	-3.47	14.54	0.27	0.49	14.747	-19.5	1
J224503.87+551319.7	105.51	-3.32	13.48	0.27	0.18	13.687	5.1	3
J224640.02+592740.1	107.67	0.34	14.23	0.68	0.42	14.447	-7.9	1
J225034.82+543719.5	105.95	-4.21	13.30	0.41	0.49	13.511	-29.9	1
J225249.50+582330.5	107.90	-0.98	15.01	0.49	0.37	15.223	-10.2	1
J225328.64+572059.3	107.52	-1.95	13.66	0.32	0.38	13.869	3.9	1
J225328.64+572059.3	107.52	-1.95	13.66	0.32	0.38	13.869	-3.9	1
J225559.62+584908.8	108.46	-0.77	14.92	0.62	0.60	15.136	-32.1	3
J225634.71+601111.6	109.11	0.43	14.38	0.84	0.60	14.601	-3.3	1
J225709.69+573327.8	108.06	-1.98	13.79	0.48	0.43	14.003	0.8	1
J225735.47+582555.6	108.48	-1.21	14.23	0.50	0.51	14.443	-7.9	1
J225851.15+594528.4	109.19	-0.08	14.19	0.69	0.68	14.408	-35.3	1
J225851.58+594808.8	109.21	-0.04	15.46	0.76	0.71	15.679	-35.2	1
J225859.68+630020.9	110.57	2.87	15.79	0.83	0.67	16.011	-32.2	3
J225922.92+582338.4	108.68	-1.34	13.45	0.36	0.38	13.660	-11.9	1
J230004.08+592657.1	109.20	-0.42	15.35	0.87	0.66	15.572	-31.0	1
J230048.21+590638.4	109.14	-0.77	15.98	0.55	0.38	16.194	-20.6	1
J230140.68+592154.4	109.35	-0.58	14.57	0.56	0.46	14.784	-15.2	1
J230215.46+565630.8	108.43	-2.82	13.66	0.48	0.50	13.873	-23.4	1
J230239.06+592622.3	109.49	-0.56	14.33	0.54	0.40	14.544	-10.7	1
J230402.62+580707.2	109.12	-1.84	14.90	0.53	0.52	15.114	-20.7	1
J230415.70+593106.4	109.71	-0.57	14.88	0.73	0.51	15.099	-20.6	1

NAME	$l(deg)$	$b(deg)$	r	r-i	r-Hα	V	$EW_{H\alpha}$	Ref.
J233514.67+644512.5	114.92	3.07	13.78	0.64	0.50	13.996	-17.7	1
J233615.33+620424.2	114.25	0.48	16.00	0.74	0.58	16.219	-19.1	1
J233632.92+620616.3	114.29	0.50	14.18	0.81	0.69	14.400	-36.5	1
J233650.81+585739.2	113.43	-2.53	13.91	0.57	0.68	14.125	-20.1	1
J233702.38+623450.4	114.48	0.94	14.84	0.90	0.59	15.063	-23.5	1
J233823.06+622325.5	114.58	0.71	15.57	0.73	0.82	15.789	-25.5	1
J233940.45+580809.0	113.56	-3.42	15.20	0.66	0.54	15.417	-20.8	1
J233941.46+623050.7	114.76	0.79	15.29	0.66	0.51	15.507	-34.4	1
J234255.79+613845.6	114.89	-0.15	13.70	0.59	0.77	13.915	-48.4	1
J234300.59+604248.4	114.66	-1.05	15.59	0.95	0.71	15.814	-26.3	1
J234317.62+603732.6	114.67	-1.15	14.05	0.74	0.66	14.269	-27.3	1
J234323.84+620151.8	115.05	0.21	14.20	0.53	0.53	14.414	-21.3	1
J234409.27+623943.9	115.29	0.79	13.78	0.44	0.38	13.992	-14.0	1
J234656.98+623355.6	115.58	0.62	13.83	0.47	0.53	14.042	-21.5	1
J234700.05+605626.6	115.19	-0.96	14.14	0.77	0.73	14.359	-41.9	1
J234719.89+612552.4	115.34	-0.49	14.06	0.54	0.50	14.274	-19.9	1
J234840.20+594117.2	115.08	-2.22	15.90	0.56	0.41	16.114	-8.8	1
J234842.28+592615.0	115.02	-2.47	15.08	0.59	0.49	15.295	-29.2	1
J234943.12+633603.4	116.14	1.55	14.60	0.67	0.46	14.817	-12.4	1
J234946.77+624236.9	115.93	0.68	13.30	0.59	0.57	13.515	-15.2	1
J234949.64+632526.4	116.11	1.37	14.12	0.72	0.58	14.338	-21.5	1
J235017.97+604242.7	115.52	-1.28	14.26	0.61	0.45	14.476	-13.3	1
J235046.75+625007.1	116.07	0.77	13.92	0.53	0.46	14.134	-9.7	1
J235119.01+591118.6	115.29	-2.79	14.03	0.48	0.48	14.243	-18.6	1
J235235.36+631554.7	116.37	1.15	14.24	0.60	0.52	14.455	-11.8	3
J235300.10+602852.8	115.79	-1.58	15.05	0.74	0.64	15.269	3.3	1
J235314.34+584234.3	115.42	-3.31	15.43	0.58	0.41	15.645	-11.1	1
J235424.49+611745.0	116.14	-0.82	14.94	0.56	0.43	15.154	-12.2	1
J235425.40+620411.0	116.31	-0.07	13.71	0.44	0.51	13.922	-18.5	1
J235443.62+631720.8	116.61	1.12	13.84	0.53	0.54	14.054	-30.6	1
J235457.41+610350.6	116.15	-1.06	15.14	0.53	0.37	15.354	-9.6	1
J235509.36+622714.9	116.48	0.29	13.41	0.32	0.41	13.619	-5.3	1
J235546.37+623533.9	116.58	0.41	14.39	0.40	0.57	14.601	-26.3	1
J235549.00+623626.6	116.58	0.42	13.33	0.50	0.80	13.543	-62.4	1
J235647.63+622134.5	116.64	0.16	14.83	0.47	0.37	15.042	-10.0	1
J235804.33+631458.9	116.97	1.00	13.25	0.43	0.51	13.461	-14.3	1
J235840.45+641332.4	117.23	1.94	14.28	0.36	0.67	14.490	-23.6	1
J235856.40+624653.0	116.97	0.52	14.62	0.63	0.63	14.836	-24.2	3
J235859.75+625145.0	116.99	0.60	15.16	0.30	0.12	15.368	8.0	3
J235956.43+634404.3	117.27	1.43	15.97	0.51	0.24	16.183	6.0	3

Table 4.3. Continued...

NAME	$l(deg)$	$b(deg)$	r	r-i	r-Hα	V	$EW_{H\alpha}$	Ref.
J230424.03+632849.0	111.32	3.05	15.28	0.88	0.61	15.502	-17.9	1
J230430.93+575918.7	109.13	-1.99	13.75	0.64	0.79	13.966	-50.3	1
J230436.93+584851.0	109.47	-1.24	15.80	0.68	0.62	16.017	-23.8	1
J230844.57+643516.8	112.19	3.88	14.35	0.49	0.39	14.563	-11.7	1
J231108.53+603503.3	110.92	0.07	13.84	0.74	0.60	14.059	-31.9	1
J231159.52+564037.6	109.55	-3.59	14.02	0.30	0.34	14.228	-9.0	1
J231220.82+605805.9	111.20	0.37	14.19	0.51	0.44	14.403	-6.1	1
J231229.94+600725.7	110.90	-0.42	14.41	0.80	0.62	14.630	-25.3	1
J231307.09+590247.9	110.57	-1.45	14.42	0.81	0.85	14.640	-46.7	1
J231331.30+601727.3	111.08	-0.31	15.84	0.72	0.69	16.058	-36.6	1
J231529.13+621733.0	112.03	1.47	13.78	0.60	0.57	13.995	-21.5	1
J231640.52+621539.0	112.15	1.39	14.38	0.73	0.80	14.599	-45.7	1
J231819.36+630345.3	112.61	2.07	14.00	0.54	0.60	14.214	-28.5	1
J231819.36+630345.3	112.61	2.07	14.00	0.54	0.60	14.214	-28.1	1
J231900.76+610845.1	112.02	0.25	13.90	0.67	0.49	14.117	-3.2	1
J231906.01+605909.2	111.97	0.09	13.26	0.49	0.48	13.473	-17.6	1
J231910.81+600917.0	111.69	-0.69	13.00	0.34	0.63	13.209	-36.6	1
J231935.58+640610.1	113.11	3.00	14.85	0.74	0.60	15.069	-31.6	1
J232418.51+620233.3	112.91	0.88	15.33	0.63	0.46	15.546	-13.2	1
J232630.27+612437.2	112.95	0.20	13.65	0.52	0.59	13.863	-27.0	1
J232917.20+610128.9	113.15	-0.28	13.54	0.45	0.55	13.752	-26.9	1
J232937.11+612749.5	113.32	0.13	13.76	0.45	0.43	13.972	-18.9	1
J233006.53+613920.6	113.44	0.29	13.63	0.72	0.71	13.848	-27.8	3
J233014.52+613401.9	113.42	0.20	14.33	0.54	0.54	14.544	-25.0	1
J233036.61+610814.6	113.33	-0.22	13.81	0.41	0.41	14.021	-11.4	1

NAME	$l(deg)$	$b(deg)$	r	r-i	r-Hα	V	$EW_{H\alpha}$	Ref.